AD NUMBER

ADC040572

CLASSIFICATION CHANGES

TO: unclassified

FROM: confidential

LIMITATION CHANGES

TO:

Approved for public release, distribution unlimited

FROM:

Controlling Office: Director, Defense Nuclear Agency, Washington, DC 20305-1000.

AUTHORITY

DSWA ltr., 13 Apr 1998; Same

DNA-5826F

DYNAMIC PRESSURE IMPULSE FOR NEAR-IDEAL AND NON-IDEAL BLAST WAVES -- HEIGHT OF BURST CHARTS (U)

E. J. Bryant
F. J. Allen
Kaman Tempo
P. O. Drawer Q Q
Santa Barbara, CA 93102

15 May 1981

Technical Report

CONTRACT No. DNA 001-80-C-0156

THIS WORK WAS SPONSORED BY THE DEFENSE NUCLEAR AGENCY
UNDER RDT&E RMSS CODE B344080464 Y99QAXSG60124 H2590D.

Prepared for
Director
DEFENSE NUCLEAR AGENCY
Washington, DC 20305-1000

CLASSIFIED BY DD Form 254, 15 February 1980, Contract No. DNA 001-80-C-0156, and multiple sources.

FORMERLY RESTRICTED DATA
Unauthorized disclosure subject to administrative and criminal sanctions. Handle as Restricted Data in foreign dissemination. Section 144.b, Atomic Energy Act, 1954.

DESTRUCTION NOTICE:

FOR CLASSIFIED documents, follow the procedures in DoD 5200.22-M, Industrial Security Manual, Section II-19 or DoD 5200.1-R, Information Security Program Regulation, Chapter IX.

FOR UNCLASSIFIED, limited documents, destroy by any method that will prevent disclosure of contents or reconstruction of the document.

Retention of this document by DoD contractors is authorized in accordance with DoD 5200.1-R, Information Security Program Regulation.

PLEASE NOTIFY THE DEFENSE NUCLEAR AGENCY, ATTN: STTI, WASHINGTON, DC 20305-1000, IF YOUR ADDRESS IS INCORRECT, IF YOU WISH IT DELETED FROM THE DISTRIBUTION LIST, OR IF THE ADDRESSEE IS NO LONGER EMPLOYED BY YOUR ORGANIZATION.

DISTRIBUTION LIST UPDATE

This mailer is provided to enable DNA to maintain current distribution lists for reports. We would appreciate your providing the requested information.

☐ Add the individual listed to your distribution list.

☐ Delete the cited organization/individual.

☐ Change of address.

NAME: _____

ORGANIZATION: _____

OLD ADDRESS	CURRENT ADDRESS
_____	_____
_____	_____
_____	_____

TELEPHONE NUMBER: ( ) _____

SUBJECT AREA(s) OF INTEREST:

_____	_____
_____	_____
_____	_____

DNA OR OTHER GOVERNMENT CONTRACT NUMBER: _____

CERTIFICATION OF NEED-TO-KNOW BY GOVERNMENT SPONSOR (if other than DNA):

SPONSORING ORGANIZATION: _____

CONTRACTING OFFICER OR REPRESENTATIVE: _____

SIGNATURE: _____

Director
Defense Nuclear Agency
ATTN: STTI
Washington, DC 20305-1000

Director
Defense Nuclear Agency
ATTN: STTI
Washington, DC 20305-1000

(This page is unclassified)

UNCLASSIFIED

SECURITY CLASSIFICATION OF THIS PAGE

AD-C040572

REPORT DOCUMENTATION PAGE

Form Approved OMB No. 0704-0188 Exp. Date: Jun 30, 1986

1a. REPORT SECURITY CLASSIFICATION CONFIDENTIAL	1b. RESTRICTIVE MARKINGS FORMERLY RESTRICTED DATA
2a. SECURITY CLASSIFICATION AUTHORITY DD Form 254, 15 February 1980, Contract No.	3. DISTRIBUTION/AVAILABILITY OF REPORT N/A since Formerly Restricted Data
2b. DECLASSIFICATION/DOWNGRADING SCHEDULE N/A since Formerly Restricted Data	
4. PERFORMING ORGANIZATION REPORT NUMBER(S) KT-81-014(R)	5. MONITORING ORGANIZATION REPORT NUMBER(S) DNA-5826F
6a. NAME OF PERFORMING ORGANIZATION Kaman Tempo 6b. OFFICE SYMBOL (If applicable)	7a. NAME OF MONITORING ORGANIZATION Director Defense Nuclear Agency
6c. ADDRESS (City, State, and ZIP Code) P.O. Drawer QQ Santa Barbara, CA 93102	7b. ADDRESS (City, State, and ZIP Code) Washington, DC 20305-1000
8a. NAME OF FUNDING/SPONSORING ORGANIZATION 8b. OFFICE SYMBOL (If applicable) SPAS (Ullrich)	9. PROCUREMENT INSTRUMENT IDENTIFICATION NUMBER DNA 001-80-C-0156
8c. ADDRESS (City, State, and ZIP Code)	10. SOURCE OF FUNDING NUMBERS PROGRAM ELEMENT NO: 62715H; PROJECT NO: Y99QAXS; TASK NO: G; WORK UNIT ACCESSION NO: DH004734

11. TITLE (Include Security Classification)
DYNAMIC PRESSURE IMPULSE FOR NEAR-IDEAL AND NON-IDEAL BLAST WAVES—HEIGHT OF BURST CHARTS (U)

12. PERSONAL AUTHOR(S)
Bryant, E. J. and Allen, F. J.

13a. TYPE OF REPORT	13b. TIME COVERED	14. DATE OF REPORT (Year, Month, Day)	15. PAGE COUNT
Technical	FROM 800215 TO 810415	810515	215

16. SUPPLEMENTARY NOTATION
This work was sponsored by the Defense Nuclear Agency under RDT&E RMSS Code B344080464 Y99QAXSG60124 H2590D. For multiple sources see List of Classification Guidance References.

17 COSATI CODES			18. SUBJECT TERMS (Continue on reverse if necessary and identify by block number)	
FIELD	GROUP	SUB-GROUP		
18	3		Nuclear Weapons Effects	Dynamic Pressure Impulse
19	4		Airblast (Nuclear)	Height of Burst
			Precursor (Nuclear)	Sachs Scaling

19. ABSTRACT (Continue on reverse if necessary and identify by block number)

Dynamic pressure impulse, I_q, was evaluated as a function of wheeled vehicle displacement (1/4 ton and 2-1/2 ton trucks) for ideal/near-ideal and non-ideal blast environments. Good correlation was obtained between dynamic pressure impulse and vehicle displacements using least squares fits. Using the quadratic equations derived by least squares fit the I_q were calculated from known vehicle displacements and these were averaged with initial estimates of I_q (ideal/near-ideal) and measured I_q (non-ideal) to obtain iterated values of I_q. Least square fits were also applied to I_q versus scaled ground range and displacement versus scaled ground range for various values of n, the exponent of yeild. The values of n providing the best fits were between 0.4 and 0.43 for displacements and n = 0.42 or 0.43 for I_q as a function of scaled range.

sub q

20. DISTRIBUTION/AVAILABILITY OF ABSTRACT	21. ABSTRACT SECURITY CLASSIFICATION
☐ UNCLASSIFIED/UNLIMITED ☒ SAME AS RPT ☐ DTIC USERS	UNCLASSIFIED
22a. NAME OF RESPONSIBLE INDIVIDUAL Betty L. Fox	22b. TELEPHONE (Include Area Code) (202)325-7042
	22c. OFFICE SYMBOL DNA/STTI

DD FORM 1473, 84 MAR — 83 APR edition may be used until exhausted. All other editions are obsolete.

SECURITY CLASSIFICATION OF THIS PAGE
UNCLASSIFIED

FORMERLY RESTRICTED DATA
Unauthorized disclosure subject to administrative and criminal sanctions. Handle as Restricted Data in foreign dissemination. Section 144.b, Atomic Energy Act, 1954.

2a. SECURITY CLASSIFICATION AUTHORITY (Continued)

DNA 001-80-C-0156 and multiple sources.

18. SUBJECT TERMS (Continued)

Light Dust Blast Wave
Heavy Dust Blast Wave

20. ABSTRACT (Continued)

I_q, displacement, and damage obtained on water and asphalt surfaces were compared with similar data obtained on the desert surfaces. I_q and displacement were less on water and asphalt. But for damage the asphalt exhibited similar results as on desert surface (Bee-6 and Met-12). Desert Rock displacement and damage were compared with the desert surface. Displacements were less and damage was equivalent in the Desert Rock sector to that along the desert line. It was concluded that surface hardness contributed to damage. Desert Rock was undisturbed desert surface and desert line was disturbed producing a fine, loose, sandy surface.

Once-iterated (near-ideal) and twice-iterated (non-ideal) $\bar{I}_q$ values were used to obtain scaled $\bar{I}_q$ versus range curves. The data on these curves were least squares fitted for various combination of events and burst heights. These curves were divided into three categories, ideal/near-ideal, light dust and heavy dust events. The $\bar{I}q$ data from asphalt surfaces were combined with I_q data from light dust events and good correlation was obtained. The data from these curves were then used to construct two HOB Charts - one for light dust/near-ideal and one for heavy dust/near-ideal. It was indicated that the surface conditions for the heavy dust events were unique and thus produced blast conditions which were unique. It was suggested that little importance be given to the heavy dust/near-ideal HOB Chart and perhaps be disregarded. The light dust/near-ideal HOB Chart which includes asphalt data is more representative of expected blast conditions over surfaces where precursors would be formed. It was also felt that resultant I_q values for these events (light dust) were caused primarily by the precursor action). The conclusion is that the light dust/near-ideal HOB Chart is the preferred chart for general applications.

PREFACE
(This Preface is Unclassified)

The authors wish to acknowledge the considerable contribution of Mrs. Jeanne Rosser to this report: skilled assistance with a variety of details necessary to the carrying out of this study including plotting figures; checking data, tabulations, and some computations; and planimetering pressure-time records. We also wish to acknowledge the assistance of Mr. John Keefer, BRL, in obtaining some of the raw data and we wish to acknowledge much helpful technical discussion with Mr. Noel Ethridge, BRL.

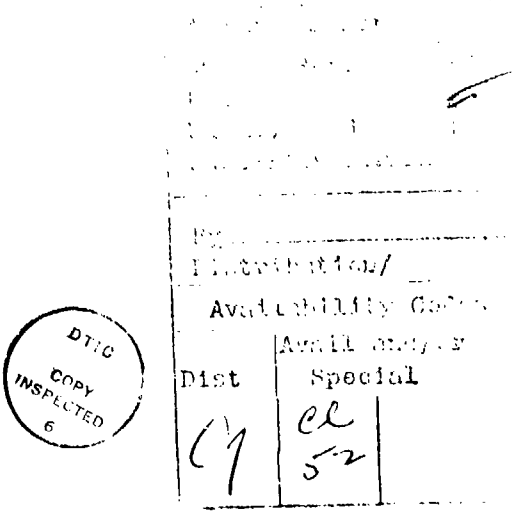

CONVERSION TABLE

(This Conversion Table Is Unclassified)

angstrom	1.000 000 X E -10	meters (m)
atmosphere (normal)	1.013 25 X E +2	kilo pascal (kPa)
bar	1.000 000 X E +2	kilo pascal (kPa)
barn	1.000 000 X E -28	meter^2 (m^2)
British thermal unit (thermochemical)	1.054 350 X E +3	joule (J)
calorie (thermochemical)	4.184 000	joule (J)
cal (thermochemical)/cm^2	4.184 000 X E -2	mega joule/m^2 (MJ/m^2)
curie	3.700 000 X E +1	*giga becquerel (GBq)
degree (angle)	1.745 329 X E -2	radian (rad)
degree Fahrenheit	$t_k = (t°f + 459.67)/1.8$	degree kelvin (K)
electron volt	1.602 19 X E -19	joule (J)
erg	1.000 000 X E -7	joule (J)
erg/second	1.000 000 X E -7	watt (W)
foot	3.048 000 X E -1	meter (m)
foot-pound-force	1.355 818	joule (J)
gallon (U.S. liquid)	3.785 412 X E -3	meter^3 (m^3)
inch	2.540 000 X E -2	meter (m)
jerk	1.000 000 X E +9	joule (J)
joule/kilogram (J/kg) (radiation dose absorbed)	1.000 000	Gray (Gy)
kilotons	4.183	terajoules
kip (1000 lbf)	4.448 222 X E +3	newton (N)
kip/inch^2 (ksi)	6.894 757 X E +3	kilo pascal (kPa)
ktap	1.000 000 X E +2	newton-second/m^2 (N-s/m^2)
micron	1.000 000 X E -6	meter (m)
mil	2.540 000 X E -5	meter (m)
mile (international)	1.609 344 X E +3	meter (m)
ounce	2.834 952 X E -2	kilogram (kg)
pound-force (lbs aviordupois)	4.448 222	newton (N)
pound-force inch	1.129 848 X E -1	newton-meter (N·m)

CONVERSION TABLE (Concluded)

pound-force/inch	1.751 268 X E +2	newton/meter (N/m)
pound-force/foot^2	4.788 026 X E -2	kilo pascal (kPa)
pound-force/inch^2 (psi)	6.894 757	kilo pascal (kPa)
pound-mass (lbm avoirdupois)	4.535 924 X E -1	kilogram (kg)
pound-mass-foot^2 (moment of inertial)	4.214 011 X E -2	kilogram-meter^2 (kg·m^2)
pound-mass/foot^3	1.601 846 X E +1	kilogram/meter^3 (kg/m^3)
rad (radiation dose absorbed)	1.000 000 X E -2	**Gray (Gy)
roentgen	2.579 760 X E -4	coulomb/kilogram (C/kg)
shake	1.000 000 X E -8	second (s)
slug	1.459 390 X E +1	kilogram (kg)
torr (mm Hg, 0°C)	1.333 22 X E -1	kilo pascal (kPa)

*The becquerel (Bq) is the SI unit of radioactivity; 1 Bq = 1 event/s.
**The Gray (Gy) is the SI unit of absorbed radiation

TABLE OF CONTENTS

(This Table of Contents Is Unclassified)

TABLE OF CONTENTS (Continued)

TABLE OF CONTENTS (Concluded)

LIST OF ILLUSTRATIONS

(This List of Illustrations Is Unclassified)

LIST OF ILLUSTRATIONS (Continued)

LIST OF ILLUSTRATIONS (Continued)

LIST OF ILLUSTRATIONS (Continued)

LIST OF ILLUSTRATIONS (Continued)

LIST OF ILLUSTRATIONS (Concluded)

LIST OF TABLES

(This List of Tables Is Unclassified)

LIST OF TABLES (Concluded)

SECTION 1
(This Section Is Unclassified)

INTRODUCTION

1.1 GENERAL

In a previous effort, we evaluated dynamic pressure impulse, I_q, for ideal/near-ideal blast waves by showing a correlation with wheeled vehicle (1/4 ton trucks) displacement (Reference 1). We found that there is a one-to-one correspondence between I_q and vehicle displacement and concluded that from known vehicle displacements the dynamic pressure impulse can be estimated with reasonable accuracy.

Here, we present the results for evaluating I_q, not only for ideal/near-ideal blast waves but also for I_q for non-ideal blast waves. We combined the data from our first evaluation with 1/4 ton truck exposures to non-ideal blast waves along with that of 2-1/2 ton truck exposures to both non-ideal and ideal/near-ideal blast environments.

Additionally, we evaluated damage to wheeled vehicles as a function of vehicle displacement. For a given displacement, the damage can then be correlated with I_q. The scaling of damage for known values of I_q is straightforward by simply using Sachs scaling. The damage itself as a function of range, however, cannot be scaled by use of a constant exponent of the weapon yield such as $W^{0.4}$. The exponent of W will vary depending on the burst height of the weapon.

To keep this report from being too cumbersome we do not include the damage versus displacement here. Instead another report was prepared to present this information. We also feel that in this way the report on I_q will be of special interest to groups dealing with airblast phenomena while the report on damage will be of special interest to groups dealing with targeting and vulnerability/survivability. This report on I_q presents the procedures for correlating I_q versus displacement, the effect of surface conditions on I_q, the construction of I_q versus range curves as well as the construction of HOB charts for iso-I_q.

1.2 OBJECTIVES

Our main objective was the evaluation of dynamic pressure impulse for ideal/near-ideal and non-ideal blast waves using wheeled vehicle response along with gage measurements. Other objectives were to correlate damage

with vehicle response, establish the influence of diffraction flow on displacement and evaluate the peak overpressure effects on damage to wheeled vehicles.

1.3 BACKGROUND

The exposure of wheeled vehicles (drag-type targets) on past nuclear and HE tests served several purposes such as troop indoctrination, damage evaluation and verification of damage predictions. Different types of vehicles were exposed under a variety of conditions. The vehicles included 1/4 ton, 3/4 ton, 2-1/2 ton, and 5 ton trucks. The majority of vehicles exposed were 1/4 ton trucks and on several occasions they were used as gages to evaluate the relative effects of nuclear blast on drag-type targets. The information on wheeled vehicle exposures has been compiled and reevaluated. A report has been prepared which covers the exposure conditions, vehicle damage, and displacements (Reference 2).

Damage to and displacements of drag-type targets under some nuclear burst conditions was far in excess of damage and displacements for other nuclear burst conditions. This was dramatically demonstrated on events of Encore-9 and Grable-10, Upshot/Knothole. The maximum damage of vehicles (1/4 ton trucks) exposed on Encore-9 was M.6 (Moderate II) and the maximum displacement was about 11 metres. On Grable-10, however, the 1/4 ton trucks were completely dismembered and displacement of parts (engine, chassis, wheels) was greater than 300 metres. The exposure of vehicles on these two events was based on peak overpressure values and it was assumed that the other blast parameters could be calculated by using the Rankine-Hugoniot relations. But the pressure waveforms measured on Encore-9 (Mach Region) were primarily steep-rising shock fronts (near-ideal), while the pressure waveforms on Grable-10 were somewhat distorted showing rounded fronts with high frequency oscillations and in some cases secondary peaks were observed (non-ideal). There was no correlation between overpressure and dynamic pressure on Grable-10. This difference in damage and displacement was then attributed to the precursor dust-laden blast wave formed on Grable-10. The dust momentum increased the total loads on the vehicles. Similar results were obtained on other precursor-forming events. Thus one of the criteria used for distinguishing between ideal/near-ideal and non-ideal blast environments was the waveform — steep rising shock front for ideal/near-ideal and a rounded front with secondary peaks for non-ideal. The non-ideal could be further divided

into light dust and heavy dust blast environment. One of the measures for this was that dynamic pressures were greater on heavy dust events than on light dust environments.

When vehicles were used as gages they were located adjacent to blast line instrumentation which consisted of overpressure, pitot-tube, differential pressure, total head, GREG and SNOB gages. In a precursor dust-laden blast environment the dust registry coefficient was known for the GREG and SNOB gages only. Many of the measurements for deriving dynamic pressure versus time in this sort of an environment were suspect. A procedure was developed to try to retrieve the suspect data (Reference 3). The technique for retrieving the suspect data was based on the comparison of measured data from two gages — one gage with a known registry coefficient and the other with an unknown coefficient. This procedure was not successful since there were a limited number of measurements with gages having a known registry coefficient. Wheeled vehicles on the other hand responded by translational and rotational motion to the actual blast load environments. The displacement of the vehicle should, therefore, be a measure of the blast loads acting on the target.

Past studies have resulted in calculational capability to compute rotational and translational motion of drag-type targets (References 4 and 5). The technique of Reference 4 calculates either translational motion or rotational motion. The technique of Reference 5 which is a multidegree-of-freedom code calculates both translation and rotation. However, for both techniques the calculation for rotation is limited up to the point of overturning. The important blast parameter considered in both techniques is dynamic pressure impulse. For fractional KT weapons, diffraction loading due to overpressure influences the motion. These calculations provide an insight for proper interpretation of the vehicle response to the blast loads.

In our initial evaluation, we were concerned about establishing the values of dynamic pressure impulse for the ideal/near-ideal blast waves to be correlated with vehicle displacements. Two approaches were used to establish these values. One approach was based on averaging the measured overpressure and positive phase duration as a function of range and then combining this with the Rankine-Hugoniot relations together with empirically derived equations to compute the peak dynamic pressures and the peak dynamic pressure impulse, respectively. Another approach was the use of theoretical and analytical computations for static pressure impulse, I_p, and I_q combined

with the average values of measured peak overpressure, P_s, and static pressure impulse. The latter approach, which was the method selected, permitted the construction of a set of curves showing the ratio of I_p/I_q versus P_s for several burst heights. The I_q was determined using the average measured values of I_p and P_s on each event. Details of this approach are given in Appendix A.

SECTION 2

(U) BLAST MEASUREMENTS AND VEHICLE EXPOSURES - NUCLEAR AND HE EVENTS

2.1 (U) TECHNICAL DATA BASE

2.1.1 (U) Operations/Events

(U) Over 400 vehicles were exposed on 19 nuclear and HE events. Blast measurements of one type or another were also obtained from these events. Of the more than 400 vehicles exposed, only 167 were used for correlation with I_q. The vehicles excluded for this correlation were those located on the asphalt and water surfaces and those located in the Desert Rock sector, and also, vehicles which were constrained to rotate without sliding. Blast overpressure measurements were obtained on the majority of these events. Only on two events, Encore-9 and Wasp-1, were the dynamic pressure measurements unavailable.

(U) The listing of the Operation/Events are given in Table 2.1. The information provided includes the yield, actual burst height, scaled burst height, scaling factors, and ambient environment. Ten of these events are additions to the events used in our first evaluation. These added events all took place at Nevada Test Site; most produced strong precursor actions (non-ideal blast waves). The nomenclature given for each event refers to the code name and to the shot number for that Operation.

2.1.2 (U) Blast Wave and Vehicle Displacement Collations

(U) The nuclear and HE events, designated as ideal/near-ideal blast waves were the assigned nine events (first evaluation) and the additional two events: Wasp-1 and Wasp Prime-9. Our initial guidance for categorizing the precursor nuclear events was based on the information given in Reference 6, i.e., whether they were light dust-laden or heavy dust-laden blast waves. The sorting of events into one of the three categories is as follows:

Ideal/Near-Ideal Blast Waves

Upshot/Knothole: Encore-9
Castle: Koon-3 and Nectar-6
Teapot: Wasp-1 and Wasp Prime-9
Redwing: Lacrosse-1, Zuni-3 and Yuma-4
HE: Canadian 20-Ton, 100-Ton and Dice Throw

Light Dust-Laden Blast Waves

Teapot: Moth-2, Turk-4, Bee-6, and Apple I-8

Heavy Dust-Laden Blast Waves

Upshot/Knothole: Grable-10
Teapot: Met-12 and Apple II-13
Plumbbob, Smoky-15

Some of the events within the light dust and heavy dust categories, however, were interchanged as will be described later in this report. The blast measurements of total pressure and overpressure as a function of time were also gathered and categorized accordingly.

(U) The wheeled vehicle exposure data were sorted into these three categories. The vehicle data pertinent to this evaluation were the location, orientations, displacements and damage. Vehicles were further sorted according to surface conditions, i.e., desert, water, asphalt.

2.2 (U) ANALYTICAL APPROACH

2.2.1 (U) Blast Data Reduction Procedures

(U) We have described the procedures used for deriving I_q for ideal/near-ideal blast conditions (see Background and Appendix A). In order to obtain the initial best estimates of I_q for the non-ideal blast conditions we reduced the data independently of the previous data reduction procedures. The procedure we followed was to integrate the total pressure-time and the static pressure-time waveforms to obtain the total pressure impulse and the static pressure impulse. A check was made for certain intervals of the total pressure-time and the static pressure-time curves to determine the range of Mach numbers for those intervals. Where appropriate the Mach compressibility corrections were made to the difference between the total pressure impulse and static pressure impulse for those intervals. The sum over these intervals yielded the dynamic pressure impulse. The details of this procedure are presented in Appendix B.

(U) We made checks of this procedure by comparing the I_q values we derived with those reported by BRL on Plumbbob, Smoky-15 (Reference 7) and on Dice Throw (Reference 8). The Mach numbers ranged as high as 2.2 in these comparisons. Waveforms on Smoky-15 displayed a considerable amount of oscillations while the waveforms selected from Dice Throw were reasonably smooth. On Smoky-15, at the first stations, we assu that the gage was plugged since

the total pressure-time curve did not return to the base line. For computing the total pressure impulse we terminated the integration of the pressure-time curve corresponding to the end of the positive-phase on the static pressure-time curve. We assumed that the error contribution to the total pressure impulse would be small at the tail-end of the waveform. The comparisons of I_q are shown in Table 2.2. The maximum difference between these two values is about 15 percent.

2.2.2 (U) Least Squares Fit Procedures

(U) All of the problems evaluated where least squares fits were applied made use of the TI-59 Programmable Calculator. The problems evaluated were:

1) Dynamic Pressure Impulse vs. Displacement [subcases included WWII and M38A1 (1/4 ton trucks) and the M35 and M135 (2-1/2 ton trucks) in both side-on and face-on orientations].

2) Damage vs. Displacement (several subcases).

3) Displacement vs. Scaled Ground Range (subcases included side-on and face-on for 1/4 ton trucks with various height of burst conditions including light and heavy dust).

4) Dynamic Pressure Impulse vs. Scaled Ground Range (subcases included air burst and surface burst as well as light and heavy dust conditions).

5) Scaled Displacement vs. Scaled Ground Range (WWII, 1/4 ton trucks, side-on and face-on, surface burst conditions).

6) Scaled Dynamic Pressure Impulse vs. Scaled Ground Range (subcases included air burst and surface burst as well as light and heavy dust conditions).

The functional forms used for least squares fits for these preliminary evaluations were as follows:

PROBLEM 1: $I_q = B\ D^m$ or $D = AI_q^{\ell}$

where: a and b are coefficients
m and n are exponents
D is displacement (metres)

PROBLEM 2: $da = a_0 + a_1 D + a_2 D^2,\ D \leq D_m$

$da = 10,\ D \geq D_m$

where: da = damage
D = displacement
D_m = value of displacement for which curve fit (first) reaches line da = 10

PROBLEMS 3 through 6: $\ell n\ y = a_0 + a_1 x + a_2 x^2$

where: y = ordinate, Displacement or I_q
x = independent variable, Scaled Ground Range

(U) A detailed description of the least squares fit procedures is given in Appendix C.

As stated previously, the above functional forms were used for the preliminary evaluations. Later, we used other functional forms and these will be defined in other Sections of this report.

2.2.3 (U) Displacement - Dynamic Pressure Impulse Least Squares Fits

(U) In Appendix A we have described how we obtained values of I_q for the ideal shots used in this report. In Appendix B we have described in considerable detail how we obtained values of I_q from gage data for the non-ideal shots of present concern. The results are contained in Table 2.3. Figures 2.1 through 2.4 show plots of these values of I_q versus vehicle displacement for the WWII and M38A1 one-quarter ton trucks in side-on and face-on orientations.

(U) We obtained least squares fits for both I_q versus displacement and for displacement versus I_q in each case following the procedures described in Appendix C. The results are given in Table 2.4. Similar results are given for the REO M35 2-1/2 ton trucks in Figures 2.5 and 2.6 and Table 2.4. (For the REO M35 improved or "first iteration" values of I_q were used as described in Section 2.2.4.)

(U) We will discuss these results in detail in Section 3.1. Here we note, however, that while the data exhibit considerable scatter, the curve fits to the data are well determined. Thus, on the average, I_q can be estimated with fair accuracy from a measurement of vehicle displacement — the fitted curve serving as a calibration and the vehicle serving as a gage. The results* in Table 2.4 show that values of I_q inferred from displacement measurements are of comparable accuracy with the gage-reduced data for the non-ideal shots discussed in Appendix B.

(U) *Note the listed values of E_I.

2.2.4 (U) Improved or "Iterated" Values of I_q

(U) One of the objectives of this report is to obtain the best, most reliable possible values of dynamic pressure impulse for non-ideal nuclear shots. Since vehicle displacement is independent of the detailed cause of the impulse to which the vehicle is subjected, i.e., whether it is caused solely by airblast or by an air-dust mixture, and since displacement-inferred values of impulse appear to be comparable in accuracy with gage-inferred values, it appears logical to use displacement-inferred results to improve our estimates of dynamic pressure impulse. Therefore, for each instance in this report where we have one or more 1/4 ton trucks exposed on a non-ideal shot, side-on and/or face-on, at the same ground range as that of a gage location — in most cases gages and vehicles were placed at the same ground range — we have averaged the values of dynamic pressure impulse inferred from the measured displacement by use of the dynamic pressure impulse versus displacement data fits. (Note that these fits are based on both ideal/near-ideal and non-ideal nuclear shot data, and include some HE shot data also.) This provides, then, a single, mean value of dynamic pressure impulse inferred from vehicle displacements.

(U) Finally, since the gage-inferred and vehicle displacement-inferred values of dynamic pressure impulse appear to be of comparable accuracy, we have averaged the (average) gage-inferred value with the (average) displacement-inferred value to obtain a "final" average or "grand" average value of dynamic pressure impulse. We note that in most cases the number of gage-inferred values producing the gage average result is 2 or 3 (i.e., 2 or 3 of the 4 possible values acceptable); the displacement-inferred result is usually based on the average of 2 results, one side-on and one face-on. However, the displacement results are independent whereas the gage-inferred results are partially dependent in a complicated way, as we have noted.

(U) The improved estimates of dynamic pressure impulse obtained for non-ideal shots by this procedure are given in Table 2.3. These results, along with our original estimates for I_q for ideal and near-ideal shots, are used in Sections 3 and 4 of this report.

(U) Having obtained the above results for the non-ideal shots as described, we could consider replotting displacement versus I_q using the improved I_q results with the expectation that data scatter would be lessened (since the average curve for the originally plotted results is used to improve

the estimates of some of the points now being replotted)! However, the diminution in the data scatter would actually be quite small: the scatter of the ideal/near-ideal data points about the curves is as great as for the non-ideal (and there are more ideal/near-ideal data points). This may seem illogical: gage data should be better for ideal shots since the gages are not subject to clogging by dust and pressure-time waveforms are freer of irregularities. It follows from this that the ideal gage data should also be better than vehicle displacement-inferred results since the latter were found to be comparable in accuracy to the gage-inferred values of I_q for non-ideal shots. For the fact that the ideal nuclear shot results show as much data scatter in the displacement-I_q plots as do the non-ideal we offer the following explanation:

1) there is a greater variety of ideal/near-ideal shots, especially with regard to the range of weapon yields in the data base;

2) our calculation of four gage-derived values of I_q, largely independent from the standpoint of data reduction procedure (see Appendix B), and intercomparison of the calculated values, after culling obviously bad gage data, resulted in elimination of most of the poor data (whether caused by a gage result or the data reduction process) before averaging to obtain the accepted gage-derived result; (the latter was then averaged with the average displacement-derived result to obtain our improved estimate).

Whether or not the above explanation accounts entirely for it, the fact is that ideal and non-ideal data have about the same scatter on the displacement versus I_q plots. Thus, while initially it seemed reasonable to improve our estimates of I_q for the non-ideal shots by using the vehicle displacement data — the "calibration" of the vehicle as a gage being determined by both the ideal/near-ideal data along with our initial estimates of non-ideal data (gage-inferred) — it now appears equally reasonable to use the vehicle displacement data to improve I_q estimates for the ideal/near-ideal shots: the results for the latter are apparently not as accurate as might have been supposed. The same rationale justifies the procedure: the central curve in the displacement-I_q plots is well determined; the data point scatter about this curve is fairly large but quite uniform. So while displacement-inferred values of I_q have considerable scatter (there being several uncontrolled variables which affect displacement, (see Section 3.1), their accuracy is comparable with that of the gage-inferred and/or calculated results for the ideal/near-ideal shots.

(U) Following the above reasoning we again used displacement-inferred values of I_q to improve our estimates in order to obtain the best possible estimates of I_q for construction of scaled HOB contours. To distinguish these results from the previous results, we now refer to the first such results (Table 2.3), applicable only to non-ideal shots, as "first iteration" results. Our second use of this procedure, which applies to both ideal and non-ideal shots and which starts with the best previous estimate (i.e., initial estimate for ideal/near-ideal shots, "improved" or "first iteration" results for non-ideal shots) — we now refer to as the "second iteration". We note here the changes produced in this iteration were quite modest. However, as will be seen in Section 4.1, it is quite difficult to determine accurately the shapes of scaled HOB I_q contours so that the best possible data should be used for this purpose. Section 4.1 is the only part of this report in which we use "second iteration" values of I_q. The second iteration i.e., final best estimates of I_q are given in Tables 4.1 through 4.4.

TABLE 2.1 (U) General Information -- Nuclear and HE Tests

CONFIDENTIAL - FORMERLY RESTRICTED DATA

OPERATION	EVENT	YIELD (KT)	HOB METRES	SCALED HOB METRES	SCALING FACTORS S_p	S_d	S_t	S_i	P_o kPa	TO °C	RH* (%)
Upshot/ Knothole	Encore-9	26.0	738.5	240	1.127	0.3244	0.3254	0.3667	89.9	16.7	19
	Grable-10	14.9	159.7	62.5	1.126	0.3909	0.3908	0.4400	90.0	14.8	32
Castle	Koon-3	150	4.15	0.78	1.005	0.1879	0.1918	0.1928	100.8	27.2	82
	Nectar-6	1700	2.13	0.18	1.007	0.0836	0.0853	0.0859	100.7	26.7	85
Teapot	Wasp-1	1.16	232.3	208	1.197	0.8963	0.8620	1.032	84.6	- 6.6	43
	Moth-2	2.39	91.4	65.0	1.163	0.7112	0.6871	0.7991	87.1	- 4.2	57
	Turk-4	43.0	152.4	41.0	1.186	0.2696	0.2653	0.3146	85.4	5.83	32
	Bee-6	7.76	152.4	73.2	1.163	0.4803	0.4719	0.5488	87.1	5.0	34
	Apple I-8	14.2	152.4	59.5	1.186	0.3901	0.3875	0.4596	85.4	11.2	54
	Wasp Prime-9	3.16	225.2	145	1.193	0.6425	0.6398	0.7633	84.9	12.6	28
	Met-12	22.0	121.9	42.0	1.132	0.3425	0.3448	0.3903	89.5	18.9	21
	Apple II-13	28.5	152.4	47.2	1.184	0.3094	0.3098	0.3668	85.6	15.6	--
Redwing	Lacrosse-1	39.5	5.18	1.52	1.006	0.2930	0.2991	0.3009	100.7	27.2	84
	Zuni-3	3500	2.74	0.18	1.005	0.0657	0.0671	0.0674	100.8	27.2	80
	†Yuma-4	0.185	62.4	109	1.012	1.748	1.785	1.806	100.1	27.5	80
Plumbbob	Smoky-15	43.7	213.4	57.3	1.185	0.2683	0.2736	0.3242	85.6	26.4	33
(HE TESTS)											
Canadian	20-Ton	0.04	0	0	1.090	2.841	2.866	3.124	93.0	20	32
	100-Ton	0.2	0	0	1.075	1.669	1.683	1.809	94.2	20	21
Dice Throw	628 Ton ANFO	1.0	-	-	1.196	0.9421	0.9334	1.116	84.7	9.7	71

* Relative Humidity

† These events and yields in combination are CONFIDENTIAL-FORMERLY RESTRICTED DATA.

CONFIDENTIAL

TABLE 2.2 (U) Comparison of Dynamic Pressure Impulse

UNCLASSIFIED

Plumbbob, Smoky-15

RANGE (Metres)	Calculated I_{q_0} psi-sec	Calculated I_{q_0} kPa-sec	BRL (Report WT-1407) I_{q_0} psi-sec	BRL (Report WT-1407) I_{q_0} kPa-sec
457	20.02	138	21.99	152
789	3.44	23.7	3.85	26.5
897	2.29	15.8	2.02	13.9
1038	2.28	15.7	2.26	15.6

Dice Throw

RANGE (Metres)	Calculated I_{q_0} psi-sec	Calculated I_{q_0} kPa-sec	BRL (Report DNA4377P-1) I_{q_0} psi-sec	BRL (Report DNA4377P-1) I_{q_0} kPa-sec
134	1.56	10.79	1.45	9.98
195	0.59	4.07	0.53	3.67
375	0.096	0.66	0.082	0.57

TABLE 2.3 (U) Dynamic Pressure Impulse vs. Range, Non-Ideal Blast Waves

UNCLASSIFIED

Event	Ground Range (m)	Gage Reduced Result (avg) (kPa-sec)	Displacement Inferred I_q (avg) (kPa-sec)	"Grand" Avg (First Iteration Result) (kPa-sec)
Grable-10	736	5.1	5.16	5.13
	844	2.5	2.87	2.69
Moth-2	287	6.75	--	6.75
	366	3.35	--	3.35
	411	2.54	2.31	2.42
	457	1.88	1.83	1.85
	518	1.35	--	1.35
Turk-4	716	20.7	--	20.7
	914	11.8	--	11.8
	1030	7.95	7.42	7.69
	1128	5.50	5.82	5.66
	1280	2.32	--	2.32
Bee-6	549	6.1	10.1	8.10
	610	3.75	4.59	4.17
	701	2.25	2.40	2.32
	777	1.35	2.47	1.91
Apple I-8	527	17.3	--	17.3
	622	9.10	--	9.10
	902	1.46	2.44	1.95
	991	0.96	1.44	1.20
	1128	0.41	0.338	0.38
Met-12	610	48.0	38.0	43.0
	686	37.2	38.0	37.6
	762	17.2	16.3	16.8
	838	11.5	16.1	13.8
	914	3.4	3.62	3.51
Apple II-13	518	41.9	--	41.9
	625	34.0	--	34.0
	808	19.3	--	19.3
	914	12.1	8.54	10.3
	1006	7.4	3.68	5.54
	1128	4.8	3.15	3.98
	1219	2.48	2.62	2.55
Smoky-15	726	22.3	34.7	28.5
	841	14.7	17.3	16.0
	897	18.2	6.81	12.5
	1038	5.96	7.84	6.9
	1181	3.96	3.54	3.75

TABLE 2.4 (U) LEAST SQUARES FIT RESULTS --
Dynamic Pressure Impulse vs. Displacement and Displacement vs. Dynamic Pressure Impulse

CONFIDENTIAL - FORMERLY RESTRICTED DATA

VEHICLE/ ORIENTATION (FIG NO.)	EVENTS INCLUDED	YIELD RANGE (KT)	N	FIT	$S_{\ell n\, I_q}$ ($S_{\ell n\, D}$)	S'_{I_q} (S'_D)	$\sigma_{\ell n\, I_q, C}$ ($\sigma_{\ell n\, D,\, C}$)	$\sigma'_{I_q, C}$ ($\sigma'_{D,\, C}$)	$E_I(\%)$ [$E_D(\%)$]	m (ℓ)	σ_m (σ_ℓ)	$\sigma_{m/m}$ ($\sigma_{\ell/\ell}$)
WWII, SO (2.1)	Koon-3 * Nectar-6 Bee-6 Apple I-8 Wasp Prime-9 Met-12 Apple II-13 Lacrosse-1 Zuni-3 *Yuma-4 Canadian 20T Canadian 100T	0.04≤Y≤3500	44	$I_q = 0.59900^{0.7884}$ $r = 0.9616$	4.711	5.956	0.3349	0.3766	36.79	0.7884	0.03471	0.0440
				$D = 2.2651 I_q^{1.173}$	(7.009)	(9.381)	(0.4085)	(0.4726)	(46.17)	(1.173)	(0.05164)	(0.0440)
M38A1, SO (2.2)	Encore-9 Grable-10 Moth-2 Turk-4 Dice Throw	1.0≤Y≤43.0	20	$I_q = 1.4170^{0.4183}$ $r = 0.9817$	0.4020	0.3798	0.1494	0.1453	13.78	0.4183	0.01912	0.0457
				$D = 0.4657 I_q^{2.304}$	(2.214)	(3.456)	(0.3507)	(0.4382)	(41.57)	(2.304)	(0.1053)	(0.0457)
WWII, FO (2.3)	Koon-3 * Nectar-6 Bee-6 Apple I-8 Wasp Prime-9 Met-12 Apple II-13 Lacrosse-1 Zuni-3	3.16≤Y≤3500	28	$I_q = 1.9100^{0.5737}$ $r = 0.9442$	4.210	4.819	0.4024	0.4305	41.48	0.5737	0.03926	0.06845
				$D = 0.4780 I_q^{1.554}$	(11.40)	(17.25)	(0.6623)	(0.8145)	(78.49)	(1.554)	(0.1064)	(0.06845)

* These events and yields in combination are CONFIDENTIAL-FORMERLY RESTRICTED DATA.

TABLE 2.4 (U) LEAST SQUARES FIT RESULTS --
Dynamic Pressure Impulse vs. Displacement and Displacement vs. Dynamic Pressure Impulse (Concluded)
CONFIDENTIAL - FORMERLY RESTRICTED DATA

VEHICLE/ ORIENTATION (FIG NO.)	EVENTS INCLUDED	YIELD RANGE (KT)	N	FIT	$S_{\ell n\ I_q}$ ($S_{\ell n\ D}$)	S'_{I_q} (S'_D)	$\sigma_{\ell n\ I_q, C}$ ($\sigma_{\ell n\ D,\ C}$)	$\sigma'_{I_q, C}$ ($\sigma'_{D,\ C}$)	$\varepsilon_I(\%)$ [$\varepsilon_D(\%)$]	m (ℓ)	σ_m (σ_ℓ)	$\sigma_{m/m}$ ($\sigma_{\ell/\ell}$)
M38A1, FO (2.4)	Encore-9 Dice Throw	1.0≤Y≤26.0	9	$I_q = 1.9990^{0.3963}$ r = 0.9483	0.2405	0.2052	0.1854	0.1712	15.10	0.3963	0.05012	0.1265
				$D = 0.20611_q^{2.269}$	(1.377)	(2.949)	(0.4436)	(0.6491)	(57.25)	(2.269)	(0.2870)	(0.1265)
REO M35, SO (2.5)	Encore-9 Grable-10 Moth-2 Turk-4 Dice Throw	1.0≤Y≤43.0	19	$I_q = 1.671D^{0.3695}$ r = 0.9699	0.7313	0.6494	0.2074	0.1954	18.49	0.3695	0.02252	0.0610
				$D = 0.2913I_q^{2.546}$	(5.039)	(11.40)	(0.5443)	(0.8191)	(77.48)	(2.546)	(0.1552)	(0.0160)
REO M35, FO (2.6)	Encore-9 Dice Throw	1.0≤Y≤26.0	7	$I_q = 2.6436^{0.4491}$ r = 0.9513	0.1372	0.1592	0.1657	0.1784	15.08	0.4491	0.06509	0.145
				$D = 0.13141_q^{2.015}$	(0.6156)	(0.4150)	(0.3509)	(0.2881)	(24.35)	(2.015)	(0.2921)	(0.145)

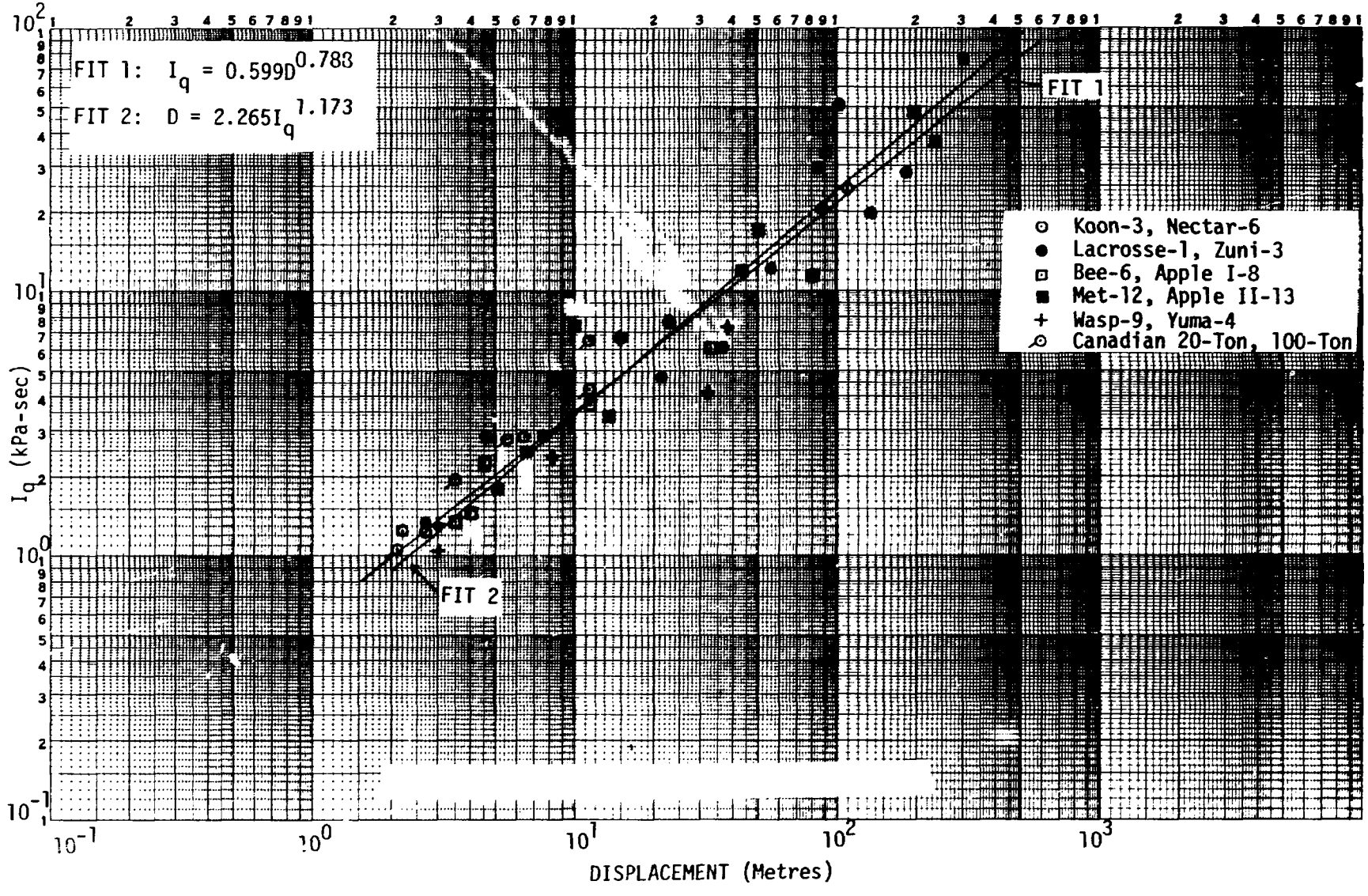

CONFIDENTIAL - FORMERLY RESTRICTED DATA

FIGURE 2.1 (U) Dynamic Pressure Impulse versus Displacement - 1/4 Ton Trucks, WWII, Side-on

CONFIDENTIAL

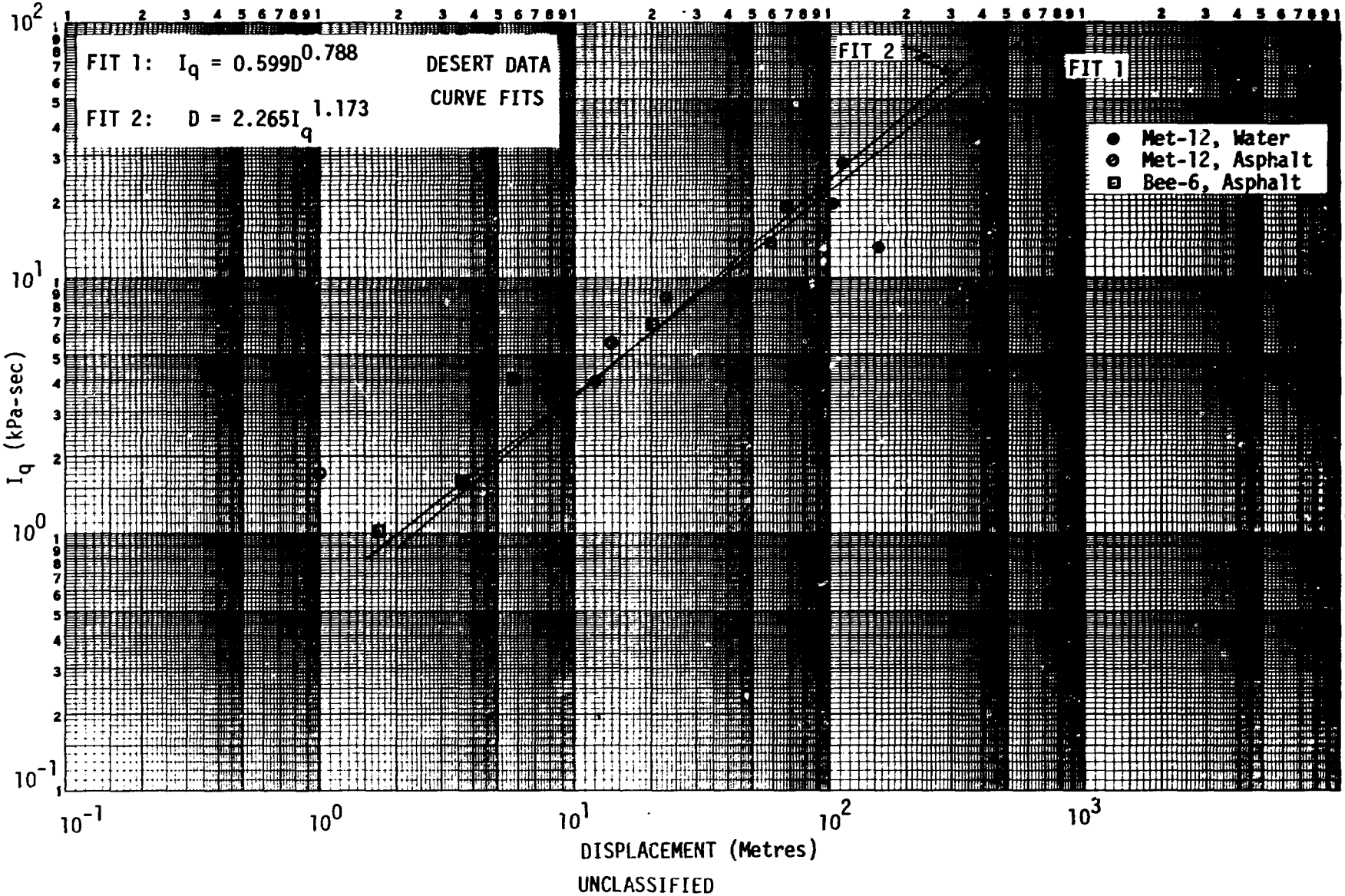

FIGURE 2.1-1 (U) Dynamic Pressure Impulse versus Displacement - 1/4 Ton Trucks, WWII, Side-on, Desert Data Curves, Non-Desert Data Points

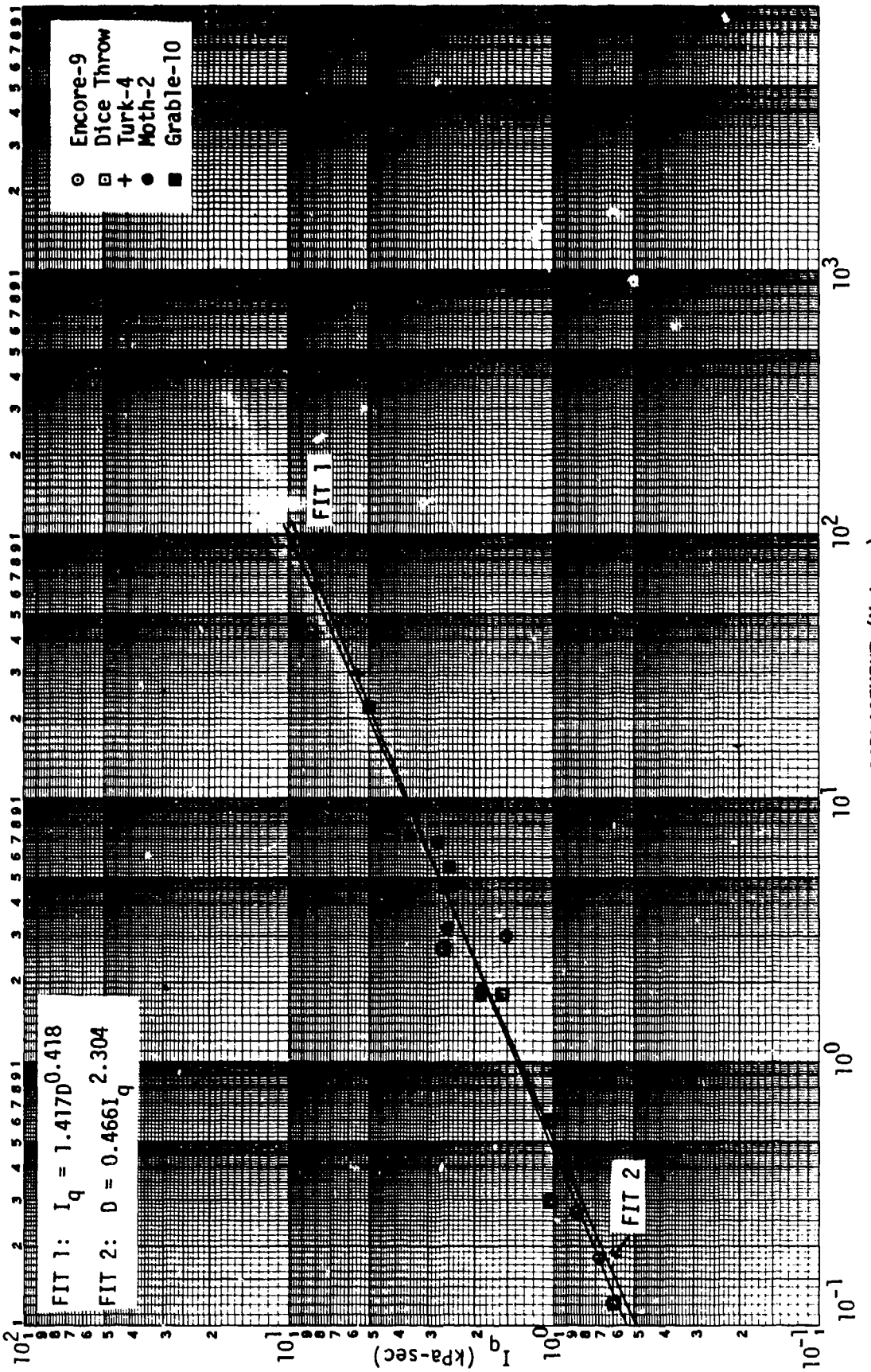

UNCLASSIFIED

FIGURE 2.2 (U) Dynamic Pressure Impulse versus Displacement - 1/4 Ton Truck, M38A1, Side-on

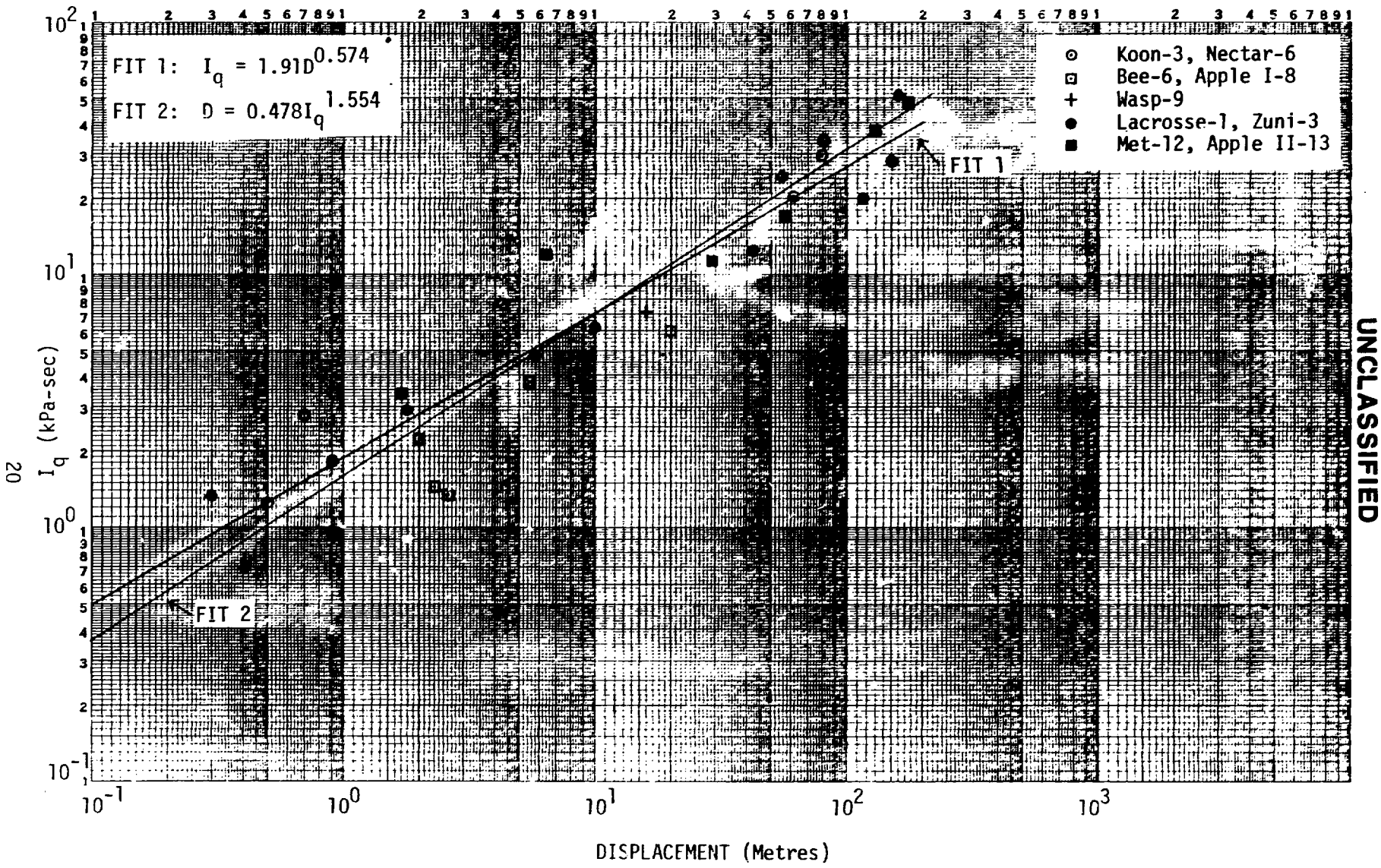

FIGURE 2.3 (U) Dynamic Pressure Impulse versus Displacement - 1/4 Ton Trucks, WWII, Face-on

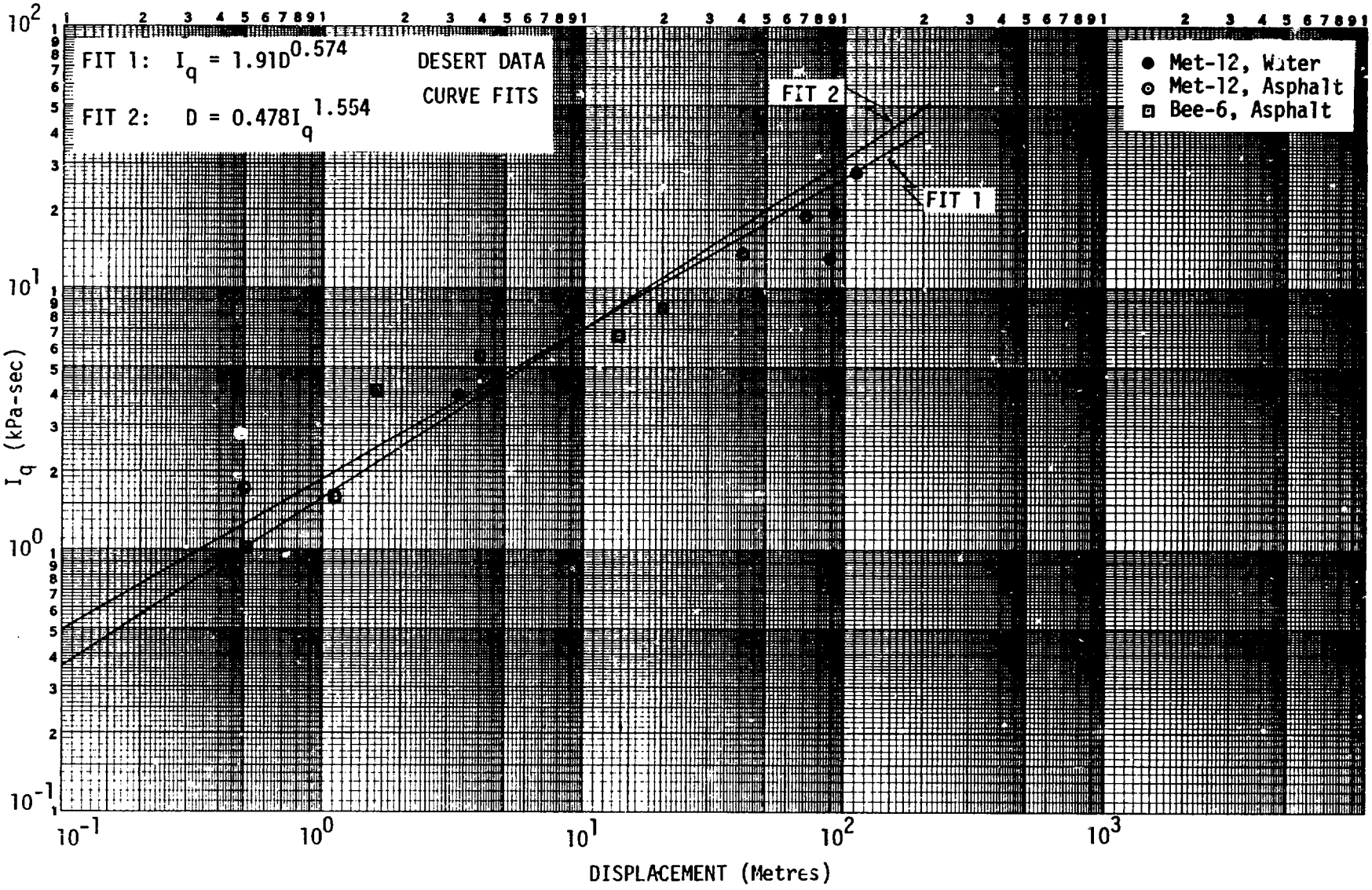

UNCLASSIFIED

FIGURE 2.3-1 (U) Dynamic Pressure Impulse versus Displacement - 1/4 Ton Trucks, WWII, Face-on, Desert Data Curves, Non-Desert Data Points

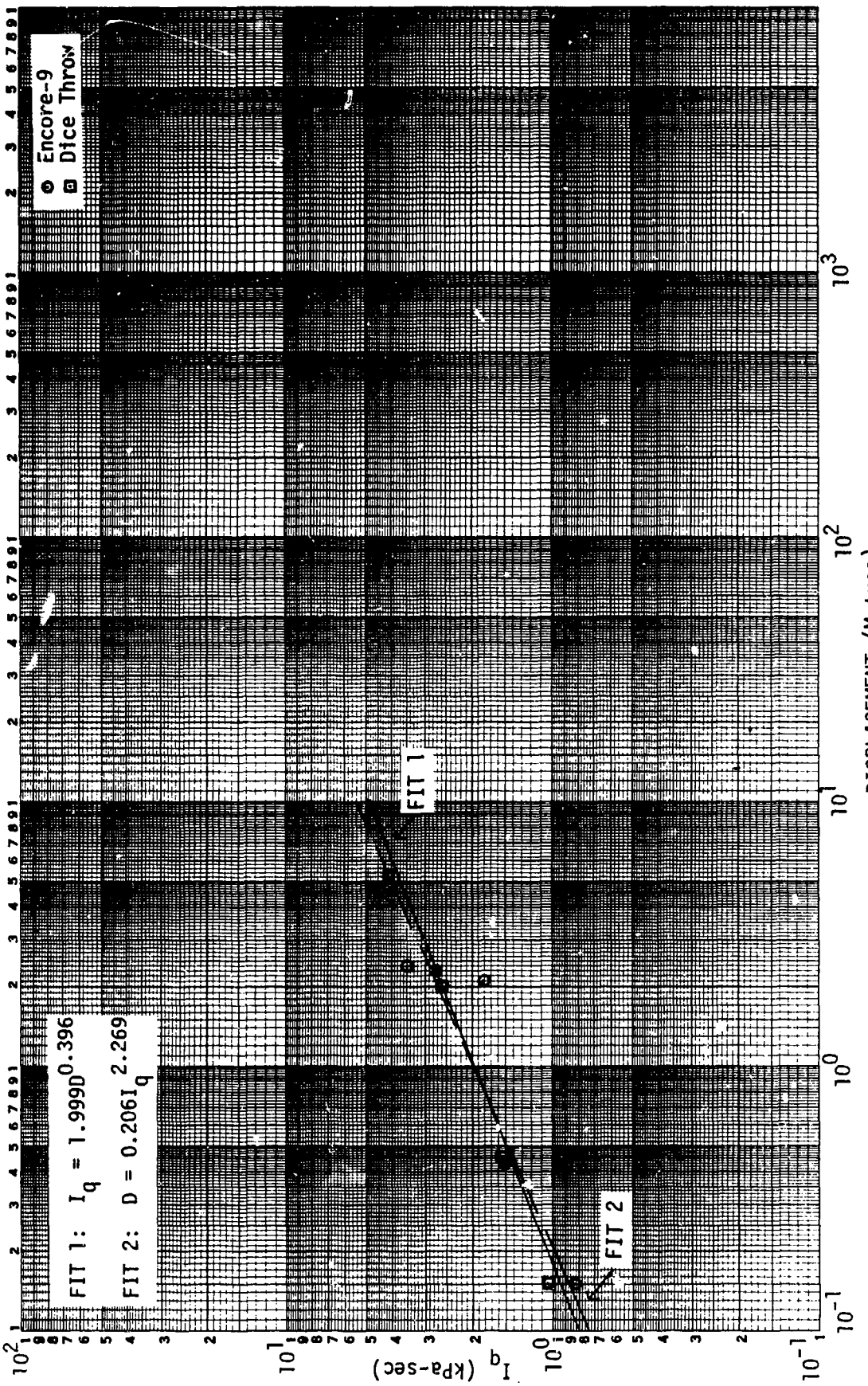

FIGURE 2.4 (U) Dynamic Pressure Impulse versus Displacement - 1/4 Ton Trucks, M38A1, Face-on

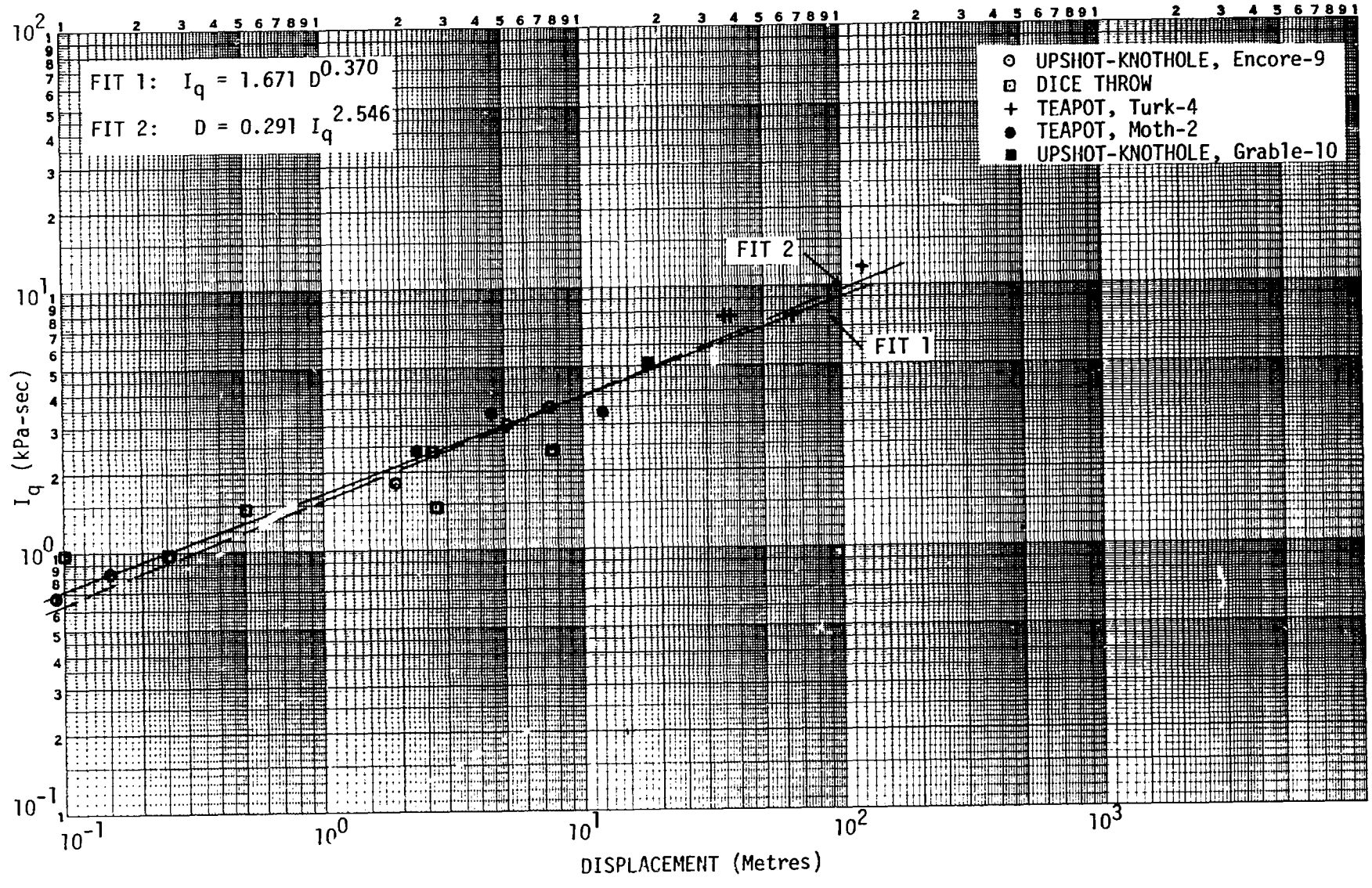

FIGURE 2.5 (U) Dynamic Pressure Impulse versus Displacement - 2-1/2 Ton Truck, REO M35, Side-on

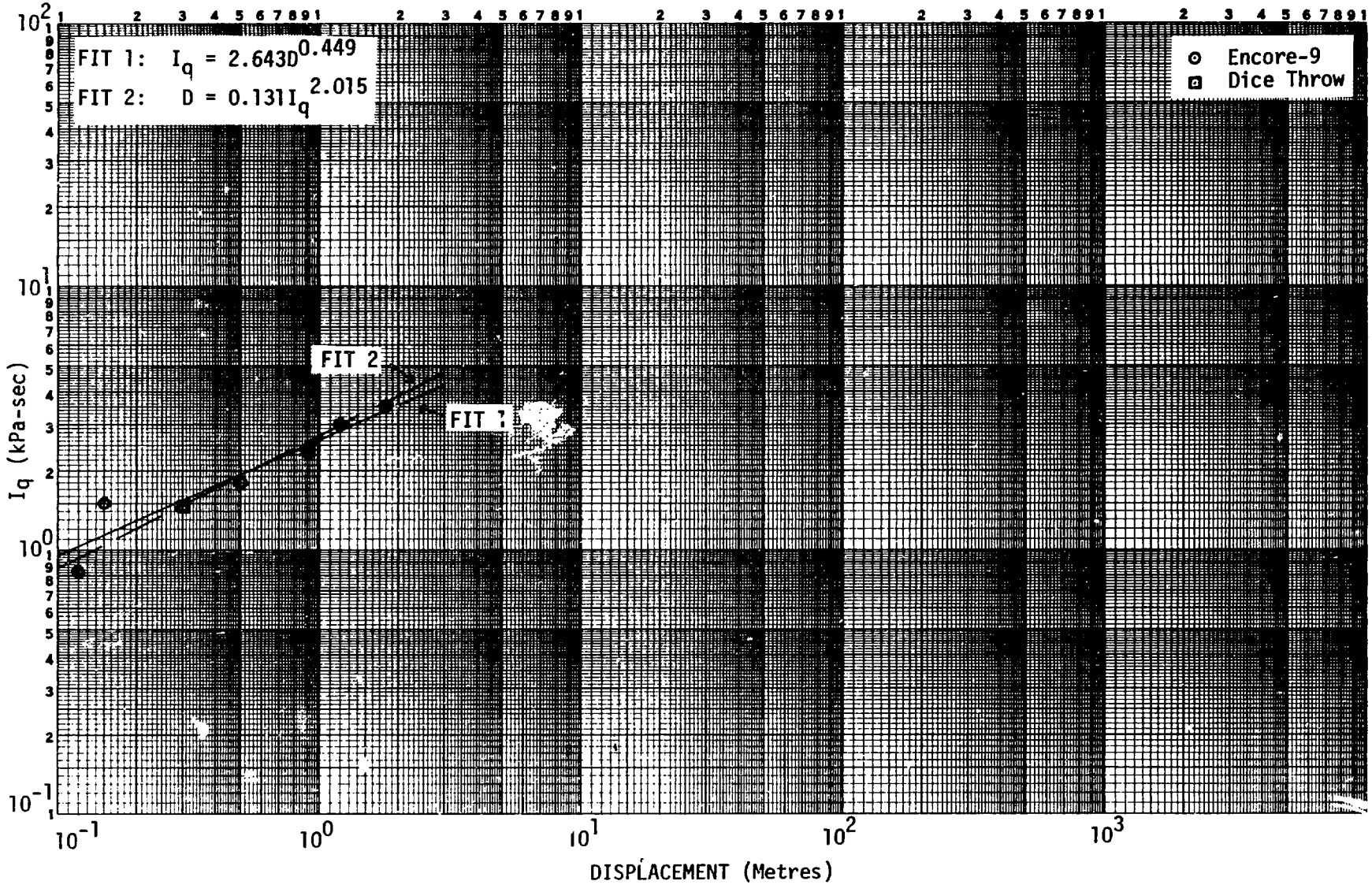

UNCLASSIFIED

FIGURE 2.6 (U) Dynamic Pressure Impulse versus Displacement - 2-1/2 Ton Truck, REO M35, Face-on

UNCLASSIFIED

SECTION 3

(U) RESULTS AND DISCUSSION

3.1 (U) ANALYSIS OF VEHICLE MOTION

3.1.1 (U) Dynamic Pressure Impulse versus Displacement Results

(U) The results for Dynamic Pressure Impulse versus Displacement are given in Figures 2.1 through 2.6 and Table 2.4.

(U) The log-log plots indicate a rather uniform scatter of the data about the straight line fits. The values of r, the coefficient of correlation, are given in the tables. While r is a measure of the goodness of fit of the selected fitting function with respect to the data (see Appendix C, "Least Squares Fitting Procedures"), it appears that better values would not be expected with a different fitting function; the data scatter preclude that.

(U) There is more data for the WWII than for the M38A1 vehicle. The fact that there is more scatter in the WWII data stems from the fact that a largernumber and variety of shots give rise to the data for the WWII. Also for some of the greater displacements, large resultant errors are introduced because of the dismemberment of the vehicles, particularly for the side-on orientations. There is some tendency for points from given shots to be above or below the fitted curve. Since this tendency has superimposed upon it the data point scatter associated with each shot, the total scatter is greater than for the M38A1 vehicle. Thus, for the WWII, side-on plot, Figure 2.1, the data corresponding to shots Koon-3, Nectar-6, Canadian 20-Ton and 100-Ton have somewhat smaller displacements for a given value of I_q than the curve fit while data from shots Wasp Prime-9, Yuma-4, Bee-6 and Apple I-8 have somewhat higher displacements. Similarly for the WWII, face-on plot, Figure 2.3, (except that here no Canadian 20-Ton and 100-Ton points are shown — see next paragraph). Thus, a small HOB effect is present in the data. The data points for the M38A1, with very limited shot variety, result in a rather uniform scatter of the data for individual shots about the curve fit as best we can judge this from the small number of data points.

3.1.1.1 (U) Effect of Diffraction

In the side-on orientation both vehicles usually turned over, thus causing displacements, as measured — before and after position of vehicle center of mass — to be larger for side-on than for face-on orienta-

tion, except possibly for very large displacements where they appear to be equal for the WWII vehicle. In the face-on orientation the vehicle turned over infrequently in the case of the WWII and not at all for the M38A1. A few points corresponding to low yield shots are not shown on the plots nor are they included in the curve fits. These show the effects of diffraction. Data for very low yield shots (10 tons) exhibit much higher values of displacement for small values of dynamic pressure impulse than the plotted data. This is because the blast wave is so short that the vehicle received almost all of the dynamic pressure impulse on its struck side while also subjected to a "static" overpressure before any significant counterpressure has affected the opposite side. In the face-on data this effect is evident also for the Canadian 20-Ton, 100-Ton and Yuma-4 (fractional KT, see Table 2.1) shots. The effect for these shots is not evident in the side-on data. We believe the reason for this is that in the side-on case vehicle turnover caused comparable displacements for low values of I_q for the higher yield shots, thus concealing the diffraction effect.

3.1.1.2 (U) Partial Interpretation of Results

(U) When a vehicle is struck by a blast wave, it will acquire a velocity proportional to the impulse received (if we ignore the effect of the motion-resisting force during the time of delivery of the impulse). Therefore, we expected to find a good correlation between displacement and I_q. In later discussion we will note that damage correlates with displacement wehreas in a wide variety of studies involving blast damage to equipment, damage seems to depend upon both pressure and impulse. We, therefore, made plots of displacement versus each of the other blast field variables, namely, overpressure, dynamic pressure, and overpressure impulse. As expected, we found in each case a very large point scatter about a trend in which displacement increases with increases in any of the blast field variables. We interpret this as follows: displacement is causally dependent upon I_q; correlation between displacement and the other blast field variables (with very large scatter) is accidental, existing only because these variables have a tendency (in the data base) to have high values when I_q has a high value (and low values when I_q has a low value).

(U) Upon analysis of the results for the two vehicles and two orientations we find that: for fairly small values of I_q turnover occurs in the side-on orientation, but not in the face-on, causing measured displacements to be larger side-on; in the data base there are no large displacements

for the M38A1, especially face-on, nor small displacements for the WWII, especially side-on; over most of the range of significant overlap of the data the disparity between side-on and face-on displacements (for a given value of I_q) is about the same for each vehicle. However, the WWII vehicles were exposed to higher values of I_q than the M38A1's and consequently suffered larger displacements. For large values of I_q (and hence displacement) the side-on and face-on displacements are close in value. This is because turnover of the vehicles (in both orientations) takes place, almost certainly, early during the blast pulse. This tends to randomize vehicle orientation, thus making the blast force on the vehicle over the remainder of the blast wave and the effective resisting force over almost all of the trajectory approximately the same for the two (initial) orientations. (We expect that this would be true for any initial orientation.)

3.1.2 (U) Calculations of Vehicle Motion

3.1.2.1 (U) Translational and Rotational Velocities

(U) We made several calculations based on vehicle characteristics in order to explain the observations and differences between the responses of the two vehicles. Most of the vehicle characteristics we require are given in Reference 2. These are given in the following table along with our estimates of the area, A, presented to the blast by each vehicle (based on overall sketches, not detailed drawings of the vehicle), and our calculation of the amount of inertia about the overturning axis for the side-on orientation, I_{OT}, (obtained by use of the parallel axis theorem and the listed values of the moment, I_{CM}, about the center of mass).

VEHICLE/ ORIENTATION	HEIGHT OF CM (cm)	HALF WIDTH OF VEHICLE (cm)	MASS OF VEHICLE, M (gms)	I_{CM} (gm cm^2)	I_{OT} (gm cm^2)	A (cm^2)	μ, COEFF. OF FRICTION
WWII, SO	64	70.2	1.09×10^6	2.54×10^9	1.25×10^{10}	2.8×10^4	0.70
WWII, FO	64		1.09×10^6			1.4×10^4	0.25
M38A1, SO	67.6	71.6	1.19×10^6	3.00×10^9	1.46×10^{10}	3.0×10^4	0.70
M38A1, FO	67.6		1.19×10^6			1.5×10^4	0.25

(U) The listed characteristics indicate that only small differences are to be expected between the responses of the two vehicles. For example, the M38A1 has a slightly larger mass and overturning moment about the center of mass than the WWII: but it also has a slightly larger area presented

to the blast direction and a slightly larger overturning moment arm. Therefore, the differences in the two vehicles tend to cancel one another both for translational and rotational response.

(U) Using the above data we first performed a few very simple calculations applicable to both vehicles.

(1) Taking I_q = 80 kPa-sec = 8 x 10^5 dyne sec/cm^2 we find, using

$MV_o = I_qA$ where M = vehicle mass and V_o = initial velocity

$$V_o \cong 2 \times 10^4 \text{ cm/sec} \cong 450 \text{ miles/hour.}$$

(This is for a side-on orientation.) In the experiments subjection of the vehicles to blast with I_q considerably less than 80 kPa-sec caused the vehicles to be demolished, as would be expected with such a value of the (calculated) initial velocity.

(2) Taking I_q = 10 kPa-sec, we obtain

$$V_o \cong 2.5 \times 10^3 \text{ cm/sec} \cong 57 \text{ miles/hour.}$$

If we assume that most of this impulse is delivered in 0.1 sec, the vehicle acceleration will be 2.5 x 10^4 cm/sec^2 and it will travel a distance of 1.3 metres.

(U) In general, such calculations show that displacement of the vehicle during the intense part of the blast wave is fairly small compared with the measured displacement of the vehicle.

(3) The average force acting on the vehicle during delivery of the impulse in (2) is:

$$\frac{10^5 \text{ dyne sec/cm}^2}{0.1 \text{ sec}} \times 3 \times 10^4 \text{ cm}^2 = 3 \times 10^{10} \text{ dynes}$$

This is much larger than the force of friction, which is

$$F_{fric} \cong 1.1 \times 10^6 \text{ gms} \times 980 \text{ dynes/gm} \times 0.7$$
$$\cong 7.8 \times 10^8 \text{ dynes.}$$

(4) If we take I_q = 1 kPa-sec delivered in 0.1 sec, the average force on the vehicle is 3 x 10^9 dynes which is still considerably larger than the opposing frictional force. Thus even for the smallest blast impulses in the experiments the force exerted by the blast wave on the vehicle is greater than the opposing frictional force. (For the face-on orientation the vehicle area is only about one-half as large but the coefficient of friction is only

slightly over one-third as large as in the side-on case, so the statement is true in both vehicle orientations.)

(5) We made similar calculations for overturning. Here we assumed that the effective moment arm for the force on the vehicle due to the blast is the height of the center of mass. Then with I_q = 10 kPa-sec, time of impulse delivery 0.1 sec, we find the angular acceleration, α, to be

$$\alpha \cong 150 \text{ radians/sec}^2$$

After 0.1 sec, the angular velocity, ω, is

$$\omega \cong 15 \text{ rad/sec} \cong 2.4 \text{ revolutions/sec}$$

and the angular displacement, θ, is

$$\theta = 1/2\ \alpha t^2 = 0.76 \text{ radian} \cong 43°.$$

Here we have ignored the torque owing to gravity, T_G, tending to prevent overturning. Again using the tabular data, we find

$$T_G \cong 1.1 \times 10^6 \text{ gms} \times 980 \text{ dynes/gm} \times 70 \text{ cm}$$
$$\cong 7.5 \times 10^{10} \text{ dyne cm}$$

The torque applied by the blast wave is [see (3) above].

$$3 \times 10^{10} \text{ dynes} \times 70 \text{ cm} \cong 2 \times 10^{12} \text{ dyne cm},$$

which is much larger than T_G.

(U) In general, the angular displacement during the blast pulse is much smaller than the angular displacement well after the pulse (as measured wherever the vehicle is found overturned) just as was found true for linear displacement; when the bulk of the blast impulse is received over a substantially larger time period, 0.5 seconds, for example, the linear and angular displacements during the pulse time become quite significant.

(6) From the calculation in (5) we see that for I_q = 10 kPa-sec the vehicle certainly overturns (side-on); for I_q = a few kPa-sec, it certainly overturns but for $I_q \sim 1$ kPa-sec it appears marginal and we cannot draw any conclusions from such a calculation. This is because as the vehicle starts to rotate a larger area is exposed to the blast wave and the effective moment arm also increases. Also, the moment arm associated with the force of gravity decreases and when the vehicle has rotated approximately 45°, the torque due to gravity reverses direction and helps to overturn the vehicle. With I_q = 1 kPa-sec, delivery time 0.1 sec, the angular displacement at 0.1 sec is

4.3° and the angular velocity is 86° per second, with the restoring torque owing to gravity rapidly diminishing.

(U) In the experiments, vehicles exposed side-on to a dynamic pressure impulse ~ 1 kPa-sec sometimes overturned and sometimes did not.

(U) The above simple calculations are applicable to both the WWII and the M38A1 vehicles, there being very little difference between the two.

3.1.2.2 (U) Models of Vehicle Motion

(U) Since the I_q versus displacement data fits for the two vehicles appear to be somewhat different and only partially accounted for in the previous discussion we attempted a further calculation. The forces we should expect to act on the vehicle during its motion, other than the blast force, are: a frictional force — during the part of the motion in which the vehicle is sliding over (or gouging) the earth; an air drag force which at least in the later stages of the motion would resemble the usual type of air drag — vehicle penetrating and imparting some of its momentum to the air in its path. Earlier in the motion when the long tail of the blast wave involves air going past the vehicle this would not seem to apply and as time progresses the air density in front of the vehicle will vary considerably as the air refills the region partially emptied of air by the blast. The I_q versus displacement plots contain data from a considerable variety of shots; the air density in front of the vehicle depends not only on the vehicle's (instantaneous) position but also on the weapon yield, height of burst, and ambient conditions. Notwithstanding these difficulties we attempted to write a (composite) "equation of motion" for a vehicle and determine an effective resistive force in agreement with the displacement versus I_q curve (for each vehicle, in each orientation).

(U) We assume the vehicle responds truly impulsively to the blast wave; that is, the blast wave imparts a velocity to the vehicle but the vehicle moves only negligibly during the blast wave. We also assume that during this time the force resisting vehicle motion is negligible. While somewhat idealized, these assumptions are in general agreement with the simple calculations already presented. We further assume that the resisting force (after the dynamic pressure impulse has been received) is, on the average, a function only of the vehicle's instantaneous velocity, i.e., we ignore fluc-

tuations associated with the vehicle's orientation (relative to both its direction of motion and the ground). This appears reasonable from one standpoint: the vehicle's instantaneous velocity is seemingly the only continuous variable during the motion to which the effective resistive force can be related. Then with M, V, A representing the vehicle's mass, velocity, and initial projected area on the blast direction, we have

$$M\frac{dV}{dt} = M\frac{dV}{dx}\frac{dx}{dt} = MV\frac{dV}{dx} = -F(V) = -\frac{V}{g(v)} \qquad (1)$$

where the resisting force or equivalently $\frac{g(V)}{V}$ is a function to be determined. Then

$$-\int_{V_o}^{o} g(V)dV = \int_{o}^{D}\frac{dx}{M} \qquad \text{where D = displacement (at end of motion)} \qquad (2)$$

But $D = CI_q^{\ell}$ from our curve fits* (3)

and $MV_o = I_qA$ (4)

---

* Here ℓ is dimensionless since

$$\ell n\ D = \ell n\ C + \ell\ \ell n\ I_q$$

so that $$\ell = \frac{d(\ell n\ D)}{d(\ell n\ I_q)} = \frac{dD/D}{dI_q/I_q} .$$

In CGS units, C has dimensions:

$$[C] = [cm]^{\ell + 1}\ [gm]^{-\ell}\ [sec]^{\ell} .$$

To obtain the values of C for the two vehicles/orientations from the fits listed in Table 2.4, where the fits are of the form $D = AI_q^{\ell}$ with D in metres and I_q in kPa-sec, we have

$$C = \frac{100A}{(10^4)^{\ell}}$$

since 1m = 100cm and 1 kPa-sec = $10^4\ \frac{\text{dynes sec}}{\text{cm}^2}$.

where V_o is the vehicle's velocity immediately after receipt of impulse I_q.

So $$D = C\left(\frac{M}{A} V_o\right)^{\ell} . \tag{5}$$

Differentiating the integral with respect to its lower limit, V_o, and substituting this relation for D on the right hand side yields:

$$-\frac{d}{dV_o} \int_{V_o}^{o} g(V)dV = \frac{d}{dV_o} \left[\int_o^D \frac{dx}{M}\right] = \frac{d}{dV_o} \left[\frac{x}{M} \Big|_o^D\right] = \frac{d}{dV_o} \left(\frac{D}{M}\right) \tag{6}$$

Thus $$g(V_o) = \frac{d}{dV_o} \left[\frac{1}{M} C\left(\frac{M}{A} V_o\right)^{\ell}\right] = \frac{C}{M} \left(\frac{M}{A}\right)^{\ell} \ell V_o^{\ell-1} . \tag{7}$$

So $$g(V) = \frac{C}{M} \left(\frac{M}{A}\right)^{\ell} \ell V^{\ell-1} \tag{8}$$

and the resisting force is given by the right hand side of the equation

$$M\frac{dV}{dt} = -\frac{V}{g(V)} = - V \frac{M}{C} \left(\frac{A}{M}\right)^{\ell} \frac{1}{\ell} V^{1-\ell} \tag{9}$$

Finally, $$M\frac{dV}{dt} = MV\frac{dV}{dx} = - \frac{M}{C\ell} \left(\frac{A}{M}\right)^{\ell} V^{2-\ell} \tag{10}$$

(U) Comparison of the resistive force, r.h.s. of Equation (10), which contains $V^{2-\ell}$ with the values of ℓ given in Table 2.4, we see that the velocity dependence of the effective resistive force varies greatly and that $2-\ell$, the exponent of V, can be either positive or negative to accord with the data fits. Thus for low values of V, the resistive force approaches zero for $2-\ell$ positive, infinity for $2-\ell$ negative, neither of which is physically realistic. This sort of occurrence can perhaps be expected with empirical data fits; it does not mean that the effective resistive force derived is necessarily invalid over substantial portions of the vehicle's motion. With the resistive force derived we can calculate velocity and displacement of the vehicle as a function of time by integrating the "equation of motion". However, we have no physical interpretation for the derived resistive force so we have only used it as a partial check on physically motivated models.

(U) The displacement versus dynamic pressure impulse curve fits contain several phenomena. For small enough values of I_q the vehicles will slide across the ground opposed by a conventional frictional force. This occurred for both vehicles in the face-on orientation and for the M38A1 side-on.

The WWII in side-on orientation was not exposed to blasts with such small values of I_q. For larger values of I_q vehicle turnover occurs quite readily in the side-on orientation, less readily face-on. The M38A1 was not exposed to any blasts with sufficiently high I_q for turnover face-on. As I_q is raised and the vehicle initial velocity increases air drag can become important, at least in the later phases of the motion when the vehicle pushes air which has moved back in toward ground zero. At sufficiently high values of I_q the vehicle can be partly or completely lifted off the ground, so that there is no ground friction term. If there is no air drag term either, the vehicle is in free flight, probably tumbling in some fashion, but is eventually pulled down and strikes the earth. Thus sliding, rolling, bouncing across the ground along with gouging of the ground all can take place at one or another time during the motion. This, along with the variety of weapon yields, burst heights, ground ranges, and ambient conditions, is the reason that the best that can be hoped for is a "composite equation of motion".

(U) With these considerations in mind we consider two cases: (1) low values of I_q such that only sliding takes place; (2) higher values where the other mentioned phenomena also take place in which we include a constant frictional resistance along with a conventional type air drag resistance. There are clearly some portions of the motion for which these assumptions are inadequate. Consider first the case of small dynamic pressure impulse so that only ground friction is important. We take the equation of motion to be (it is a legitimate equation for this very restricted case):

$$M\frac{dV}{dt} = MV\frac{dV}{dx} = -K \quad \text{where K is the constant} \qquad (11)$$

frictional resisting force. Integrating this equation yields

$$D = MV_o^2/2K \quad . \qquad (12)$$

The coefficient of friction, μ, is then

$$\mu = K/Mg \quad . \qquad (13)$$

For the M38A1 in side-on orientation, we have for $I_q = 1$, D = 46.6 cm; with values of $I_q \leq 1$ kPa-sec, the M38A1 did not turn over.

(U) Using the tabulated data of vehicle characteristics (A and M values) we then obtain

$$\mu = 0.71$$

Such good agreement with the measured value of 0.7 is probably fortuitous. (In fact over the range of the data $0.597 \leq I_q \leq 1.04$ kPa-sec where vehicle turnover does not play a role, such calculations provide values of μ between 0.68 and 0.83.)

(U) For higher values of I_q we include air drag in a "composite equation of motion" in order to check the result against experiment. Our starting equation is then:

$$M\frac{dV}{dt} = MV\frac{dV}{dx} = -(K_1 + K_2V^2), \quad \text{which upon integration and a} \qquad (14)$$

little simplification yields

$$D = \frac{M}{2K_2}\, \ell n\, (1 + \frac{K_2}{K_1} V_o^2) \quad . \qquad (15)$$

Since $MV_o = I_qA$, Equation (4), we can simply take two values of I_q in the desired range, calculate V_o and find D from our curve fits, then use Equation (15) to determine K_1 and K_2. However, the results are quite sensitive to the choices of I_q values. We found, however, that by fitting the data (for a given vehicle/orientation) over a limited range to the expression for D (somewhat crudely — we have no convenient least squares program for such a functional dependence) we can obtain reasonable results. [That this expression for D cannot fit the data over a large range is clear since it is incompatible with the fit $D = AI_q^{\ell}$; the latter fit corresponds to the resistive force previously derived, $F(V) = \frac{M}{C\ell}\,(\frac{A}{M})^{\ell}\, V^{2-\ell}$. Equation (10).]

(U) We note that for small V_o, i.e., small I_q, according to Equation (15),

$$D \rightarrow \frac{M}{2K_2}\, \frac{K_2}{K_1}\, V_o^{\,2} = \frac{M}{2K_1} V_o^{\,2} \ ,$$

the same result achieved with no air drag. For large V_o,

$$D \rightarrow \frac{M}{2K_2}\, \ell n\, (\frac{K_2}{K_1} V_o^{\,2}) \ \ \alpha\ 2\ \ell n\ V_o$$

or D becomes proportional to $\ell n\ I_q$. So Equation (15) can only be fitted to very limited ranges of data.

(U) We fitted Equation (15) to data over a limited region for a few cases. Taking the WWII vehicle, face-on, over the region $1 \leq I_q \leq 8$ kPa-sec we determined reasonable values of K_1 and K_2 [such that Equation (15)

predicts displacement to within 15%]:

$$K_1 = 2.35 \times 10^8$$

$$K_2 = 850$$

Then $$\mu = \frac{K_1}{Mg} = 0.22$$

which is in reasonable agreement with the measured value, $\mu = 0.25$.

(U) Computing $K_2V_o^2$ we find that for $I_q = 8$, K_2V^2, the air drag term in the (composite) model, is almost 4 times as great as the frictional term (initially). For $I_q = 1$, $K_2V_o^2 << K_1$ so that here the air drag term is negligible throughout the motion.

(U) We also used Equation (15) for the M38A1, face-on, over the range $1 \leq I_q \leq 4$ kPa-sec (about the range of the data for this case). Following the same procedure we obtained a value for the coefficient of friction $\mu = 0.30$ which is to be compared with the experimental value 0.25. In these cases there were no vehicle turnovers.

(U) Finally we used Equation (15) for the WWII, side-on, over the range $1 \leq I_q \leq 8$. We obtained the result $\mu = 0.15$.

(U) This is much smaller than the measured value of 0.70, corresponding to the fact that all of the vehicles turned over, almost all 180°; thus the vehicles rolled, bounced, and may have partially or completely lost ground contact for part of the motion. Thus the measured coefficient of friction is much greater than the physically effective value.

(U) Again, calculating $K_2V_o^2$ we find that for $I_q = 1$ the air drag force is (initially) a little less than one-half the frictional force while for $I_q = 8$ the force attributed to air drag in this model is initially 27 times as large as the frictional force — clearly an important effective force over a significant portion of the vehicle motion, even if not a conventional air drag force.

(U) Finally, each of the "composite equations of motion", Equations (10), (11), and (14), can be integrated enabling us to obtain vehicle velocity and displacement as functions of time. (However, we have no experimental data with which to compare such model-predicted values.) In general, we find that the vehicle motion takes place over a time period ~ one to a few seconds. Thus in most cases, all three models predict that vehicle motion persists considerably longer than the intense portion of the

blast wave, but in some cases not longer, or not much longer, than the positive phase duration. Therefore, in some cases the air drag in our model corresponds at least roughly to a conventional air drag term (with varying air density) while in other cases it may bear little resemblance to a conventional air drag force.

(U) In sum, the various calculations described provide some insight into the meaning of the displacement versus I_q curves. Further, they indicate that differences in results for the two vehicles are not explained to any significant degree by differences in the physical characteristics of the WWII and M38A1 vehicles.

3.1.2.3 (U) Surface Effects and Explanation of Remaining Discrepancies Between Results for the WWII and M38A1 Vehicles

(U) Most of the differences in results for the two 1/4 ton trucks have already been explained, the causes for the differences being: exposure to different ranges of I_q values; relatively small regions of overlap of the data for the two vehicles compared with the total data range for each vehicle; fairly large scatter of the data points, especially for the WWII vehicle, this in turn being caused by the variety of shots which give rise to the data for this vehicle — there being a small, but not completely negligible height of burst effect present in the data. We note that the curve fits, good straight lines on the log-log plots over the range of data for each vehicle/orientation, would not necessarily be well represented by such straight lines if the data extended over a larger range — as it does when we combine the data for the two vehicles, which it now seems reasonable to do since differences in the data for the two vehicles appear to result from causes other than differences in the physical characteristics of the two vehicles.

(U) The previously described calculations and data comparisons led us to look carefully at the displacement versus I_q data for the two vehicles in the region of overlap of the respective data ranges (in each orientation) and to associate the vehicle overturn data with the results while making the comparisons. For the two vehicles in face-on orientation no vehicle overturns occur in the region of overlap of the data. In this region there are only a few data points for each vehicle, 10 for the WWII and 7 for the M38A1. There is considerable scatter. The combination of few data points and large scatter causes considerable difference in least squares fits to the data for the two vehicles in their common region.

However, the data for the two vehicles appear to be quite compatible in this region; there certainly is no large difference. (The overlap region only spans $1.3 \leq I_q \leq 4$ kPa-sec.)

(U) In side-on orientation there are many more data points for each of the vehicles in the region of overlap of the data. The range of overlap is $1 \leq I_q \leq 8$ kPa-sec. The slopes of curves for the two vehicles in this region are quite different. However, the only significant difference in the data sets lies in the region $1 \leq I_q \leq 3$ kPa-sec. Now as we have seen $I_q \sim 1$ kPa-sec is marginal for vehicle turnover. The WWII vehicle was not exposed to any blasts with $I_q < 1$. The M38A1 data contain 5 points with $I_q \leq 1.04$; in 4 of these cases the vehicle did not turn over. The 5th instance, $I_q = 1.04$, D = 0.3m appears peculiar in that a 90° turnover occurred — and a 90° turnover results in a measured displacement of about 1.4m. In most cases examination of our data shows, for small and moderate displacements, that the displacement associated with turnover (90° or 180°) accounts for a large part of the measured displacement, the latter almost always being somewhat larger than the turnover-caused fraction of the measured displacement. (This statement applies to side-on orientation; there were no turnovers face-on with only small or moderate displacement; when a very large displacement occurs, in either orientation, the vehicle may turn over 360° or more which is not evident in our data — or it may be demolished, which is evident.)

(U) In tracing back the difference in responses of the two vehicles in the region $1 \leq I_q \leq 3$ kPa-sec, we found first that the M38A1 turned over 90° whereas when the WWII turned over it was turned 180°. There were a couple of instances with $I_q \sim 3$ kPa-sec in which the WWII vehicle did not turn over; each occurred with a low yield shot so that, because of the diffraction effect previously described, the displacement was considerably larger than occurs for a similar I_q value associated with a higher yield shot (longer blast wave). A 180° overturn causes twice the displacement as a 90° overturn and, since most of the measured displacement is caused by overturning, the WWII exhibited larger displacements in the region $1 \leq I_q \leq 3$ kPa-sec than the M38A1 in all cases (owing either to 180° overturn, as opposed to 90° for the M38A1, or to a low yield diffraction effect). Upon further inquiry we found that the WWII vehicle had been exposed to the blast while standing on loose soil while the M38A1 stood on firm ground. We believe this accounts for the 180° WWII overturns compared with the 90° M38A1 overturns for the following

reason. As the vehicle starts to slide (and rotate simultaneously) the loose dirt will be pushed ahead of the tires. When the vehicle has rotated 90° the top of the side of the vehicle farthest from ground zero strikes loose dirt pushing it in somewhat. Thus the vehicle actually rotates somewhat more than 90° in a single overturn, the tires elevated a little with a pile of displaced loose dirt under them and the top of the vehicle side farthest from ground zero depressed a little. This makes it easier for the vehicle to overturn again than if it were lying horizontal. Therefore, over a small range of I_q just above $I_q \sim 1$ kPa-sec, we should expect the WWII, placed on loose dirt, to be likely to overturn 180° while the M38A1, placed on firm soil, is likely to overturn only 90°.

(U) This explanation, qualitatively, appears capable of accounting for the only as yet unexplained difference in the data for the two 1/4 ton trucks. We also note in this connection that the results for the 2-1/2 ton trucks, Figures 2.5 and 2.6, and Table 2.4 are very similar to those for the M38A1 1/4 ton trucks. The 2-1/2 ton trucks also stood on firm soil.

(U) As we noted in a previous section, the displacement versus I_q plots and fits are based on gage-derived I_q values for both near-ideal and non-ideal shots. As discussed elsewhere in this report we have been able to improve upon the I_q estimates for non-ideal shots by use of displacement data (the vehicle in essence playing the role of a gage, after being properly calibrated). If we were to use the best I_q estimates we have obtained for plots of displacement versus I_q we would find not only a rather modest improvement but also that the discrepancy between data for the two vehicles is somewhat diminished where the data scatter is large. This tends to corroborate the finding that there is no significant difference between the two vehicles and that our explanation of the differences in the response data is correct.

(U) Finally, since we have found that the differences in data for the two vehicles are due to factors other than differences in the physical characteristics of the two vehicles, it is meaningful to combine the data for the two 1/4 ton trucks, in each orientation, and to obtain curve fits for the combined data.

3.1.2.4 (U) Final Dynamic Pressure Impulse versus Displacement Least Squares Fits

(U) We combined data for the two 1/4 ton trucks and obtained

fits for I_q versus displacement and displacement versus I_q as shown in Figures 3.1 and 3.2. When the data are combined the ranges of displacement and I_q (in each orientation) are greater than for either vehicle alone and a straight line log-log fit is not as good as a quadratic; there is a significant curvature. The statistical measures associated with the fits are given in Table 3.1.

(U) We likewise combined the data for the 2-1/2 ton trucks, REO M35 and GMC M135. There is insufficient data for a side-on fit for the GMC M135 and no face-on data for this vehicle. Therefore, we obtained data fits for the REO M35, side-on and face-on, and a combined fit to the side-on for the two vehicles. (The few data points for the GMC M135 do appear to have slightly higher I_q values for a given displacement than is the case for the REO M35.)

(U) We obtained both linear (log-log) and quadratic fits to the combined data; the latter is the better and is shown in Figure 3.3. The results are shown in Table 3.1. The results for REO M35 alone, side-on and face-on, are given in Figures 2.5 and 2.6 and Table 2.4.

(U) For the combined displacement-I_q fits for the two 1/4 ton trucks, and for all of the displacement-I_q fits for the 2-1/2 ton trucks, we used the iterated (improved) I_q values previously discussed for the non-ideal shots.

3.2 (U) DISPLACEMENT VERSUS SCALED GROUND RANGE. Results are given in Figures 3.4 through 3.11 and Table 3.2.

3.2.1 (U) Scaling

(U) Scaling ground ranges used here and elsewhere in this report are given by

$$x = S_d R \qquad \text{(Modified Sachs scaling)} \tag{16a}$$

or by

$$x = S'_d R \quad . \tag{16b}$$

Here

$$S_d = \left(\frac{P_o}{14.7}\right)^{1/3} \frac{1}{W^{1/3}} \tag{17a}$$

and

$$S'_d = \left(\frac{P_o}{14.7}\right)^{1/3} \frac{1}{W^n} \tag{17b}$$

where P_o = ambient pressure,
n = a number used in the assumed scaling law, and
W = weapon yield (KT).

(U) We tried several values of n (in addition to 1/3) for each subcase: n = 0.37, 0.4, and 0.43, and in some instances, additional values of n. In most of the subcases in this section the optimum value of n was found to be near 0.4

(U) In general, the data have a rather large scatter (since there are many uncontrolled variables involved). Thus fairly large errors can be expected in inferring displacement from scaled ground range. (See Table 3.2.)

(U) We also attempted to determine "scaled displacement versus scaled ground range" (analagous to "scaled impulse vs. scaled ground range", Section 3.3). To do this we proceeded as follows. For the scaled impulse case we have

$$S_i I_q = f(S_d R) \tag{18}$$

where $$S_i = \left[\frac{T_o\ (°C) + 273}{288}\right]^{1/2} \left(\frac{14.7}{P_o}\right)^{2/3} \frac{1}{W^{1/3}} \tag{19}$$

(Modified Sachs Scaling),

T_o = ambient temperature

and f indicates a functional relationship.

Then $$I_q = \frac{1}{S_i} f(S_d R) \tag{20}$$

and since displacement, $D = AI_q^{\ell}$ (see Section 3.1.2.2 and/or Appendix C) we have $D = A\left[\frac{1}{S_i} f(S_d R)\right]^{\ell}$. This can be rewritten

$$S_i^{\ell} D = A[f(S_d R)]^{\ell}\ , \tag{21}$$

where the left hand side now represents scaled displacement. In individual cases, i.e., specified vehicle and orientation, we know A and ℓ from our data fits of "Displacement versus Dynamic Pressure Impulse". From out data fits of "Scaled Impulse versus Scaled Ground Range" we also have a functional form f containing coefficients a_0, a_1, and a_2 whose values we have determined. If we use these results, scaled displacement may be regarded as known and no fitting of data is required. However, there is considerable scatter in the data determining A and ℓ (i.e., the data for "Displacement versus Dynamic Pressure Impulse") and there is also scatter in the data for determining $f(S_d R)$ (i.e., the data for

"Scaled Dynamic Impulse versus Scaled Ground Range"). Therefore, we simply took $S_I^{\ell}D = G(S_dR)$ where $G(S_dR)$ is a function to be determined by the data and it not required that $G(S_dR) = A[f(S_dR)]^{\ell}$ (the right hand side being already determined by the above mentioned data fits). This expresses "scaled displacement" as a function of scaled ground range.

(U) We fitted scaled displacement, $S_I^{\ell}D$, to the functional form of Equation (2), Appendix C, with $x_1 = x$ = scaled ground range and $x_2 = x^2$ (in two cases where we have sufficient data for such a fit: WWII Vehicle, Ideal Surface Burst with Yield > 1 KT, side-on and face-on vehicle orientations). We regarded ℓ as fixed. The resulting fits were not quite as good as the fits obtained without scaling displacements. It is, of course, possible that by also varying ℓ the results could be improved. This, however, appears unwarranted: if the value of ℓ to be used in an application of these results cannot be that obtained from "Displacement versus Scaled Dynamic Pressure Impulse" results, scaling the displacement has no utility. Therefore, we pursued this no further.

3.2.2 (U) Effect of Dust

(U) Having obtained plots and data fits of displacement versus scaled ground range for various burst conditions we compared the results. (The grouping of the shots according to burst conditions will be discussed in the next section.) Comparing Figure 3.5 with 3.4 (surface burst) we see that the effect of dust over a limited span of scaled ground ranges is to greatly enhance the displacement. (Since n = 0.4 for both of these figures scaled ground ranges are directly comparable. Both figures pertain to the WWII vehicle side-on.) At very short range displacement is enhanced by a factor of 6. At long range the dust-laden blast wave is weaker than the ideal since energy is sapped from the wave by the dust and the dust ultimately falls behind the wave, no longer contributing significantly to the dynamic pressure impulse.

(U) Similarly comparing Figure 3.7a with 3.6 (air burst) we again see that the effect of dust is to increase displacement by up to a factor of 6 over a limited spatial region. In this case n = 0.43 for both figures and the vehicle involved is the M38A1 in side-on orientation.

(U) Finally, comparing Figure 3.11 (light dust) and 3.10a (near-ideal air burst) we obtain the same result for dust enhancement of displacement, this time for 2-1/2 ton trucks (with n = 0.43 for both figures).

3.3 (U) DYNAMIC PRESSURE IMPULSE AND SCALED DYNAMIC PRESSURE IMPULSE VERSUS SCALED GROUND RANGE

(U) Results are given in Figures 3.12 through 3.21 and Tables 3.3 and 3.4.

3.3.1 (U) Surface Burst

(U) We first discuss the surface burst data, ideal/near-ideal blast data spanning the yield range of 20 tons - 3.5 MT. Here, as in the case of displacement versus scaled ground range, we consider both scaled and unscaled dynamic pressure impulse and use both

$$x = S_d R \quad \text{and} \quad x = S_d' R \ . \qquad (16a,b)$$

In the latter case we again took values of n (in addition to 1/3) of 0.37, 0.4, 0.43, and in some cases additional values — somewhat higher values when data over a very large range of yields were fitted.

(U) For both scaled and unscaled dynamic pressure impulse we obtained two sets of fits to the experimental data, one using only nuclear shots ranging in yield from 39.5 KT to 3500 KT and one including these shots along with HE shots extending the yield range downward to 20 tons. We consider first of all the nuclear case.

3.3.1.1 (U) Nuclear Events

(U) For both scaled and unscaled impulse we have two fits, one extending over the entire scaled ground range and one over the large scaled ground range domain of the data. See Figures 3.12a, 3.12b, and 3.13. In each case the data fit over the entire range reaches a minimum near the end of the data range (and would thus be incapable of extrapolation). Comparing the fits over the entire data range we see that (Tables 3.3 and 3.4) the statistical measures of goodness of fit are a little better for scaled than for unscaled impulse even with optimum value of n, 0.425 in this case. [The ground range scaling factor, S_d', depends upon n. See Equation (17b).] The results with n = 0.4, however, are not greatly inferior to those with n = 0.425. Comparing the statistical measures for the scaled and unscaled impulse fits we have: scaled, $\sigma_{\ell n\ I,C} = 0.1637$, $\sigma'_{I,C} = 0.1611$ and $E_I = 15.11\%$; unscaled corresponding values 0.1756, 0.1774, and 16.64%, respectively. We note that this is in spite of the fact that $1-R^2$ is 0.0120 for the unscaled case and 0.0173 for the scaled case. Thus R^2 cannot be used to determine which is the better of two fits when one or both variables are different in one fit than in the other.

(U) Comparing the two fits over the large scaled ground range end of the data range, again with n = 0.425 determining S'_d, we see that in this case the statistical measures of goodness of fit are a little better for unscaled than for scaled impulse. (See Tables 3.3 and 3.4.) In each case the minimum of the fitted function here is well beyond the range of the data so that reasonable extrapolation is possible.

(U) In obtaining data fits over the large x end of the data region there is some arbitrariness concerning just how much of the data range to include. There is in each case substantially more data in the low and moderate x than in the large x portion of the data range. In each case we obtained additional fits covering a greater or smaller range than indicated in Figures 3.12a, 3.12b, and 3.13. We selected what we regarded as the best fit on the basis of accuracy of fit to the data points used, number of data points used and a subjective criterion: that when the fit obtained is coupled with the portion of the total data fit covering the remainder (small x) part of the scaled ground range domain — the result is a curve over the entire range essentially coinciding with a good eye-drawn curve.

(U) In further analyzing these results we can say that the prediction capability afforded is quite good. There is much less data scatter than in corresponding displacement plots. This is partly due to the fact that more uncontrolled variables affect displacement than dynamic pressure impulse, but is also partly due to the fact that in the data reduction process (by many persons over a long time period) there has inevitably been some smoothing of data for the blast field variables as a function of ground range for each shot. Also, some of the latter results are based, at least in part, on calculations. (This is not the case for displacement values.)

(U) Finally, we remark that in neither the scaled nor unscaled impulse plots is the scaling (only ground range is scaled in the latter case) perfect; i.e., the data for the 4 shots do not coalesce perfectly. In both cases the Nectar-6 points lie a little above the Zuni-3 (and curve slopes based on each set separately would differ slightly). These points make up the upper end of the curves. Similarly lower down on the curve the Koon-3 points lie a little above the Lacrosse-1 points in their (small) region of overlap.

(U) Overall there is not much difference between the reliability of the two sets of fits. Both are quite good; the scaled or unscaled impulse results may be used with equal confidence.

3.3.1.2 (U) Nuclear Plus HE Events

(U) We now consider the corresponding sets of scaled and unscaled impulse data curve fits over the entire yield range of 20 tons to 3500 KT. For the unscaled impulse data we found that for the scaled ground range $x = S_d'R$, the optimum value of n (upon which S_d' depends) is about 0.46, the larger value of n in this case being required to coalesce the low yield (non-nuclear) data on the same curve as the higher yield shot data — causing somewhat more separation of the Nectar-6 and Zuni-3 points at the upper end of the curve. See Figures 3.14 and 3.15.

(U) The comparisons for the curve fits for scaled and unscaled impulse are very similar to those just discussed over the smaller yield range: the statistical measures are a little better for the scaled impulse fits for the whole data range fits but a little better for the unscaled impulse curve fits over the large x end of the data. (See Tables 3.3 and 3.4.) Again the whole data range fits have a minimum near the end of the data range; the large x region fits have minima well beyond the data range and are capable of reasonable extrapolation beyond the data range. Once again, the data for the several shots are not completely coalesced under the scalings used. In addition to a moderate separation of the Nectar-6 and Zuni-3 points at the upper end of the curves, the Dice Throw (1 KT, HE) points are somewhat above the curve except at large x. (The scaled impulse curve contains one more Dice Throw point than the unscaled total data fit. As can be seen from Figure 3.14, the Dice Throw point at $x = 574.7$ cannot reasonably be included in the curve fit over the total data range without considerable worsening of the fit. Thus the total data fit does not extend to this scaled ground range, though the fit to the large scaled ground range data includes this point. We have no reason to suppose this to be a bad data point; the functional form selected for fitting the data, however, does not provide as accurate and reliable a predictive capability when this point is included in the fit over the entire data range.) At the large x end of the data the Koon-3 points are somewhat higher than the other data points. Deviations from the curves are modest, however, and considering the large yield range encompassed by the data, the scalings used coalesce the data quite well. Again, good eye-drawn curves would coincide rather well with the combined curves formed by the large scaled ground region fits and the non-overlapping regions of the total data curve fits. (At the low ground range end where the curves are very

steep, eye-drawn curves could improve on the fitted curves somewhat more here than in the all-nuclear shot case previously discussed where the yield range covered is much smaller.)

(U) Finally, the predictive accuracy is somewhat diminished as compared with the all-nuclear, smaller yield range data fits. (See Table 3.3 and 3.4.) For example, the RMS errors, E, for the scaled impulse versus scaled ground range fits over the whole data range and over the yield ranges (20 tons - 3500 KT) and (39.5 KT to 3500 KT) are 19.24% and 15.11%, respectively. The corresponding results for (unscaled) impulse versus scaled ground range are: 20.22% and 16.64%, respectively. Similar results hold for the other statistical measures.

(U) Once more from an overall viewpoint there is little difference in reliability between the two sets of curve fits to the data. Both are good. The scaled or unscaled impulse versus scaled ground range curve fits may be used with equal confidence.

3.3.1.3 (U) Comparison of Scaled and Unscaled Dynamic Pressure Impulse Results

(U) To show that this is true we compared values of I_q obtained by one of the scaled and unscaled fits for a matrix of values of yield and ground range. (We ignored effects of ambient conditions here which are small and have a negligible effect on the comparison.) We chose weapon yields W, of 0.1, 10, and 1000 KT and values of $R/W^{1/3}$ of 150, 200, 300, 400 and 600 metres. Here R is the ground range and the specification of $R/W^{1/3}$ was simply for convenience in the computation using the scaled I_q versus scaled ground range fits. The actual domain of ground range R in the matrix of R, W values is $69.62 \leq R \leq 6000$ metres. We used Figures 3.14 and 3.15 and the data fits listed thereon. For the selected matrix of values we thus calculated 15 values of I_q over the very large span of yields and ground ranges using both the scaled and unscaled I_q data fits. (The range of R extended into the extrapolated region of the data fits - large x region.) The average percent difference between the two sets of results was 13.6%.

3.3.2 (U) Non-Surface Bursts (HOB and Surface Effects)

(U) In section 3.2.2 we compared displacements for near-ideal bursts with those for bursts which gave rise to appreciable dust in the blast wave. Prior to plotting and fitting this data, however, it was necessary to group

the shots. In order to do this we must have some criterion since the amount of dust will vary with each shot for each ground range. Since a primary objective of the present study is to obtain good estimates of I_q, especially for non-ideal shots, we first plotted scaled I_q versus scaled ground range for the various shots. We made this choice because the scaled I_q plots involve $W^{1/3}$ in scaled ground range — whereas (unscaled) I_q plots involve W^n with n variable, at least over a limited range of values. Having done this, however, we find the results obtained to be consistent for scaled and unscaled I_q and also for displacement versus scaled ground range. The resulting grouping is as follows: "Light Dust" - Grable-10, Moth-2, Turk-4, Bee-6, Apple I-8, and Smoky-15; "Heavy Dust" - Met-12 and Apple II-13; "Non-Surface Near-Ideal" - Encore-9, Wasp Prime-9, Yuma-4 (and Wasp-1, although we have no I_q data for this shot except what can be derived from I_q versus displacement; but all vehicle displacements were very small for Wasp-1, hence inference of I_q is very inaccurate). This grouping is somewhat coarse since the data do not warrant fine distinctions as to degree of dust. See, however, Section 4.

(U) This grouping parallels the scaled HOB grouping for the shots — see Table 2.1, with one exception: by virtue of its scaled HOB we would expect Turk-4 to be in the "Heavy Dust" group with Met-12 and Apple II-13. However, Turk-4 was exploded over a well-vegetated region, thus creating less dust than shots over desert at the same selected HOB. As far as dynamic pressure impulse is concerned, the dust, not the scaled HOB, is the relevant factor.

(U) Figures 3.16a, 3.16b, and 3.17 show that the data for the various shots, grouped as indicated, fall into a reasonably compact set. The Bee-6 points are a little high, perhaps indicating somewhat more dust than other shots in the group. These figures are for "Light Dust". Figures 3.18 and 3.19 for "Heavy Dust" exhibit somewhat more data scatter. See Section 4. (In the case of Figure 3.18 the value of n is almost irrelevant since Met-12 and Apple II-13 have scaling factors which are close in value; thus changing n produces very little change in the relative positions of the data points for the two shots.)

(U) Finally, we wish to evaluate the effect of dust on I_q. Comparing Figures 3.16a and 3.12b (each of which has n = 0.4) we see that light dust increases I_q by a factor of about 1.2 to 1.6 over the region of scaled ground range overlap of the data. Likewise comparing Figures 3.18 and 3.12b (n = 0.4

for both) we see that heavy dust enhances I_q by a factor varying from about 1.5 to 3 over the scaled ground range region common to the two figures.

(U) The effect of dust on I_q can also be seen by comparing the scaled I_q versus scaled ground range plots. Thus comparing Figures 3.17 and 3.13 (or 3.15) we see that over the common region of scaled ground range light dust increases (scaled) I_q by a factor varying from about 1 to 3. Again for larger ground range values (scaled) I_q falls off much more rapidly when dust is present than when it is not. Comparing Figures 3.19 and 3.13 (or 3.15) we see that heavy dust enhances (scaled) I_q by a factor of about 3 to 5 over a limited spatial region; thereafter (scaled) I_q falls off very rapidly with increasing ground range.

(U) Generally comparing Figures 3.21 and 3.13 (or 3.15) we see that at large scaled ground ranges I_q falls off more slowly for a near-ideal air burst than for an ideal surface burst. For small scaled ground range I_q is much greater for a near-ideal surface burst than for a near-ideal air burst; however, our data does not extend to very small ground ranges. We note also that the scaled HOB's for the shots we have grouped in the near-ideal air burst category differ considerably from one another, which probably explains at least partly the lack of good coalescence of the data for the separate shots in Figures 3.20a, 3.20b and 3.21.

3.3.2.1 (U) Comparison of Scaled and Unscaled Dynamic Pressure Impulse Results

(U) We used both the scaled and unscaled I_q versus scaled ground range plots (separately) in obtaining preliminary scaled I_q HOB contours. (In Section 4 we describe the method we finally used in obtaining these contours; however, the effort described here provides a good comparison of the use of the scaled and unscaled dynamic pressure impulse results.) Except for the surface bursts each shot provided data points on the contours at its scaled HOB, the latter being different for each non-surface shot. In using the figures just discussed we followed the fitted curve for the shot group in general, but allowed for deviations of the individual shots from the group curve (since the shots do not coalesce perfectly on the group curve). That is, we assume that there are real physical deviations of individual shots from the group curves (certainly there are various degrees of dust) — the deviations are not due only to inaccuracy of our knowledge of I_q. In any given case we cannot know to what extent our inaccurate knowledge of I_q and to what extent real physical differences account for deviations from the group curve. However, the group

curve served as an excellent guide in all cases; in many cases there would not be sufficient data to determine a reliable curve for a single shot. The results obtained in this way, using separately the scaled and unscaled I_q versus scaled ground range fits, for obtaining values of $S_i I_q$ for the HOB contours were very close — nearly always within about 2% of one another.

3.4 (U) BEST VALUE OF n

(U) When we started fitting displacement and I_q versus scaled ground range, the first several cases we tried seemed to have their optimum values of n in the vicinity of 0.4. As we have seen, comparisons of figures can be made directly only when the values of n are the same. So we adopted n = 0.4 as a "standard" for comparison purposes. For our scaled I_q versus scaled ground range fits, however, the value of n is fixed at n = 1/3 (modified Sachs scaling). There is a theoretical basis for this, although effect of dust is not included; we have seen, however, that it is not useful to scale displacement. Therefore, having improved our estimates of I_q and obtained fits for a considerable variety of cases we wish to establish our "optimum" overall value of n — one which could be used for cases not treated herein with the expectation that reasonably accurate results would be achieved.

(U) In Tables 3.2 and 3.3 we list the results for many cases we have fitted. The values of n are optimum within approximately $\pm$ 0.01 when only one value of n is listed. (In a few cases, as mentioned previously, changing n does not shift the points very much relative to one another so that the results are almost independent of n. This can happen when only two or three shots supply data for a curve to be fitted*; generally when there are three or more shots, however, the results vary quite significantly with n.) In several cases we list the results for the optimum value of n and also for n = 0.4. Comparison then shows how much better the optimum is than that obtained with n = 0.4. A graphical comparison is obtained by comparing Figures 3.7a, 3.7b; 3.8a, 3.8b; 3.12a, 3.12b; 3.16a, 3.16b**; 3.20a, 3.20b. The two

(U) * When only two shots contribute data it may also happen that their data ranges don't overlap in I_q or scaled I_q (or overlap is based on one or two data points) so that the data can be "coalesced" by a single curve within a wide range of n (including n = 1/3).

(U)** The fits in Figures 3.16a and 3.16b illustrate the case in which one statistical measure of goodness of fit is slightly better for n = 0.4, the other two slightly better for n = 0.37. See Table 3.3. The optimum value of n in this case is probably between these two values.

figures in each pair differ only in their values of n. Inspection of the entire set of results, Tables 3.2 and 3.3, shows that the optimum-value of n, overall, is about n = 0.42 or 0.43. Most of the cases for which the data are best and there are the most data points cluster about such a value. In fact all of the "good" cases and almost all of the "fair" and "not so good" cases lie within the range $0.40 \leq n \leq 0.46$. Perhaps the two best cases, 3.12a and 3.14, all nuclear near-ideal surface burst and nuclear + HE near-ideal surface burst I_q versus scaled ground range, have optimum values of n of 0.425 and 0.46, respectively, the latter comparatively high value of n being needed to coalesce the data over the very large yield range of $0.04 \leq Y \leq 3500$ KT. As would be expected with many data fits, a goodly fraction of which have rather few data points with considerable scatter, values of optimum n will vary somewhat more than is physically realistic. Figures 3.9, 3.10b, 3.20a and 3.20b may well be examples of this.

(U) So while we have no criterion which allows us to determine "the" optimum overall value of n, a value of n = 0.42 or n = 0.43 appears to be a very good choice and one which can be used with some confidence for a broader class of data than encompassed herein. References 4 and 9 show similar values of n for blast damage to drag-type targets.

3.5 (U) EFFECTS OF NON-DESERT SURFACE (WATER, ASPHALT, DESERT ROCK)

(U) In shot Met-12 gages and vehicles were placed not only on desert surface but also on water (over desert), asphalt and desert rock; on shot Bee-6 similar data were taken over asphalt. We did not use any of this data in obtaining the fitted curves. We now wish to compare this data with the corresponding desert surface results. We start with I_q (and scaled I_q) versus scaled ground range.

3.5.1 (U) Effect on Dynamic Pressure Impulse

(U) Placing the data points for a water surface on Figure 3.18 and 3.19 we see that the I_q values for water are substantially lower than the desert values (except for the lowest point). See Figures 3.18-1 and 3.19-1. The I_q values for asphalt are lower than those for water over the whole range and much lower than desert, a factor of 2 or more. Placing the asphalt data for shot Bee-6 on Figure 3.16a again shows the asphalt I_q values to be lower than those for desert (3 of the 4 data points lower, fourth about the same). See Figure 3.16a-1. On the average the asphalt I_q values are lower by a factor

of about 1.4. Use of Figure 3.17 with the asphalt data produces the same result; see Figure 3.17-1.

3.5.2 (U) Effect on Displacement

(U) We next compare displacements for the desert and non-desert data. Referring to Figure 3.5-1 (side-on) we see that displacements for vehicles on a water surface are about the same as for desert (although the I_q values for water are somewhat lower than for desert). Use of Figure 3.9-1 provides the same result; in this case we compare face-on displacements. Using the same figures we see that vehicle displacement on asphalt is much smaller than on desert surface. This is consistent with the considerably lower I_q values found over asphalt.

(U) We also find that vehicles placed on Desert Rock are displaced about the same as on asphalt — if we assume no difference between the M38A1 and WWII vehicles. This is a good assumption since the displacements involved here are large (see Section 3.1.2.3).

(U) In the case of the 2-1/2 ton trucks placing the Met-12 (heavy dust shot over the desert portion of the terrain) displacements (Desert Rock) on the light dust plot for 2-1/2 ton trucks, Figure 3.11, the most comparable data we have — we see that the displacements over Desert Rock are uniformly substantially lower than over desert in agreement with the above result for 1/4 ton trucks. See Figure 3.11-1.

3.5.3 (U) Effect on Displacement versus Dynamic Pressure Impulse

(U) We next compare displacement versus I_q for desert and non-desert cases. Comparing vehicle displacements over water with those over desert, Figures 2.1-1 and 2.3-1, we see that the differences are rather small. There is not sufficient data to determine whether or not this is significant.

(U) Comparing displacements over asphalt with those over desert, again using Figures 2.1-1 (side-on) and 2.3-1 (face-on), we see that there is no difference in the face-on orientation, while the only significant difference in the side-on orientation occurs for one Met-12 point with I_q value in the vicinity of 1 kPa-sec, i.e., the marginal region for turnover.

(U) Thus as far as displacement is concerned for a specified value of I_q, there is not much difference among water, asphalt and desert. (See, however, Section 3.1.2.3 for effect of surface on vehicle turnover in cases where I_q value is marginal for vehicle turnover.)

3.5.4 (U) Effect on Damage

(U) Finally we come to a comparison of damage between desert and non-desert surfaces. The damage data have inherently large scatter.* Referring to Figure 3.3-1, we see that the results for water differ little from those for desert, though one point appears low — this is in face-on orientation. Using Figure 3.1-1, side-on, we see that two of the water points lie far below the curve (while the other 3 are on the curve in the damage = 10 region). For one of the two points, the vehicle apparently was supported by a dike retaining the water; in any case it did not turn over despite a large displacement (12 metres). In the second case, 78 metre displacement, the vehicle probably turned over 360° — but was not damaged as it would have been had it been bouncing and/or scraping the earth.

(U) For asphalt, comparing the side-on data with that of desert, Figure 3.1-1, we find that 8 of the 9 points are within 1σ of the curve (mostly above); the ninth is a damage = 10 point 3σ above the curve, yet not very far (to the low displacement side) from other (desert) damage = 10 points. In the face-on case comparison, Figure 3.3-1, 6 of the 9 points are within 1σ of the curve again mostly above. Two of the remaining 3 are damage = 10 points, one of these not far from other such points. The other was evaluated as damage = 10 owing to fire rather than blast damage; the blast damage was moderate. The remaining point corresponds to a vehicle for which part of the damage was caused by debris rather than blast. Overall, then, damage for a given displacement appears to average somewhat higher on an asphalt surface than on desert surface. (As we have seen, for a specified displacement, I_q is about the same on desert and asphalt surfaces, so that any dependence of damage on I_q over and above that owing to displacement —

(U) * The damage data and results are discussed in a separate report, Reference 17; figures from that report used here follow Figure 3.21 in this report. Figures 2.1, 2.2, 2.3, and 2.8 of Reference 17 correspond to Figures 3.1-1, 3.2-1, 3.3-1, and 3.8-1, respectively, of the present report. The curve fit shown is, in each case in both reports, the damage-displacement least squares data fit for vehicles on a desert surface. However, in Reference 17 the (desert) data points used in the fit are shown whereas in the present report the data points shown are non-desert data points (and are not used in obtaining the fitted curve).

which is in turn caused by the dynamic pressure impulse, I_q — is not a factor here.)

(U) Lastly, comparing damage over a Desert Rock surface with that over desert we have recourse to Figures 3.2-1 and 3.8-1. From Figure 3.2-1, we see that there are not sufficient Desert Rock data points on which to base a judgement; however, the Desert Rock points do exhibit somewhat more damage for a given displacement than the desert points. In the case of Figure 3.8-1 (2-1/2 ton trucks) the result is more clear cut: there are 8 desert rock data points, none in the damage = 10 region and all above both curve fits, averaging more than 2σ above curve fit 1 and 1.5σ above fit 2. Thus, it is clear that for a given displacement vehicle damage is greater on a Desert Rock surface than on desert.

(U) Thus the pattern is consistent: for a given I_q value, displacement is, at least approximately, independent of the surface on which the vehicle is placed (provided, for the side-on orientation case, that I_q is above the marginal region for vehicle turnover, ~1 kPa-sec); but for a given displacement damage is greater on the harder surfaces, asphalt and Desert Rock, than on desert and greater on desert than on water (over desert), i.e., a soft, mushy surface. This is quite plausible since bouncing, scraping and gouging a hard surface would be expected to do considerable damage to a vehicle, whereas a soft, mushy surface has a cushioning effect.

3.5.5 (U) Plumbbob, Smoky-15 Results

(U) The data for Plumbbob, Smoky-15 differ moderately from other desert data:

(1) As far as I_q and scaled I_q versus scaled ground range are concerned, the data appear consistent with other shot data. See Figures 3.16a, 3.16b, and 3.17.

(2) As far as displacement versus I_q is concerned, the Smoky-15 data are within the data scatter. Smoky-15 data are included in these figures.

(3) For displacement versus scaled ground range, the Smoky-15 points are somewhat low, both side-on and face-on; we did not use them in the fits. (They are comparable with the asphalt points here.)

(4) For damage versus displacement* we did not use the Smoky-15 data in the fits. On comparing the data with the fits, however, we found that the Smoky-15 points averaged somewhat below the desert data curve in side-on orientation and above the desert data curve in face-on orientation.

(U) There are only a few points in each instance so that it is difficult to draw clear-cut conclusions. However, it appears probable that the (modest) discrepancies can be accounted for by combination of the usual data scatter and a small inaccuracy in our estimates of dynamic pressure impulse. (Our estimate of dynamic pressure impulse may be a little high.)

(U) * Damage results are reported in Reference 17.

TABLE 3.1 (U) LEAST SQUARES FIT RESULTS --
Combined Vehicles - 1/4 Ton and 2-1/2 Ton Trucks (Iterated I_q Values)

CONFIDENTIAL - FORMERLY RESTRICTED DATA

VEHICLE/ ORIENTATION (FIG. NO.)	EVENTS INCLUDED	YIELD RANGE (KT)	N	FIT	
M38A1 & WWII, SO (3.1)	Koon-3 Nectar-6 Bee-6 Apple I-8 Wasp Prime-9 Met-12 Apple II-13 Lacrosse-1 Zuni-3 *Yuma-4 Canadian 20T Canadian 100T Smoky-15 Encore-9 Grable-10 Moth-2 Turk-4 Dice Throw	* $0.04 \leq Y \leq 3500$	69	$\ell n\ I_q = 0.1329 + 0.3759\ \ell n\ D + 0.05658\ (\ell n\ D)^2$ $R^2 = 0.9394$ $\ell n\ D = -0.2226 + 2.222\ \ell n\ I_q - 0.2142\ (\ell n\ I_q)^2$ $R^2 = 0.9315$	$\sigma_{\ell n\ D,\ C} = 0.4689$ $\sigma'_{D,\ C} = 0.5656$ $E_D = 55.32\%$ $\sigma_{\ell n\ I_q,\ C} = 0.2891$ $\sigma'_{I_q,\ C} = 0.3243$ $E_{I_q} = 32.43\%$
M38A1 & WWII, FO (3.2)	Koon-3 Nectar-6 Bee-6 Apple I-8 Wasp Prime-9 Met-12 Apple II-13 Lacrosse-1 Zuni-3 Encore-9 Dice Throw Smoky-15	* $1.0 \leq Y \leq 3500$	42	$\ell n\ I_q = 0.7317 + 0.4654\ \ell n\ D + 0.02204\ (\ell n\ D)^2$ $R^2 = 0.9407$ $\ell n\ D = -1.362 + 2.081\ \ell n\ I_q - 0.09982\ (\ell n\ I_q)^2$ $R^2 = 0.9381$	$\sigma_{\ell n\ D,\ C} = 0.5272$ $\sigma'_{D,\ C} = 0.5869$ $E_D = 56.55\%$ $\sigma_{\ell n\ I_q,\ C} = 0.2935$ $\sigma'_{I_q,\ C} = 0.3351$ $E_{I_q} = 32.29\%$

(U) * This event and yield in combination are CONFIDENTIAL - FORMERLY RESTRICTED DATA.

CONFIDENTIAL

TABLE 3.1 (U) LEAST SQUARES FIT RESULTS --
Combined Vehicles - 1/4 Ton and 2-1/2 Ton Trucks (Iterated I_q Values) (Concluded)
CONFIDENTIAL - FORMERLY RESTRICTED DATA

VEHICLE/ ORIENTATION (FIG. NO.)	EVENTS INCLUDED	YIELD RANGE (KT)	N	FIT	
REO M35 & GMC M135, SO (3.3)	Encore-9 Grable-10 Moth-2 Turk-4 Dice Throw	$1.0 \leq Y \leq 43.0$	25	$\ell n\ I_q = 0.4288 + 0.3325\ \ell n\ D + 0.02753\ (\ell n\ D)^2$ $R^2 = 0.9466$ $\ell n\ D = -1.365 + 3.339\ \ell n\ I_q - 0.4259\ (\ell n\ I_q)^2$ $R^2 = 0.9495$	$\sigma_{\ell n\ D,\ C} = 0.4977$ $\sigma'_{D,\ C} = 0.6628$ $E_D = 62.18\%$ $\sigma_{\ell n\ I_q,\ C} = 0.2109$ $\sigma'_{I_q,\ C} = 0.2047$ $E_{I_q} = 19.20\%$

TABLE 3.2 (U) LEAST SQURES FIT RESULTS --
Displacement vs. Scaled Ground Range

UNCLASSIFIED

VEHICLE ORIENTATION (FIG. NO.)	BURST CONDITIONS	EVENTS INCLUDED	YIELD RANGE (KT)	N	n	FIT (R^2)	x_{min} (x_{max})	$x_{max,data}$ ($x_{min,data}$)	$S_{\ell n\ D}$	S'_D	$\sigma_{\ell n\ D,C}$	$\sigma'_{D,C}$	E_D (%)
WWII, SO (3.4)	Near-Ideal Surface Burst	Koon-3 Nectar-6 Lacrosse-1 Zuni-3	39.5≤Y≤3500	20	0.4	$\ell n\ D = 7.956 - 0.02979x + 0.00002470\ x^2$ ($R^2 = 0.9622$)	603.1 (——)	336.1 (81.5)	1.577	1.888	0.3046	0.3332	30.72
WWII, SO (3.5)	Light and Heavy Dust	Bee-6 Apple I-8 Met-12 Apple II-13	7.76≤Y≤28.5	16	0.4	$\ell n\ D = 9.423 - 0.01951x - 0.00002377\ x^2$ ($R^2 = 0.9249$)	—— (——)	(368.7) (170.0)	3.589	5.219	0.5254	0.6336	57.11
M38A1, SO (3.6)	Near-Ideal Air Burst	Encore-9 Wasp-1	7.16≤Y≤26.0	11	0.43	$\ell n\ D = 7.868 - 0.03583x + 0.00003246\ x^2$ ($R^2 = 0.8731$)	552.0 (——)	539.9 (178.9)	3.293	8.142	0.6416	1.009	86.03
M38A1, SO (3.7a)	Light Dust	Moth-2 Turk-4 Grable-10	2.39≤Y≤43.0	9	0.43	$\ell n\ D = 13.07 - 0.05621x + 0.00004728\ x^2$ ($R^2 = 0.9928$)	594.4 (——)	401.7 (193.1)	0.2183	0.2086	0.1907	0.1865	15.22
(3.7b)				9	0.4	$\ell n\ D = 18.24 - 0.08489x + 0.00008874\ x^2$ ($R^2 = 0.9876$)	487.3 (——)	435.5 (216.2)	0.3770	0.3213	0.2507	0.2314	18.89
WWII, FO (3.8a)	Near-Ideal Surface Burst	Koon-3 Nectar-6 Lacrosse-1 Zuni-3	39.5≤Y≤3500	16	0.43	$\ell n\ D = 9.571 - 0.05921x + 0.00007726\ x^2$ ($R^2 = 0.9760$)	383.2 (——)	289.4 (75.6)	1.965	2.043	0.3888	0.3964	35.74
(3.8b)				16	0.4	$\ell n\ D = 10.81 - 0.06000x + 0.00007236\ x^2$ ($R^2 = 0.9670$)	414.6 (——)	336.1 (96.5)	2.492	3.674	0.4378	0.5317	47.92

TABLE 3.2 (U) LEAST SQUARES FIT RESULTS --
Displacement vs. Scaled Ground Range (Concluded)

UNCLASSIFIED

VEHICLE ORIENTATION (FIG. NO.)	BURST CONDITIONS	EVENTS INCLUDED	YIELD RANGE (KT)	N	n	FIT (R^2)	x_{min} (x_{max})	$x_{max,data}$ ($x_{min,data}$)	$S_{\ell n\, D}$	S'_D	$\sigma_{\ell n\, D,C}$	$\sigma'_{D,C}$	E_D (%)
WWII, FO (3.9)	Light and Heavy Dust	Bee-6 Apple I-8 Met-12 Apple II-13	$7.76 \le Y \le 28.5$	13	1/3	$\ell n\, D = 14.96 - 0.0531x + 0.00003367\, x^2$ ($R^2 = 0.9031$)	788.5 (——)	440.0 (208.9)	5.444	9.027	0.7378	0.9502	83.33
REO M35 & GMC M135, SO (3.10a)	Near-Ideal Air Burst	Encore-9 Wasp-1	$1.16 \le Y \le 26.0$	17	0.43	$\ell n\, D = 9.397 - 0.05119x + 0.00005870\, x^2$ ($R^2 = 0.7962$)	436.0 (——)	472.5 (178.9)	5.054	8.295	0.6008	0.7697	69.85
REO M35, SO (3.10b)	Near-Ideal Air Burst	Encore-9 Wasp-1	$1.16 \le Y \le 26.0$	11	0.45	$\ell n\, D = 9.108 - 0.05086x + 0.00005848\, x^2$ ($R^2 = 0.8857$)	434.9 (——)	442.7 (167.7)	2.623	3.787	0.5726	0.6880	58.67
REO M35 & GMC M135, SO (3.11)	Light Dust	Moth-2 Turk-4	$2.39 \le Y \le 43.0$	13	0.43	$\ell n\, D = 1.955 + 0.04384 - 0.00001781\, x^2$ ($R^2 = 0.9345$)	—— (123.1)	268.7 (171.4)	1.617	1.797	0.4021	0.4239	37.18

TABLE 3.3 (U) LEAST SQURES FIT RESULTS -- Dynamic Pressure Impulse vs. Scaled Ground Range

UNCLASSIFIED

BURST CONDITIONS	EVENTS INCLUDED	YIELD RANGE (KT)	N	n	FIT Range of x (x_{min})	R^2	$S_{\ell n\ I_q}$	S'_{I_q}	$\sigma_{\ell n\ I_q,C}$	$\sigma'_{I_q,C}$	E_I (%)
Surface Near-Ideal All Nuclear (3.12a)	Koon-3 Nectar-6 Lacrosse-1 Zuni-3	39.5≤Y≤3500	25	0.425	$\ell n\ I_q = 6.136 - 0.03042x + 0.00003299\ x^2$ $66.44 \leq x \leq 499.3$ (461.1) FIT 1	0.9880	0.6784	0.6922	0.1756	0.1774	16.64
	Koon-3 Lacrosse-1		7	0.425	$\ell n\ I_q = 4.132 - 0.01719x + 0.00001370\ x^2$ $230 \leq x \leq 627.4$ (627.4) FIT 2	0.9812	0.06768	0.07396	0.1301	0.1360	10.28
(3.12b)	Koon-3 Nectar-6 Lacrosse-1 Zuni-3		25	0.4	$\ell n\ I_q = 6.466 - 0.02872x + 0.00002797\ x^2$ $80.7 \leq x \leq 565.7$ (513.3) FIT 1	0.9847	0.9088	0.8663	0.2032	0.1984	18.61
	Koon-3 Lacrosse-1		7	0.4	$\ell n\ I_q = 3.755 - 0.01352x + 0.000008922\ x^2$ $270 \leq x \leq 757.7$ (757.7) FIT 2	0.9683	0.1139	0.1276	0.1688	0.1786	13.50
Surface Near-Ideal (3.14)	Koon-3 Nectar-6 Lacrosse-1 Zuni-3 Dice Throw Canadian 20T Canadian 100T	0.04≤Y≤3500	41	0.46	$\ell n\ I_q = 5.485 - 0.02937x + 0.00003240\ x^2$ $49.94 \leq x \leq 446.0$ (453.3) FIT 1	0.9859	1.643	1.676	0.2079	0.2100	20.22

TABLE 3.3 (U) LEAST SQUARES FIT RESULTS -- Dynamic Pressure Impulse vs. Scaled Ground Range (Continued)

(This Portion of TABLE 3.3 Is CONFIDENTIAL - FORMERLY RESTRICTED DATA)

BURST CONDITIONS	EVENTS INCLUDED	YIELD RANGE (KT)	N	n	FIT Range of x (x_{min})	R^2	$S_{\ell n\, I_q}$	S'_{I_q}	$\sigma_{\ell n\, I_q,C}$	$\sigma'_{I_q,C}$	E_I (%)
Surface Near-Ideal (3.14)	Koon-3 Lacrosse-1 Canadian 20T Canadian 100T Dice Throw	$0.04 \leq Y \leq 3500$	15	0.46	$\ell n\, I_q = 3.296 - 0.01437x + 0.000008389\, x^2$ $240 \leq x \leq 856.6$ FIT 2 (856.6) (Max x_{data} = 574.7)	0.9852	0.1260	0.1366	0.1025	0.1067	9.54
Light Dust (3.16a)	Grable-10 Bee-6, Moth-2 Turk-4 Apple I-8 Smoky-15	$2.39 \leq Y \leq 43.7$	26	0.4	$\ell n\, I_q = 5.967 - 0.01979x + 0.000006549\, x^2$ $150.3 \leq x \leq 368.7$ FIT 1 (1511.1)	0.9484	1.334	1.353	0.2408	0.2426	22.81
(3.16b)			26	0.37	$\ell n\, I_q = 5.732 - 0.01566x - 0.0000007637\, x^2$ $168.2 \leq x \leq 399.3$ FIT 2 (—)	0.9405	1.539	1.322	0.2587	0.2397	22.55
Heavy Dust (3.18)	Met-12 Apple II-13	$22.0 \leq Y \leq 28.5$	12	0.4	$\ell n\, I_q = 4.244 + 0.004793x - 0.00005522\, x^2$ $128.2 \leq x \leq 301.7$ (Max : x_i = 43.40)	0.9090	1.060	1.087	0.3431	0.3476	30.10
Air Near-Ideal (3.20a)	Encore-9 Wasp Prime-9 *Yuma-4	* $0.185 \leq Y \leq 26.0$	13	0.46	$\ell n\, I_q = 4.376 - 0.02217x + 0.00002617\, x^2$ $131.6 \leq x \leq 428.5$ (423.6)	0.8437	1.157	1.272	0.3401	0.3567	31.28

(U)* Yuma-4 yield is CONFIDENTIAL-FORMERLY RESTRICTED DATA.

TABLE 3.3 (U) LEAST SQUARES FIT RESULTS --
Dynamic Pressure Impulse vs. Scaled Ground Range (Concluded)

(This Portion of TABLE 3.3 Is CONFIDENTIAL - FORMERLY RESTRICTED DATA)

BURST CONDITIONS	EVENTS INCLUDED	YIELD RANGE (KT)	N	n	FIT Range of x (x_{min})		R^2	$S_{\ell n\, I_q}$	S'_{I_q}	$\sigma_{\ell n\, I_q,C}$	$\sigma'_{I_q,C}$	E_1 (%)
Air Near-Ideal (3.20b)	Encore-9 Wasp Prime-9 *Yuma-4	* $0.185 \leq Y \leq 26.0$	13	0.50	$\ell n\, I_q$ = 4.389 - 0.02308x + 0.00002778 x^2	$125.7 \leq x \leq 376.0$ (415.4)	0.8986	0.7504	0.9509	0.2739	0.3084	27.05

(U)* Yuma-4 yield is CONFIDENTIAL-FORMERLY RESTRICTED DATA.

TABLE 3.4 (U) LEAST SQUARES FIT RESULTS -- Scaled Dynamic Pressure Impulse vs. Scaled Ground Range

UNCLASSIFIED

BURST CONDITIONS (FIG. NO.)	EVENTS INCLUDED	YIELD RANGE (KT)	N	FIT Range of x (x_{min})	R^2	$S_{\ell n\, S_i I_q}$	$S_{S_i I_q}$	$\sigma_{\ell n\, S_i I_q, C}$	$\sigma_{S_i I_q, C}$	$E_i(\%)$
Surface Near-Ideal All Nuclear (3.13)	Koon-3 Nectar-6 Lacrosse-1 Zuni-3	39.5≤Y≤3500	25	$\ell n\, S_i I_q = 3.753 - 0.01614x + 0.00001033\, x^2$ $132.5 \le x \le 790.3$ FIT 1 (781.3)	0.9827	0.5896	0.5708	0.1637	0.1611	15.11
			10	$\ell n\, S_i I_q = 2.126 - 0.009248x + 0.000003965\, x^2$ $345 \le x \le 1166.1$ FIT 2 (1165.1)	0.9752	0.1577	0.1417	0.1501	0.1423	11.91
Surface Near-Ideal (3.15)	Koon-3 Nectar-6 Lacrosse-1 Zuni-3 Dice Throw Canadian 20T Canadian 100T	0.04≤Y≤3500	42	$\ell n\, S_i I_q = 4.060 - 0.01776x + 0.00001204\, x^2$ $93.8 \le x \le 790.3$ FIT 1 (737.4)	0.9780	1.366	1.554	0.1872	0.1996	19.24
			9	$\ell n\, S_i I_q = 2.606 - 0.01132x + 0.000005839\, x^2$ $345 \le x \le 969.8$ FIT 2 (969.8)	0.9776	0.1014	0.1030	0.1360	0.1310	10.70
Light Dust (3.17)	Grable-10 Moth-2 Turk-4 Bee-6 Apple 1-8 Smoky-15	2.39≤Y≤43.7	26	$\ell n\, S_i I_q = 3.720 - 0.006629x - 0.00001184\, x^2$ $193.0 \le x \le 440.0$ (—)	0.9518	0.9918	1.205	0.2077	0.2289	21.53

TABLE 3.4 (U) LEAST SQUARES FIT RESULTS --
Scaled Dynamic Pressure Impulse vs. Scaled Ground Range (Concluded)

(This Portion of TABLE 3.4 Is CONFIDENTIAL - FORMERLY RESTRICTED DATA

BURST CONDITIONS (FIG. NO.)	EVENTS INCLUDED	YIELD RANGE (KT)	N	FIT Range of x (x_{min})	R^2	$S_{\ell n\, S_i I_q}$	$S'_{S_i I_q}$	$\sigma_{\ell n\, S_i I_q, C}$	$\sigma'_{S_i I_q, C}$	$\bar{S}_i(x)$
Heavy Dust (3.19)	Met-12 Apple II-13	$22.0 \leq Y \leq 28.5$	12	$\ell n\, S_i I_q = 3.460 + 0.002209x - 0.00003250\, x^2$ $160.3 \leq x \leq 377.2$ (Max : $x' = 33.99$)	0.9048	1.126	1.149	0.3537	0.3573	30.94
Air Near-Ideal (3.21)	Encore-9 Wasp Prime-5 *Yuma-4	*$0.185 \leq Y \leq 26.0$	13	$\ell n\, S_i I_q = 3.261 - 0.01301x + 0.000009050\, x^2$ $132.8 \leq x \leq 647.5$ (718.9)	0.9276	0.9402	1.277	0.3066	0.3574	31.34

*Yield Is CONFIDENTIAL-FORMERLY RESTRICTED DATA.

CONFIDENTIAL

TABLE 3.5 (U) Non-Desert Surface Data

UNCLASSIFIED

VEHICLE TYPE	GROUND RANGE (M)	I_q (kPa-sec)	Displacement (M)	da	SURFACE
		TEAPOT, Bee-6, Side-on			
WWII	549	6.59	20.1	7	Asphalt
WWII	610	4.16	5.7	3	Asphalt
WWII	701	1.60	3.6	3	Asphalt
WWII	777	1.02	1.7	3	Asphalt
		TEAPOT, Bee-6, Face-on			
WWII	549	6.59	13.4	3	Asphalt
WWII	610	4.16	1.6	7	Asphalt
WWII	701	1.60	1.1	2	Asphalt
WWII	777	1.02	0.5	3	Asphalt
		TEAPOT, Apple I-8, Side-on			
M38A1	869	--	2.7	3	Desert Rock
		TEAPOT, Met-12, Side-on			
WWII	610	28.1	113	10	Water
WWII	686	19.6	103	10	Water
WWII	762	13.1	157	10	Water
WWII	838	7.55	78	5	Water
WWII	914	3.94	12	1	Water
WWII	610	19.0	68	10	Asphalt
WWII	686	13.7	59	10	Asphalt
WWII	762	8.4	23	10	Asphalt
WWII	838	5.58	14	6	Asphalt
WWII	914	1.72	1.0	1	Asphalt
		TEAPOT, Met-12, Side-on			
M38A1	610	--	81.0	10	Desert Rock
M38A1	686	--	54	10	Desert Rock
M38A1	762	--	22	9	Desert Rock
M38A1	838	--	11.8	6	Desert Rock
REO M35	762	--	15.3	8	Desert Rock
REO M35	762	--	8.1	9	Desert Rock
REO M35	762	--	16.9	7	Desert Rock
REO M35	838	--	10.3	6	Desert Rock
REO M35	914	--	5.7	6	Desert Rock
GMC M135	686	--	16.7	9	Desert Rock
GMC M135	762	--	13.1	8	Desert Rock
GMC M135	838	--	6.7	5	Desert Rock

TABLE 3.5 (U) Non-Desert Surface Data (Concluded)

UNCLASSIFIED

VEHICLE TYPE	GROUND RANGE (M)	I_q (kPa-sec)	Displacement (M)	da	SURFACE
		TEAPOT, Met-12, Face-on			
WWII	610	28.1	110	10	Water
WWII	686	19.6	91.4	10	Water
WWII	762	13.1	88	10	Water
WWII	838	7.55	8.8	1	Water
WWII	914	3.94	3.3	1	Water
WWII	610	19.0	71.3	.9	Asphalt
WWII	686	13.7	41.4	10	Asphalt
WWII	762	8.4	20	10	Asphalt
WWII	838	5.58	4.0	3	Asphalt
WWII	914	1.72	0.5	3	Asphalt

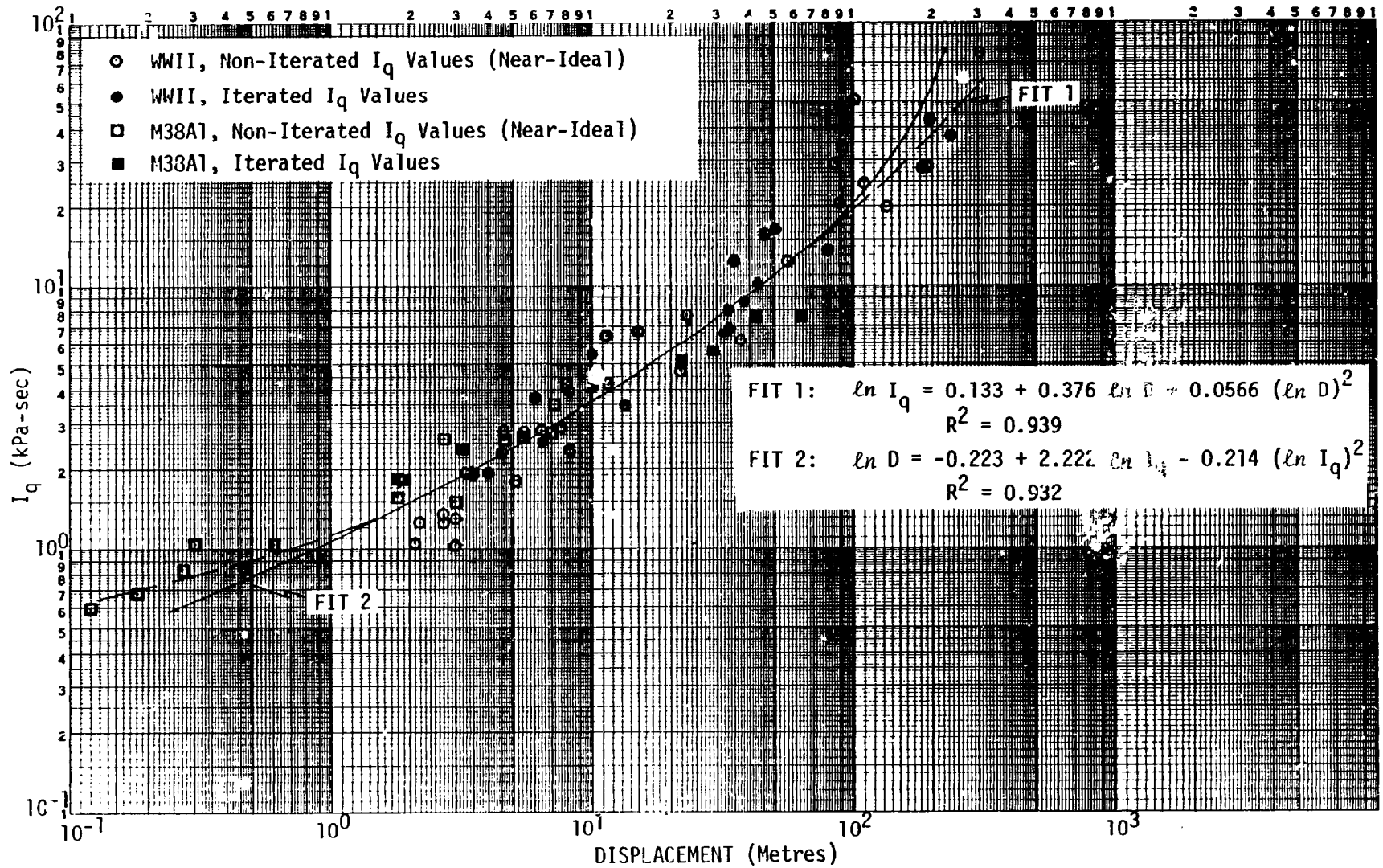

FIGURE 3.1 (U) Dynamic Pressure Impulse versus Displacement - WWII and M38A1, Side-on

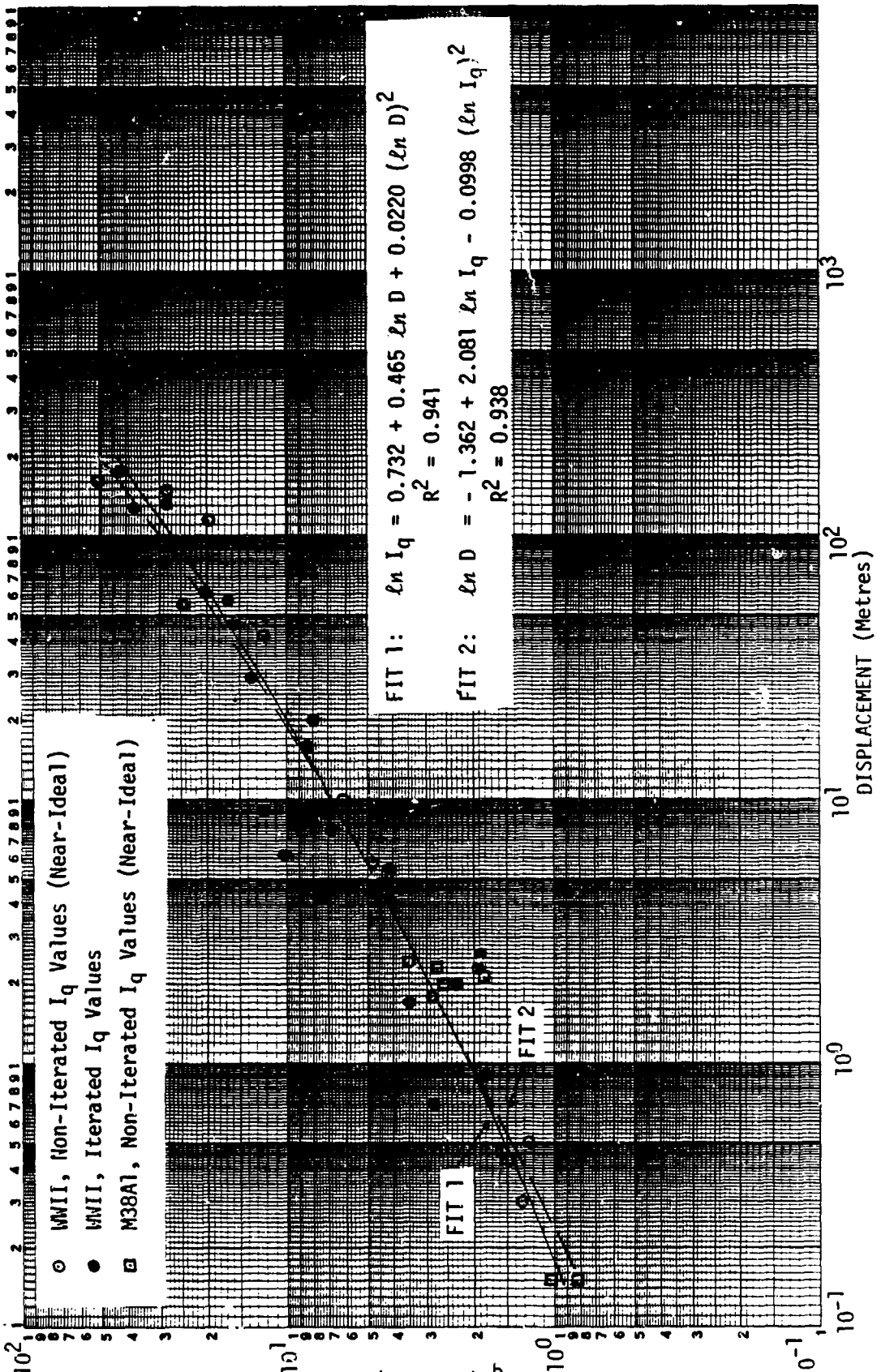

UNCLASSIFIED

FIGURE 3.2 (U) Dynamic Pressure Impulse versus Displacement - WWII and M38A1, Face-on

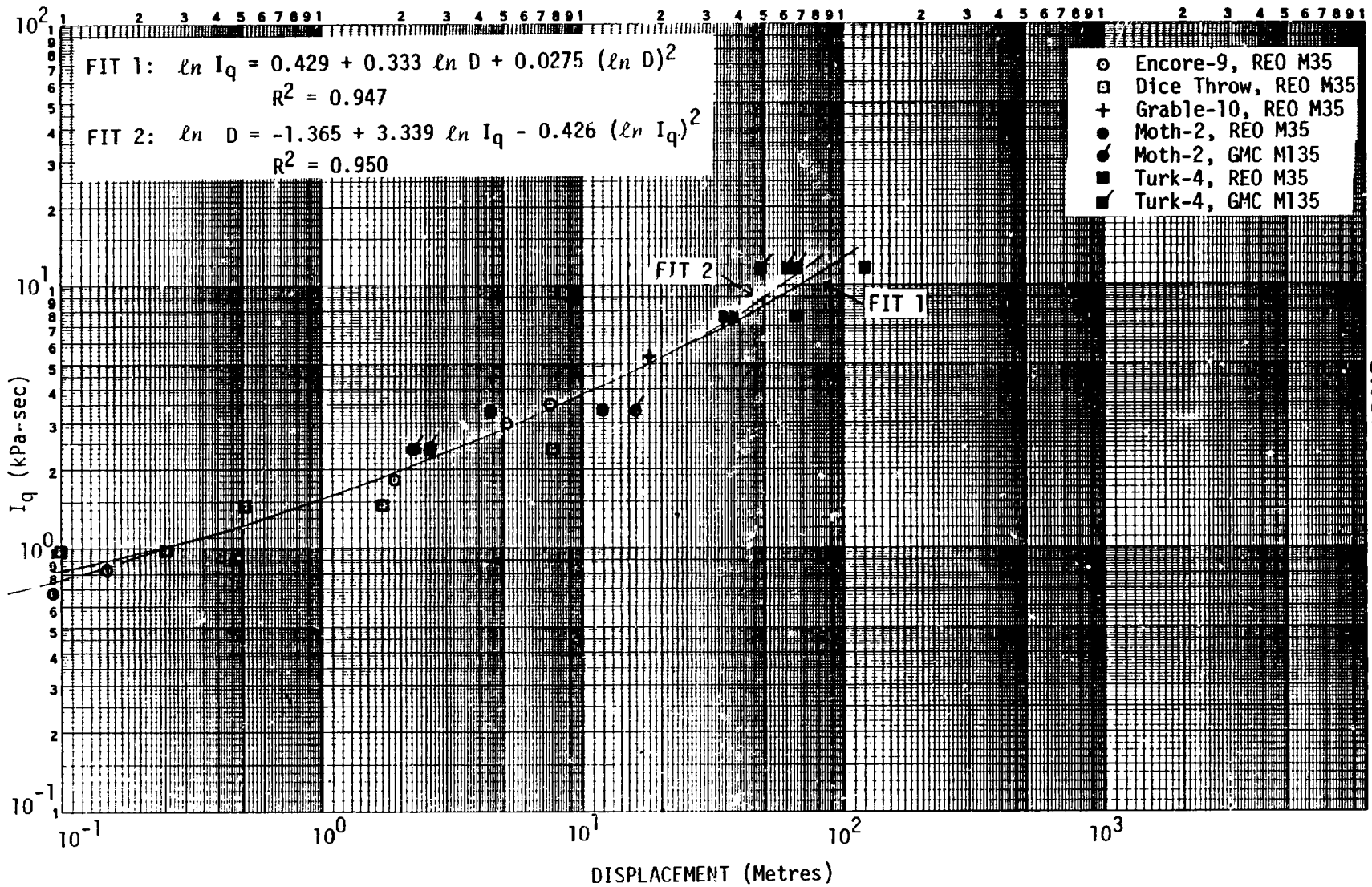

FIGURE 3.3 (U) Dynamic Pressure Impulse versus Displacement - 2-1/2 Ton Trucks, GMC M135 and REO M35, Side-on

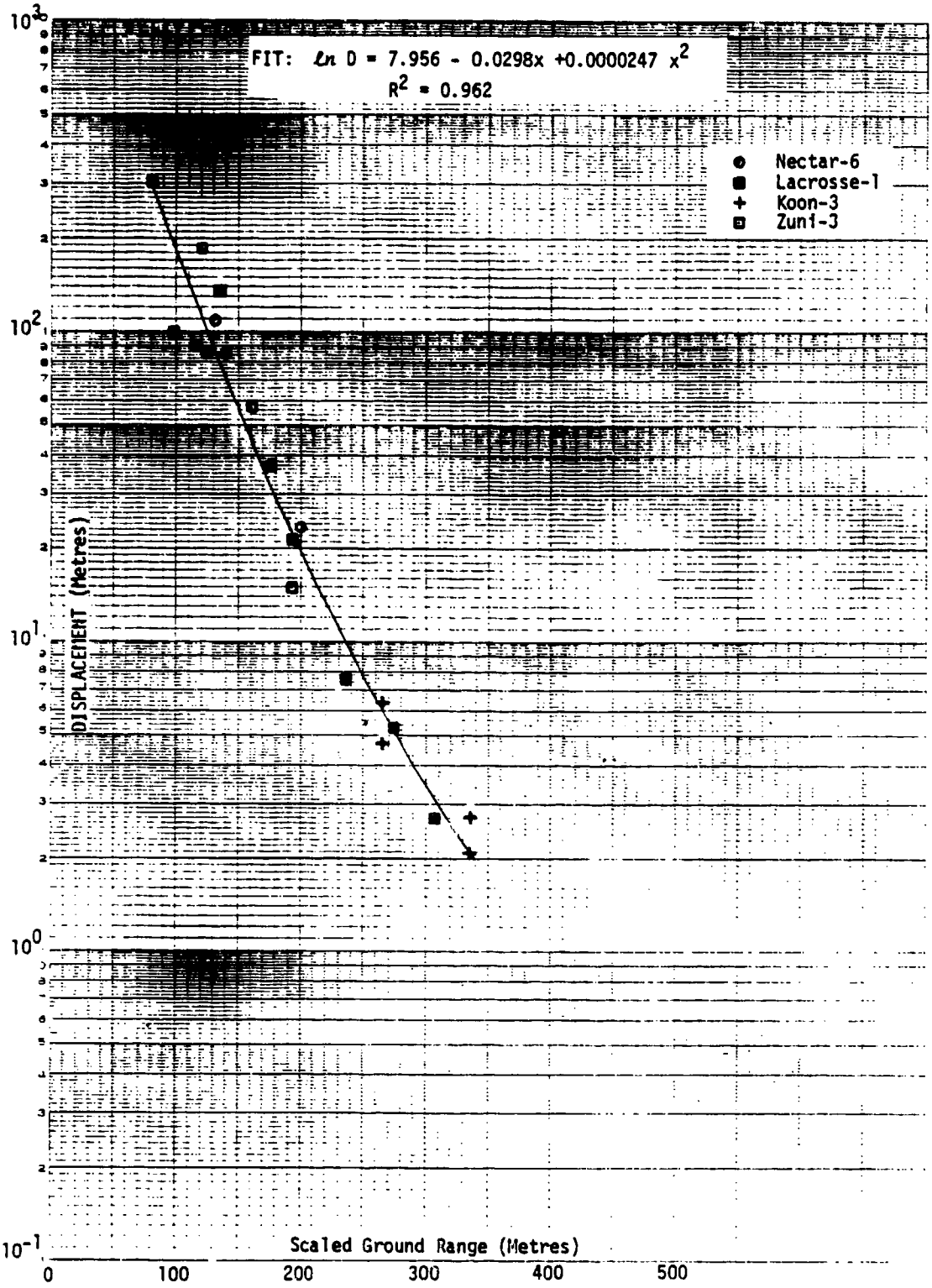

UNCLASSIFIED

FIGURE 3.4 (U) Displacement versus Scaled Ground Range - 1/4 Ton Trucks, WWII, SO, Near-Ideal Surface Burst, n = 0.4

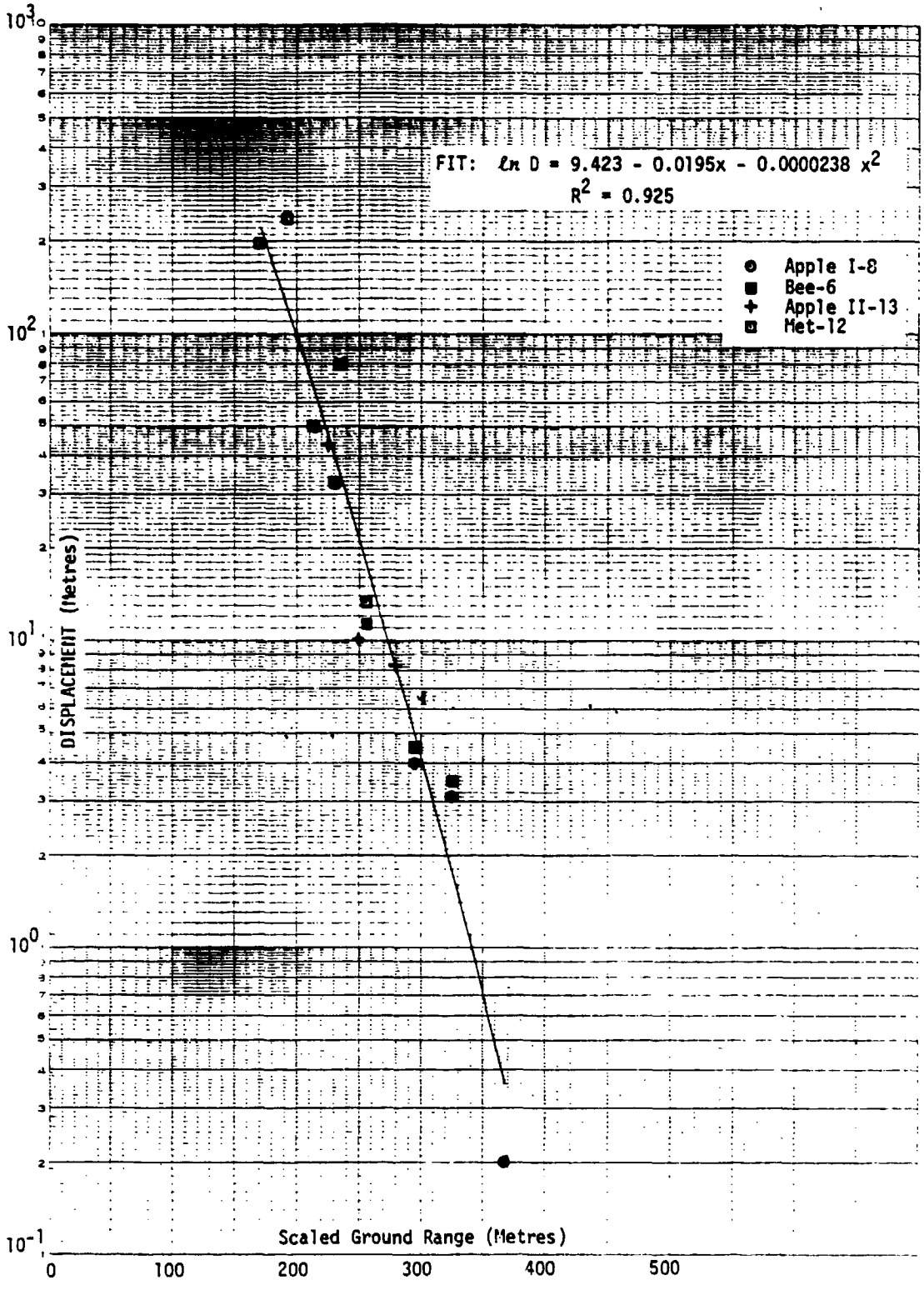

UNCLASSIFIED

FIGURE 3.5 (U) Displacement versus Scaled Ground Range - 1/4 Ton Trucks, WWII, Side-on, Light and Heavy Dust, n = 0.4

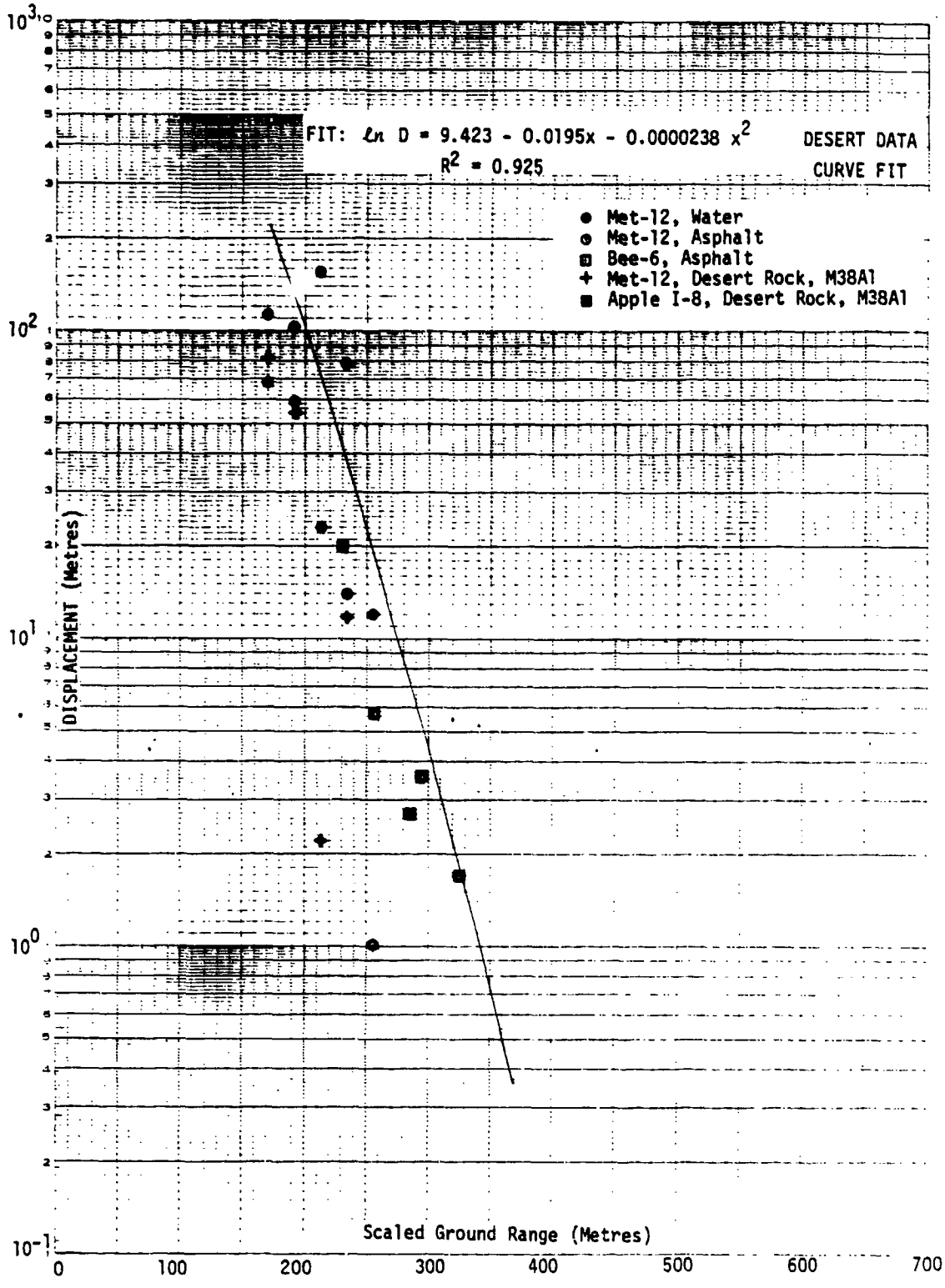

UNCLASSIFIED

FIGURE 3.5-1 (U) Displacement versus Scaled Ground Range - 1/4 Ton Trucks, WWII, Side-on, Light and Heavy Dust, n = 0.4, Desert Data Curve, Non-Desert Data Points

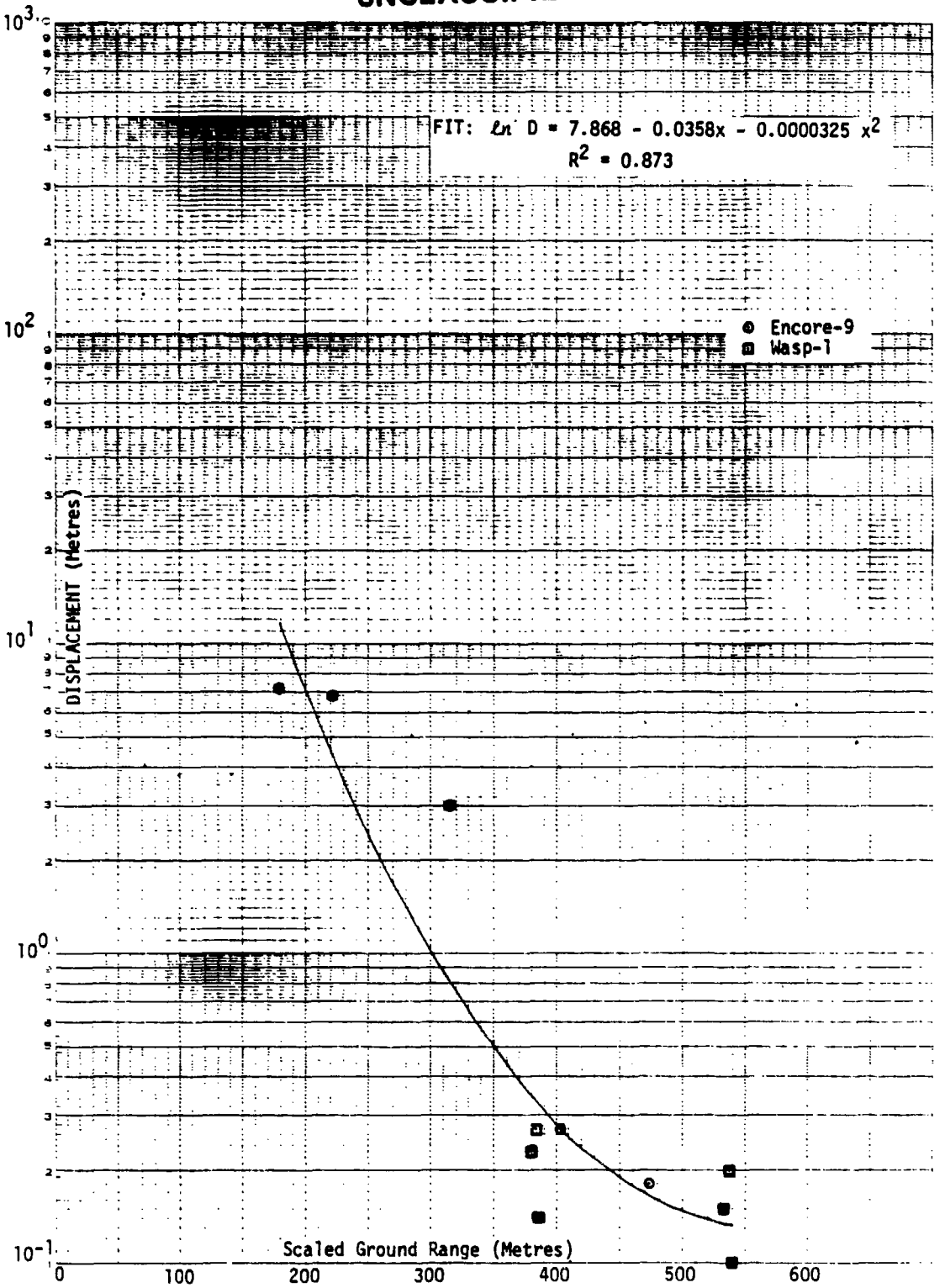

UNCLASSIFIED

FIGURE 3.6 (U) Displacement versus Scaled Ground Range - 1/4 Ton Trucks, M38A1, Side-on (Near-Ideal Air Burst), n = 0.43

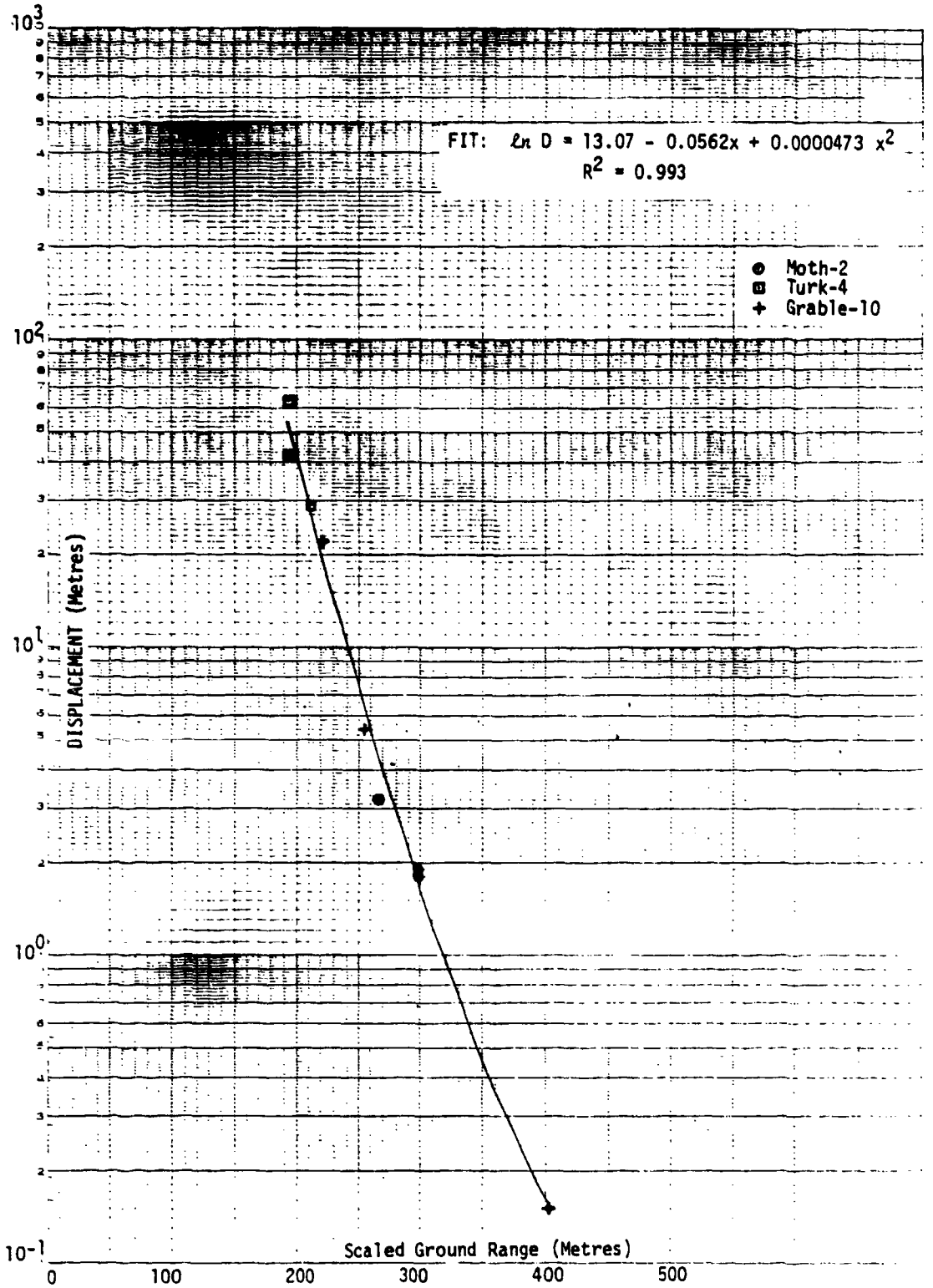

UNCLASSIFIED

FIGURE 3.7a (U) Displacement versus Scaled Ground Range - 1/4 Ton Trucks M38A1, Side-on, Light Dust, n = 0.43

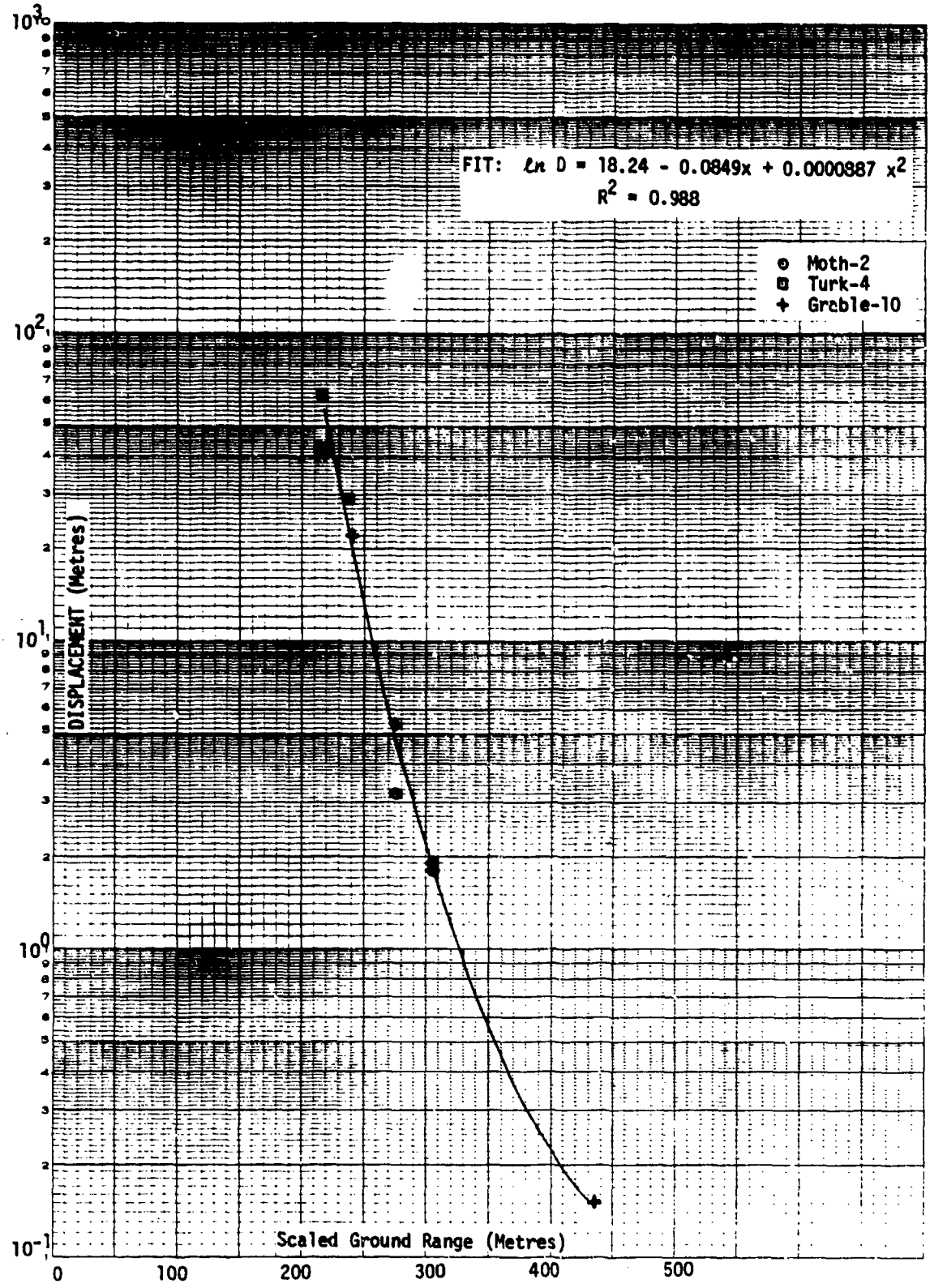

UNCLASSIFIED

FIGURE 3.7b (U) Displacement versus Scaled Ground Range - 1/4 Ton Trucks, M38A1, Side-on, Light Dust, n = 0.4

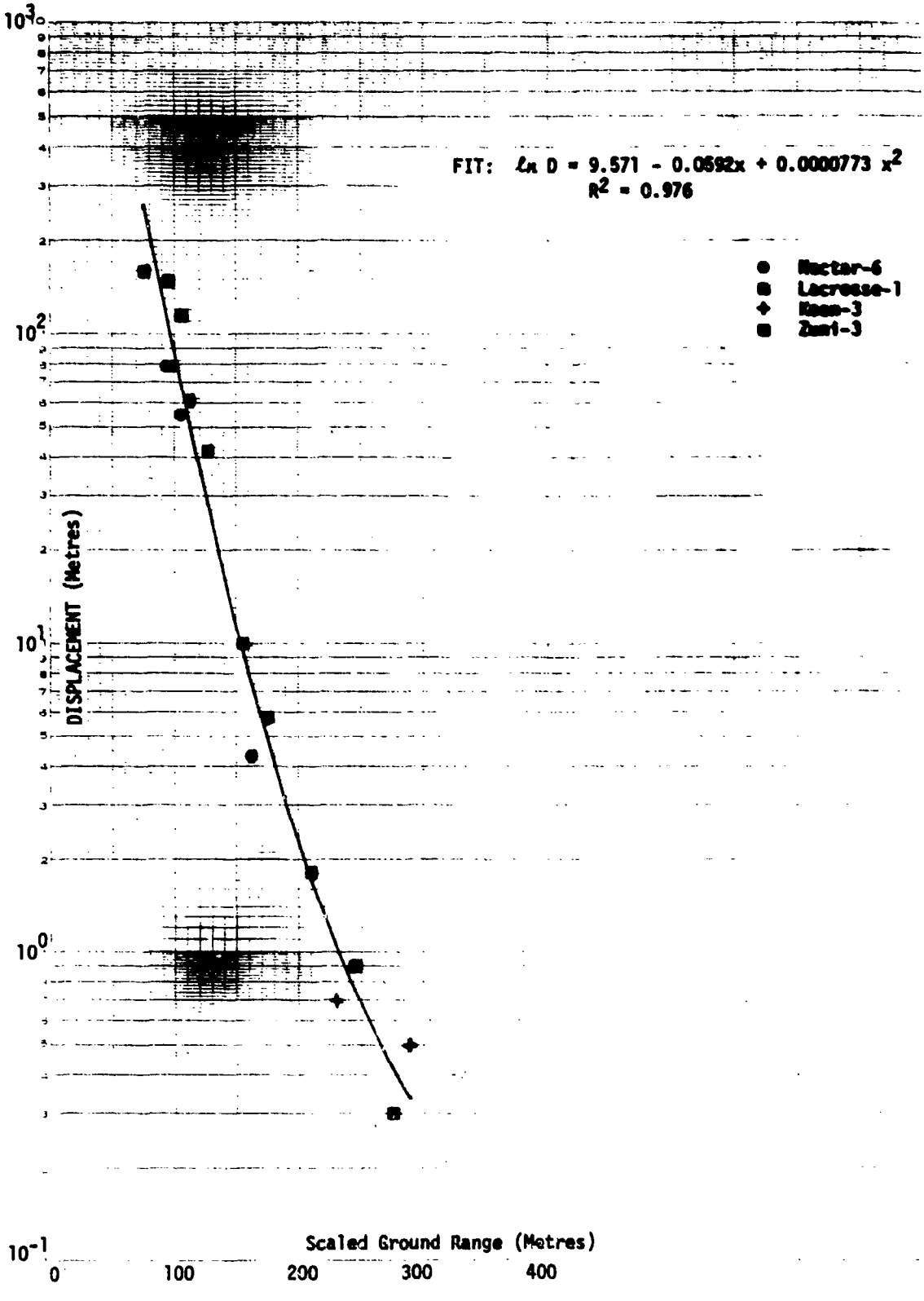

UNCLASSIFIED

FIGURE 3.8a (U) Displacement versus Scaled Ground Range - 1/4 Ton Trucks, WWII, Face-on, Near-Ideal Surface Burst, n = 0.43

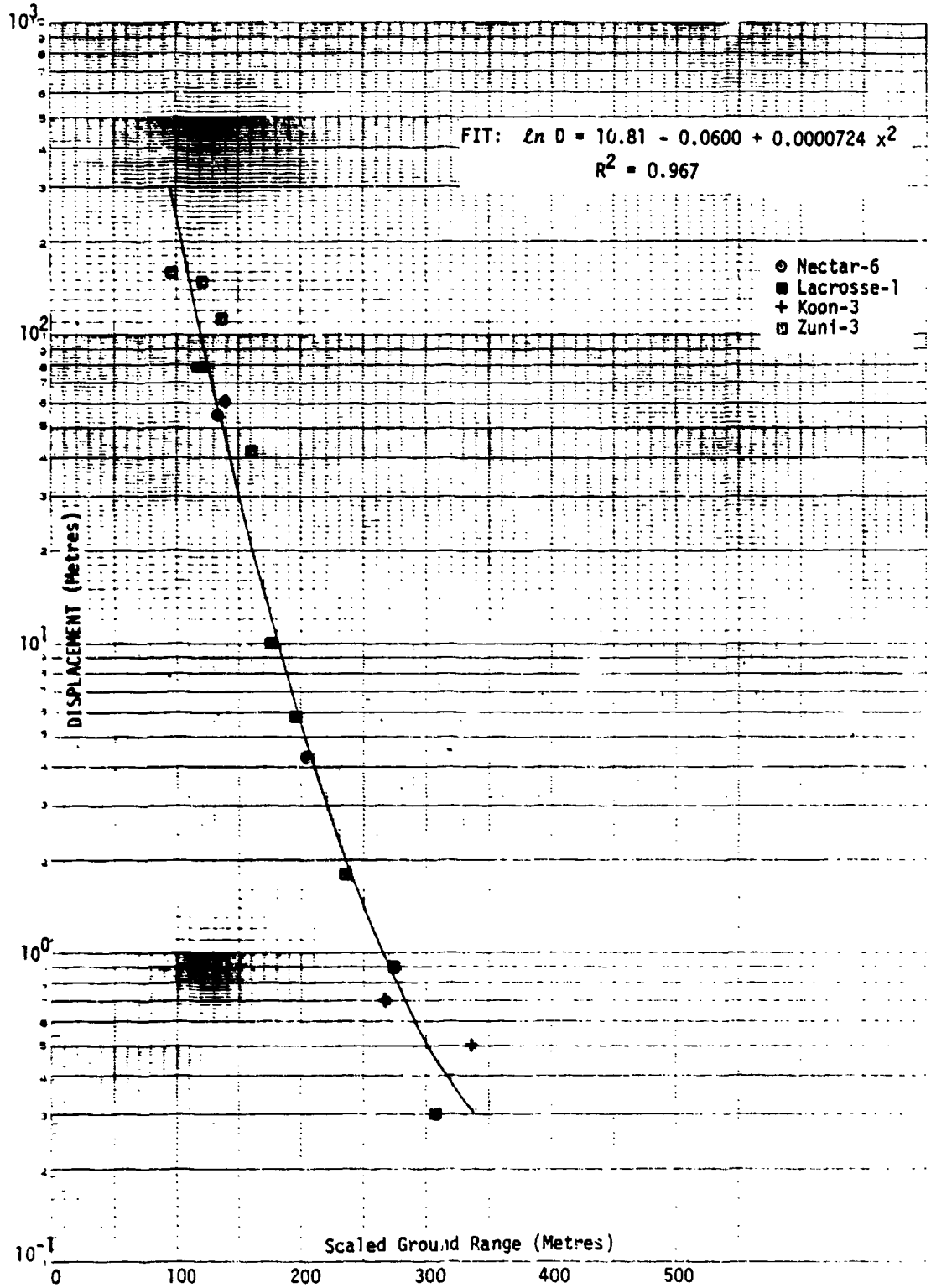

UNCLASSIFIED

FIGURE 3.8b (U) Displacement versus Scaled Ground Range - 1/4 Ton Trucks, WWII, Face-on, Near-Ideal Surface Burst, n = 0.4

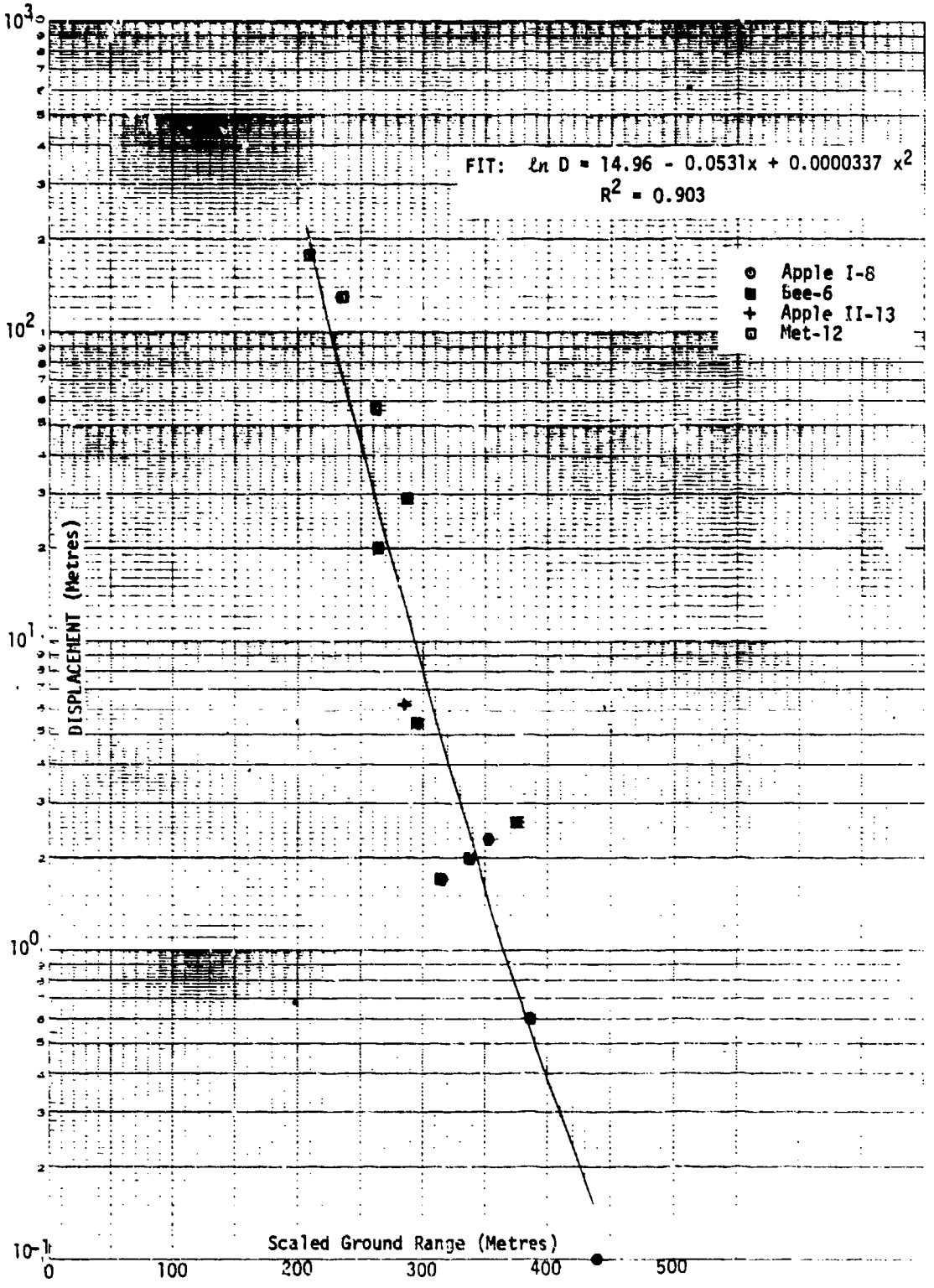

UNCLASSIFIED

FIGURE 3.9 (U) Displacement versus Scaled Ground Range - 1/4 Ton Trucks, WWII, Face-on, Light and Heavy Dust, n = 1/3

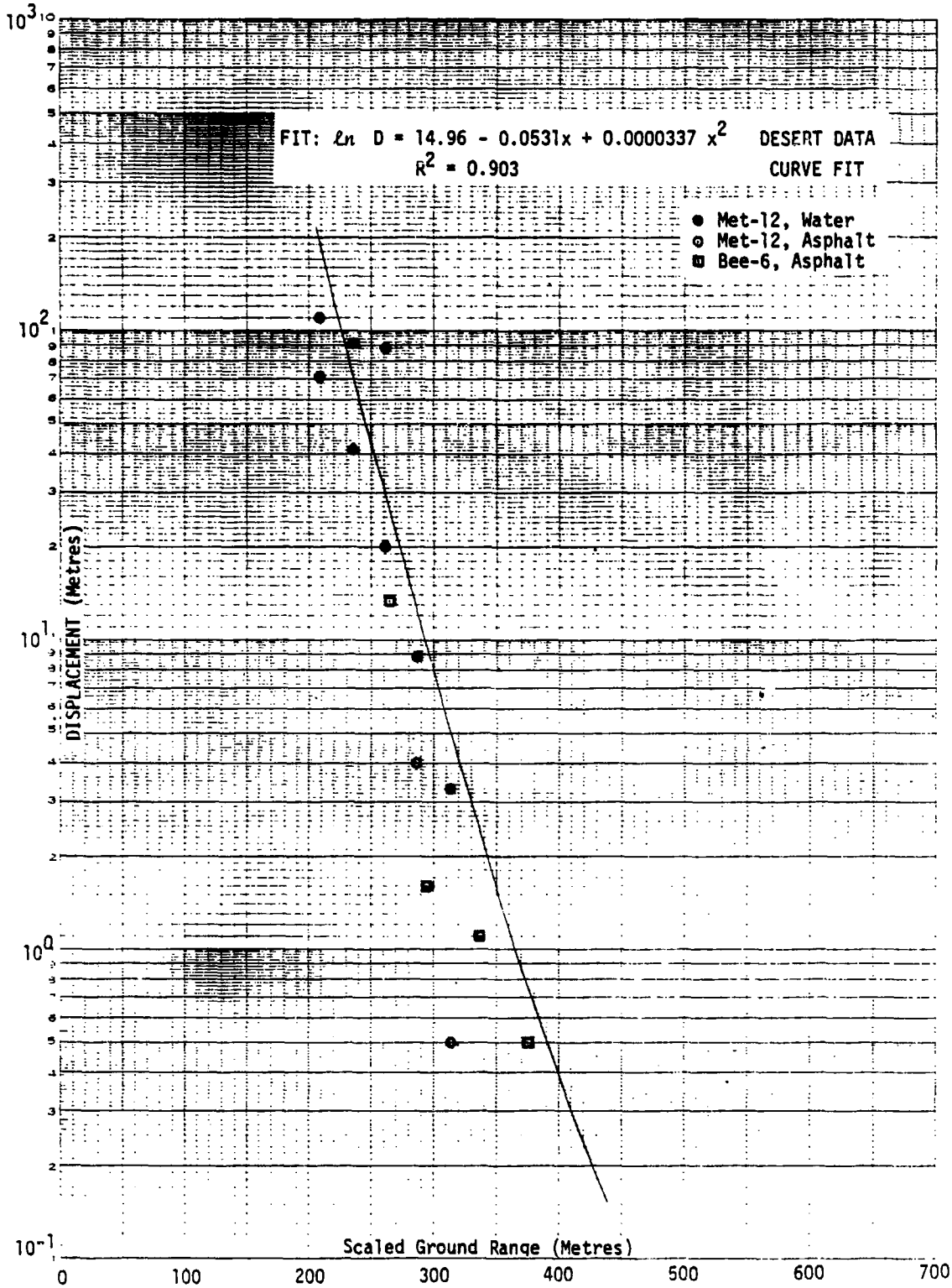

UNCLASSIFIED

FIGURE 3.9-1 (U) Displacement versus Scaled Ground Range - 1/4 Ton Trucks, WWII, Face-on, Light and Heavy Dust, n = 1/3, Desert Data Curve, Non-Desert Data Points

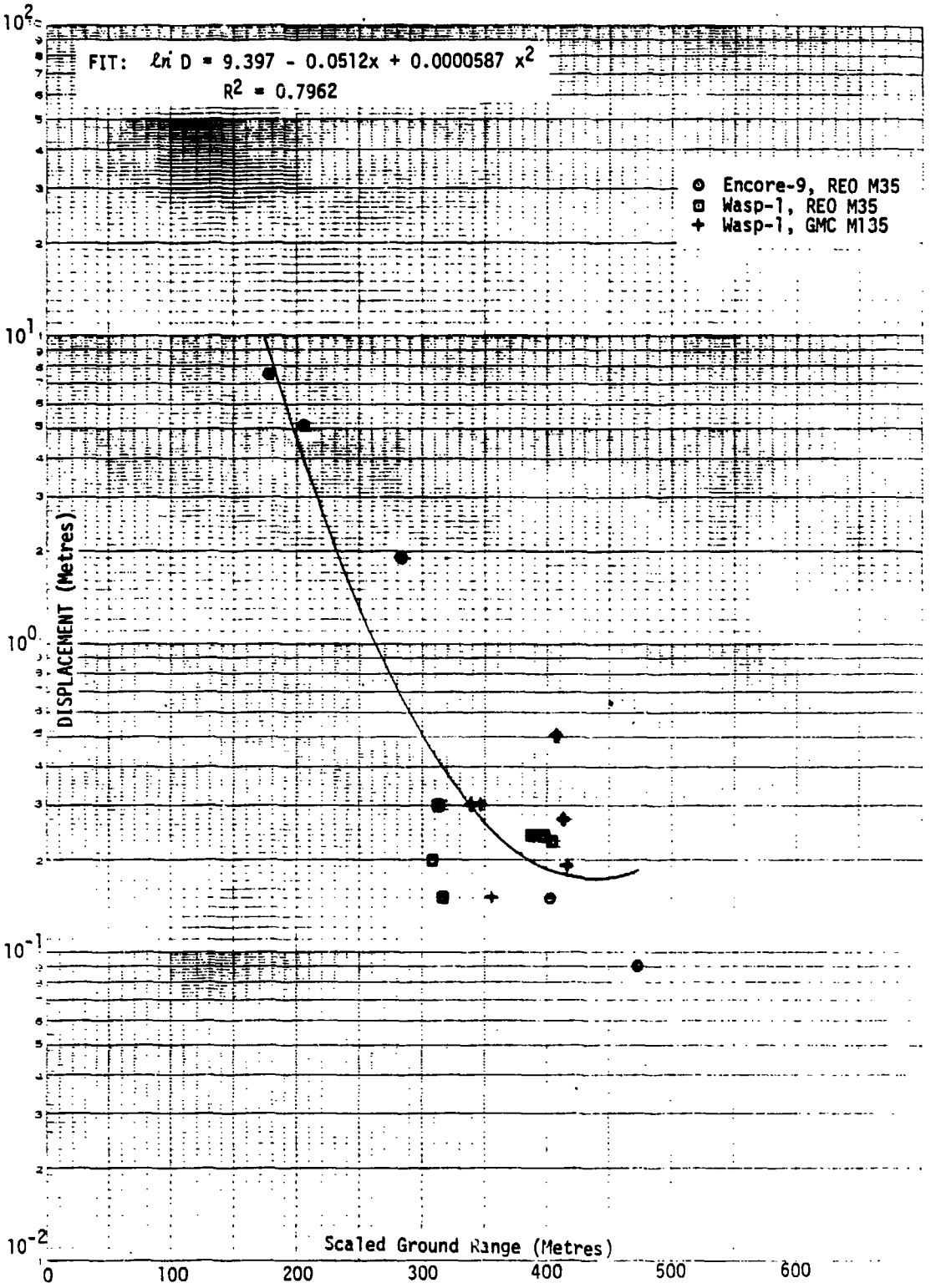

UNCLASSIFIED

FIGURE 3.10a (U) Displacement versus Scaled Ground Range - 2-1/2 Ton Trucks, REO M35 and GMC M135, Side-on, Near-Ideal Air Burst, n = 0.43

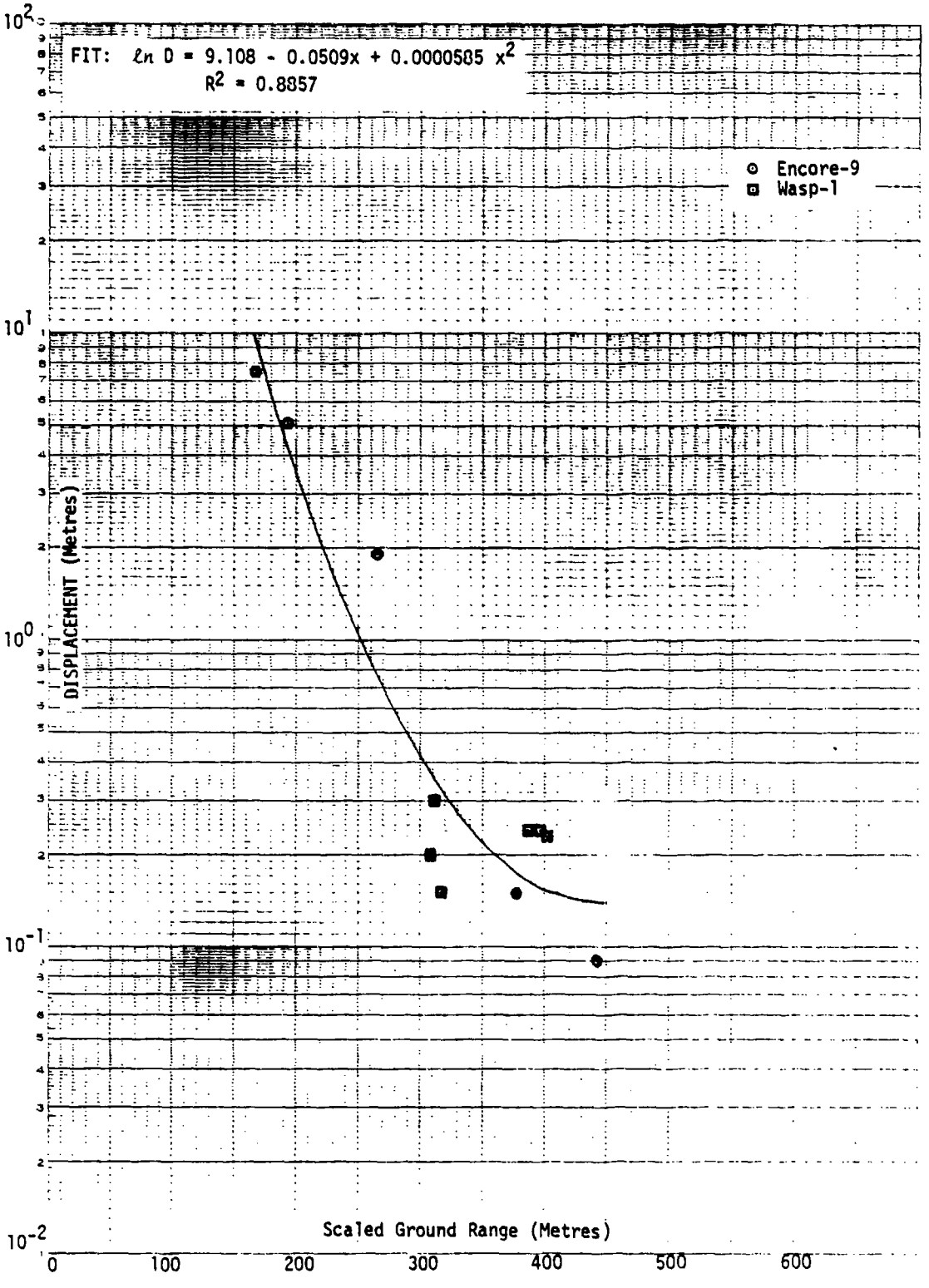

UNCLASSIFIED

FIGURE 3.10b (U) Displacement versus Scaled Ground Range - 2-1/2 Ton Trucks, REO M35, Side-on, Near-Ideal Air Burst, n = 0.45

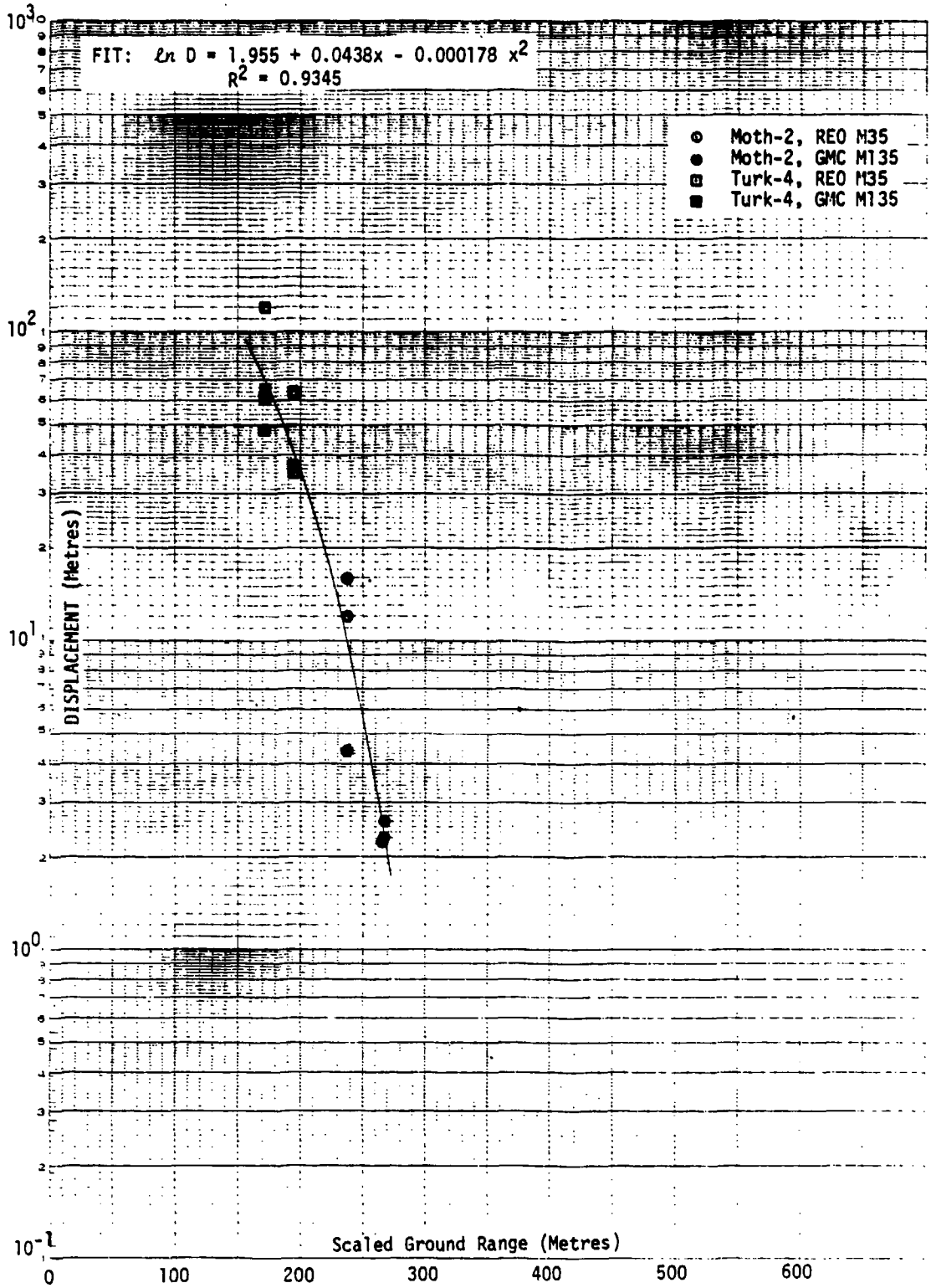

UNCLASSIFIED

FIGURE 3.11 (U) Displacement versus Scaled Ground Range - 2-1/2 Ton Trucks, REO M35 and GMC M135, Side-on, Light Dust, n = 0.43

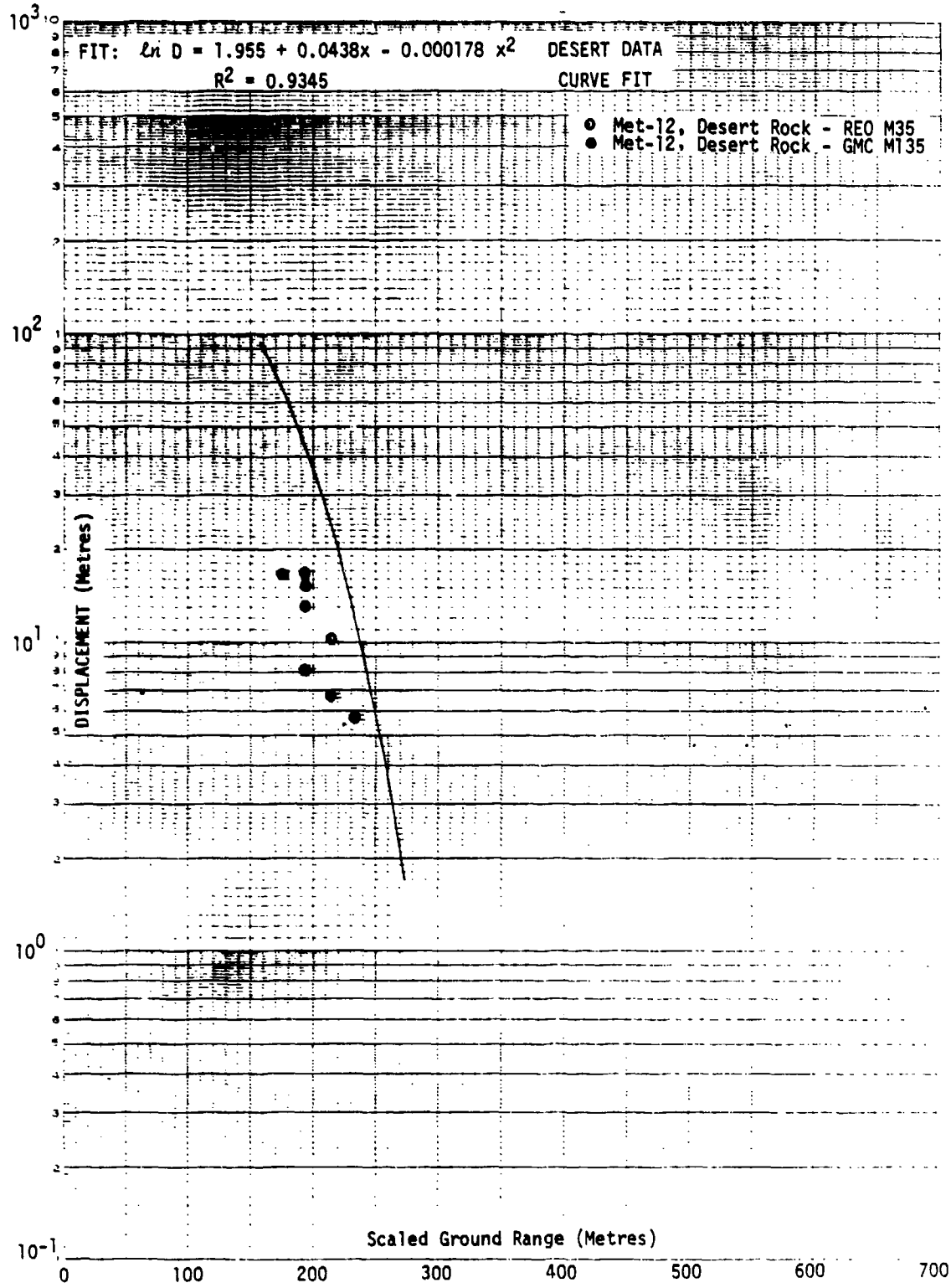

UNCLASSIFIED

FIGURE 3.11-1 (U) Displacement versus Scaled Ground Range - 2-1/2 Ton Trucks, REO M35 and GMC M135, Side-on, Light Dust, n = 0.43, Desert Data Curve, Non-Desert Data Points

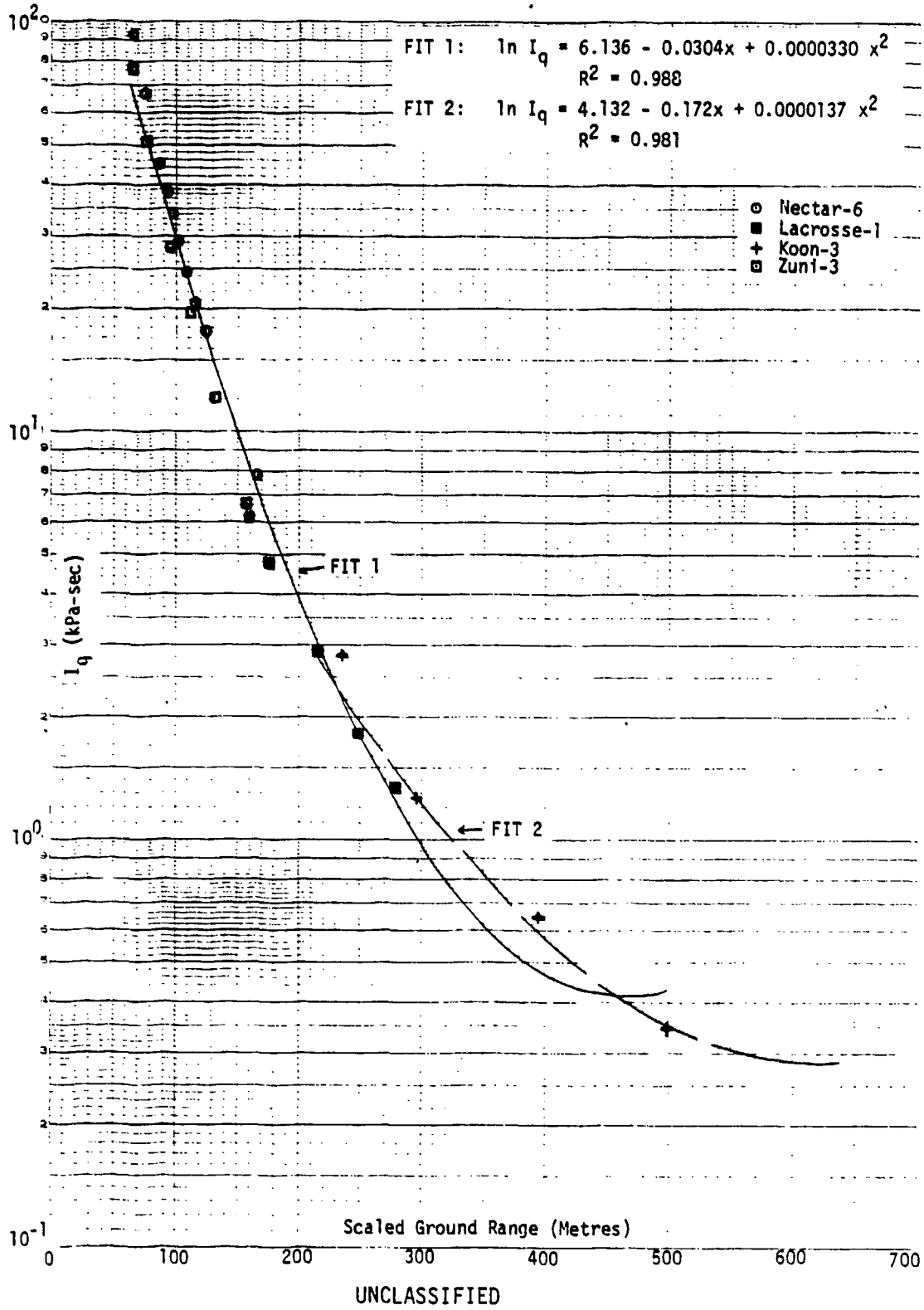

UNCLASSIFIED

FIGURE 3.12a (U) Dynamic Pressure Impulse versus Scaled Ground Range - Near-Ideal Surface Burst, n = 0.425

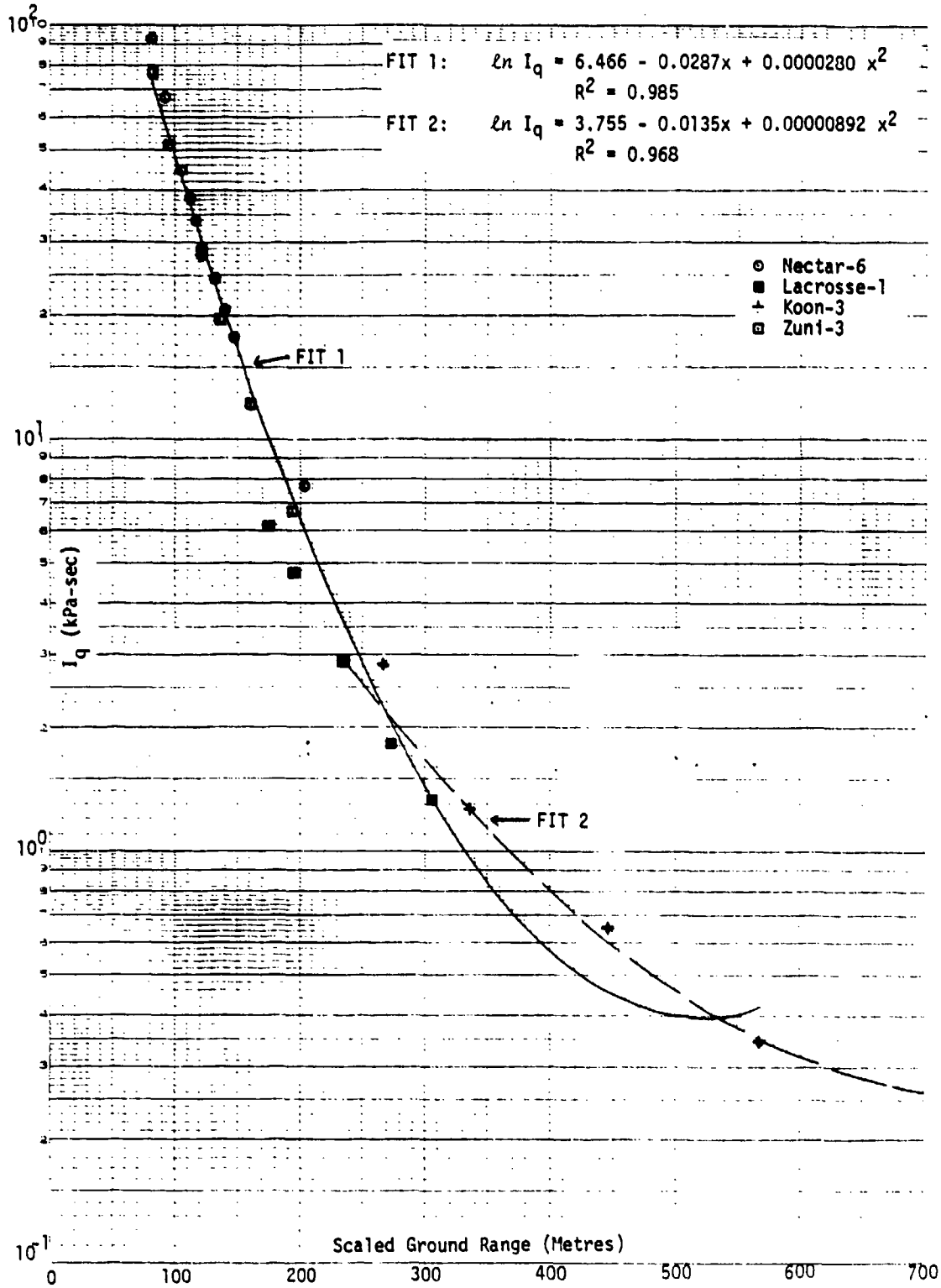

UNCLASSIFIED

FIGURE 3.12b (U) Dynamic Pressure Impulse versus Scaled Ground Range - Near-Ideal Surface Burst, n = 0.4

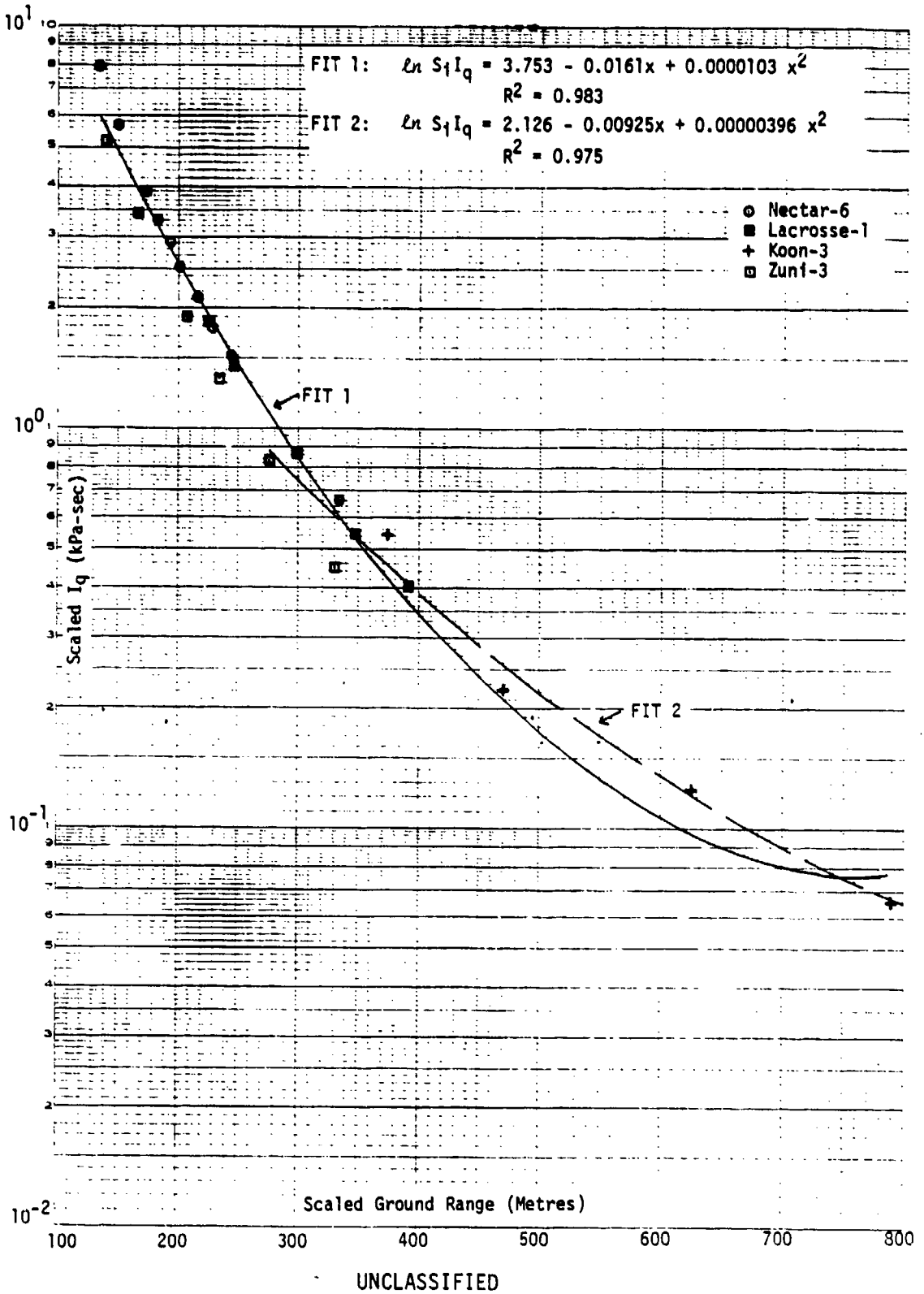

FIGURE 3.13 (U) Scaled Dynamic Pressure Impulse versus Scaled Ground Range - Near-Ideal Surface Burst

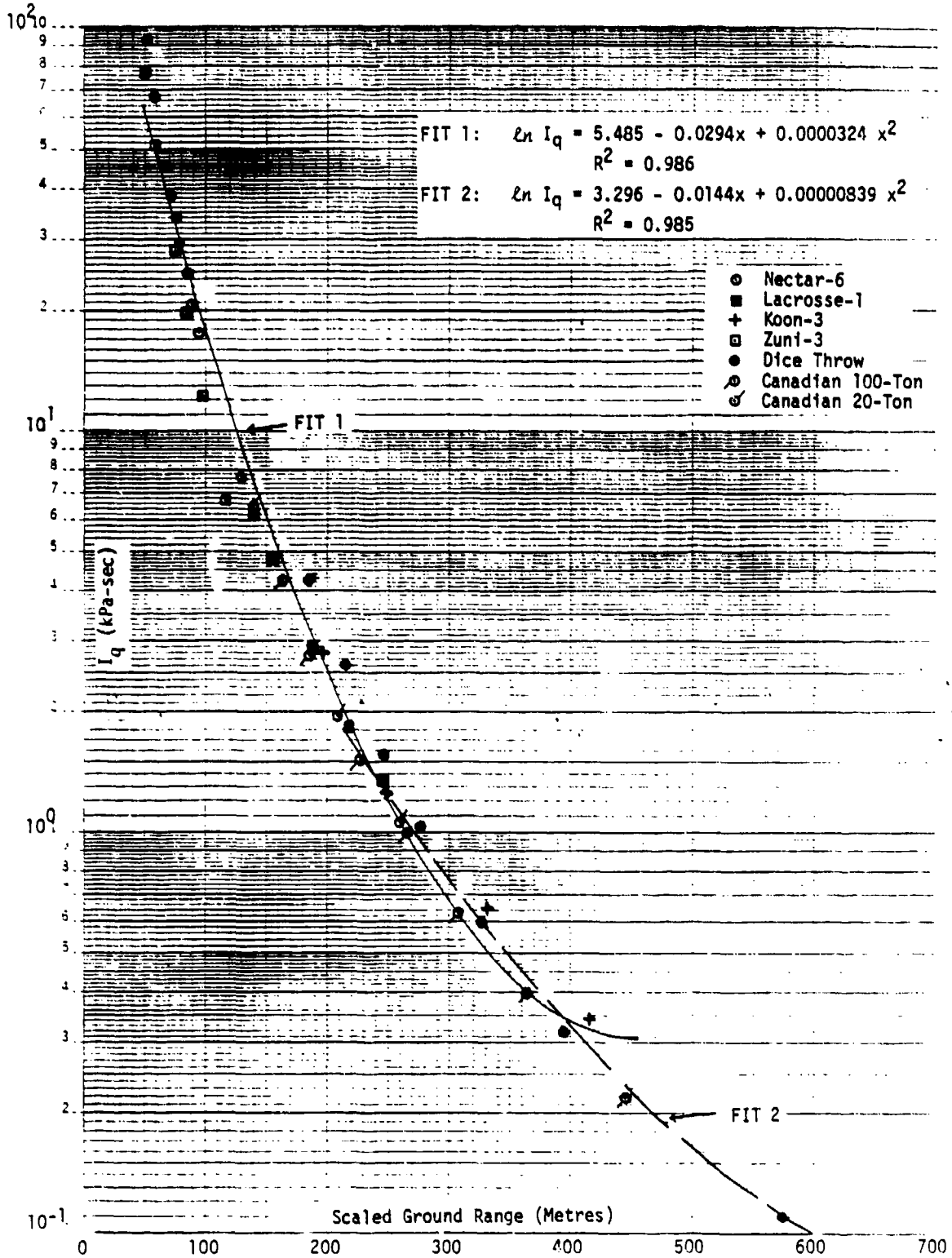

UNCLASSIFIED

FIGURE 3.14 (U) Dynamic Pressure Impulse versus Scaled Ground Range - Near-Ideal Surface Burst, n = 0.46

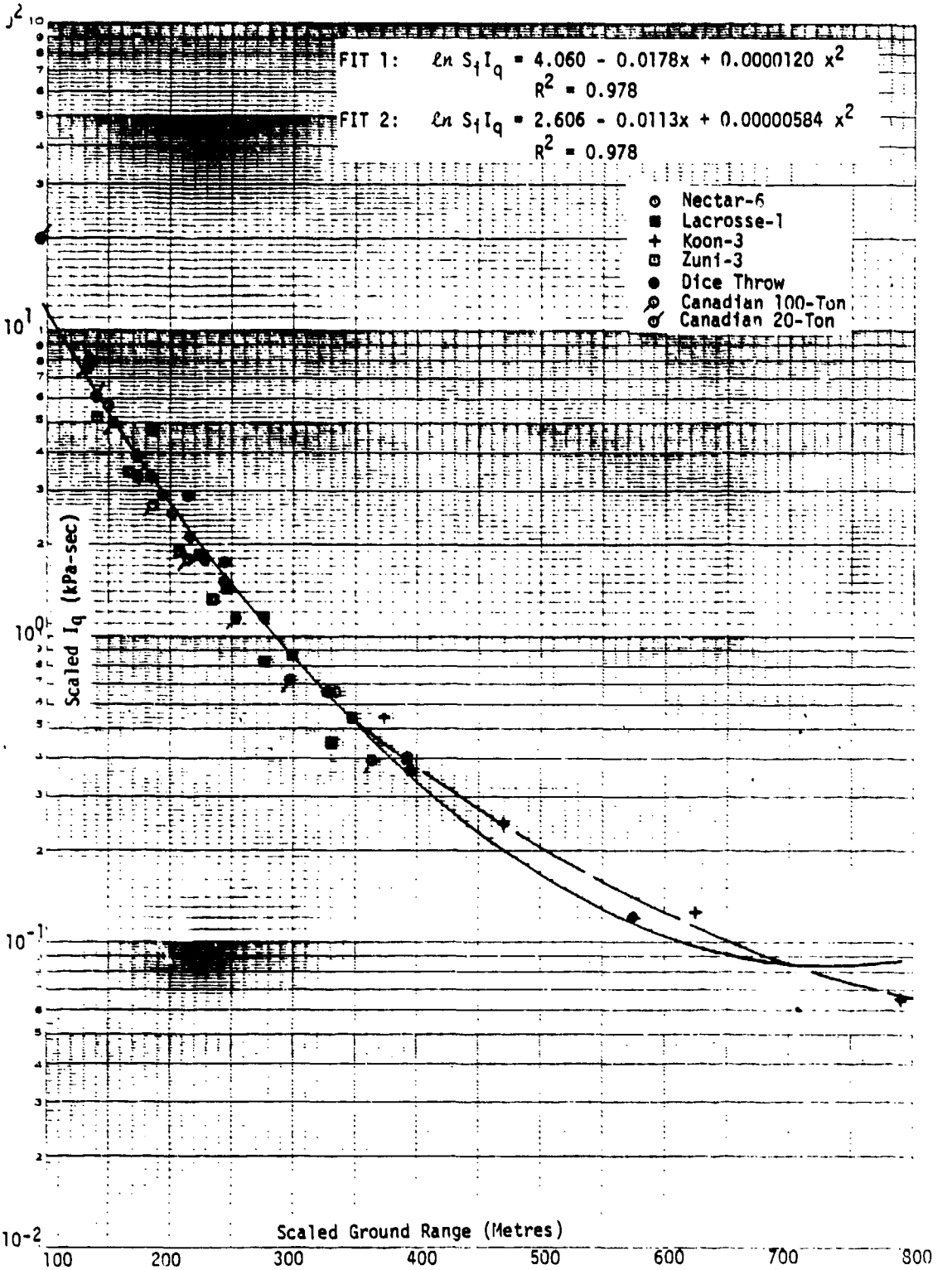

UNCLASSIFIED

FIGURE 3.15 (U) Scaled Dynamic Pressure Impulse versus Scaled Ground Range - Near-Ideal Surface Burst

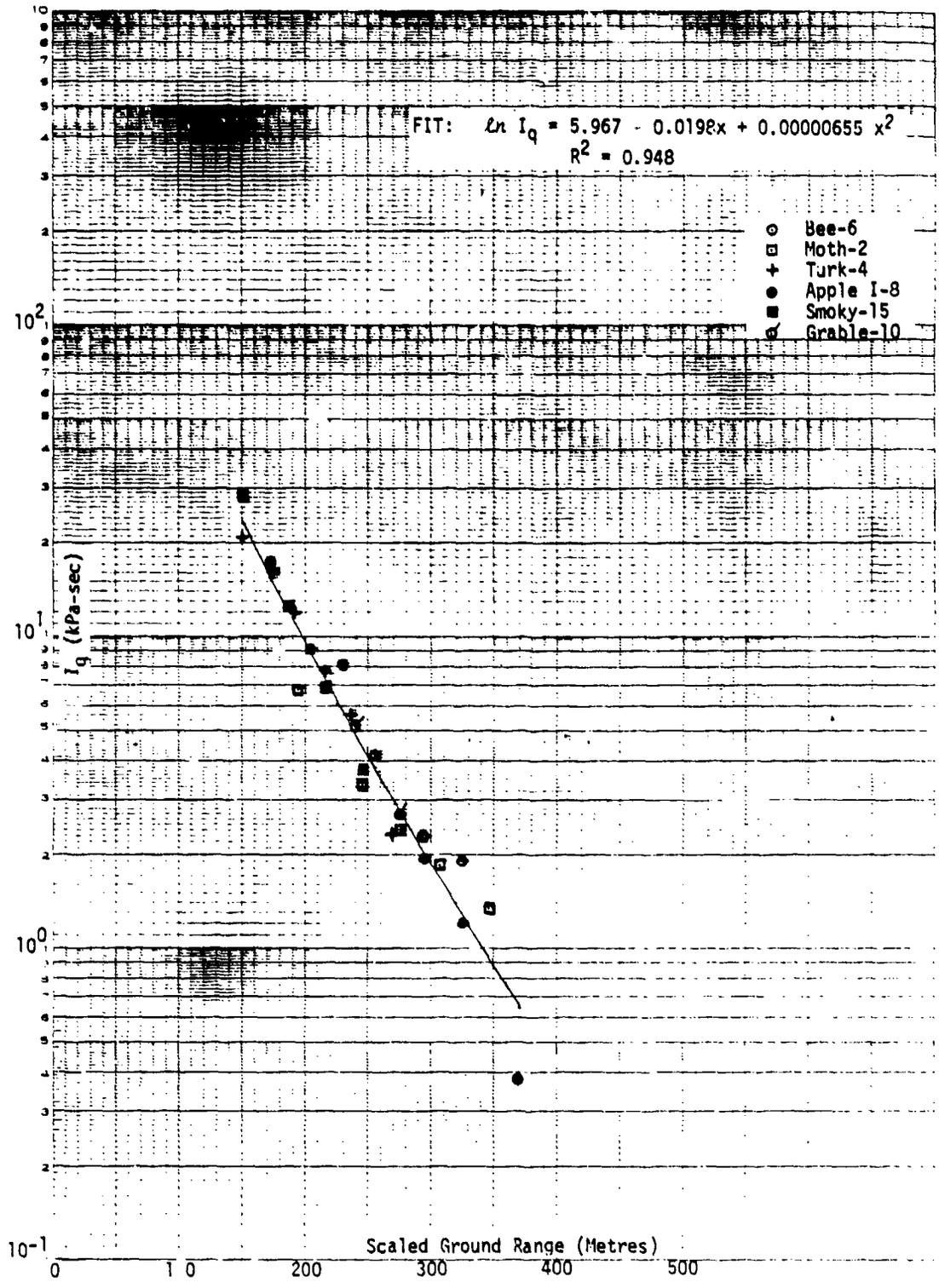

UNCLASSIFIED

FIGURE 3.16a (U) Dynamic Pressure Impulse versus Scaled Ground Range - Light Dust, n = 0.4

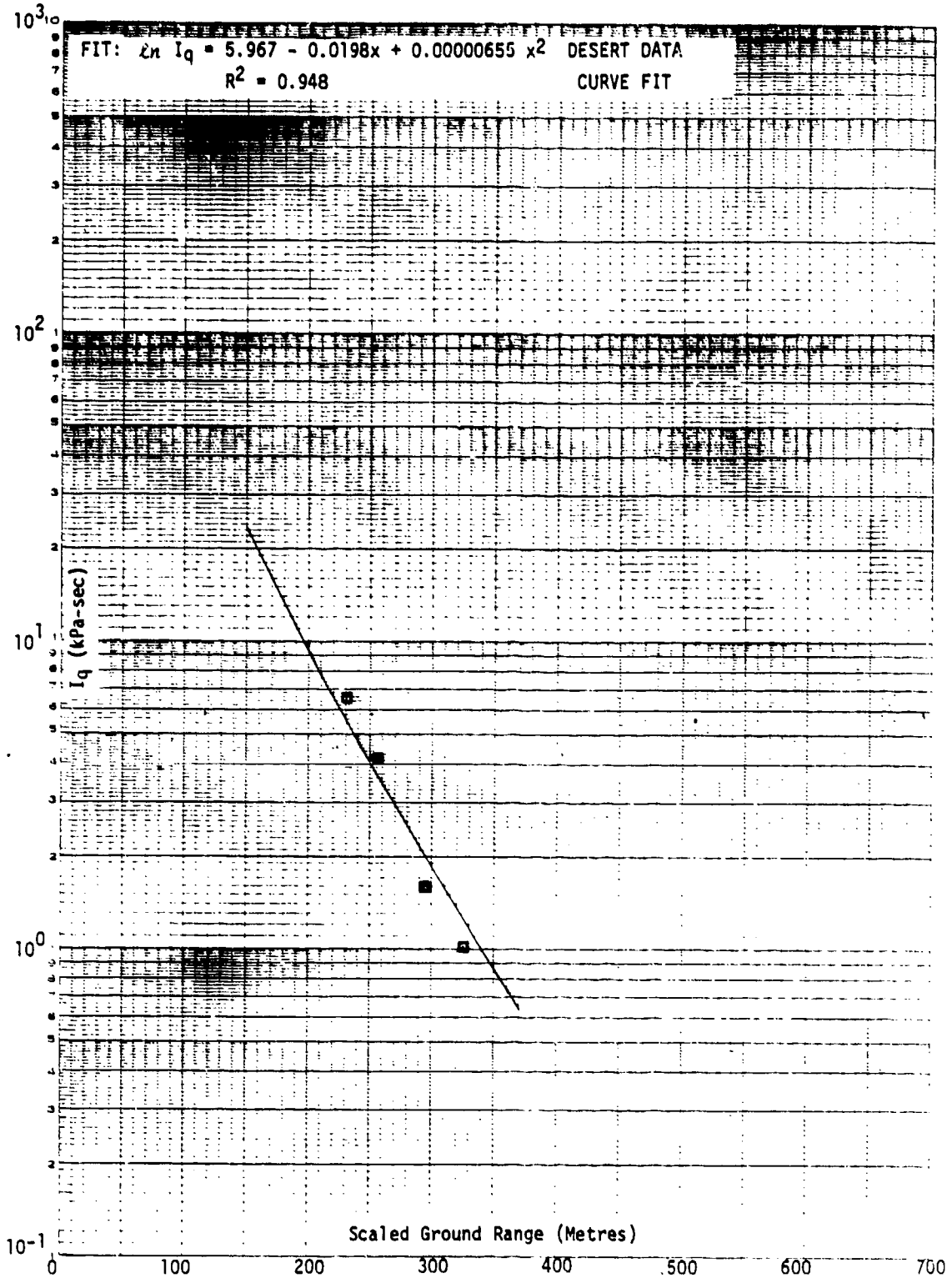

UNCLASSIFIED

FIGURE 3.16a-1 (U) Dynamic Pressure Impulse versus Scaled Ground Range - Light Dust, n = 0.4, Desert Data Curve, Non-Desert Data Points, Bee-6, Asphalt

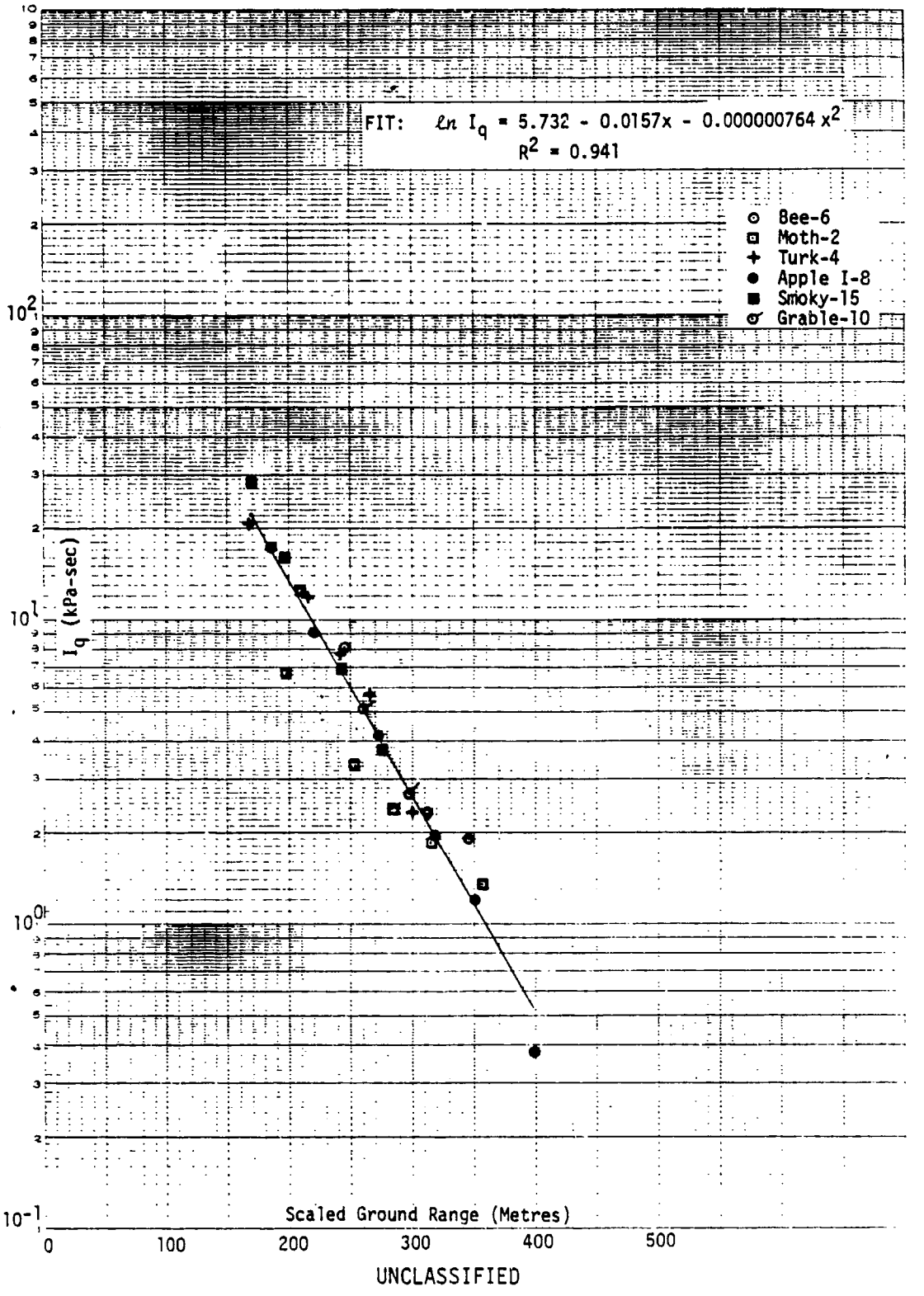

FIGURE 3.16b (U) Dynamic Pressure Impulse versus Scaled Ground Range - Light Dust, n = 0.37

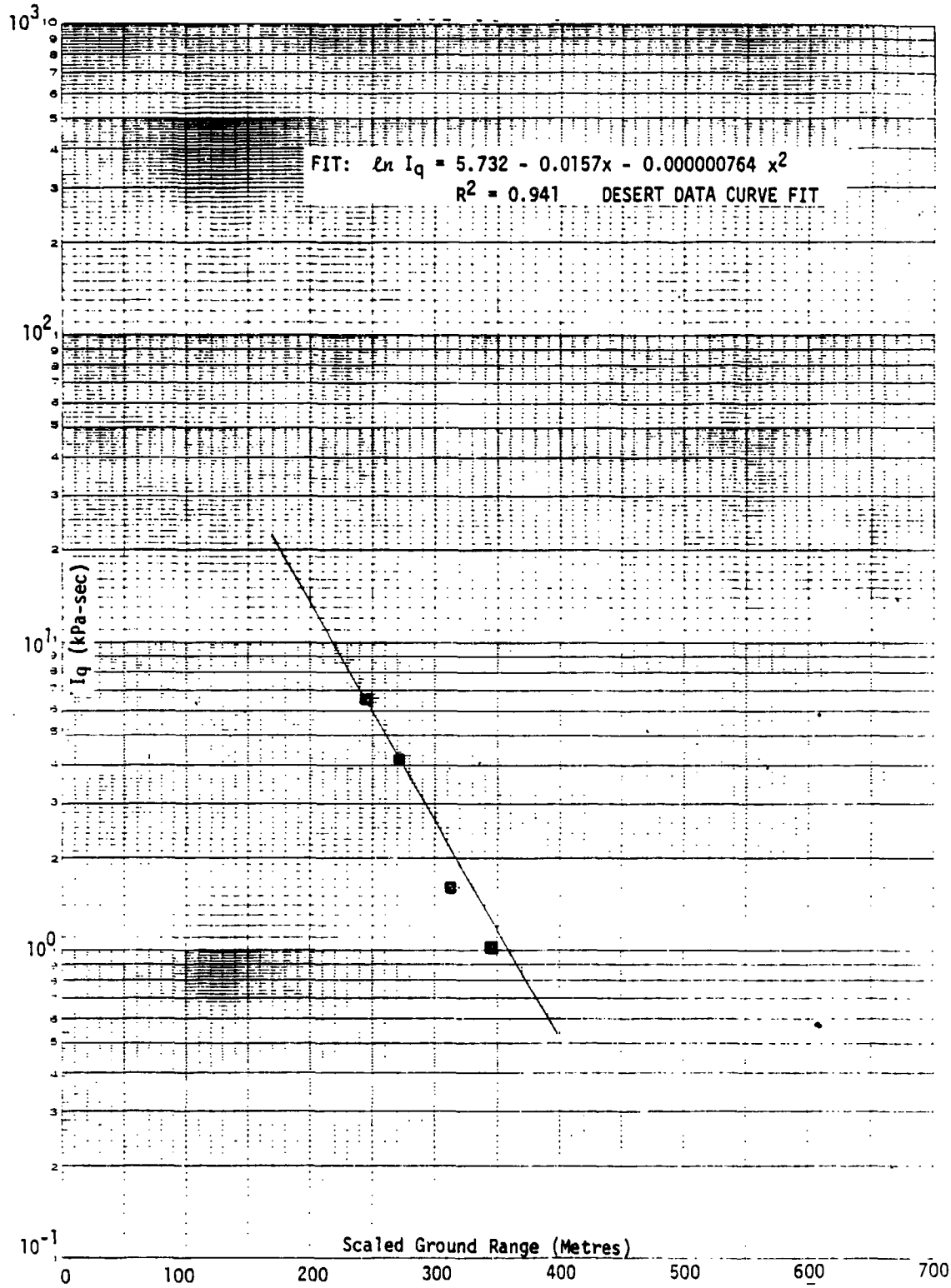

UNCLASSIFIED

FIGURE 3.16b-1 (U) Dynamic Pressure Impulse versus Scaled Ground Range - Light Dust, n = 0.37, Desert Data Curve, Non-Desert Data Points, Bee-6, Asphalt

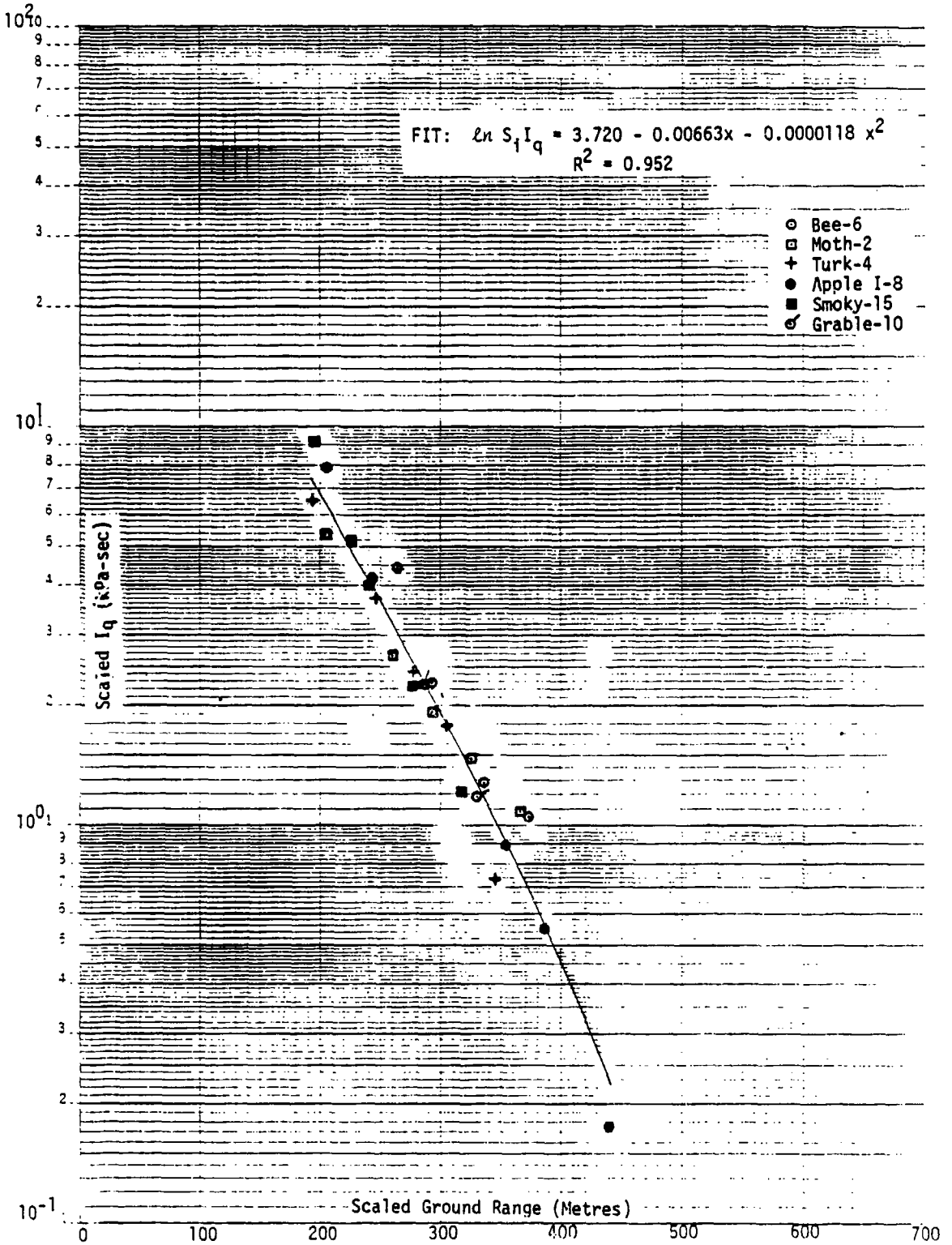

UNCLASSIFIED

FIGURE 3.17 (U) Scaled Dynamic Pressure Impulse versus Scaled Ground Range - Light Dust

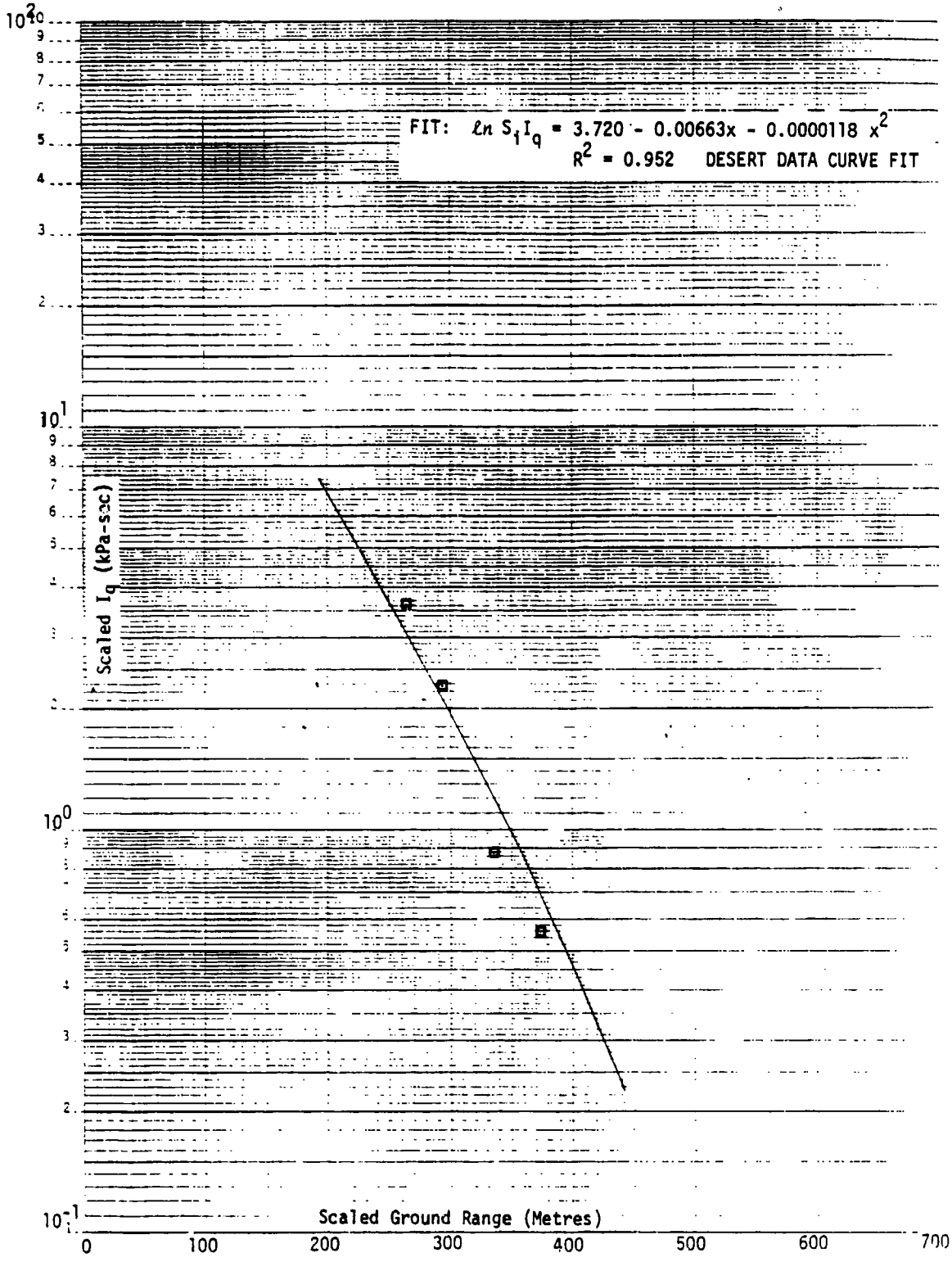

UNCLASSIFIED

FIGURE 3.17-1 (U) Scaled Dynamic Pressure Impulse versus Scaled Ground Range - Light Dust, Desert Data Curve, Non-Desert Data Points, Bee-6, Asphalt

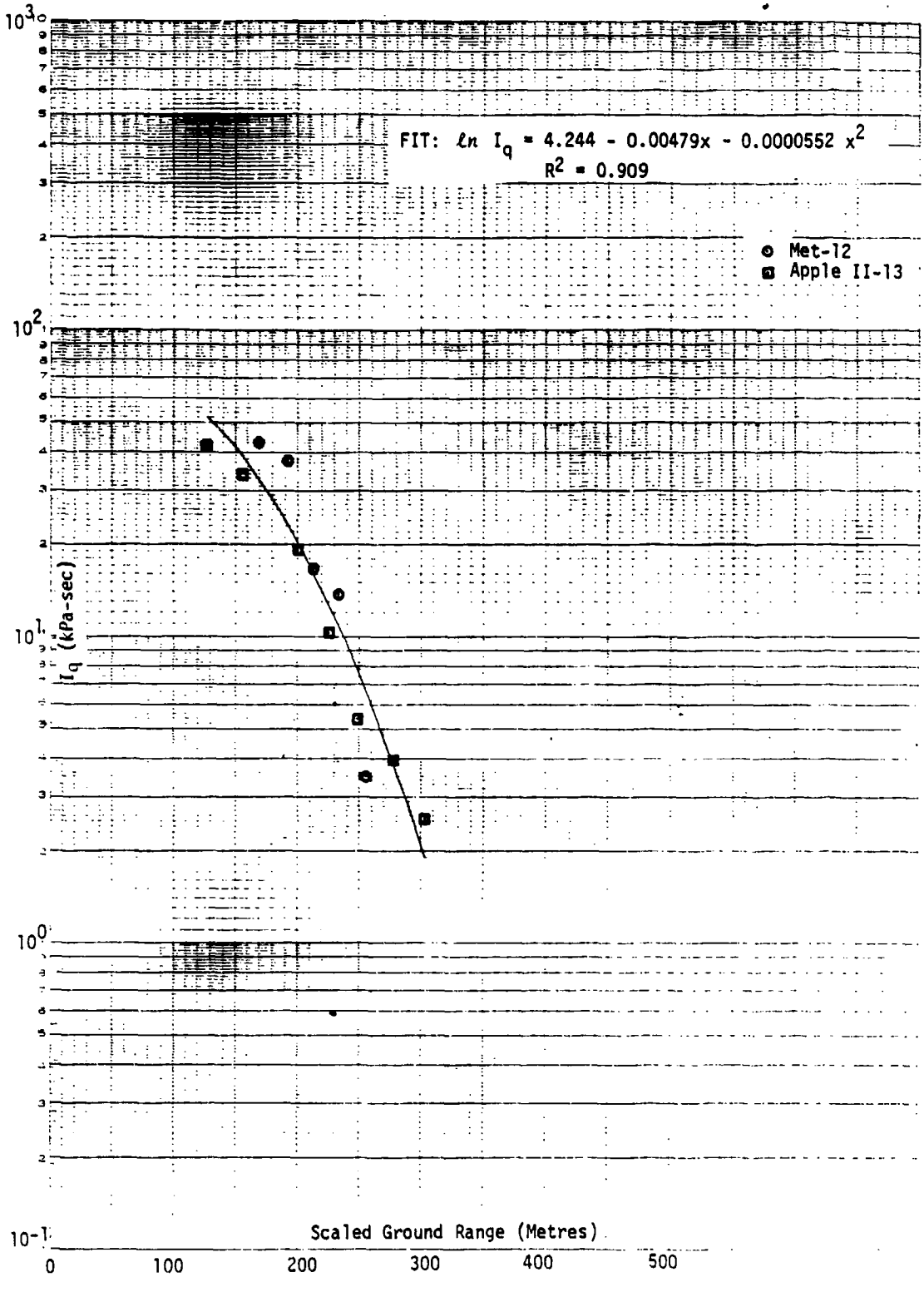

UNCLASSIFIED

FIGURE 3.18 (U) Dynamic Pressure Impulse versus Scaled Ground Range - Heavy Dust, n = 0.4

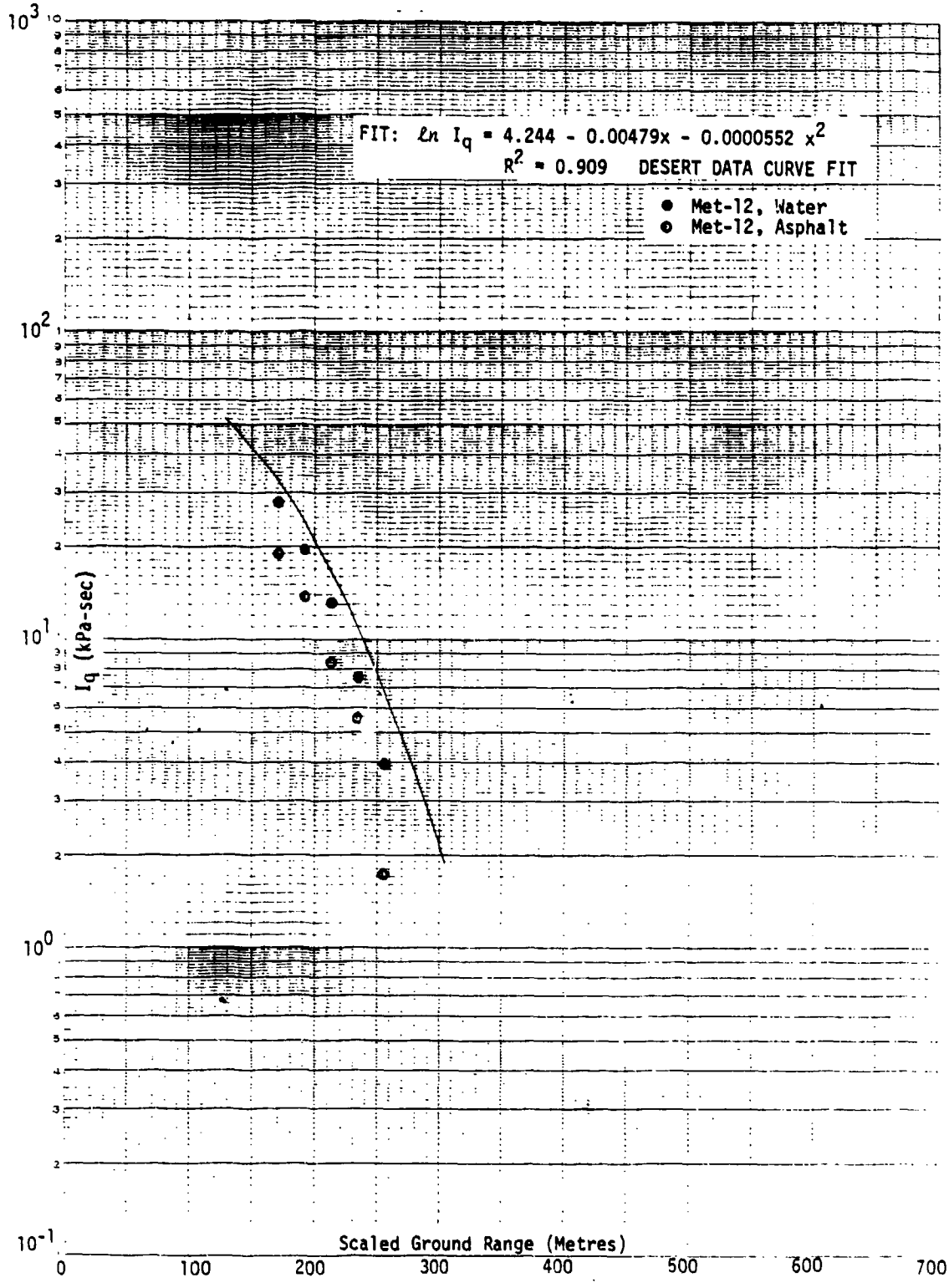

UNCLASSIFIED

FIGURE 3.18-1 (U) Dynamic Pressure Impulse versus Scaled Ground Range - Heavy Dust, n = 0.4, Desert Data Curve, Non-Desert Data Points

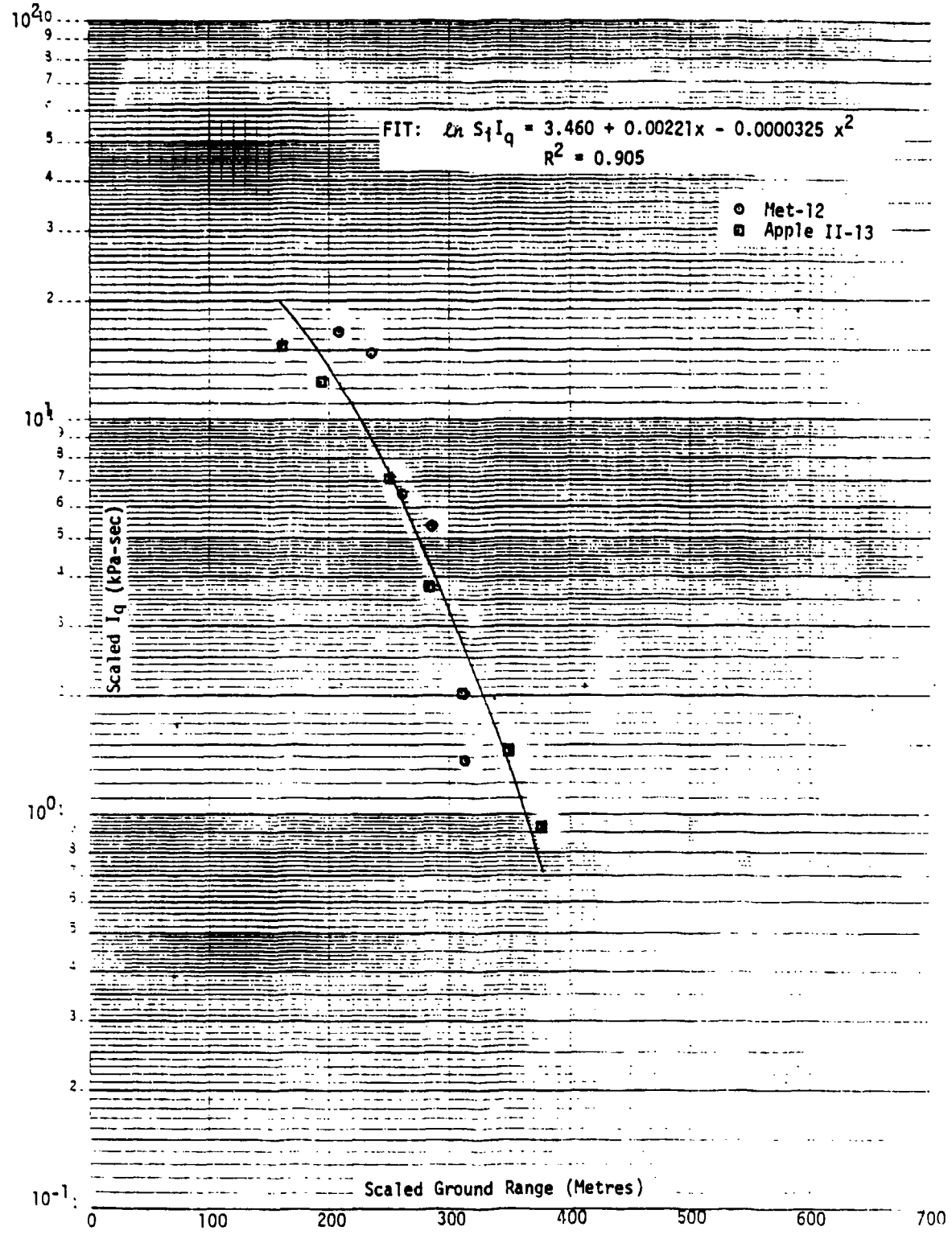

UNCLASSIFIED

FIGURE 3.19 (U) Scaled Dynamic Pressure Impulse versus Scaled Ground Range - Heavy Dust

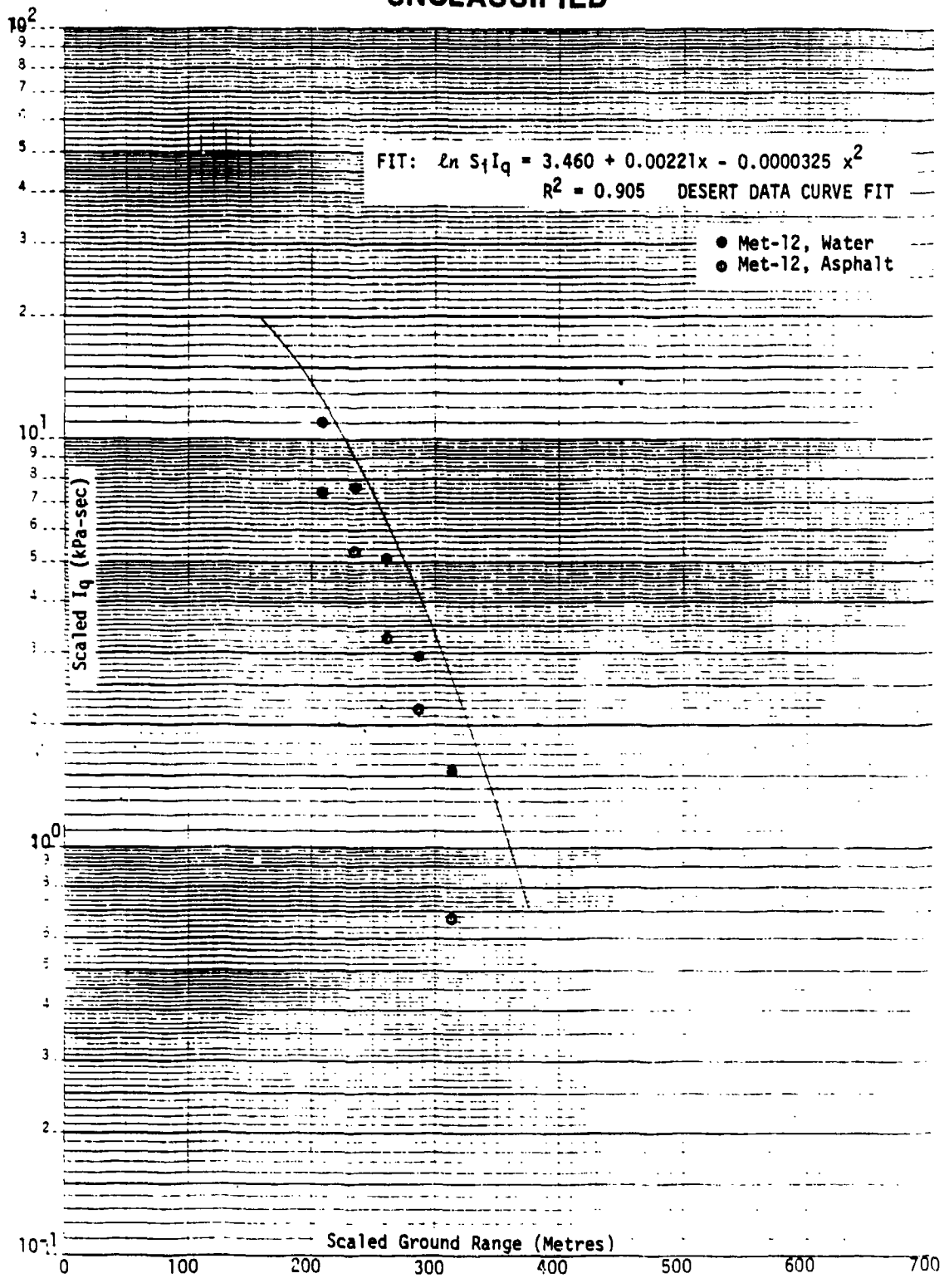

FIGURE 3.19-1 (U) Scaled Dynamic Pressure Impulse versus Scaled Ground Range - Heavy Dust, Desert Data Curve, Non-Desert Data Points

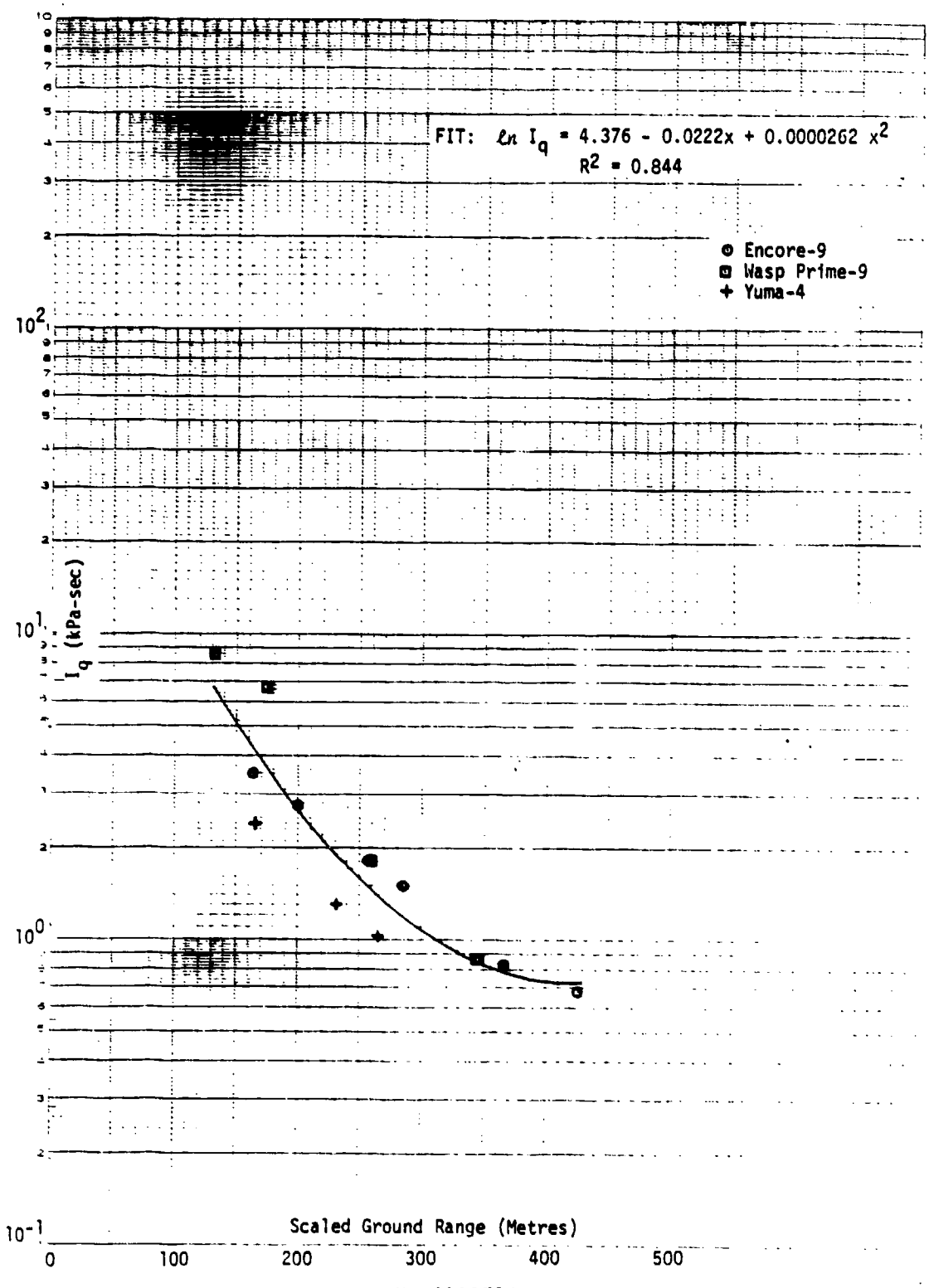

UNCLASSIFIED

FIGURE 3.20a (U) Dynamic Pressure Impulse versus Scaled Ground Range - Near-Ideal Air Burst, n = 0.46

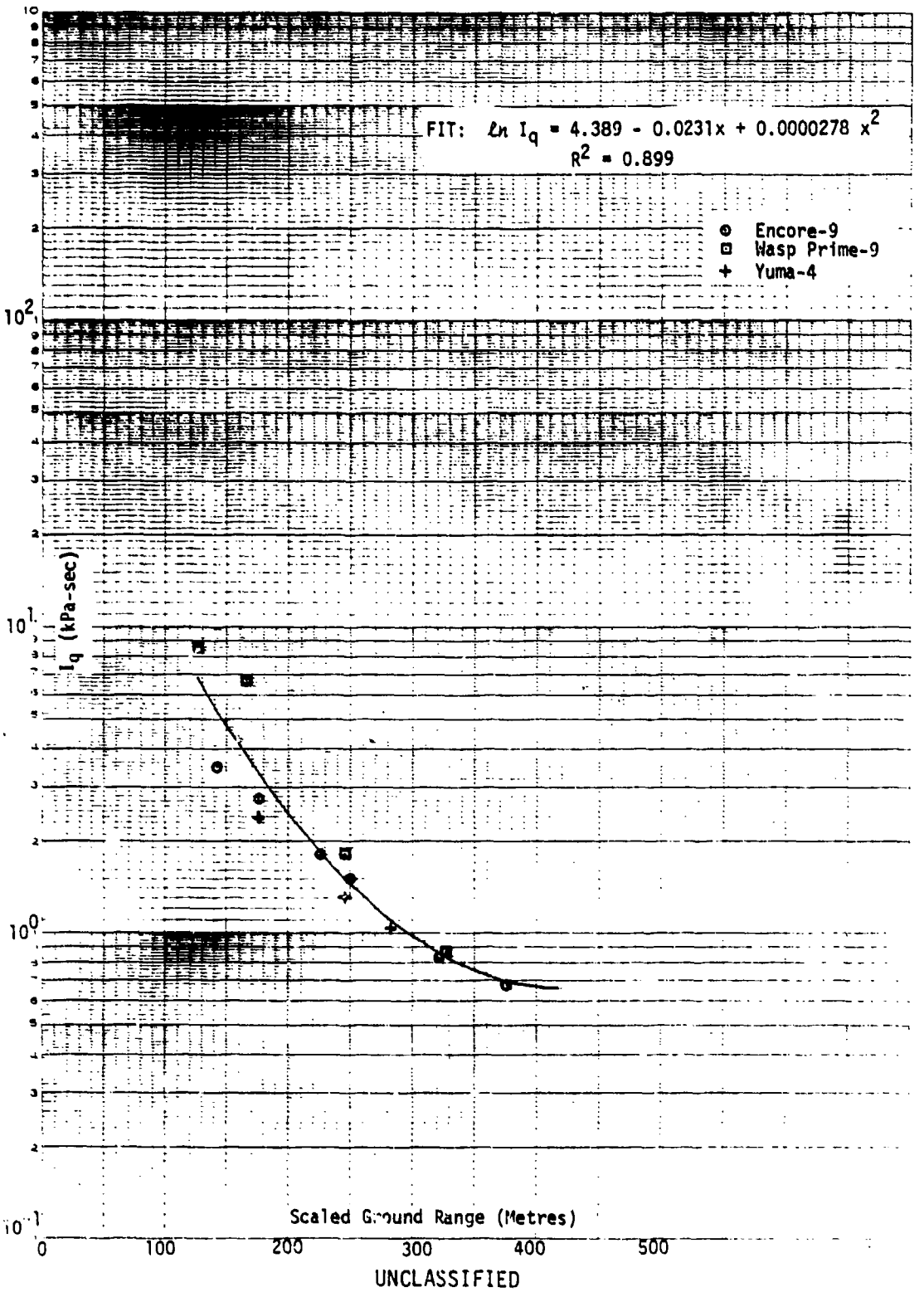

UNCLASSIFIED

FIGURE 3.20b (U) Dynamic Pressure Impulse versus Scaled Ground Range - Near-Ideal Air Burst, n = 0.50

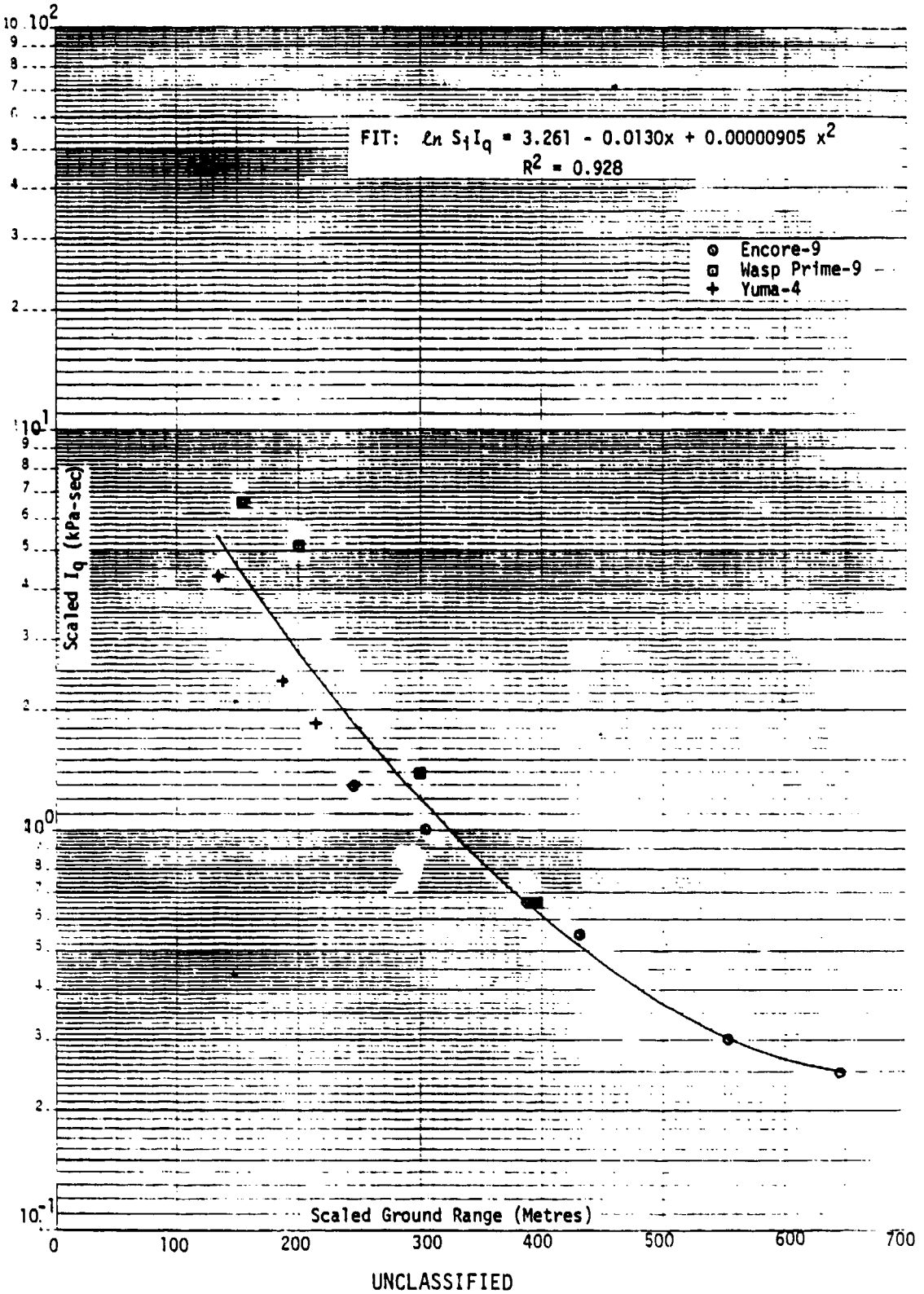

UNCLASSIFIED

FIGURE 3.21 (U) Scaled Dynamic Pressure Impulse versus Scaled Ground Range - Near-Ideal Air Burst

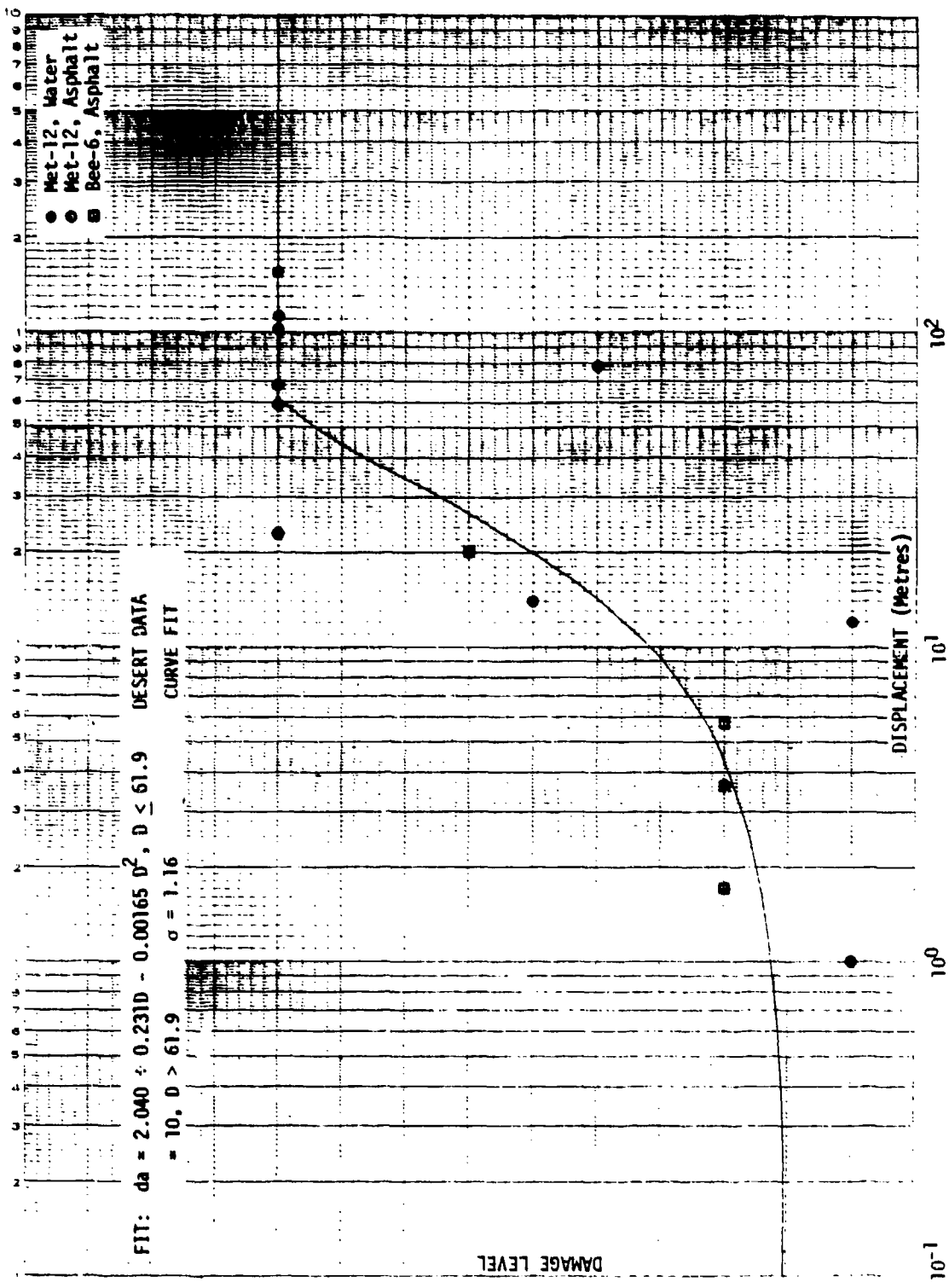

FIGURE 3.1-1 (U) Damage versus Displacement - 1/4 Ton Trucks, WWII, Side-on, (Reference 17) Desert Data Curve, Non-Desert Data Points (Yield > 1 KT)

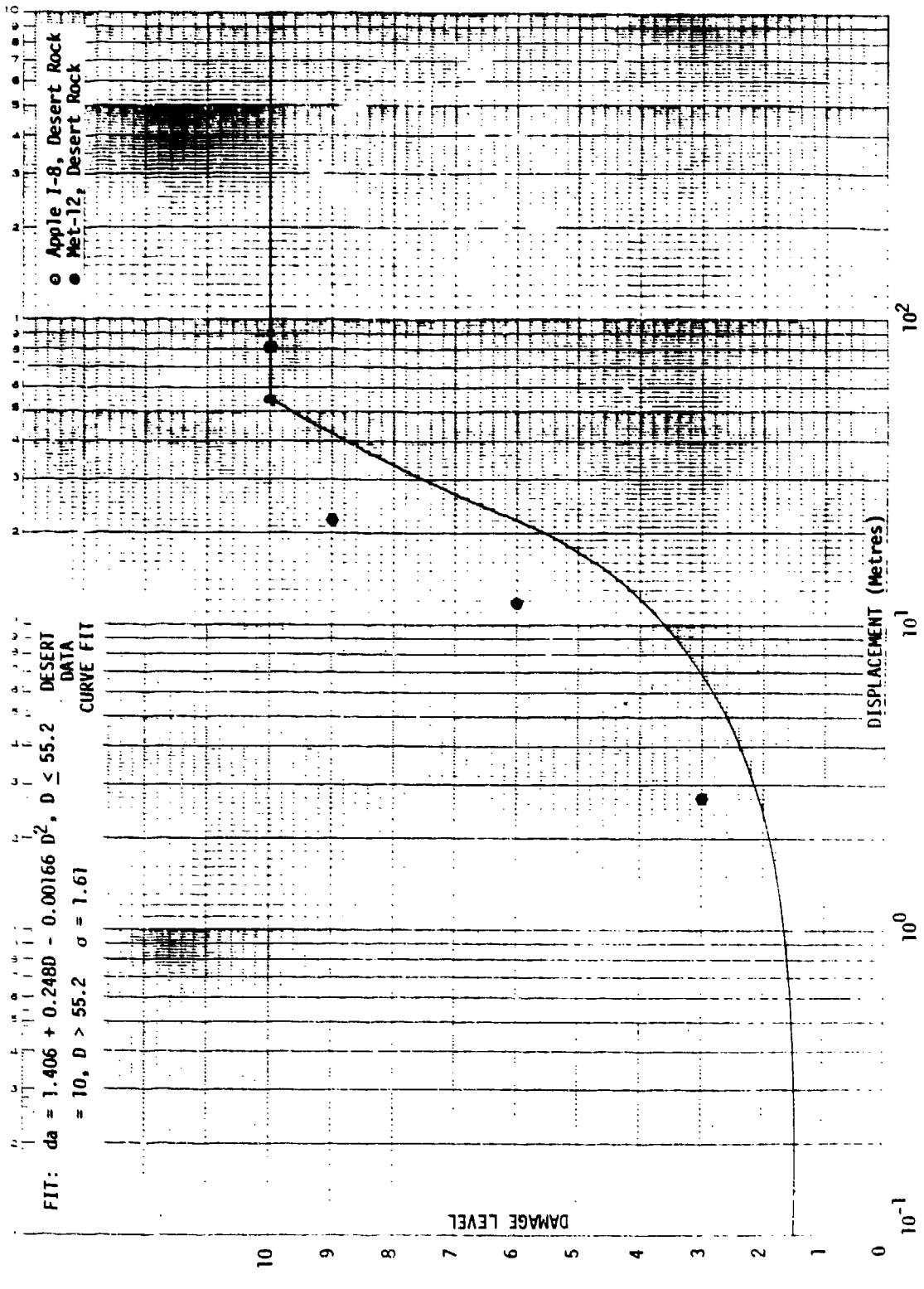

UNCLASSIFIED

FIGURE 3.2-1 (U) Damage versus Displacement - 1/4 Ton Trucks, M38A1, Side-on, (Reference 17) Desert Data Curve, Non-Desert Data Points (Yield > 1 KT)

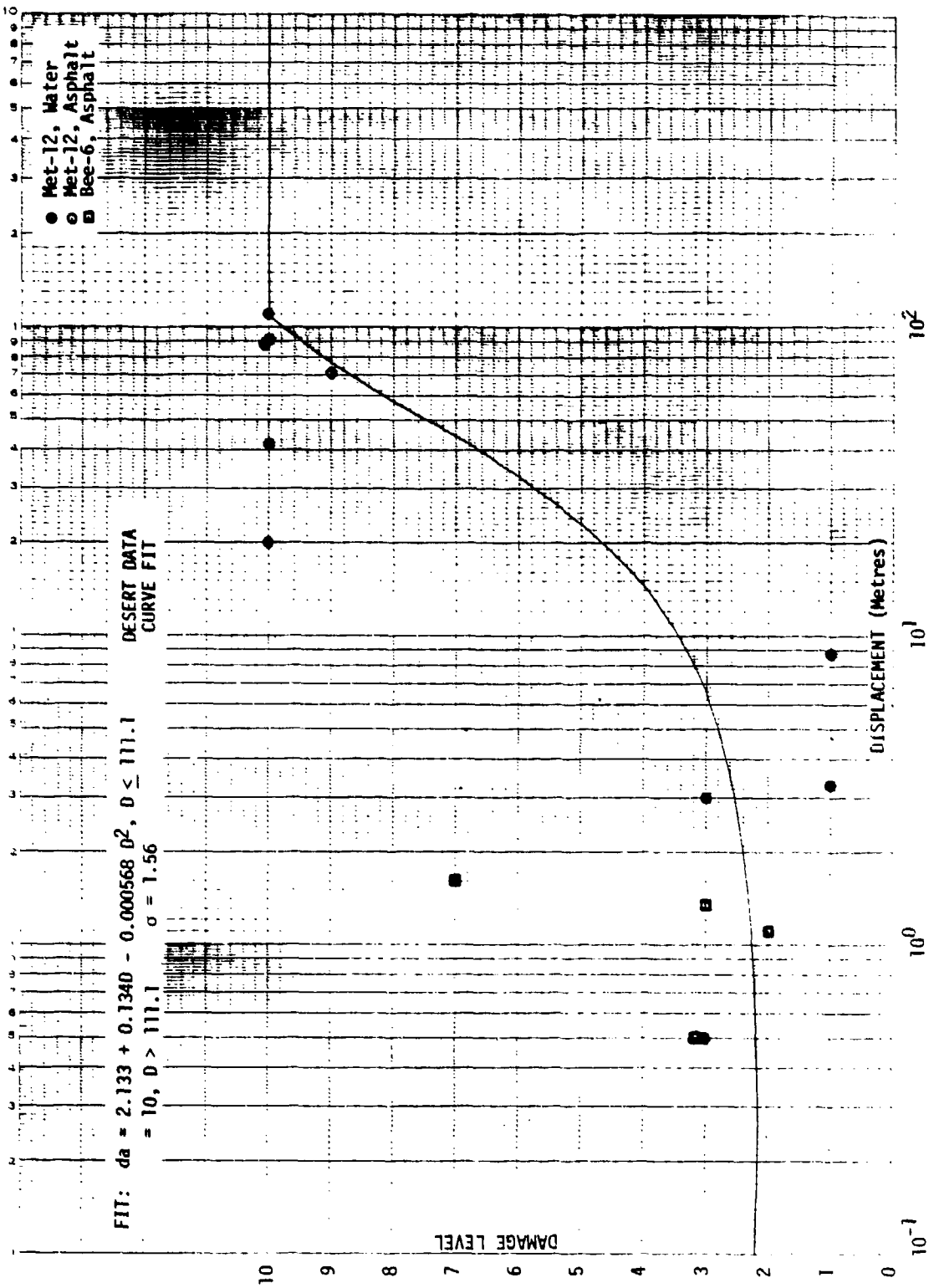

FIGURE 3.3-1 (U) Damage versus Displacement - 1/4 Ton Trucks, WWII, Face-on, (Reference 17) Desert Data Curve, Non-Desert Data Points (Yield > 1 KT)

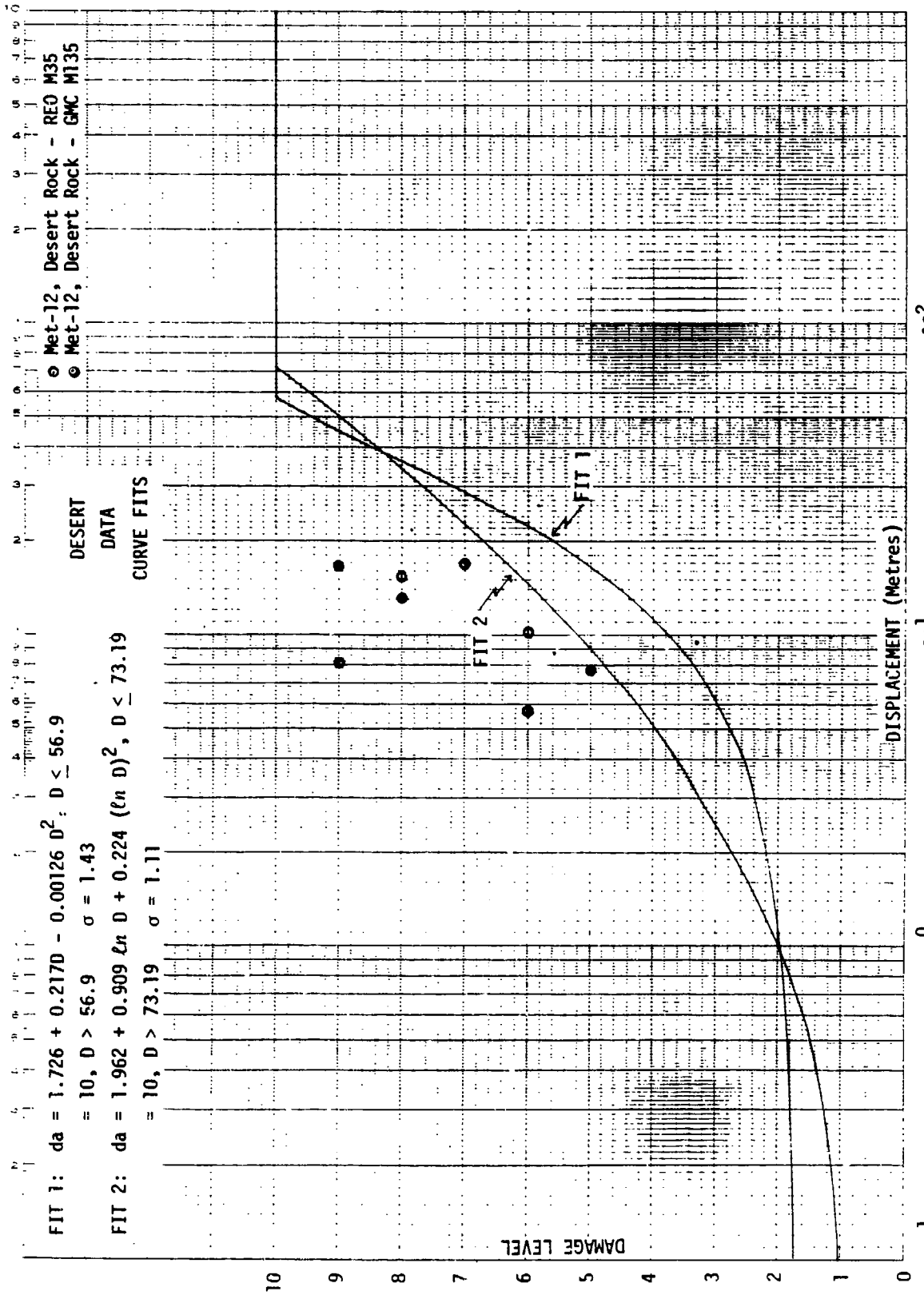

FIGURE 3.8-1 (U) Damage versus Displacement, 2-1/2 Ton Trucks, REO M35 and GMC M135, Side-on, Desert Data Curves, Non-Desert Data Points (Yield > 1 KT)

THIS PAGE IS INTENTIONALLY LEFT BLANK.

(U) SECTION 4

(U) HEIGHT OF BURST CHARTS FOR I_q

4.1 (U) SCALED DYNAMIC PRESSURE IMPULSE VERSUS SCALED GROUND RANGE CURVES

(U) Prior to constructing the Height of Burst (HOB) Charts, we again went through an iterative procedure to obtain $\bar{I}_q$ values as a function of range for each nuclear event (HE information was not used in constructing the HOB Charts). The procedure used was similar to that described in Section 2.2.4, except that we used the quadratic least squares fits (see Section 3.1.2.4) for the combined WWII and M38A1 (1/4 ton trucks) and for the combined M35 and M135 (2-1/2 ton trucks) to obtain $I_{q_{avg}}$. The $\bar{I}_q$ data for each nuclear event are shown in Tables 4.1 through 4.3 (I_q derived from Desert Rock or from water surfaces were not used in these Tables). Tables 4.1 and 4.2 show the data for ideal/near-ideal blast environments for surface bursts (4 events) and for air burst (4 events), respectively. Table 4.3 shows the data for non-ideal blast waves (8 events). I_{q0} in these Tables represents the original estimates (non-iterated) for the ideal/near-ideal events and the first iteration for the non-ideal events. $I_{q_{avg}}$ represents the calculated values from vehicle displacements (both 1/4 ton and the 2-1/2 ton trucks). The I_{q0} and $I_{q_{avg}}$ were then averaged to produce $\bar{I}_q$ (actual). Note that in some cases there were no derived $I_{q_{avg}}$ values. In these cases, vehicles were not located at these ranges so only I_{q0} was used and these were then labeled as $\bar{I}_q$. The $\bar{I}_q$ along with range were scaled to 1 KT sea level conditions using modified Sachs scaling. The scaled $\bar{I}_q$ versus scaled range data for each event were grouped according to their scaled height of burst. Our procedures described in this Section on grouping and applying least squares fits to the data for various burst conditions are similar but a refinement to that described in Section 3.3.

(U) The ideal/near-ideal surface bursts were comprised of four events: Koon-3, Nectar-6, Lacrosse-1, and Zuni-3. Least squares fits were made to these four events. Of the four ideal/near-ideal air bursts, there is some uncertainty about Yuma-4, i.e., whether it was ideal/near-ideal or non-ideal. We previously considered this to be an ideal/near-ideal blast event since the waveforms displayed steep-rising shock fronts (one of the measures for identifying blast wave categories). However, in our final resolution of $\bar{I}_q$ for Yuma-4 these values are all above our initial estimates

(see Appendix A), implying that these higher values of $\bar{I}_q$ could be the result of precursor action. But Yuma-4 was a fractional KT device and diffraction could contribute to the motion. The derived $I_{q_{avg}}$ from vehicle displacements would then indicate higher values. Data on Yuma-4 is insufficient to be able to distinguish the discrepancy between diffraction effects and precursor action. Another questionable event is Wasp-1. Only peak pressure values were obtained on this event so the I_{q_0} values for Wasp-1 were obtained by scaling Encore-9 to the actual Wasp-1 conditions. The scaling using modified Sachs is straightforward and there is no reason to doubt the validity of the I_{q_0} values on Wasp-1. However, there are two factors which contribute to the questionable data on Wasp-1. First, the actual ground zero was somewhat distant from the intended ground zero causing the orientation of the vehicles to be at some angle other than side-on or face-on. Our I_q versus displacement correlations are either for side-on or face-on orientations. The second factor was that the displacements were fractions of a metre. Both factors would contribute to large errors in computing $I_{q_{avg}}$ from displacements. Nevertheless, least squares fits were made where we grouped Wasp Prime-9 with Yuma-4 and Encore-9 with Wasp-1.

(U) There were eight non-ideal air bursts within the scaled HOB from about 40 to 73 metres. Various combinations of these events were used for obtaining least squares fits. We combined light dust events with heavy dust events in an attempt to evaluate any significant differences between these two categories. After establishing which of the events were light dust or heavy dust blast waves we used the $\bar{I}_q$ values derived from the asphalt surfaces for comparisons (see Table 4.4) with the light dust events.

(U) A total of 23 least squares fits were made to the scaled $\bar{I}_q$ versus scaled ground range data. Table 4.5 lists the combination of events, the burst conditions, the number of data points used in the fit, the derived functional least squares equation, the associated statistical data, and comments regarding what was used in the fits and the scaled range applicable to the fit. Under the remarks column we make a distinction between $\bar{I}_q$ and I_q measured. The $\bar{I}_q$ is, of course, the average of I_{q_0} and $I_{q_{avg}}$ and I_q measured are the measured values only. The I_q measured were used as additional points for the fits as well as to establish the validity of the measurements. In one case we fitted the data using only I_q measured (Met-12 and Apple II-13). The values for these events are given in Table 4.6. Also,

in a couple of cases we fitted the curves by eye because of lack of data points, e.g., Bee-6 and Wasp Prime-9. The total number of Figures prepared for the various combinations of events was 18 and the results are shown in Figures 4.1 through 4.18. These curves are shown in sequence according to the average burst height.

(U) Two least squares fits were made for the surface bursts (Figure 4.1). The reason for this is that the functional form selected did not fit the data points at the larger ranges. Fit 1 and Fit 2 are of the same functional form but Fit 1 contains all data points used and Fit 2 contains 10 of these points which were arbitrarily selected to fit the data points at the larger ranges. We place high confidence on these fits because of the high coefficient of determination, R^2, (see Table 4.5) and the low values for the statistical parameters and in particular the percentage errors, $E_I(\%)$, which are about 13 percent. Again, these scaled $\bar{I}_q$ values represent the ideal/near-ideal blast waves.

(U) The next set of curves, Figures 4.2 through 4.6 represent the scaled $\bar{I}_q$ for non-ideal blast waves. The average range for the HOB is from 41.5 metres out to 44.6 metres — an arbitrary selection for the HOB. Note on Figure 4.2 that the asphalt data on Met-12 fits reasonably with the data of Turk-4, which we later defined to be light dust. The asphalt data includes the $I_{q_{avg}}$ calculated from vehicle displacements over asphalt surface using the quadratic fits to the I_q versus displacement which were obtained for the desert surface (Nevada Test Site) and for the coral surface (Pacific), Section (3.1.2.4). The I_q versus displacement for the asphalt surface are comparable to the desert and coral surfaces (see Section 3.5.3).

(U) Figures 4.3 and 4.4 combine what we consider to be light dust and heavy dust-laden blast waves. Met-12 $\bar{I}_q$ values are generally higher than the Turk-4 or Apple II-13 $\bar{I}_q$ values (Figure 4.3). The Turk-4 data and Apple II-13 data appear to coalesce. Matter of fact, when we fit just the $\bar{I}_q$ values on Turk-4 and Apple II-13 we get good agreement (Figure 4.4, Fit 2). This is not the case when we included the I_q measured values (Figure 4.4, Fit 1). The trend here shows an increase in I_q values at closer in ranges for Apple II-13 than for Turk-4. We did note that as reported in Reference 9 (WT-1123) the damage to vehicles (likewise displacements) on Apple II-13 was not as extensive as for other events. The reason given was that the vehicles were located on a surface which was unusually soft and sandy. We proceeded to

compare only Apple II-13 and Met-12 wherein the surface was also unusually soft and sandy, particularly along the desert blast line. These comparisons are shown in Figures 4.5, Fits 1 and 2 and Figure 4.6, Fit 3. The scatter of data is about the same for Fits 1 and 3 and somewhat larger for Fit 2 (see Table 4.2). When deriving the $\bar{I}_q$ values for Apple II-13, the $I_{q_{avg}}$ derived from vehicle displacements and averaged with I_{q_0} (measured) tended to lower the $\bar{I}_q$ values relative to I_{q_0}. The opposite of this tendency was the case for the majority of $\bar{I}_q$ on other events, i.e., the $I_{q_{avg}}$ derived from vehicle displacements averaged with I_{q_0} values increased $\bar{I}_q$ relative to I_{q_0}. We, therefore, compared only the measured I_q on Apple II-13 with Met-12, Figure 4.6. Above I_q = 10 kPa-sec the comparison is poor but for the remaining I_q values there is good agreement. Note that the percentage difference in range for the three Fits is small for $\bar{I}_q$ between 0.8 kPa-sec and 10 kPa-sec. If we believe the measurements (our inclination is that they are valid and reasonable) then we have a dichotomy with regard to Apple II-13.

(U) On the one hand, just using $\bar{I}_q$ values for Apple II-13 and combining with Turk-4 indicates that Apple II-13 could be considered a light dust event or we could argue that Turk-4 is a heavy dust event. However, Turk-4 I_q data at close in ranges are definitely below the Met-12 data (one of the measures for heavy dust and light dust) so Turk-4 was classified as light dust. Apple II-13 when combined with the Met-12 data could be classified as a heavy dust event (all previous evaluations stress the fact that Met-12 was a heavy dust event) since there is some agreement when the data from these two events are combined. We dwell on this matter to point out that the data per se for a number of events does not permit a clear distinction between light dust and heavy dust blast waves throughout the I_q versus range curves. All one can do is surmise that the type of surface conditions will produce varying amounts of dust content in the blast wave.

(U) Now we come to the I_q versus range curves, Figures 4.7 to 4.13, which we classified as light dust events since all the $\bar{I}_q$ data on these curves are lower, particularly at the close in range than the heavy dust events. These curves are for HOB ranging from 46.8 metres out to 66.9 metres. If one were to superimpose these curves on top of one another they would not vary by more than 13 percent in range and this is mainly in the region of $\bar{I}_q$ from 0.6 kPa-sec to 0.8 kPa-sec. As before, in this set of curves we made use of the I_q measured as well as $\bar{I}_q$. It is to be noted that

the asphalt results, Met-12 have also been included with Turk-4 and Smoky-15. Here, we classify Smoky-15 as a light dust event. The asphalt results fit reasonably well with the other data (Figure 4.7). We observe the same situation when we included asphalt results from Bee-6 with Moth-2 and Grable-10 (Figure 4.13). Again the asphalt $\bar{I}_q$ values from Bee-6 include the $I_{q_{avg}}$ from vehicle displacements over the asphalt using the quadratic fits (Section 3.1.2.4). An interesting observation about Grable-10 is that this event was detonated in the Frenchman's Flat area as was Met-12, yet we consider Grable-10 as producing light dust-laden blast waves. We pointed out in our initial evaluation (Reference 1) that on Met-12 the vehicle response along the desert line (disturbed, very fine loose soil) was greater than the vehicle response along the Desert Rock sector (same soil but undisturbed). For Met-12, the Iq_{avg} (calculated from vehicle displacements) was greater on the desert line than on the Desert Rock sector. We can safely assume, therefore, the higher Iq_{avg} along the desert line was the result of the disturbed surface (producing higher dust concentrations in the blast wave). The Frenchman's Flat soil consists of alluvial deposits which are fine microsize particles similar to talcum powder. The desert line region was disturbed by construction of test items, digging up cable ditches, and high concentration of daily traffic prior to detonating the device. These are somewhat unique conditions. No such activity took place in the Desert Rock sector. The vehicles on Grable-10 were located in the Desert Rock sector and thus, had lower values of I_q equivalent to the $\bar{I}_q$ values of Moth-2, Apple I-8 and Smoky-15, which were classified as light dust events (see Figure 4.11). We also note that Fits 1 and 2, Figure 4.11 nearly coincide over the total range of $\bar{I}_q$ values and this is the same situation for Fits 1 and 2, Figure 4.10.

(U) The next curve, Figure 4.14, is a fit to the data obtained on Grable-10, Moth-2 and Bee-6 (Fit 2). Two of the $\bar{I}_q$ data points do not significantly alter the curve, however, as for example, Fit 1 for Moth-2 and Bee-6, Figure 4.15. The curves of Fit 2 (Figure 4.14) and Fit 1 (Figure 4.15) are about the same. Since these two points did not necessarily influence the fit we decided to fit the data points by eye. The reason for this is that we assumed that Bee-6 could be considered to produce heavy dust-laden blast waves. The desert surface on Bee-6 was a fine, soft sandy soil similar to Apple II-13. However, the four data points on Bee-6 do not necessarily validate this assumption.

(U) The next set of curves, Figures 4.16, 4.17 and 4.18 deal with near-ideal blast waves. The average HOB for these curves range from 127 metres up to 240 metres. The HOB = 127 metres is represented by Yuma-4 (HOB = 109 metres), and Wasp Prime-9 (HOB = 145 metres) shown in Figure 4.16, Fit 1. We do not feel that this curve, Fit 1, is representative for the I_q values at this average HOB for several reasons. First, we mentioned previously that we questioned the I_q values on Yuma-4; second, the scatter of the data is large between those two events; and third, the large difference in HOB (36 metres) between these two events could be a factor in the noted scatter. We feel, therefore, that in spite of the lack of data, the fit by eye to the Wasp Prime-9 event is more reasonable. The remaining two curves, the combined events, Encore-9 and Wasp-1, Figure 4.17 and Encore-9, Figure 4.18, do not show any substantial difference. The maximum difference between these curves is less than 9 percent and that falls close to the scatter for each curve (see Table 4.2). Because of the uncertainty of the data on Wasp-1 (vehicle orientations and small displacements which poorly determined $I_{q_{avg}}$ values) we consider the Encore-9 curve only to be more reliable.

(U) To recap, we place high confidence on the I_q data for the surface bursts (ideal/near-ideal) and for the HOB range from about 40 to 70 metres (light dust). There is less confidence in the height of burst at HOB from 109 metres out to 240 metres. But this is only because of the small amount of data available at these burst heights. Nevertheless, the $\bar{I}_q$ values seem reasonable, except for Yuma-4. The heavy dust events, represented by Bee-6, Met-12 and Apple II-13, indicate $\bar{I}_q$ values to be 2 to 3 times the values for the light dust events (compare Figure 4.5, Fit 1, Heavy Dust with Figures 4.2 and 4.7). The surface conditions for the heavy dust events producing these blast environments were unique, particularly the Frenchman's Flat area. Only under these conditions would a similar blast environment be produced and these surface conditions would be rare to find in many other parts of the world. We tend to believe the validity of the measurements (there are some exceptions of course) but the $\bar{I}_q$ which combine measurements and $I_{q_{avg}}$ from vehicle displacements should, in general, be more reliable which is what we wanted to show.

4.2 (U) DYNAMIC PRESSURE IMPULSE, $\bar{I}_q$, HOB CHARTS

(U) We presented various scaled $\bar{I}_q$ versus scaled range curves for three

types of blast environments; ideal/near-ideal, light dust, and heavy dust (see Section 4.1). The procedures for classifying each event or a group of events into one of the above categories were outlined. Use was made of these curves for each type of blast category to prepare Tables which list the $\bar{I}_q$ values as a function of range for different burst heights. The scaled $\bar{I}_q$ values in these Tables extend from 0.4 kPa-sec out to 10 kPa-sec. The scaled range for each $\bar{I}_q$ value was selected by eye from the fitted curves. Tables 4.7, 4.8, and 4.9 give this information for ideal/near-ideal, light dust and heavy dust blast environments, respectively. The $\bar{I}_q$ values given are for a height of 0.91 metres (3 feet) above the ground surface.

(U) The $\bar{I}_q$ versus range data for the ideal/near-ideal blast waves are given for five burst heights (Table 4.7). Two of these burst heights include the $\bar{I}_q$ values from Yuma-4 (HOB = 127 metres) and Wasp-1 (HOB = 224 metres) which yielded questionable data (see Section 4.1). However, a comparison of the ranges for several $\bar{I}_q$ values for HOB = 127 metres and 145 metres shows the percentage difference is less than 9 percent. The exceptions are for $\bar{I}_q$ of 5 kPa-sec and 4 kPa-sec. Here, the differences are about 21 percent for $\bar{I}_q$ = 5 kPa-sec and 14 percent for $\bar{I}_q$ = 4 kPa-sec.

(U) The next set of $\bar{I}_q$ versus range data is for the light dust events (Table 4.8). The averaged HOB in this set of data extends from 41.5 metres out to 66.9 metres. If we neglect the extrapolated values of $\bar{I}_q$ = 10 kPa-sec, the maximum percentage difference in range for given values of $\bar{I}_q$ is about 17 percent for these burst heights and this difference is due primarily to the extrapolated values for the lower $\bar{I}_q$ values. If we further neglected all of the extrapolated values then the percentage difference would be about 10 percent. This indicates that these data could be consolidated into one averaged burst height and least squares fitted without introducing large errors.

(U) The heavy dust $\bar{I}_q$ versus range data spans the averaged HOB from 43.4 out to 73.2 metres (Table 4.9). In this set of data, there are some events that we classified as light dust which have been combined with the heavy dust events. In Section 4.1, we indicated the difficulties encountered in attempting to distinguish between light dust and heavy dust events over the total $\bar{I}_q$ versus range curves. The events which we feel clearly fall into the heavy dust category based on the measures used for distinguishing light and heavy dust, are Met-12 and Apple II-13. The surfaces for both these events were fine, loose sandy soil and the magnitudes of dynamic pressure

impulse were 2 to 3 times greater than for the light dust events. Bee-6 could fall into this category as well. Similar surface conditions existed but the maximum difference in $\bar{I}_q$ was only about 1-1/2 times greater than for light dust and this was over a small portion of the range (compare Bee-6 and Moth-2, Figure 4.15). The set of $\bar{I}_q$ versus range data from Table 4.9 that could then be interpreted to be representative of heavy dust events are only two, HOB = 44.6 metres and 73.2 metres. Between these two burst heights the difference in range for constant $\bar{I}_q$ is small, less than 8 percent. Even over this whole span of HOBs, neglecting the extrapolated values, the range differences for constant $\bar{I}_q$ values decreases from about 29 percent down to 10 percent with decreasing I_q.

(U) For constructing the HOB Charts, the $\bar{I}_q$ versus range data from the three types of blast conditions have been combined and placed into two categories — light dust/near-ideal and heavy dust/near-ideal blast waves. The HOB Charts are shown in Figures 4.19 and 4.20, one for light dust/near-ideal and the other for heavy dust/near-ideal blast environments, respectively. The burst heights selected for constructing these charts were: three for the near-ideal, 0, 145, and 240 metres; two for the light dust, 49.2 and 61.1 metres (Fit 1); and two for the heavy dust, 44.6 (Fit 1) and 73.2 metres (eye-fit). The selection of only two HOBs for the light dust events was mainly to minimize clutter of data on the charts. As we pointed out for the light dust events there were small differences in $\bar{I}_q$ versus range curves over the span of HOB from 41.5 to 66.9 metres. As mentioned previously, only two of the $\bar{I}_q$ versus range curves could be interpreted to be heavy dust events. Thus, the five burst heights selected from each combination were sufficient to, at least, determine the trend of the iso-$\bar{I}_q$ contours. The error bands have not been placed in the contours but these can be readily obtained from the statistical data derived by least squares fit procedures (see Table 4.5).

(U) Upon inspection of these Charts we note the effect of HOB on range for equivalent $\bar{I}_q$ values. As the burst height increases, the range initially increases and then decreases, but for some low values of $\bar{I}_q$ the range increases with increasing HOB. Moreover, the iso-$\bar{I}_q$ are not everywhere parallel. We also note that from about HOB = 40 metres to 70 metres the range is reasonably constant for given $\bar{I}_q$ values for either the light dust or the heavy dust events.

(U) Although the $\bar{I}_q$ values from the heavy dust events (HOB = 44.6 metres) were 2 to 3 times higher than the light dust events (HOB = 49.2 metres) the comparison of $\bar{I}_q$ as a function of range shows that the range difference is about 27 percent greater for the heavy dust events at the higher $\bar{I}_q$ than for the light dust events. The range difference then decreases to about 10 percent at the lower $\bar{I}_q$. As the burst height is increased up to about 70 metres the range difference between these two types of blast environments becomes smaller, down to about 6 percent. These curves, heavy dust and light dust, converge at the lower $\bar{I}_q$ values.

(U) Here, we are comparing the heavy dust data from three events which are unique and one of these (Bee-6) has only limited data with data from five light dust events which we feel are reasonably reliable. Under these circumstances and since the range differences are not that large, our tendency is to place more importance on the HOB Chart which includes the light dust events than the chart which includes the heavy dust events. Other observations, but somewhat qualitative, which further lead us toward this trend are the surface conditions of the light dust events, the pressure-time measurements, and the agreement between $\bar{I}_q$ derived from the light dust events and the asphalt surfaces of Bee-6 and Met-12. The light dust events were detonated over surfaces which consisted of rough gravel mixed in with sand and, in some cases, vegetation was interspersed throughout the area. For all of these events except Smoky-15, only BRL mechanical self-recording gages were used along the blast line. Cable ditches or any major obstruction were not required to install the gages. The surface conditions were more or less undisturbed. Additionally, a cursory examination of the pressure-time measurements made on the light dust events shows less high frequency oscillations than for the heavy dust events. This implies that the influence of dust on these measurements (light dust) was minimal. We, therefore, believe that the main influences on the derived $\bar{I}_q$ for the light dust events was the result of precursor action and not necessarily the dust. This is somewhat borne out by the $\bar{I}_q$ values obtained over the asphalt surfaces on Bee-6 and Met-12. The asphalt $\bar{I}_q$ were combined with $\bar{I}_q$ from the light dust events and both are represented reasonably well by a single curve for that specific averaged burst height (see Figures 4.2 and 4.13). No significant amount of dust was present over the asphalt surface. For these reasons we tend to consider the HOB Chart which includes the

light dust to be more representative of the expected blast conditions over various surfaces where precursors (non-ideal) would be formed.

(U) Since the surface conditions (disturbed, micro-size particles) of the heavy dust events such as on Frenchman's Flat area were unique, the blast environments produced were also unique. These unique surface conditions gave rise to heavy dust loading of the blast wave (precursor) producing much higher $\bar{I}_q$ than for the light dust events. We, therefore, tend to place less importance on the heavy dust events and perhaps even to disregard them.

TABLE 4.1 (U) Dynamic Pressure Impulse versus Range,
Final Averages -- Ideal/Near-Ideal Blast Waves, Surface Bursts

UNCLASSIFIED

OPERATION/EVENT	ACTUAL RANGE Metres	SCALED RANGE Metres	I_{q_0} kPa-sec	$I_{q_{avg}}$ kPa-sec	ACTUAL $\bar{I}_q$ kPa-sec	SCALED $\bar{I}_q$ kPa-sec
Castle, Koon-3	1981	372.2	2.83	2.29	2.56	0.494
	2499	469.6	1.26	1.62	1.43	0.278
	3322	624.2	0.647	--	0.647	0.125
	4206	790.3	0.346	--	0.346	0.067
Castle, Nectar-6	2316	193.6	33.9	22.1	28.0	2.41
	2408	201.3	29.4	21.5	25.4	2.18
	2591	216.6	24.7	21.8	23.0	1.96
	2743	229.3	20.7	19.8	20.3	1.74
	2920	244.1	17.7	--	17.7	1.52
	3990	333.6	7.73	5.38	6.56	0.563
Redwing, Lacrosse-1	762	223.3	6.18	8.05	7.12	2.14
	844	247.3	4.78	5.58	5.18	1.56
	1021	299.2	2.89	2.92	2.90	0.873
	1189	348.4	1.82	2.22	2.02	0.608
	1334	390.9	1.34	1.49	1.42	0.427
Redwing, Zuni-3	2135	140.3	77.4	62.5	70.0	4.72
	2530	166.2	51.4	30.4	40.9	2.76
	3170	208.3	28.3	37.4	32.8	2.21
	3566	234.3	19.8	29.5	24.6	1.66
	4206	276.3	12.3	14.6	13.4	0.903
	5029	330.4	6.71	4.79	5.75	0.389

TABLE 4.2 (U) Dynamic Pressure Impulse versus Range, Final Averages -- Ideal/Near-Ideal Blast Waves/Air Bursts

CONFIDENTIAL - FORMERLY RESTRICTED DATA

OPERATION/EVENT	ACTUAL RANGE Metres	SCALED RANGE Meters	Iq_0 kPa-sec	Iq_{avg} kPa-sec	ACTUAL Iq kPa-sec	SCALED Iq kPa-sec
Upshot-Knothole, Encore-9	756	245.2	3.52	3.17	3.38	1.24
	872	282.9	3.00	2.84	2.92	1.07
	933	302.7	2.75	3.01	2.88	1.06
	1198	388.6	1.82	2.45	2.13	0.781
	1329	431.1	1.51	1.64	1.58	0.579
	1704	552.8	0.830	0.870	0.850	0.312
	1996	647.5	0.680	0.759	0.719	0.264
Teapot, Wasp-1	354	317.3	0.917	0.979	0.948	0.978
	393	352.2	0.779	1.12	0.951	0.981
	434.5	389.4	0.643	0.80	0.722	0.745
	460.8	413.0	0.567	1.05	0.808	0.834
	607.3	544.3	0.315	0.688	0.502	0.518
Teapot, Wasp Prime-9	237	152.3	8.63	9.24	8.94	6.83
	311	199.8	6.75	8.38	7.57	5.78
	465	298.8	1.82	--	1.82	1.39
	618	397.1	0.871	--	0.871	0.665
Redwing, Yuma-4*	76	132.8	2.38	3.23	2.81	5.07
	107	187.0	1.30	1.85	1.56	2.82
	122	213.3	1.03	1.85	1.44	2.60

(U) *Yield from the above information makes this event CONFIDENTIAL - FORMERLY RESTRICTED DATA

TABLE 4.3 (U) Dynamic Pressure Impulse versus Range, Final Averages -- Non-Ideal Blast Waves/Air Bursts

UNCLASSIFIED

OPERATION/EVENT	ACTUAL RANGE Metres	SCALED RANGE Metres	I_{q_0} kPa-sec	$I_{q_{avg}}$ kPa-sec	ACTUAL I_q kPa-sec	SCALED I_q kPa-sec
Upshot-Knothole,	736	287.7	5.13	5.66	5.39	2.37
Grable-10	844	329.9	2.69	2.53	2.61	1.11
(Desert Rock)	1335	433	--	0.686	0.686	0.302
Teapot, Moth-2	287	204.1	6.75	--	6.75	5.39
	366	260.3	3.35	3.86	3.61	2.88
	411	292.3	2.42	2.05	2.24	1.79
	457	325.0	1.88	1.47	1.68	1.34
	518	368.4	1.35	--	1.35	1.08
Teapot, Turk-4	716	193.0	20.7	--	20.7	6.51
	914	246.4	11.8	10.5	11.2	3.52
	1030	277.7	7.69	9.81	8.75	2.75
	1128	304.1	5.66	7.77	6.72	2.11
	1280	345.1	2.32	--	2.32	0.730
Teapot, Bee-6	549	263.7	8.10	9.36	8.73	4.79
(Desert)	610	293.0	4.17	4.44	4.31	2.37
	701	336.7	2.32	2.59	2.46	1.35
	777	373.2	1.91	2.66	2.28	1.25
Teapot, Apple I-8	527	205.6	17.3	--	17.3	7.95
	622	242.6	9.10	--	9.10	4.18
	902	351.9	1.95	2.62	2.29	1.05
	991	386.6	1.20	1.77	1.48	0.68
	1128	440	0.38	0.76	0.57	0.262
Teapot, Met-12	610	208.9	43.0	41.0	42.0	16.4
(Desert)	686	235.0	37.6	41.1	39.3	15.3
	762	261.0	16.8	15.7	16.3	6.36
	838	287.0	13.8	15.2	14.5	5.66
	914	313.0	3.51	3.57	3.54	1.38
Teapot, Apple II-13	518	160.3	41.9	--	41.9	15.4
	625	193.4	34.0	--	34.0	12.5
	808	250.0	19.3	--	19.3	7.08
	914	282.8	10.3	7.81	9.06	3.32
	1006	311.3	5.54	3.66	4.60	1.19
	1128	349.0	3.98	3.23	3.61	1.32
	1219	377.2	2.55	2.81	2.68	0.983
Plumbbob, Smoky-15	457	122.6	138	--	138	44.7
	726	194.8	28.5	36.8	32.6	10.6
	789	211.7	23.7	--	23.7	7.68
	841	225.6	16.0	14.1	15.1	4.90
	897	240.7	12.5	7.70	10.1	3.27
	1038	278.5	6.90	7.22	7.06	2.29
	1181	316.9	3.75	3.59	3.67	1.19

TABLE 4.4 (U) Dynamic Pressure Impulse versus Range,
Final Averages, Asphalt Surface -- Non-Ideal Blast Waves/Air Burst

UNCLASSIFIED

OPERATION/EVENT	ACTUAL RANGE Metres	SCALED RANGE Metres	I_{q_0} kPa-sec	$I_{q_{avg}}$ kPa-sec	ACTUAL I_q kPa-sec	SCALED I_q kPa-sec
Teapot, Bee-6	549	263.7	6.59	6.97	6.78	3.72
	610	293.0	4.16	2.61	3.38	1.85
	701	336.7	1.60	2.10	1.85	1.02
	777	373.2	1.02	1.24	1.13	0.62
Teapot, Met-12	610	208.9	19.0	18.9	19.0	7.42
	686	235.0	13.7	14.8	14.2	5.54
	762	261.0	8.40	8.34	8.37	3.27
	838	287.0	5.58	4.38	4.98	1.94
	914	313.0	1.72	1.37	1.54	0.60

TABLE 4.5 (U) LEAST SQUARES FIT RESULTS --
Scaled Dynamic Pressure Impulse vs. Scaled Ground Range for Various Combinations of Events

UNCLASSIFIED

EVENTS INCLUDED	BURST CONDITIONS	HOB AVERAGE Metres	FIG. #	N	FIT		R^2	$S_{\ell n\ I}$	S'_I	$\sigma_{\ell n\ I,C}$	$\sigma'_{I,C}$	EI(%)	COMMENTS
Koon-3 Nectar-6 Lacrosse-1 Zuni-3	Surface Near-Ideal	0	4.1	21	FIT 1:	$\ell n\ I_q = 3.24-0.0137x+0.000008x^2$	0.980	0.468	0.369	0.161	0.143	13.3	Use of $\bar{I}_q$ $140.3 < R < 790.3$
			4.1	10	FIT 2:	$\ell n\ I_q = 1.945-0.0085x+0.0000034x^2$	0.961	0.246	0.190	0.186	0.165	13.7	Use of $\bar{I}_q$ $276.3 < R < 790.3$
Turk-4 Met-12	Air Light Dust/ Non-Ideal	41.5	4.2	10		$\ell n\ I_q = 2.060+0.00926x-0.000049x^2$	0.881	0.782	0.632	0.442	0.325	25.1	Use of $\bar{I}_q$ & I_q Measured Met-12 Asphalt $193 < R < 345.1$
Turk-4 Met-12 Apple II-13	Air Light & Heavy Dust/ Non-Ideal	43.4	4.3	12		$\ell n\ I_q = 11.65-0.0553x+0.000064x^2$	0.849	1.418	1.776	0.397	0.444	38.5	Use of $\bar{I}_q$ $208.9 < R < 377$
Turk-4 Apple II-13	Air Light & Heavy Dust/ Non-Ideal	44.1	4.4	12	FIT 1:	$\ell n\ I_q = 5.040-0.0148x+0.0000021x^2$	0.913	0.905	0.943	0.317	0.324	28.0	Use of $\bar{I}_q$ & I_q Measured $160.3 < R < 377$
			4.4	7	FIT 2:	$\ell n\ I_q = 3.068-0.00486x-0.0000009x^2$	0.941	0.081	0.091	0.142	0.150	11.4	Use of $\bar{I}_q$ $246.4 < R < 377$
Met-12 Apple II-13	Air Heavy/Dust Non-Ideal	44.6	4.5	9	FIT 1:	$\ell n\ I_q = 11.06-0.0488x+0.000051x^2$	0.920	0.730	0.848	0.349	0.376	30.7	Use of $\bar{I}_q$ $208.9 < R < 377$
			4.5	12	FIT 2:	$\ell n\ I_q = 3.760-0.000085x-0.000029x^2$	0.889	1.374	1.524	0.391	0.412	35.6	Use of $\bar{I}_q$ & I_q Measured $160.3 < R < 377$
			4.6	12	FIT 3:	$\ell n\ I_q = 3.318+0.00326x-0.000034x^2$	0.902	1.108	1.030	0.351	0.338	29.3	Use of I_q Meas. $160.3 < R < 377$

TABLE 4.5 (U) LEAST SQUARES FIT RESULTS --
Scaled Dynamic Pressure Impulse vs. Scaled Ground Range for Various Combinations of Events (Continued)

UNCLASSIFIED

EVENTS INCLUDED	BURST CONDITIONS	HOB AVERAGE Metres	FIG. #	N	FIT		R^2	$S_{\ell n\ I}$	$S_{\bar{I}}$	$\sigma_{\ell n\ I,C}$	$\sigma_{\bar{I},C}$	EI(%)	COMMENTS
Turk-4 Met-12 Smoky-15	Air Light Dust/ Non-Ideal	46.8	4.7	17		$\ell n\ \bar{I}_q = 6.401-0.0235x+0.000012x^2$	0.939	1.055	0.884	0.275	0.251	22.8	Use of $\bar{I}_q$ & I_q Measured Met-12 Asphalt 122.6 < R < 345.1
Turk-4 Smoky-15	Air Light Dust/ Non-Ideal	49.2	4.8	12		$\ell n\ \bar{I}_q = 6.771-0.0278x+0.000023x^2$	0.965	0.441	0.442	0.221	0.217	19.2	Use of $\bar{I}_q$ & I_q Measured 122.6 < R < 345.1
Turk-4 Apple I-8 Smoky-15	Air Light Dust/ Non-Ideal	52.6	4.9	17		$\ell n\ \bar{I}_q = 6.337-0.0244x+0.000017x^2$	0.975	0.539	0.517	0.204	0.199	18.0	Use of $\bar{I}_q$ & I_q Measured 122.6 < R < 440
Apple I-8 Smoky-15	Air Light Dust/ Non-Ideal	58.4	4.10	12	FIT 1:	$\ell n\ \bar{I}_q = 6.724-0.0268x+0.00002x^2$	0.987	0.204	0.257	0.151	0.169	14.6	Use of $\bar{I}_q$ & I_q Measured 122.6 < R < 440
			4.10	8	FIT 2:	$\ell n\ \bar{I}_q = 5.85-0.0214x+0.00012x^2$	0.977	0.225	0.234	0.212	0.216	17.1	Use of $\bar{I}_q$ 194.8 < R < 440
Grable-10 Moth-2 Apple I-8 Smoky-15	Air Light Dust/ Non-Ideal	61.1	4.11	20	FIT 1:	$\ell n\ \bar{I}_q = 6.334-0.244x+0.00017x^2$	0.976	0.626	0.751	0.192	0.194	19.4	Use of $\bar{I}_q$ & I_q Measured 122.6 < R < 440
			4.11	14	FIT 2:	$\ell n\ \bar{I}_q = 5.566-0.0194+0.000009x^2$	0.980	0.265	0.280	0.155	0.160	14.1	Use of I_q 194.8 < R < 440
Grable-10 Moth-2	Air Light Dust/ Non-Ideal	63.7	4.12	8		$\ell n\ \bar{I}_q = 3.127-0.005x-0.000011x^2$	0.972	0.138	0.052	0.166	0.102	8.06	Use of $\bar{I}_q$ & I_q Measured 204.1 < R < 433

UNCLASSIFIED

UNCLASSIFIED

TABLE 4.5 (U) LEAST SQUARES FIT RESULTS --
Scaled Dynamic Pressure Impulse vs. Scaled Ground Range For Various Combinations of Events (Concluded)

UNCLASSIFIED

EVENTS INCLUDED	BURST CONDITIONS	HOB AVERAGE Metres	FIG. #	N	FIT		R^2	$S_{\ell n\ I}$	S'_I	$\sigma_{\ell n\ I,C}$	$\sigma'_{I,C}$	EI(%)	COMMENTS
Grable-10 Moth-2 Bee-6	Air Light Dust	66.9	4.13	12	FIT 1:	$\ell n\ I_q = 3.650-0.0078x-0.000008x^2$	0.960	0.272	0.336	0.174	0.167	16.7	Use of $\bar{I}_q$ & I_q Measured Bee-6 Asphalt 204.1 < R < 433
Grable-10 Moth-2 Bee-6	Air, Light & Heavy Dust/ Non-Ideal	66.9	4.14	12	FIT 2:	$\ell n\ I_q = 2.733-0.0183x-0.000016x^2$	0.913	0.562	0.699	0.250	0.279	24.1	Use of $\bar{I}_q$ & I_q Measured 204.1 < R < 433
Moth-2 Bee-6	Air Light & Heavy Dust/ Non-Ideal	69.1	4.15	9		$\ell n\ I_q = 4.849-0.0176x+0.000013x^2$	0.874	0.355	0.479	0.243	0.282	23.1	Use of $\bar{I}_q$ 204.1 < R < 373.2
Wasp Prime -9 Yuma-4	Air Near-Ideal	127	4.16	7		$\ell n\ I_q = 2.921-0.0082x-0.0000007x^2$	0.880	0.508	0.657	0.356	0.405	30.6	Use of $\bar{I}_q$ 132.8 < R < 397.1
Encore-9 Wasp-1	Air Near-Ideal	224	4.17	12		$\ell n\ I_q = 0.754-0.0015x-0.0000027x^2$	0.937	0.169	0.169	0.137	0.137	11.9	Use of $\bar{I}_q$ 245.2 < R < 647.5
Encore-9	Air Near-Ideal	240	4.18	7		$\ell n\ I_q = 1.273-0.0043x+0.00000024x^2$	0.984	0.041	0.397	0.101	0.100	7.53	Use of $\bar{I}_q$ 245.2 < R < 647.5

TABLE 4.6 (U) Dynamic Pressure Impulse versus Range for Met-12 and Apple II-13 -- Measured Values

UNCLASSIFIED

ACTUAL RANGE Metres	I_{q_0} kPa-sec	SCALED RANGE Metres	I_{q_0} kPa-sec
	MET-12		
610	48.0	208.9	18.7
686	37.2	235.0	14.5
762	17.2	261.0	6.71
838	11.5	287.0	4.49
914	3.4	313.0	1.33
	APPLE II-13		
518	41.9	160.3	15.4
625	34.0	193.4	12.5
808	19.3	250.0	7.08
914	12.1	282.8	4.44
1006	7.4	311.3	2.71
1128	4.8	349.0	1.76
1219	2.48	377.2	0.910

TABLE 4.7 (U) Height-Of-Burst For Dynamic Pressure Impulse Versus Ground Range At 0.91 Metres Above Surface

Ideal/Near-Ideal

UNCLASSIFIED

I_q (kPa-sec)	Average HOB (Metres) 0	127	145 (EYE-FIT)	224	240
10	87*	--	--	--	--
5	128*	158	191	--	--
4	143	184	210	--	--
3	174	218	237	--	--
2	212	260	277	--	--
1.5	240	300	307	--	--
1.2	261	325	330	258	262
1.0	281	346	350	317	301
0.8	306	372	372	382	353
0.6	341	402	402*	458	422
0.4	395	445*	445*	553	522

* Extrapolated

TABLE 4.8 (U) Height-Of-Burst For Dynamic Pressure Impulse Versus Ground Range At 0.91 Metres Above Surface

Light Dust/Non-Ideal

UNCLASSIFIED

I_q (kPa-sec)	Average HOB (Metres) 41.5	46.8	49.2	52.6	58.4 (FIT 1)	58.4 (FIT 2)	61.1 (FIT 1)	61.1 (FIT 2)	63.7	66.9 (FIT 2)
10	165*	190	188	190	192		190		--	151*
5	230	227	229	230	231		231		210	215
4	246	241	241	245	245		245		233	235
3	265	258	260	263	264		262		261	260
2	288	282	288	290	291	*About*	290	*About*	299	293
1.5	304	299	308	304	311	*the*	311	*the*	322	317
1.2	315	312	321	323	328	*Same*	328	*Same*	340	334
1.0	320	322	335	338	341	*as FIT 1*	341	*as FIT 1*	354	348
0.8	330	336	350*	355	358		360		370	365
0.6	343	353*	371*	378	380		383		390	386
0.4	358*	383*	401*	416	417		418		419	415

*Extrapolated

UNCLASSIFIED

TABLE 4.9 (U) Height-Of-Burst For Dynamic Pressure Impulse Versus Ground Range At 0.91 Metres Above Surface

Heavy Dust/Non-Ideal

UNCLASSIFIED

I_q (kPa-sec)	Average HOB (Metres) 43.4	44.1 (FIT 1)	44.1 (FIT 2)	44.6 (FIT 1)	44.6 (FIT 2)	44.6 (FIT 3)	66.9 (FIT 2)	69.1 (FIT 1)	73.2 (EYE-FIT)
10	231	190	--	238	225	228	124*	--	--
5	260	238	--	269	272	278	215	215	250
4	270	256	240	279	288	292	240	235	265
3	285	277	270	294	303	310	268	262	285
2	308	307	310	317	325	331	303	300	315
1.5	330	329	337	335	340	347	327	332	336
1.2	348	345	357	350	350	357	343	360	354
1.0	369	359	373	364	358	365	357	381	368
0.8	397*	376	392*	381*	368	375	374	--	--
0.6	--	--	--	405*	381*	--	395	--	--
0.4	--	--	--	440*	400*	--	424	--	--

*Extrapolated

UNCLASSIFIED

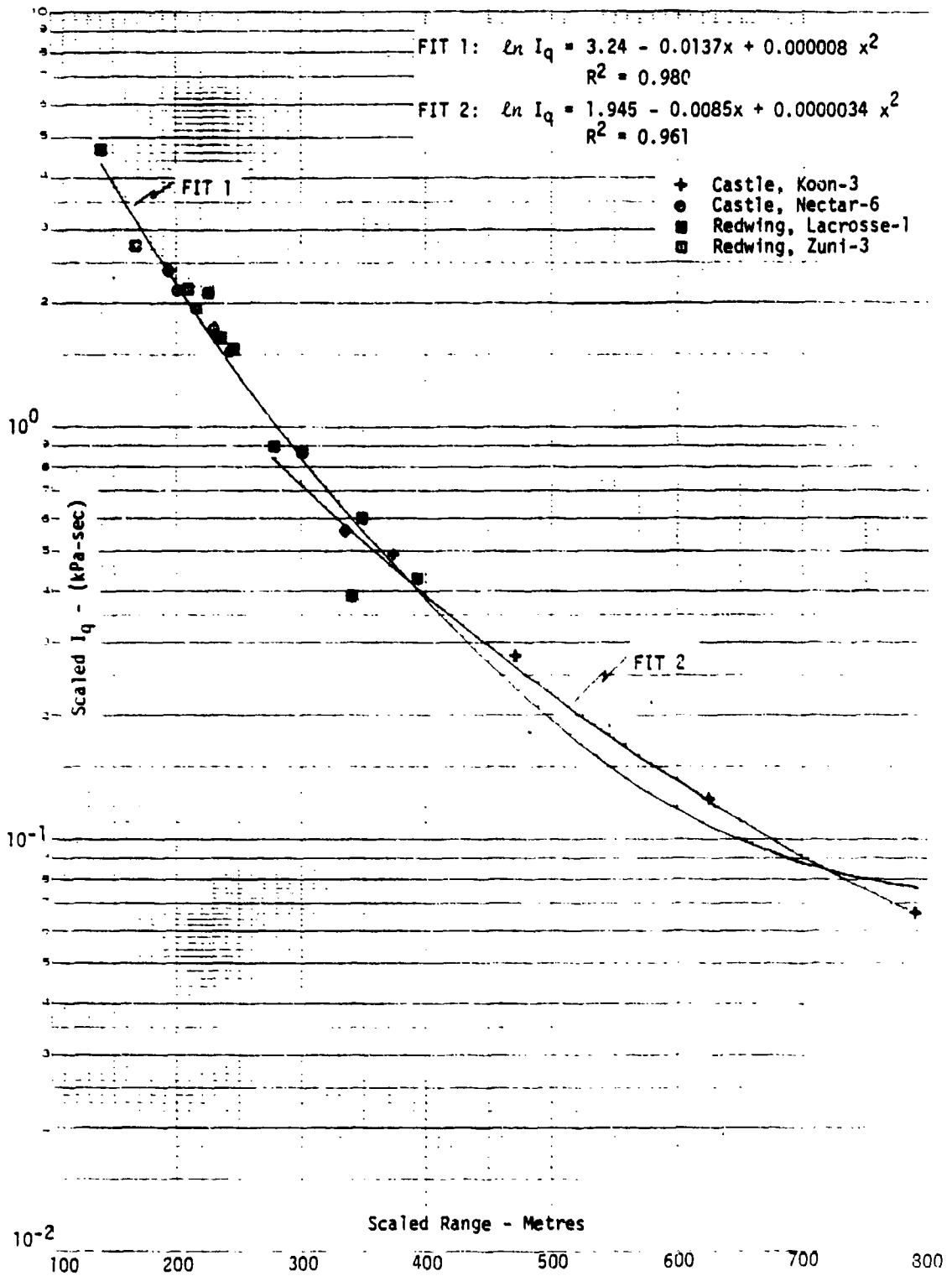

UNCLASSIFIED

FIGURE 4.1 (U) Dynamic Pressure Impulse vs. Range - Surface Bursts Scaled to 1 KT

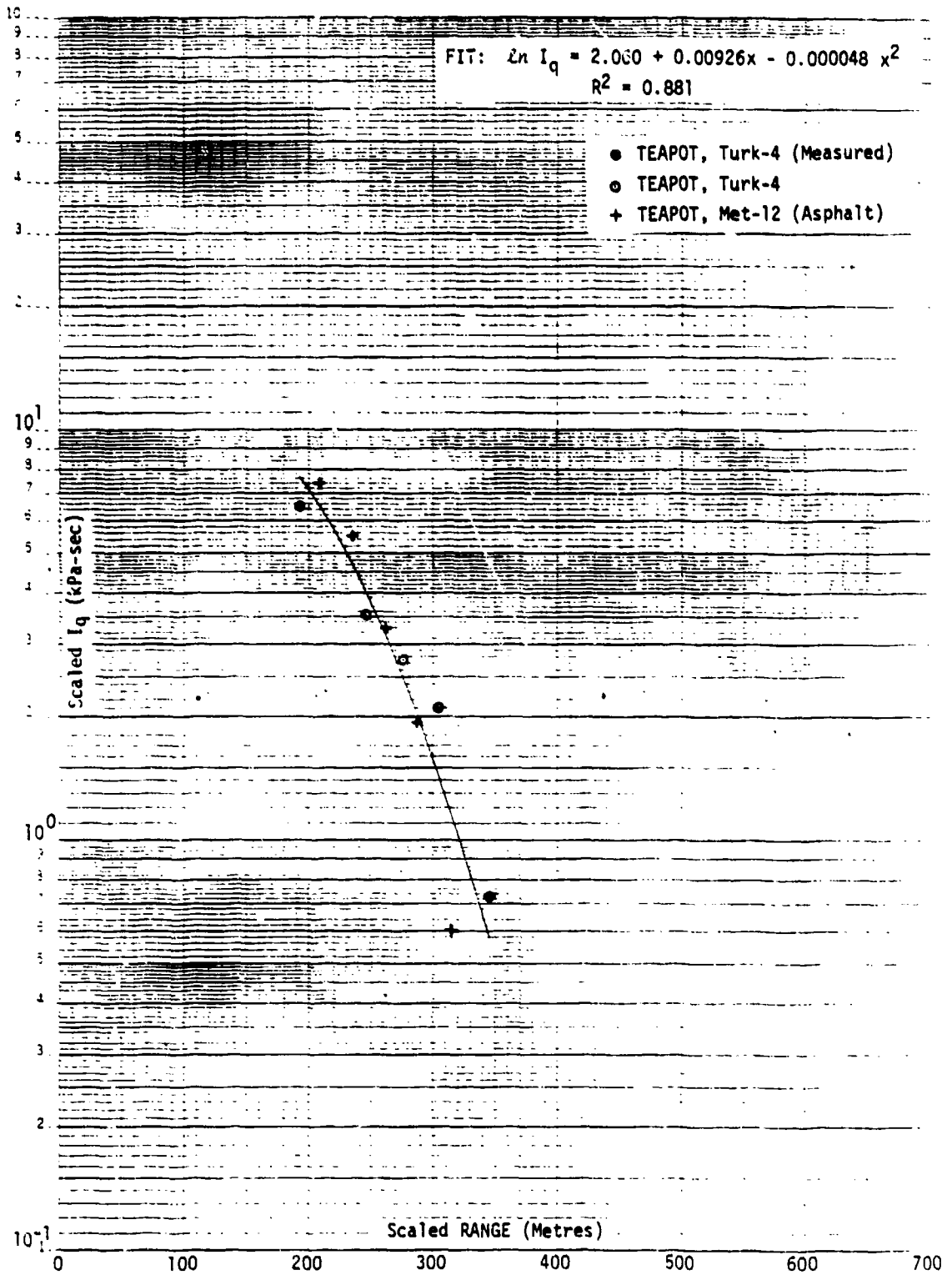

UNCLASSIFIED

FIGURE 4.2 (U) Dynamic Pressure Impulse vs. Range -- Average HOB = 41.5 Metres, Scaled to 1 KT

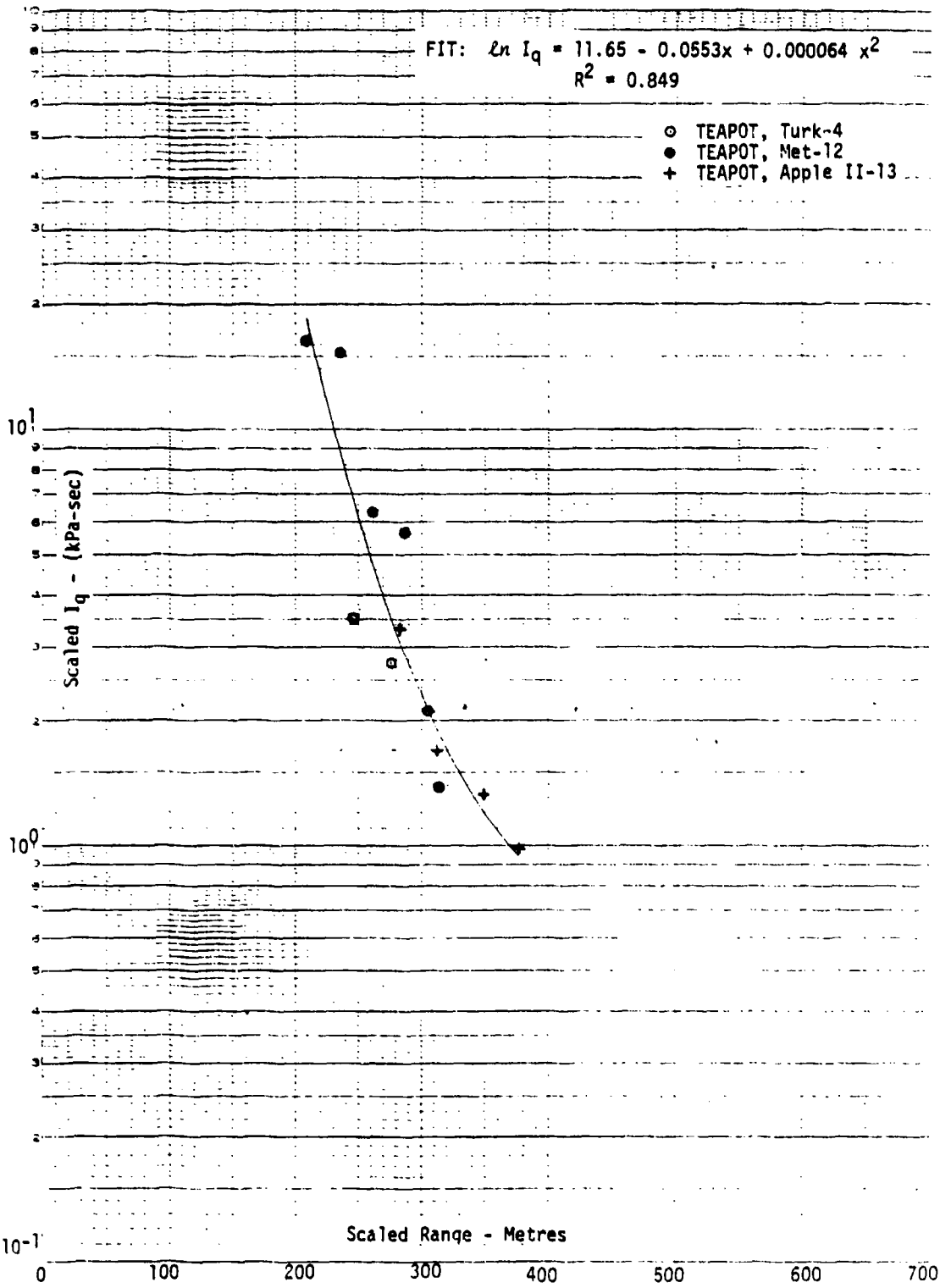

UNCLASSIFIED

FIGURE 4.3 (U) Dynamic Pressure Impulse vs. Range - Average HOB = 43.4 Metres, Scaled to 1 KT

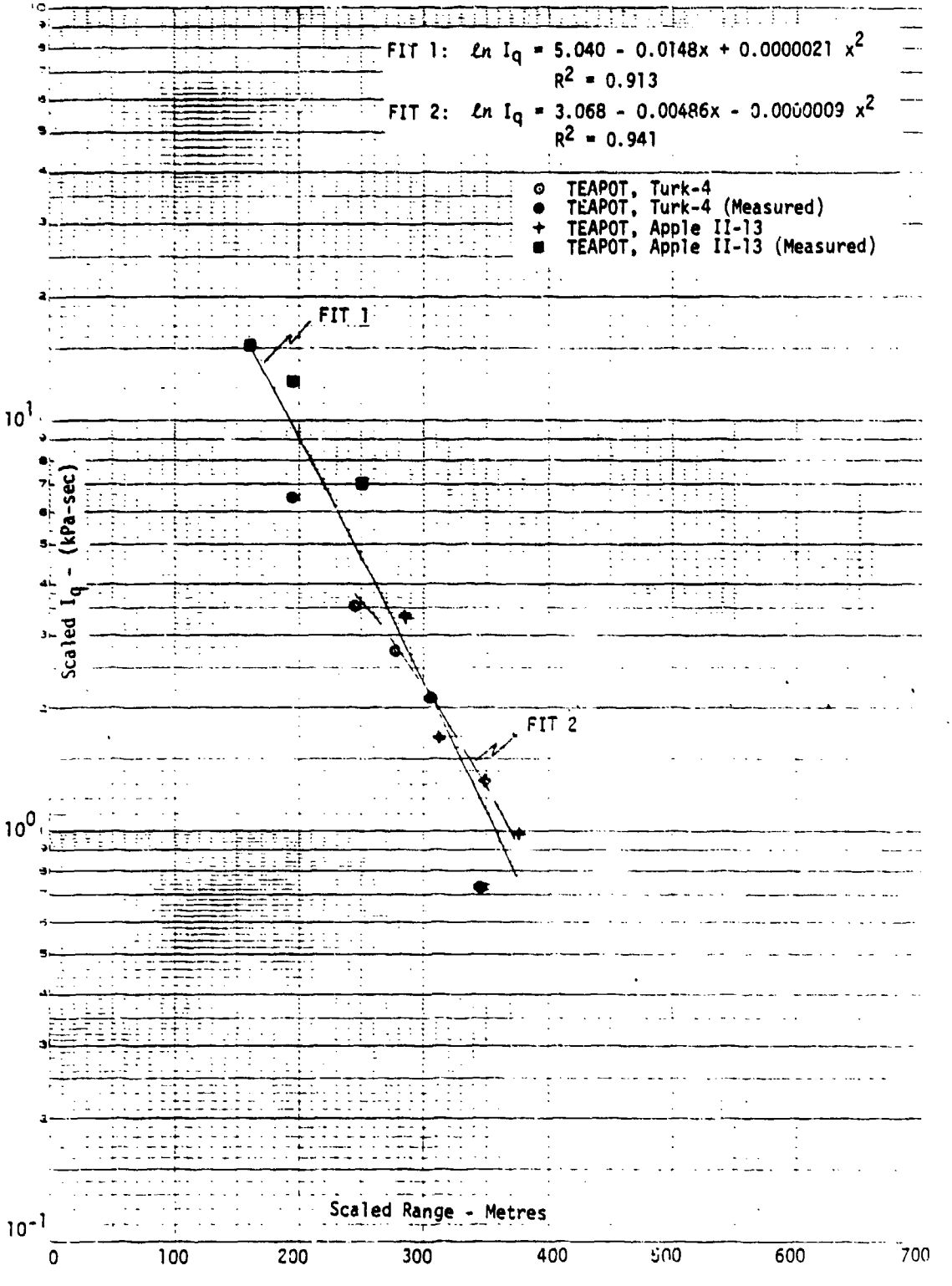

UNCLASSIFIED

FIGURE 4.4 (U) Dynamic Pressure Impulse vs. Range - Average HOB = 44.1 Metres, Scaled to 1 KT

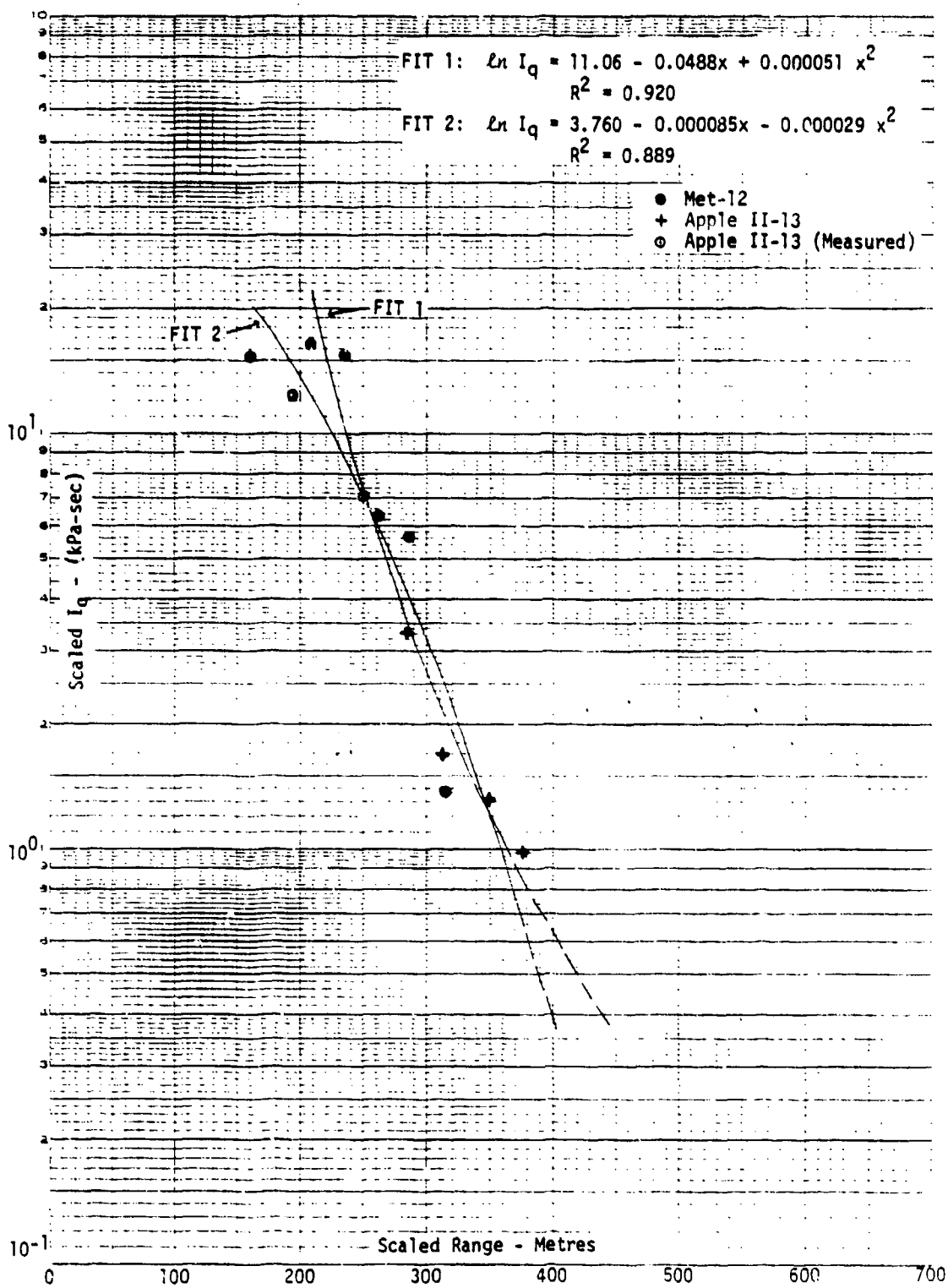

UNCLASSIFIED

FIGURE 4.5 (U) Dynamic Pressure Impulse vs. Range - Average HOB = 44.6 Metres, Scaled to 1 KT

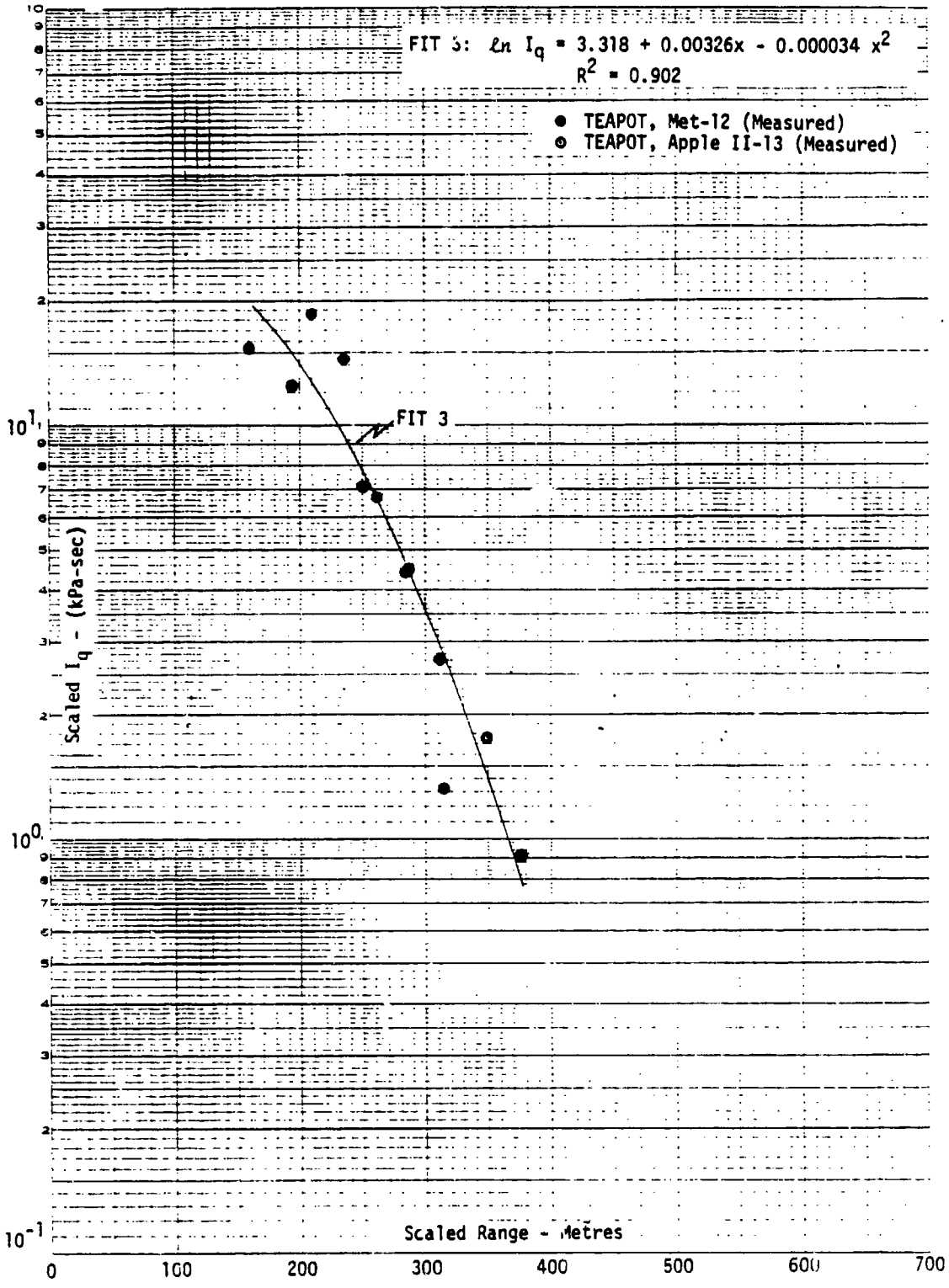

UNCLASSIFIED

FIGURE 4.6 (U) Dynamic Pressure Impulse vs. Range - Average HOB = 44.6 Metres, Scaled to 1 KT

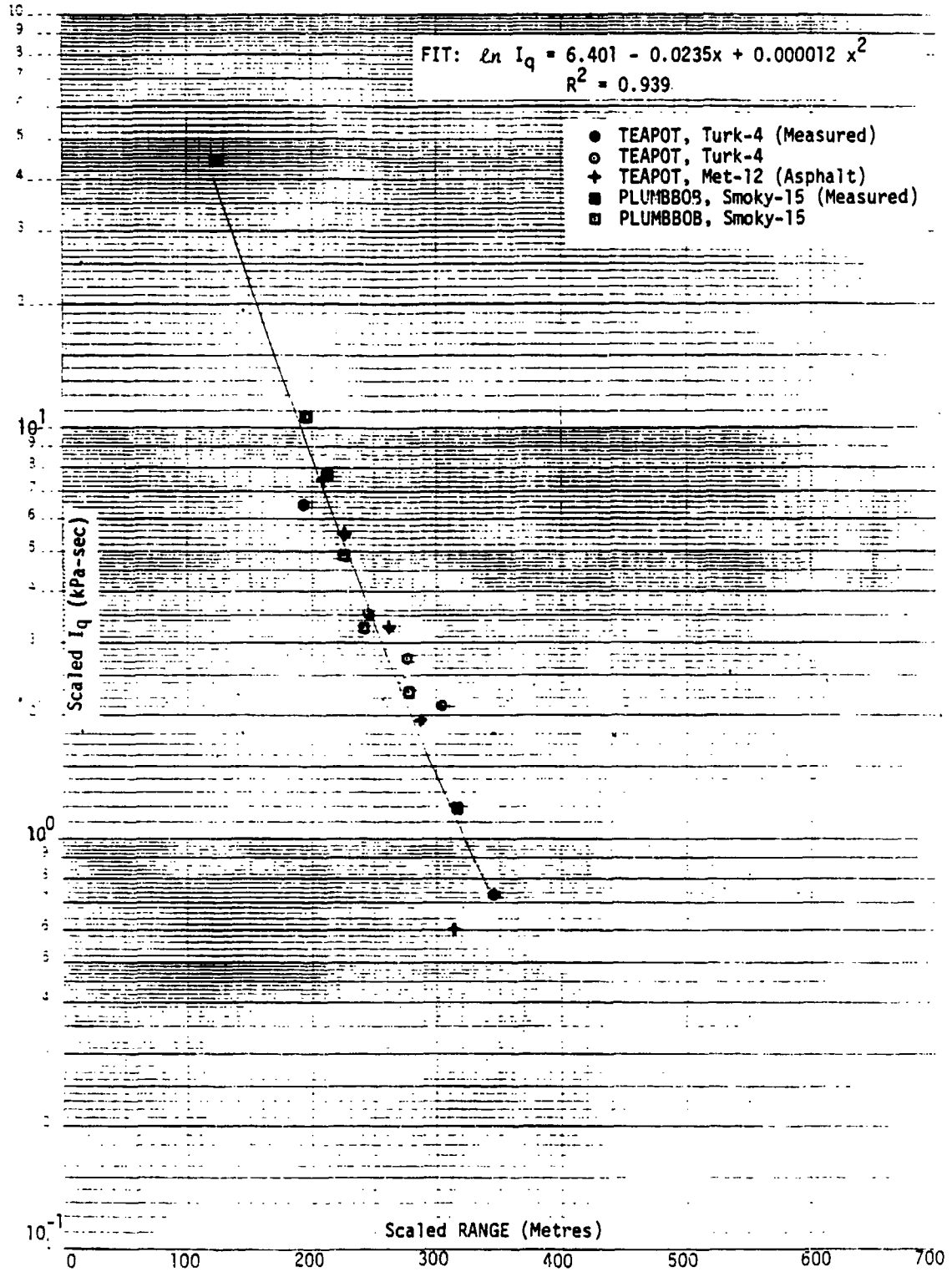

UNCLASSIFIED

FIGURE 4.7 (U) Dynamic Pressure Impulse vs. Range - Average HOB = 46.8 Metres, Scaled to 1 KT

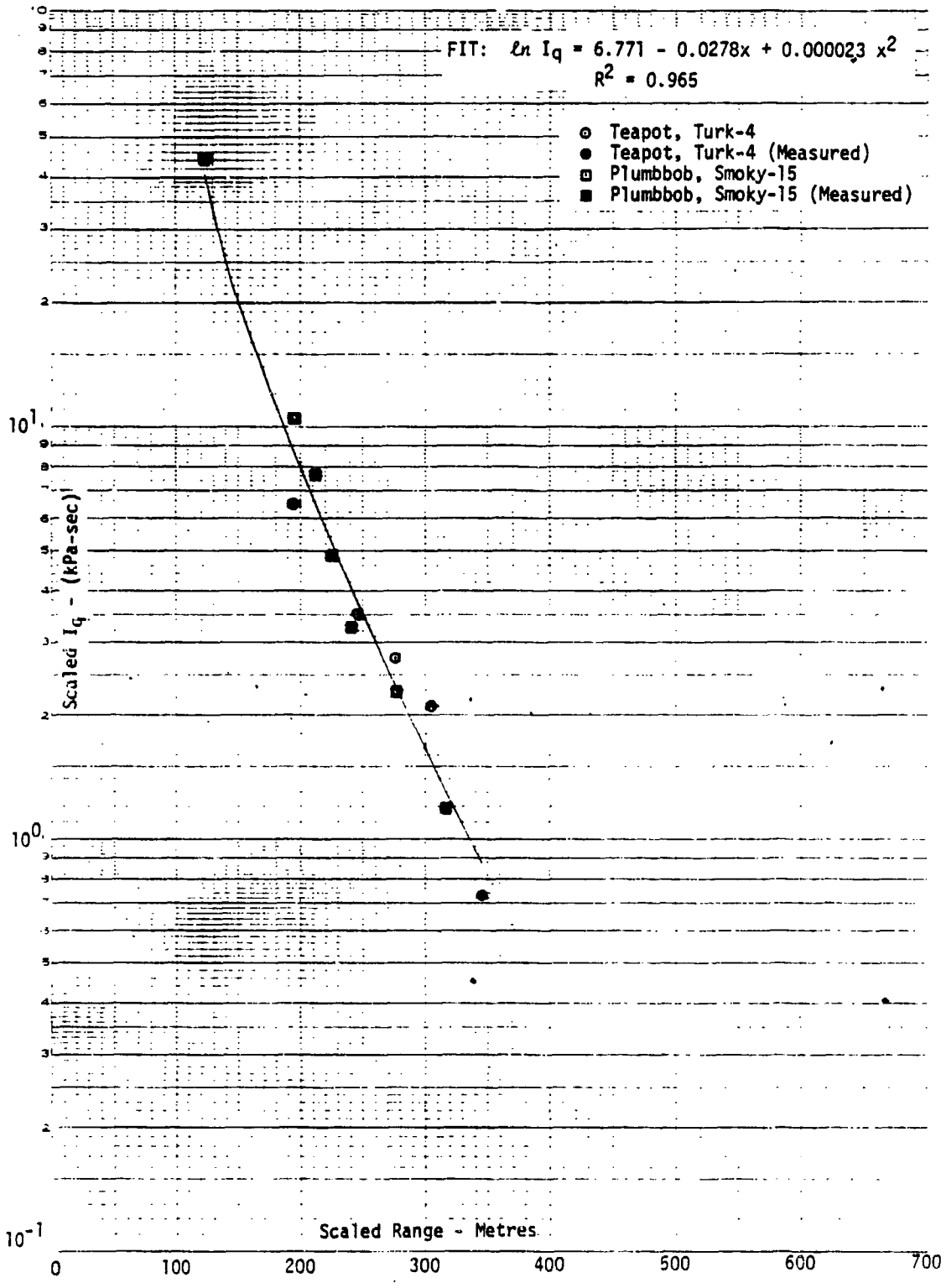

UNCLASSIFIED

FIGURE 4.8 (U) Dynamic Pressure Impulse vs. Range - Average HOB = 49.2 Metres, Scaled to 1 KT

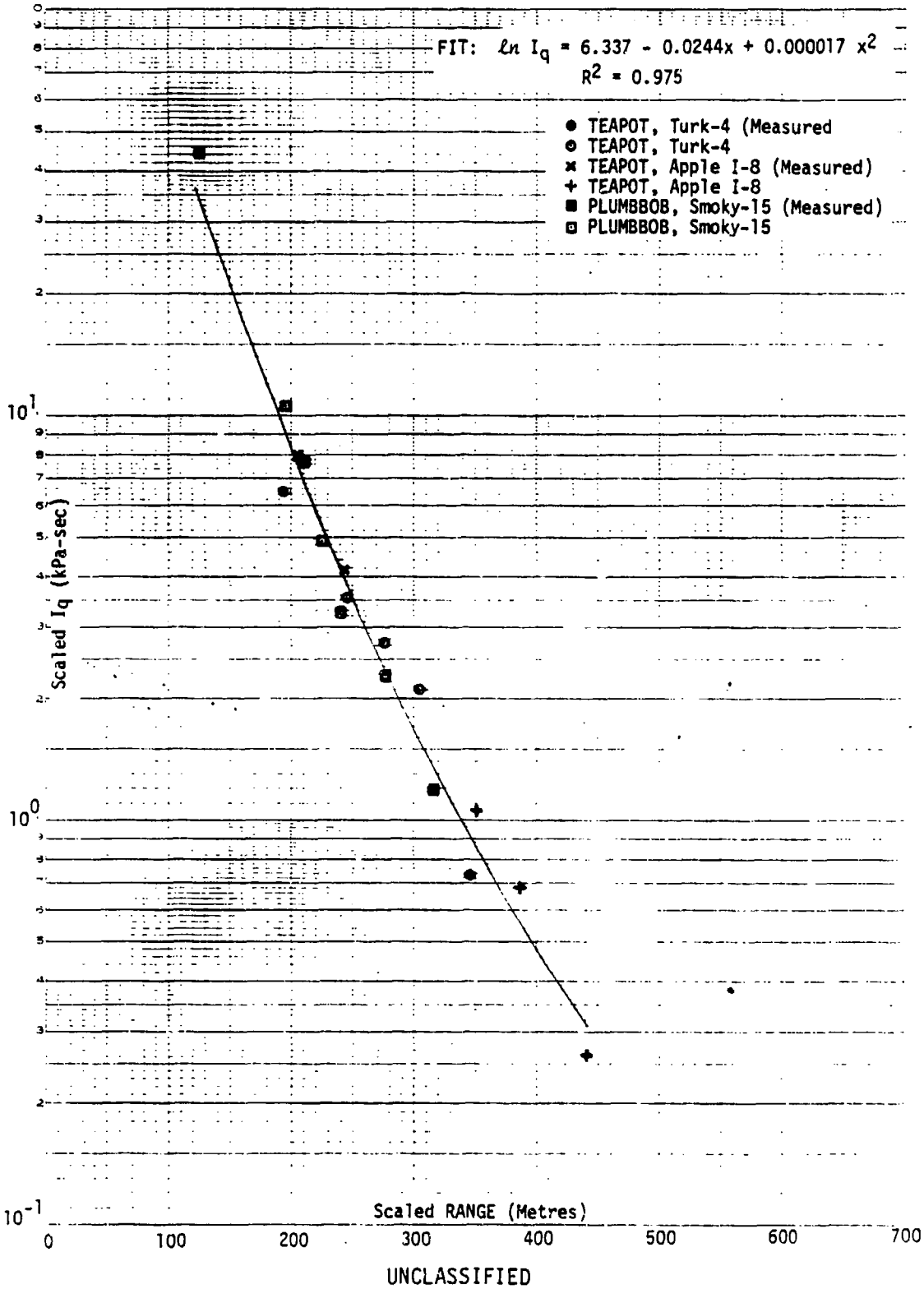

UNCLASSIFIED

FIGURE 4.9 (U) Dynamic Pressure Impulse vs. Range - Average HOB = 52.6 Metres, Scaled to 1 KT

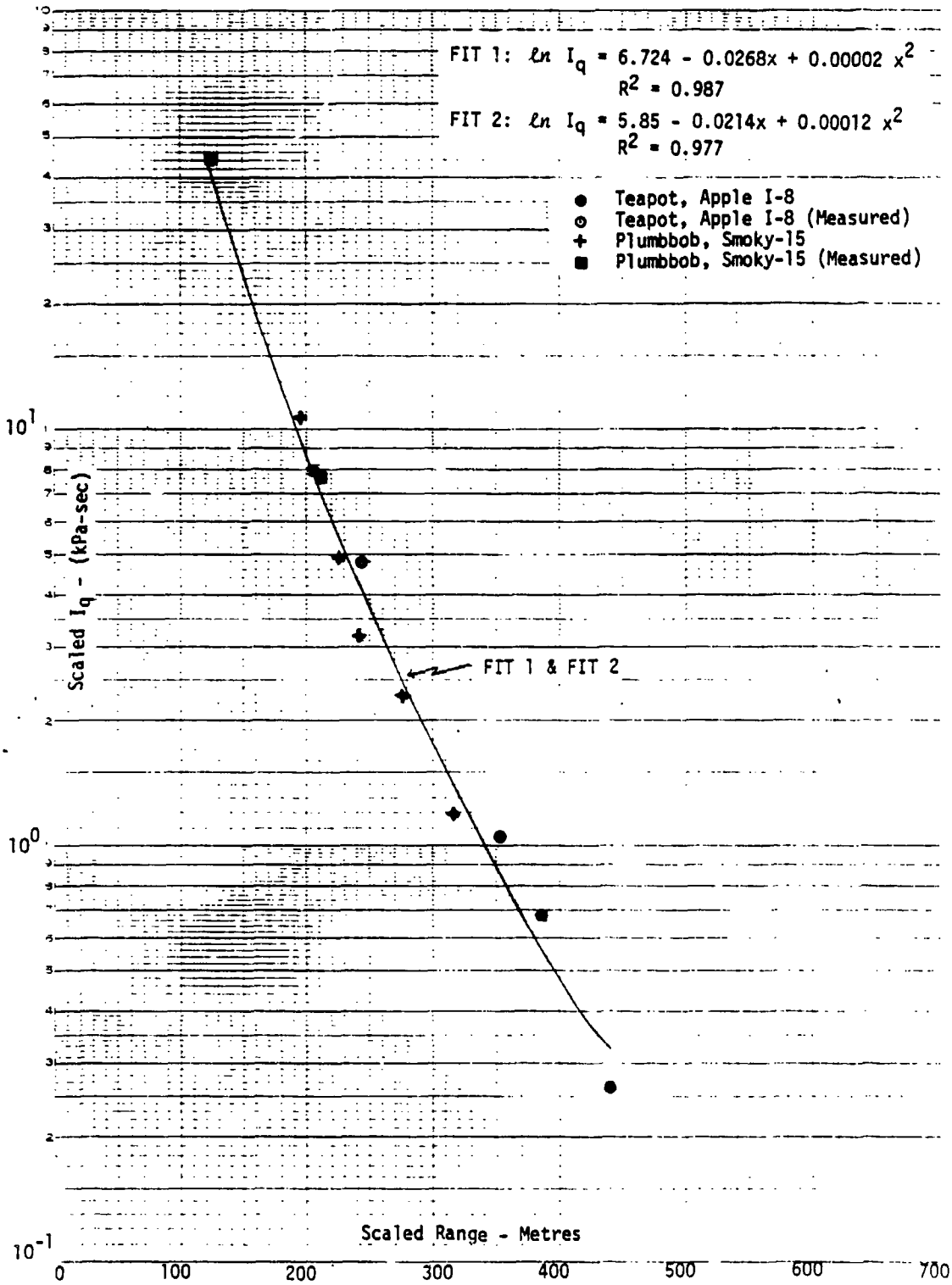

UNCLASSIFIED

FIGURE 4.10 (U) Dynamic Pressure Impulse vs. Range - Average HOB = 58.4 Metres, Scaled to 1 KT

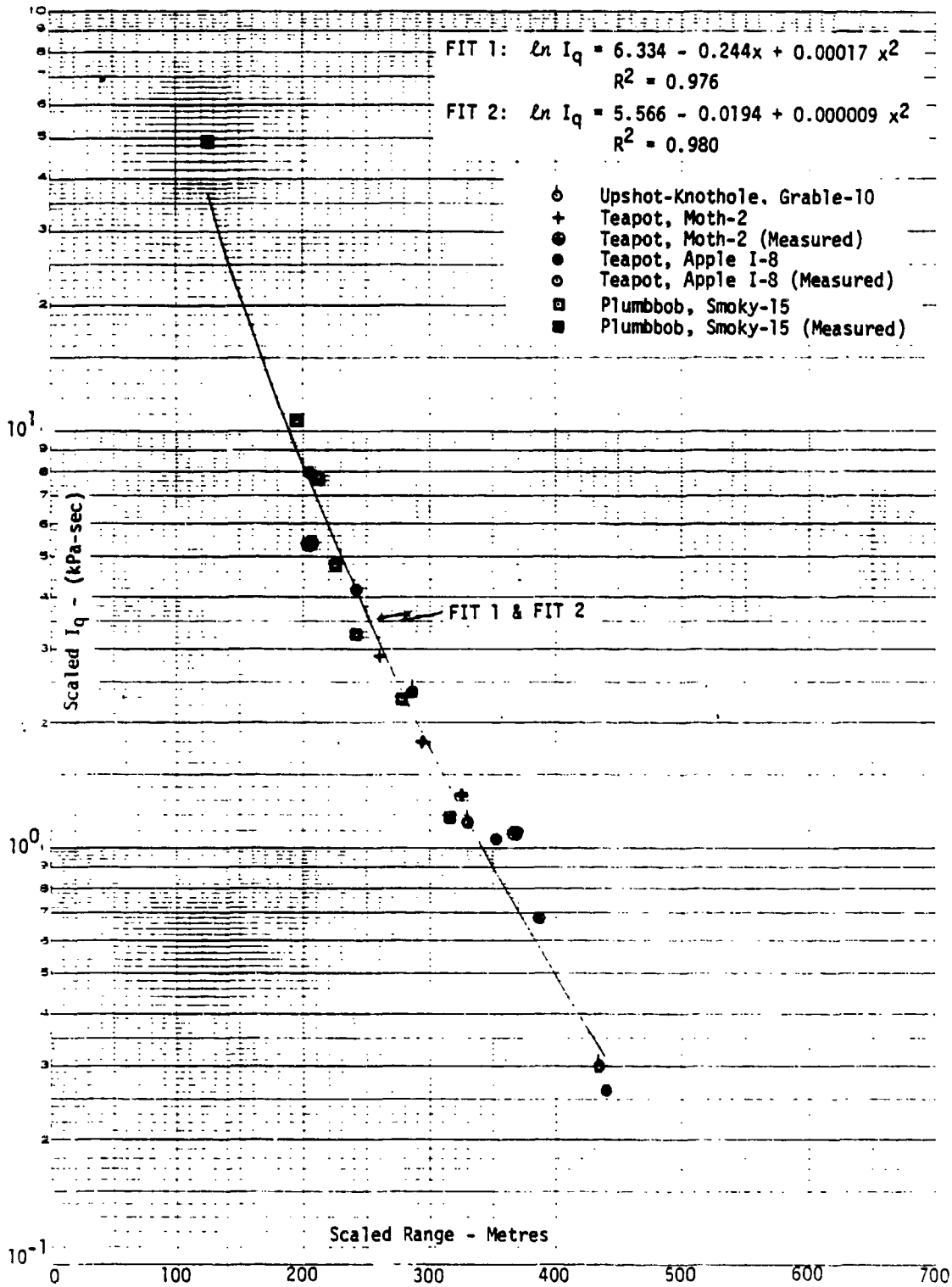

UNCLASSIFIED

FIGURE 4.11 (U) Dynamic Pressure Impulse vs. Range - Average HOB = 61.1 Metres, Scaled to 1 KT

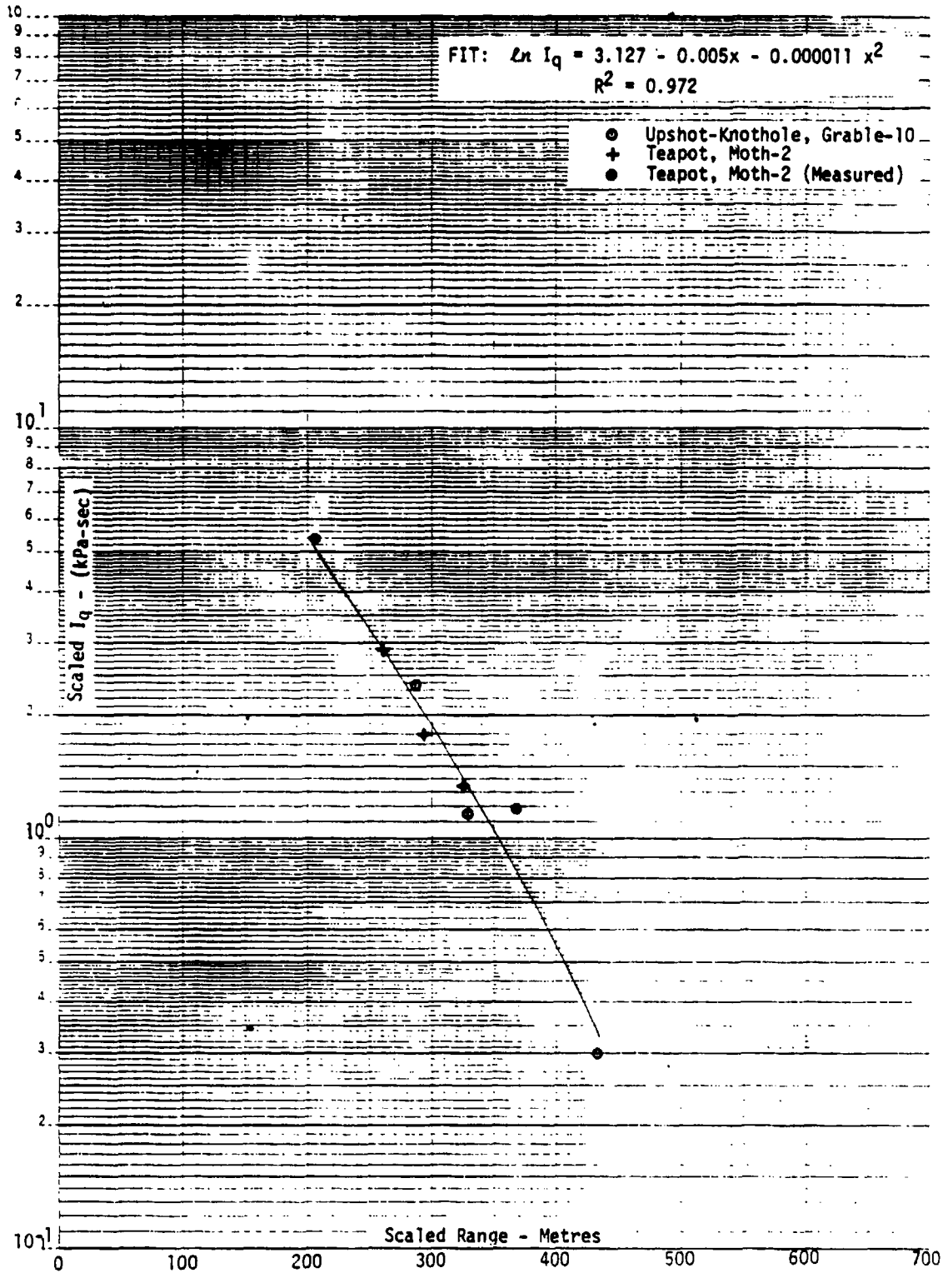

UNCLASSIFIED

Figure 4.12 (U) Dynamic Pressure Impulse vs. Range - Average HOB = 63.7 Metres, Scaled to 1 KT

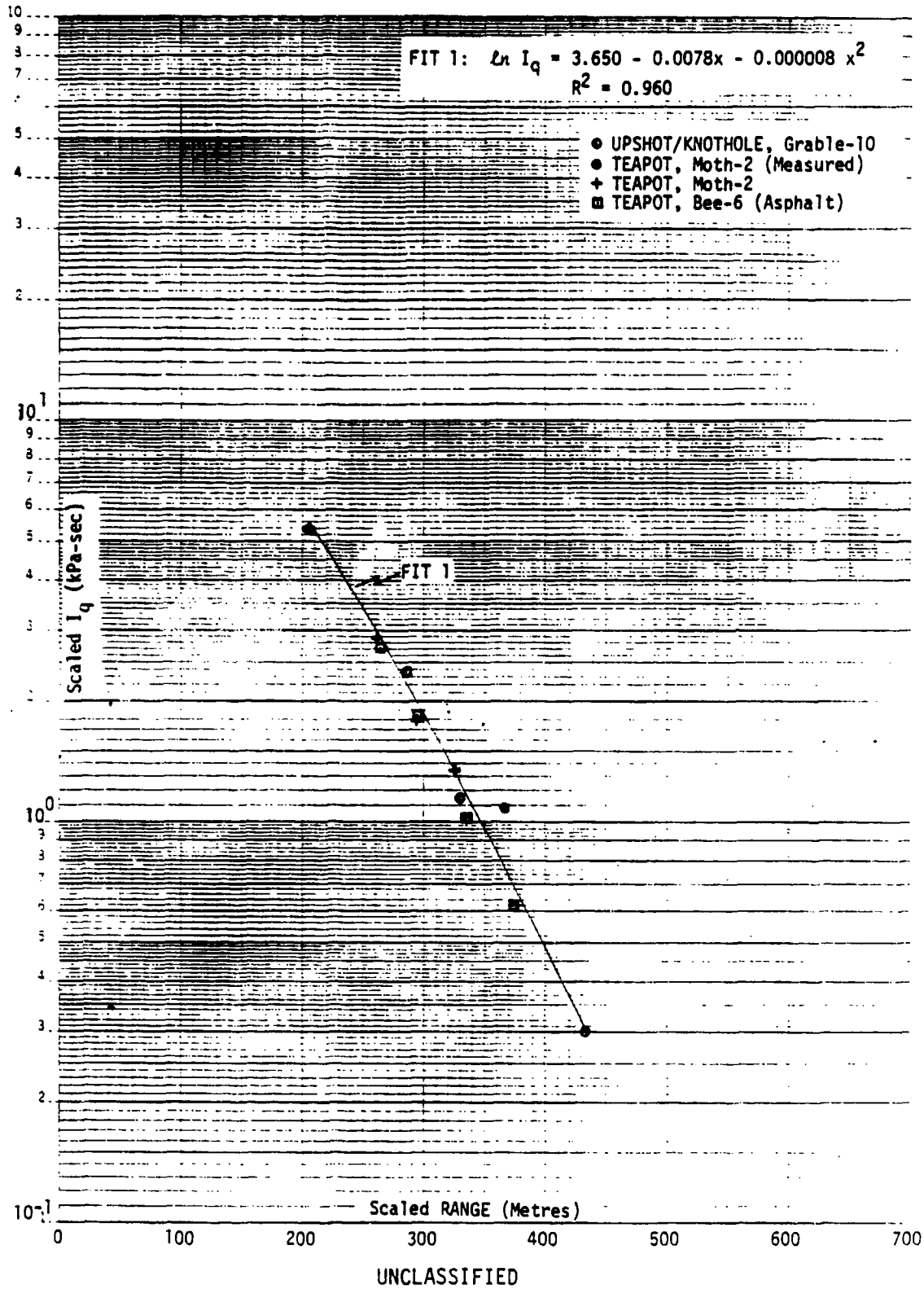

FIGURE 4.13 (U) Dynamic Pressure Impulse vs. Range - Average HOB = 66.9 Metres, Scaled to 1 KT

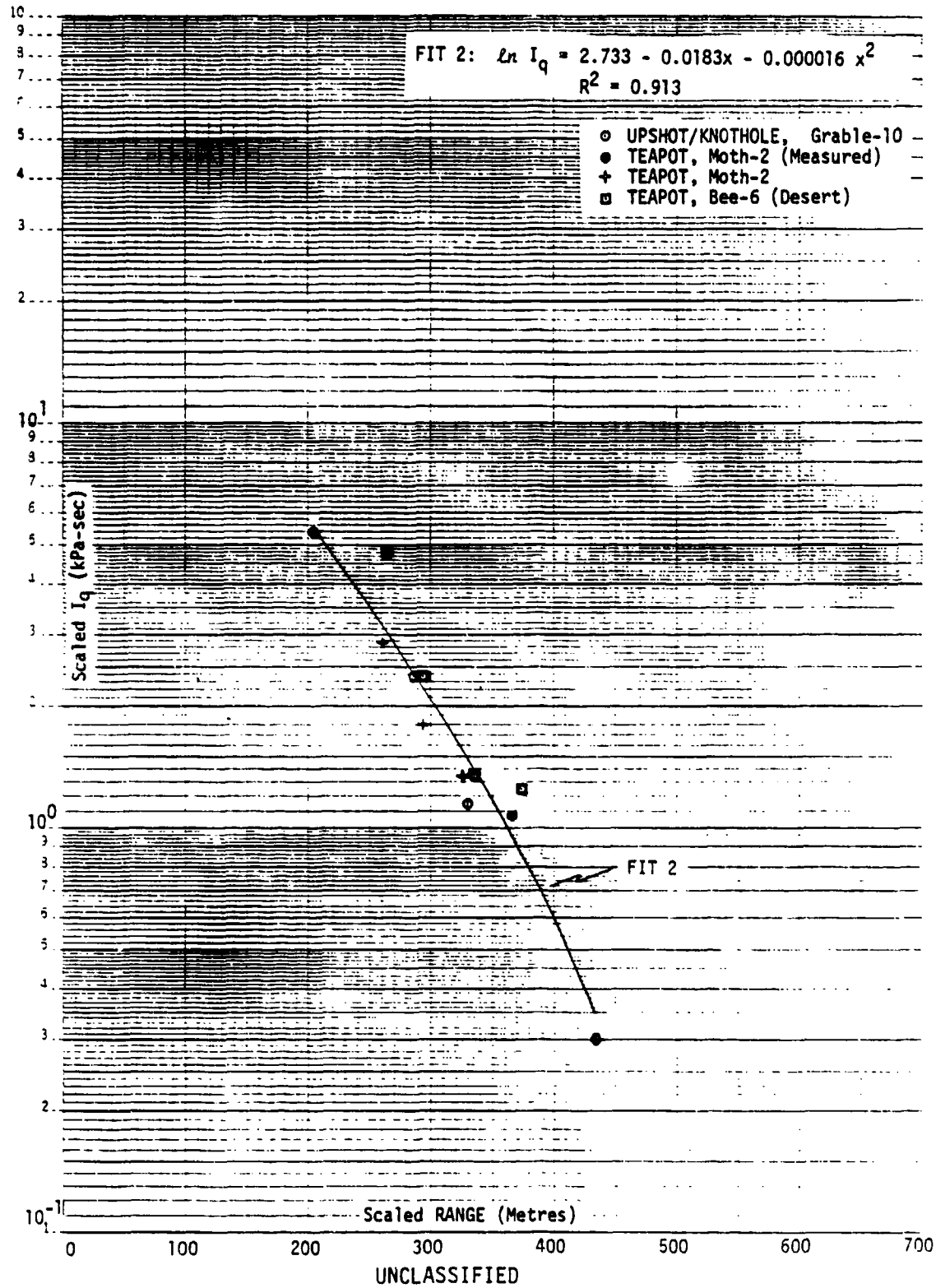

FIGURE 4.14 (U) Dynamic Pressure Impulse vs. Range - Average HOB = 66.9 Metres, Scaled to 1 KT

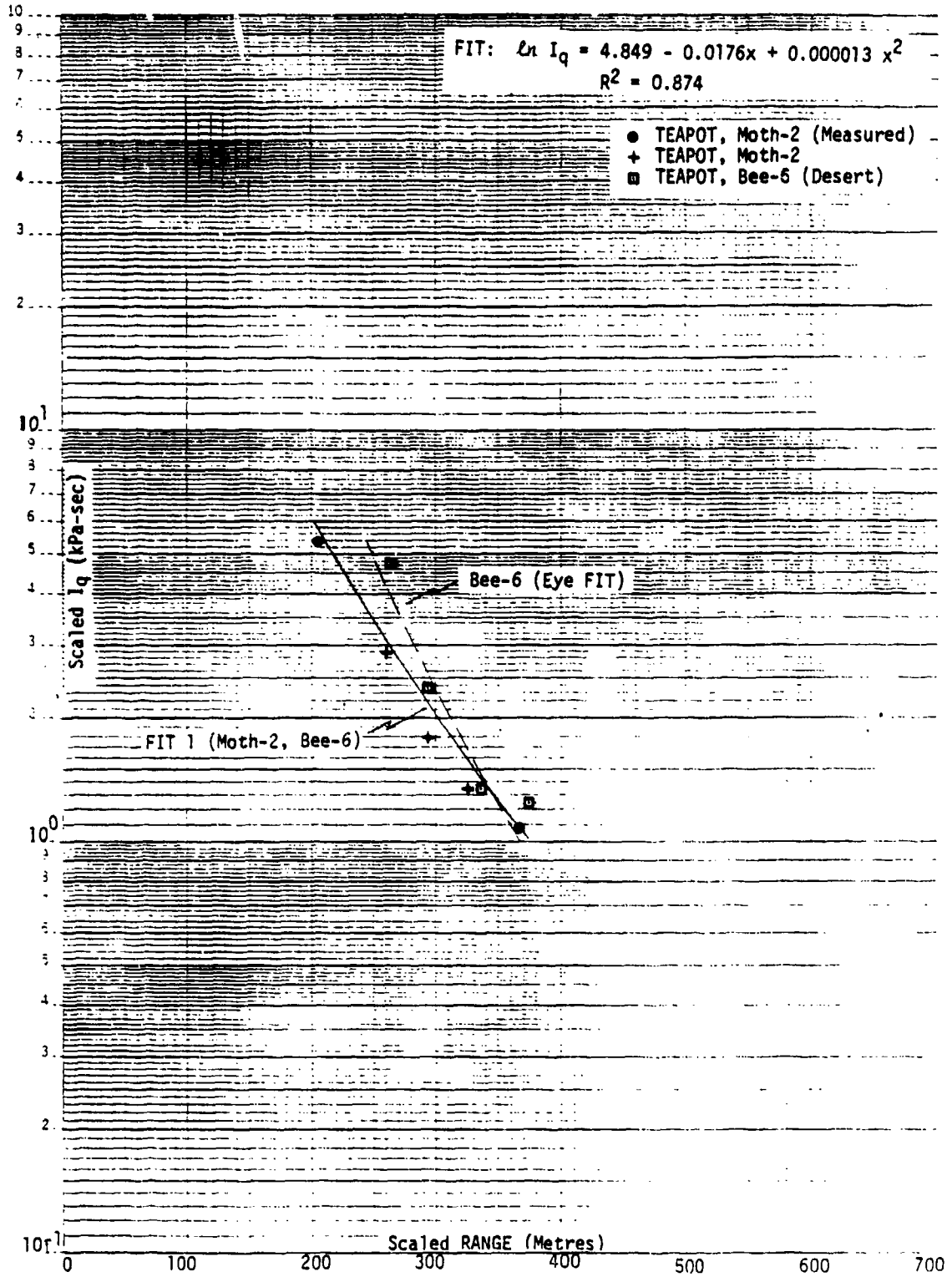

UNCLASSIFIED

FIGURE 4.15 (U) Dynamic Pressure Impulse vs. Range - Average HOB = 69.1 Metres, Scaled to 1 KT

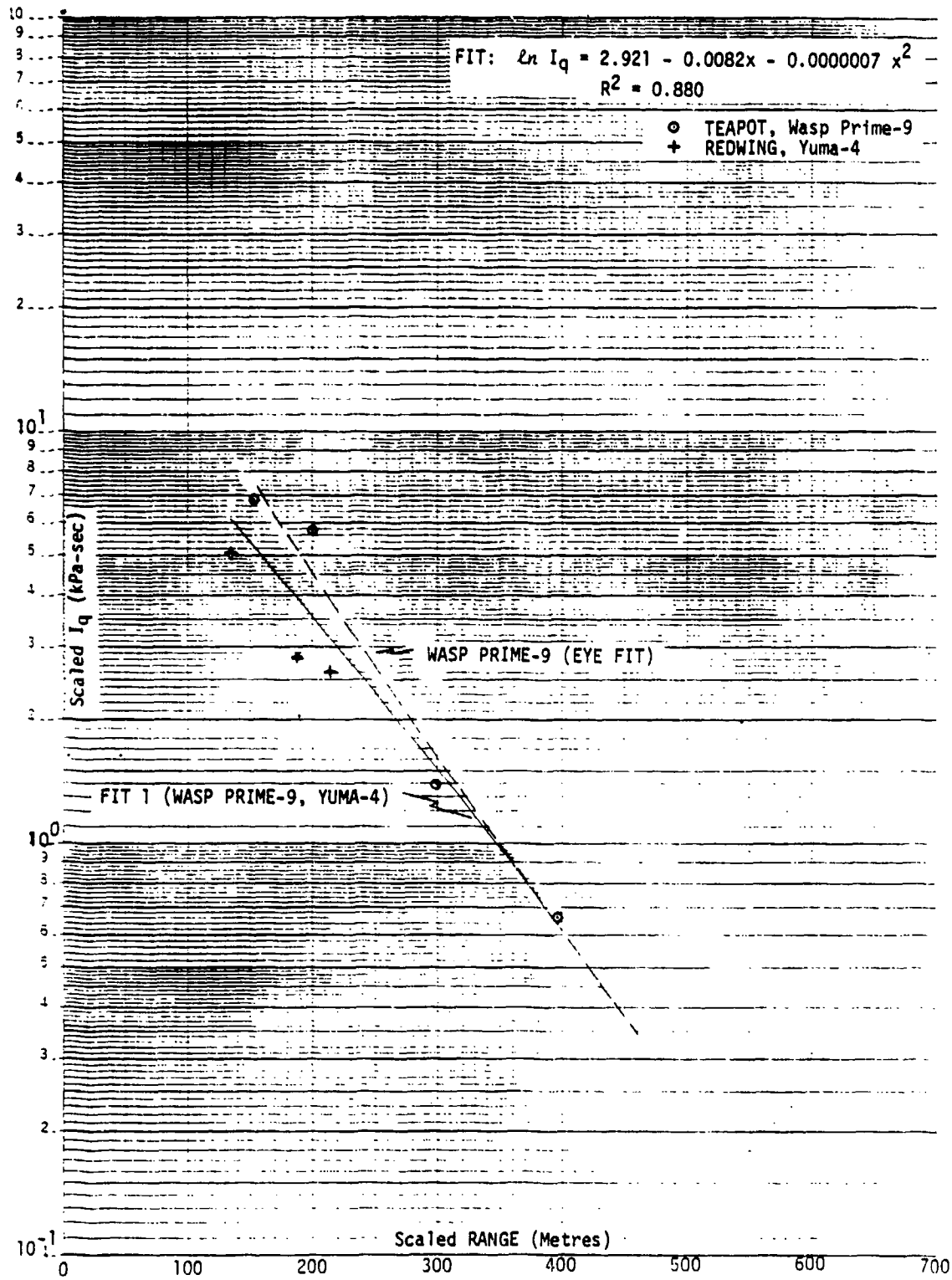

UNCLASSIFIED

FIGURE 4.16 (U) Dynamic Pressure Impulse vs. Range - Average HOB = 127.0 Metres, Scaled to 1 KT

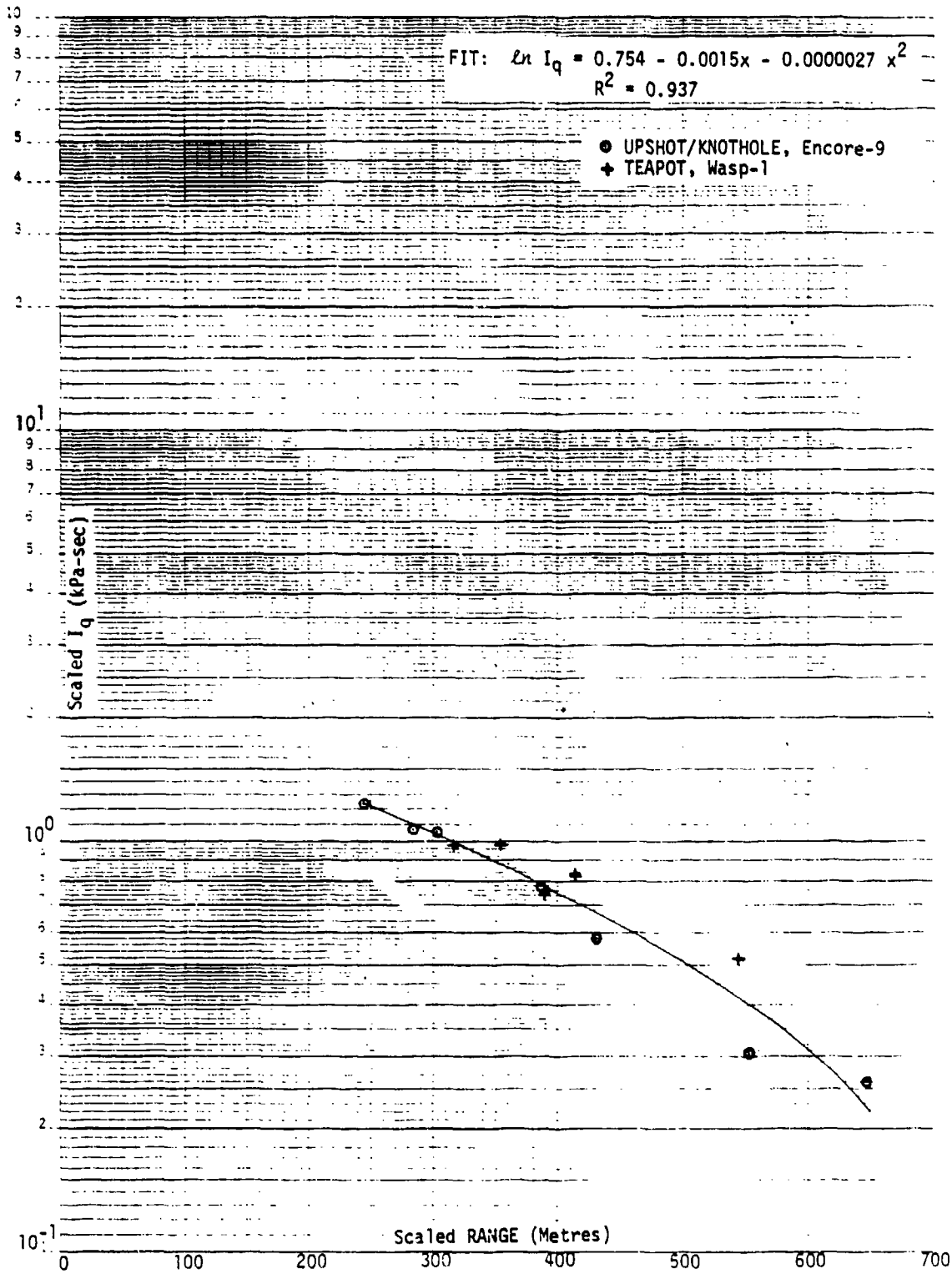

UNCLASSIFIED

FIGURE 4.17 (U) Dynamic Pressure Impulse vs. Range - Average HOB = 224.0 Metres, Scaled to 1 KT

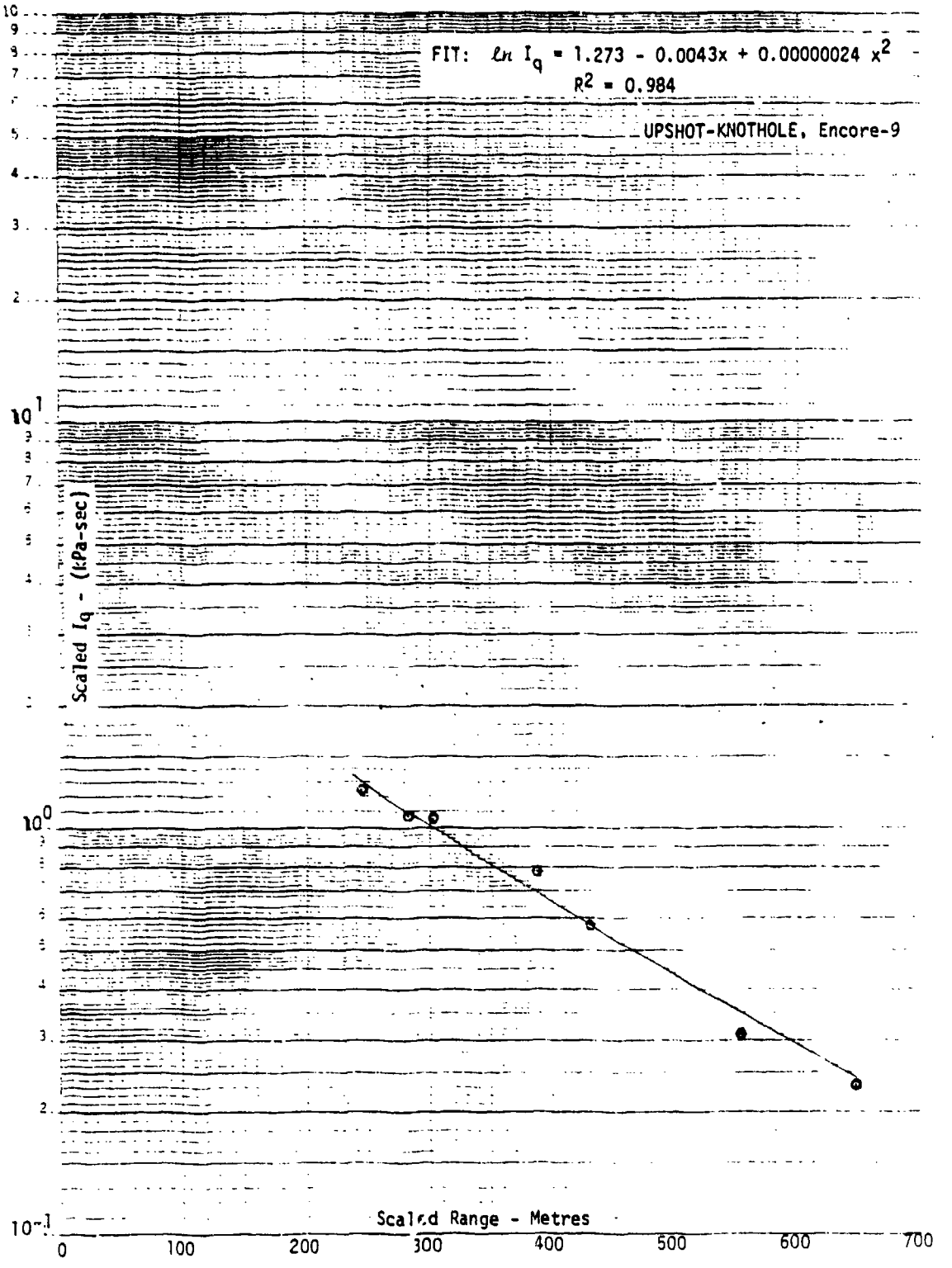

UNCLASSIFIED

FIGURE 4.18 (U) Dynamic Pressure Impulse vs. Range - Average HOB = 240.0 Metres, Scaled to 1 KT

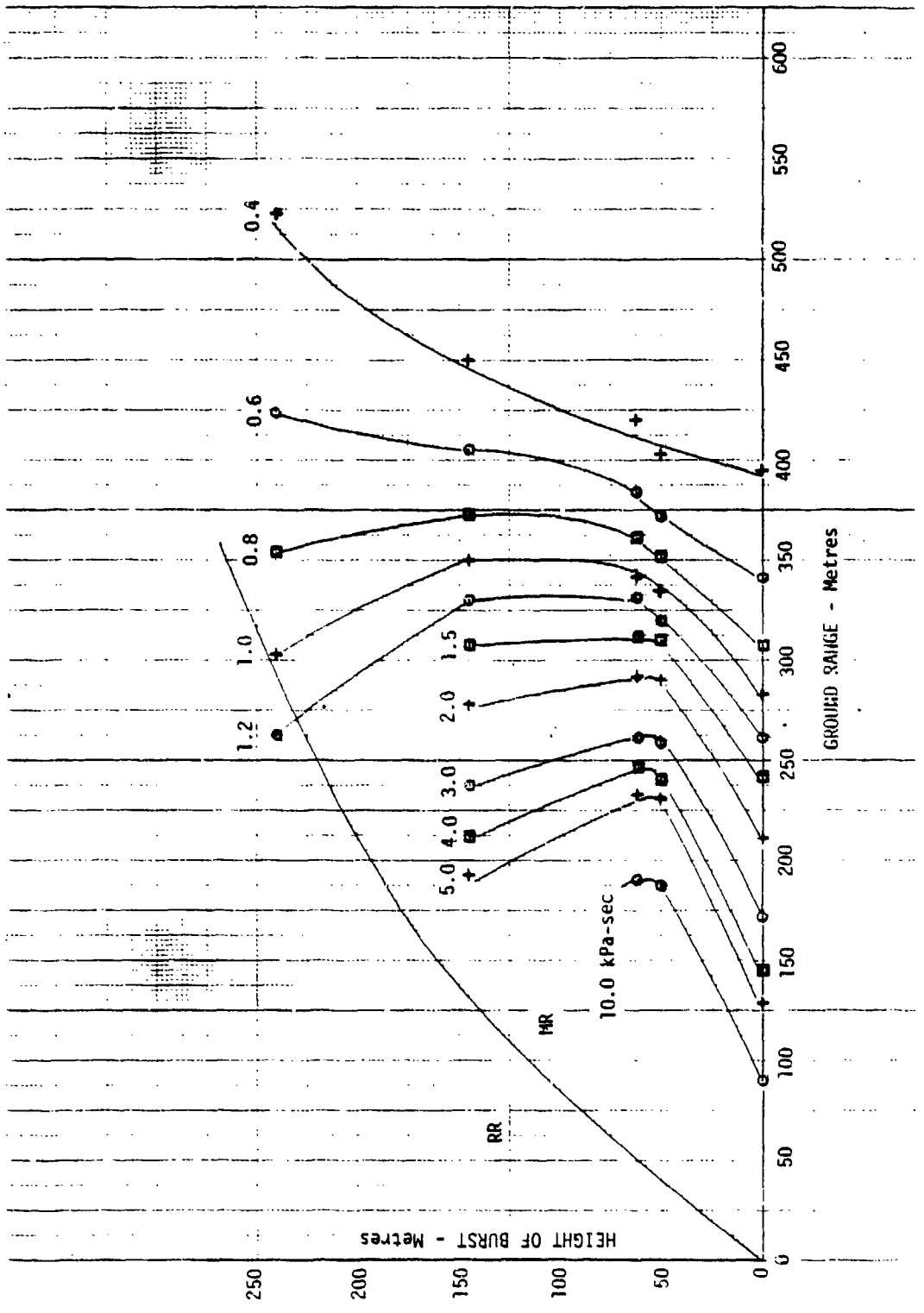

UNCLASSIFIED

FIGURE 4.19 (U) Dynamic Pressure Impulse vs. Ground Range at 0.91 Metres Above Surface -- Light Dust/Near-Ideal Surface, Scaled to 1 KT

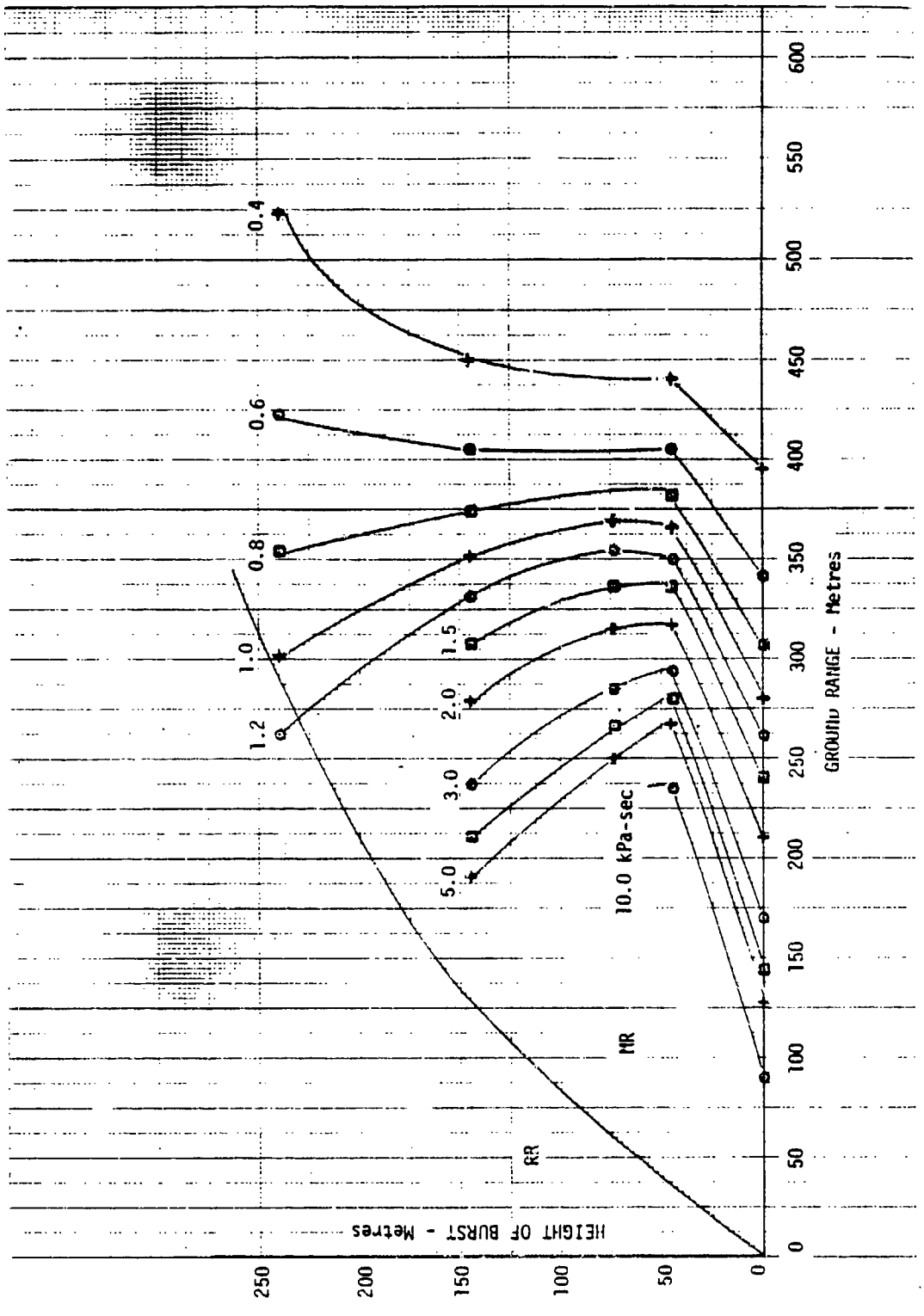

UNCLASSIFIED

FIGURE 4.20 (U) Dynamic Pressure Impulse vs. Ground Range at 0.91 Metres Above Surface -- Heavy Dust/Near-Ideal Surface, Scaled to 1 KT

SECTION 5
(This Section is Unclassified)

SUMMARY, CONCLUSIONS, AND RECOMMENDATIONS

5.1 SUMMARY AND CONCLUSIONS

5.1.1 Dynamic Pressure Impulse versus Displacement Displacement versus Dynamic Pressure Impulse

Two types of functions have been used for least squares fit to dynamic pressure impulse versus displacement and vice versa. The power functions were used to separately fit the data for the WWII and the M38A1 1/4 ton trucks. After further analysis in which we pointed out that these two vehicles could be treated as one type of truck, we combined the data for the 1/4 ton trucks as well as for the 2-1/2 ton trucks (M35 and M135) and used quadratic functions for least squares fits. Also, the I_q values for the non-ideal events were iterated and used in the latter least squares fits. The resultant equations for I_q versus displacement are:

Combined Vehicles: M38A1 and WWII -

SO $\ell n\ I_q = 0.133 + 0.376\ \ell n\ D + 0.0566\ (\ell n\ D)^2$

FO $\ell n\ I_q = 0.732 + 0.465\ \ell n\ D + 0.0220\ (\ell n\ D)^2$

Combined Vehicles: REO M35 and GMC M135 -

SO $\ell n\ I_q = 0.429 + 0.333\ \ell n\ D + 0.0275\ (\ell n\ D)^2$

and for displacement versus I_q the equations are:

Combined Vehicles: M38A1 and WWII -

SO $\ell n\ D = -0.223 + 2.222\ \ell n\ I_q - 0.214\ (\ell n\ I_q)^2$

FO $\ell n\ D = -1.362 + 2.081\ \ell n\ I_q - 0.0998\ (\ell n\ I_q)^2$

Combined Vehicles: REO M35 and GMC M135 -

SO $\ell n\ D = -1.365 + 3.339\ \ell n\ I_q - 0.4259\ (\ell n\ I_q)^2$

We find good correspondence between dynamic pressure impulse and displacement, in spite of the large scatter of data. A number of uncontrolled variables present in the experiments, which we described, contributed to the scatter. These variables are statistically averaged out in the use of least squares fit. One, therefore, can calculate with reasonable confidence the I_q from known vehicle displacements and calculate displacements (such as onset of motion) for given values of dynamic pressure impulse.

5.1.2 Displacement versus Scaled Ground Range

For different combinations of events we fitted the displacement versus scaled ground range using various values of n (the exponent of W used in scaling ground range). The best value of n is somewhat dependent on the burst height and surface conditions. The values of n for best fit of data were from n = 0.4 to n = 0.43. Our reason for these fits was to determine the feasibility of scaling the ground range for displacement since we correlated vehicle damage with displacement (Reference 17). Thus, for known displacements as a function of scaled ground range damage can be then predicted for different yields. The utility of this scheme needs further evaluation.

5.1.3 Dynamic Pressure Impulse (Unscaled and Scaled) versus Scaled Ground Range

We again fitted the unscaled dynamic pressure impulse versus scaled ground range using different values of n. The values of n which best fitted the data were n = 0.42 or n = 0.43. These were then compared to the scaled dynamic pressure impulse versus scaled ground range. We concluded from an overall viewpoint there is little difference in reliability between the two sets of curve fits to the data. The scaled or unscaled impulse versus scaled ground range curve fits may be used with equal confidence.

5.1.4 Surface Effects on Dynamic Pressure Impulse, Displacement and Damage

Comparing the data from water, asphalt, and Desert Rock for the same events, (Bee-6 and Met-12) we conclude the following:

1) The I_q for asphalt are lower than those for water and both are lower than for the desert line, (Met-12). On Bee-6, again, the I_q for asphalt are lower than for the desert line.

2) Displacements of vehicles on the water line are similar to the desert line, (Met-12) while the displacements on asphalt are smaller than on desert surface. The vehicle displacements on the Desert Rock are about the same as on the asphalt surface (Bee-6 and Met-12).

3) Comparison of displacement versus dynamic pressure impulse for desert and non-desert cases shows that there is no substantial difference among desert, water and asphalt surfaces.

4) Damage on the water surface was somewhat lower than on the desert surface while the damage on the asphalt surface on the average was somewhat higher than on the desert surface. The damage on Desert Rock

for a given displacement was higher than that on the desert line. Thus, for a given I_q value, displacement is at least approximately independent of the surface on which the vehicle is placed but for a given displacement damage is greater on the harder surfaces.

5.1.5 Scaled Dynamic Pressure versus Scaled Ground Range

We used the once-iterated I_q values (ideal/near-ideal, blast waves) and twice-iterated I_q values (non-ideal blast waves) for constructing scaled $\bar{I}_q$ versus range for several combinations of yield and burst heights. For most of the events we were able to distinguish the ideal/near-ideal blast environments from non-ideal blast environments. The non-ideal blast environments were further divided into light dust and heavy dust events.

We have high confidence in the scaled $\bar{I}_q$ versus range data for the surface bursts (ideal/near-ideal) and for the HOB span from about 40 to 70 metres (light dust events). There is less confidence on the $\bar{I}_q$ data above 70 metres but this is only because of the small amount of data available above this burst height.

We concluded that the surface conditions for the heavy dust events were unique and similar surface conditions would be rare in other parts of the world. We also concluded that dynamic pressure measurements were reasonable. More importantly, combining the I_q results from gages and those calculated from vehicle displacement results in greater reliability and accuracy in the I_q values. We also conclude that the I_q data obtained on the asphalt surface (Bee-6 and Met-12) fit reasonably well with data from the light dust events having similar burst heights.

5.1.6 Dynamic Pressure Impulse, $\bar{I}_q$, HOB Charts

Two HOB charts have been constructed, one for light dust/near-ideal and one for heavy dust/near-ideal. The light dust and heavy dust portions of the charts apply to HOB from 40 to 70 metres and the near-ideal apply to surface bursts and to HOB above 70 metres.

A comparison of heavy dust and light dust events shows that the $\bar{I}_q$ values for heavy dust are from 2 to 3 times the $\bar{I}_q$ values for light dust events. In terms of range, however, for equal $\bar{I}_q$ values the heavy dust is greater by about 27 percent at the higher I_q than for light dust and then they both converge to about the same range for lower $\bar{I}_q$ values.

In the HOB region from 40 to 70 metres the range for iso-I_q seem to be about the same for either the light dust or heavy dust events.

Because of unique surface conditions for the heavy dust events the blast environments produced were unique. Our tendency is to place less importance on the heavy dust events and perhaps even to disregard them. We consider the HOB charts which include the light dust events to be more representative of the expected blast conditions over various surfaces where precursors (non-ideal) would be formed. We feel that the resultant $\bar{I}_q$ values for these events (light dust) were caused principally by the precursor action (based on comparison of asphalt and light dust $\bar{I}_q$ values). The conclusion is that the light dust/near-ideal HOB chart (nomenclature here may now be a misnomer) is the preferred chart for application to other targets.

5.2 RECOMMENDATIONS

1) A procedure similar to that presented should be used for other drag-type targets to extend the region for I_q to higher values than 10 kPa-sec and for I_q to lower values than 0.4 kPa-sec. To obtain the higher values, heavier and harder drag-type targets such as tanks & howitzers can be used. For the lower values, lighter and softer targets such as antennas & communication equipment can be used. Additionally, different drag-type targets were exposed to nuclear blast at burst heights other than those used here. The evaluation of this information would allow greater confidence in the construction of the iso-$\bar{I}_q$ contours.

2) There is a need to develop predictions of dynamic pressure waveforms for the non-ideal blast environment. Current waveform predictions are based on the data obtained on heavy dust events which we consider to be unique. Application of waveform predictions is needed not only for determining loading and response of drag-type targets but diffraction type targets as well.

3) After a thorough evaluation of data for increasing the confidence in constructing HOB charts for $\bar{I}_q$ there is a need to construct composite HOB charts representing overpressure, dynamic pressure, static pressure impulse and dynamic pressure impulse. Various types of targets are sensitive to different blast mechanisms causing failure. For targeting and vulnerability evaluations an HOB chart of this nature would show the advantages or disadvantages against an array of targets, particularly when constructed by collateral damage (non-damage or limited damage to friendly targets).

SECTION 6
(This Section Is Unclassified)

LIST OF REFERENCES

1. E. J. Bryant and F. J. Allen, "Dynamic Pressure Impulse and Damage Derived From Vehicle Displacements For Ideal and Near-Ideal Blast Waves" (U), ARBRL-CR-00443, January 1981, Confidential-Formerly Restricted Data

2. E. J. Bryant and J. M. Hovanec, "Blast Damage and Displacements of Military Wheeled Vehicles", Volumes 1 and 2, KAMAN-TEMPO, DASIAC SR-176-1 and -2, to be published, Confidential-Formerly Restricted Data

3. J. R. Kelso, Editor, "Data Reduction Procedures For Nuclear Air Blast Instrumentation", AFWSP 1084, August 1959.

4. Noel H. Ethridge, "Blast Overturning Model For Ground Targets", BRL 1889, June 1976.

5. W. N. Lee and N. P. Hobbs, "TRUCK 30 - An Improved Digital Computer Program For Calculating the Response of Army Vehicles to Blast Waves", KAMAN-AVIDYNE, KA TR-171, September 1979.

6. F. M. Sauer, "Nuclear Airblast Precursor Dynamic Pressures Related to Surface Parameters", ARBRL-CR-00415, March 1980.

7. E. J. Bryant and J. H. Keefer, "Basic Airblast Phenomenon", Operation Plumbbob, Project 1.1, WT-1401, June 1962

8. "Proceedings of the Dice Throw Symposium, 21-23 June 1977", Volume 1, GE-TEMPO, DASIAC, DNA 4377P-1, July 1977.

9. R. J. Hesse, MAJ, CE, USA, "Damage to Field Military Equipment From Nuclear Detonations", AFSWP-511, 1 September 1955, Headquarters, Armed Forces Special Weapons Project, Washington, DC.

10. E. J. Bryant, N. H. Ethridge, and M. R. Johnson, 2LT, USA, "Response of Drag-Type Equipment Targets in the Precursor Zone, Operation Teapot, Project 3.1, WT-1123, July 1959, Confidential-Formerly Restricted Data

11. C.N. Kingery and B. F. Pannill, "Parametric Analysis of the Regular Reflection of Air Blast", BRL 1249, June 1964.

12. E. J. Bryant, N. H. Ethridge, and J. H. Keefer, "Measurements of Air Blast Phenomena with Self-Recording Gages, Operation Teapot, Project 1.14b, WT-1155, July 1959.

13. P. G. Guest, "Numerical Methods of Curve Fitting", Cambridge University Press, 1961.

14. Paul G. Hoel, "Introduction to Mathematical Statistics", John Wiley and Sons, Inc., New York, 1954.

15. Irvin Guttman and S.S. Wilks, "Introduction to Engineering Statistics", John Wiley and Sons, Inc., New York, 1965.

16. Ya-lun Chou, "Statistical Analysis", Holt, Rinehart and Winston, New York, Second Edition, 1975.

17. Bryant, E. J. and F. J. Allen, "Blast Damage to Military Field Equipment and Blast Damage Scaling (U)", DASIAC SR-209, Kaman Tempo, 31 October 1984 Confidential-Formerly Restricted Data

THIS PAGE IS INTENTIONALLY LEFT BLANK.

APPENDIX A
(This Section is Unclassified)

IDEAL/NEAR-IDEAL DYNAMIC PRESSURE IMPULSE

The procedure selected to provide us with initial dynamic pressure impulse values for ideal/near-ideal blast environments to be correlated with vehicle displacements was based on theoretical calculations and analytical techniques along with the use of measured blast parameters (Reference 1). From the theoretical calculations and the analytical techniques we obtained the ratio of static pressure impulse to dynamic pressure impulse, I_p/I_q, as a function of overpressure, P_s. The theoretical calculations consisted of the HULL code computations for Dice Throw and for 1 KT nuclear detonation at HOB = 60 $W^{1/3}$. The analytical technique used was that of Ethridge (Reference 4) for a 500 ton HE hemispherical charge. These ratios of I_p/I_q as a function of overpressure are shown in Figure A.1.

We pointed out in Reference 1 that the best measurements of blast parameters which were reasonably reliable were overpressure and static pressure impulse. Thus, for each ideal/near-ideal blast event, we obtained the average values of the measured overpressure and static pressure impulse at each vehicle location. These values were then used in conjunction with Figure A.1 to obtain the dynamic pressure impulse.

The curve designated as 1 KT 60 $W^{1/3}$ (Figure A.1) was used to derive the ratios of I_p/I_q as a function of P_s for Upshot/Knothole, Encore-9 and Redwing, Yuma-4. The scaled height of burst for these two events were: Encore-9, 240 $W^{1/3}$ metres and Yuma-4, 109 $W^{1/3}$ metres. The curve, NHE, was used for Castle, Koon-3 and Nectar-6; Redwing, Lacrosse-1 and Zuni-3; and for the Canadian 20 Ton and 100 Ton events. Both of the Canadian events were hemispherical and burst at ground surface. The nuclear events were surface bursts and it is to be noted that the NHE curve is a good approximation of a 1 KT nuclear weapon burst on the surface. And, of course, for Dice Throw the HULL calculations were used.

The values of dynamic pressure impulse derived by this procedure were checked using the Rankine-Hugoniot and empirical relations. The percentage difference between these two procedures in the majority of cases was about 10 percent, although some were as large as 25 percent.

The initial estimates of dynamic pressure impulse for the nine events

are shown in Figures A.2 through A.10 (solid lines). We also plotted the first iteration of $\bar{I}_q$ on these Figures (see Section 4.1). We note again that $I_{q_{avg}}$ which was combined with I_{q_0} to obtain $\bar{I}_q$, was derived from vehicle displacements using the quadratic fits (Section 3.1.2.4). Overall the agreement between the initial estimates and $\bar{I}_q$ are good with some exceptions. One of the exceptions is Yuma-4 which we discussed previously (Section 4.1). Other exceptions are 1 or 2 points such as on Nectar-6 and Zuni-3 where the $\bar{I}_q$ is $\pm$ 18 to 22 percent from the initial estimates.

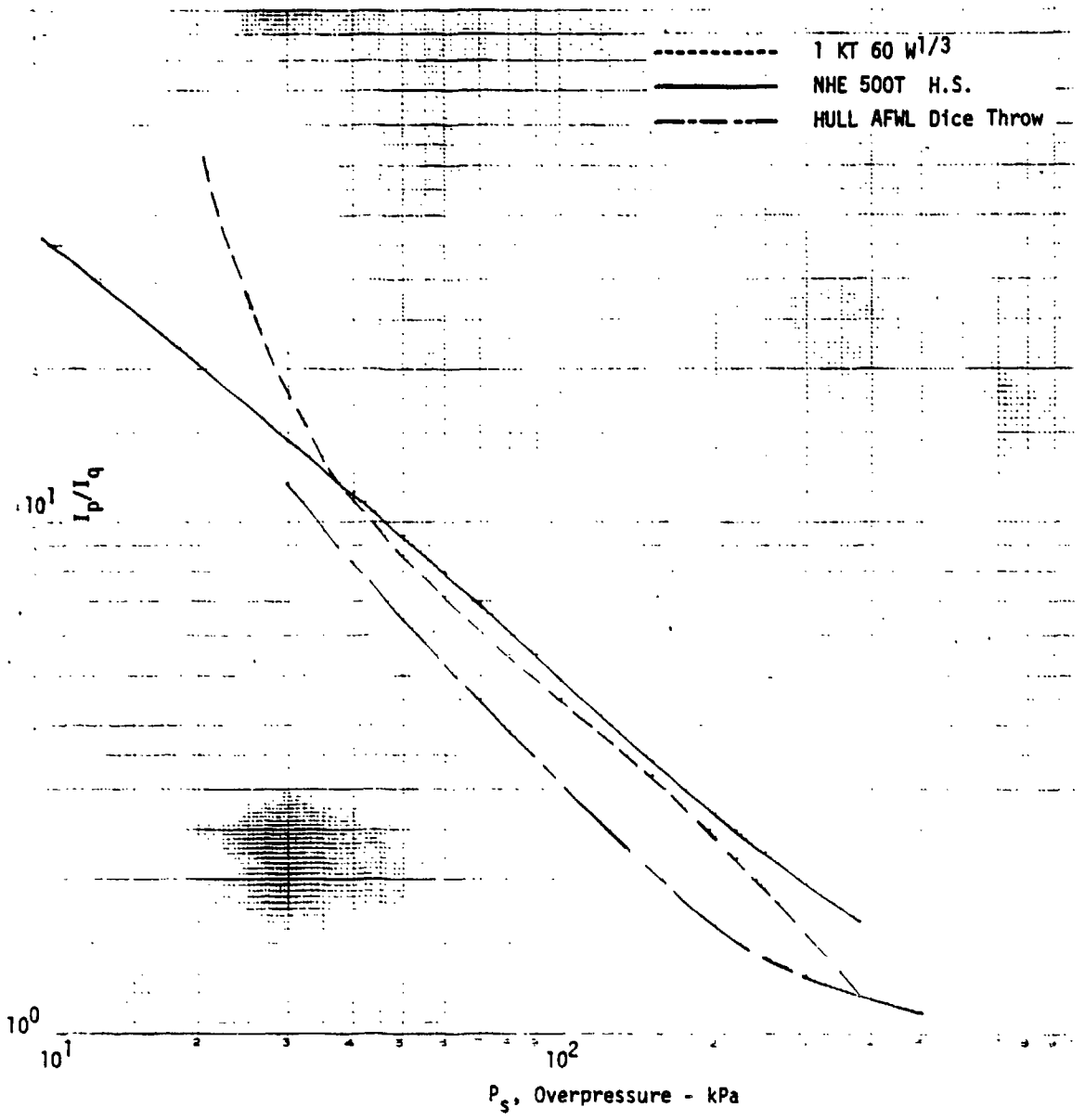

UNCLASSIFIED

FIGURE A.1 (U) Ratio of I_p/I_q versus Overpressure

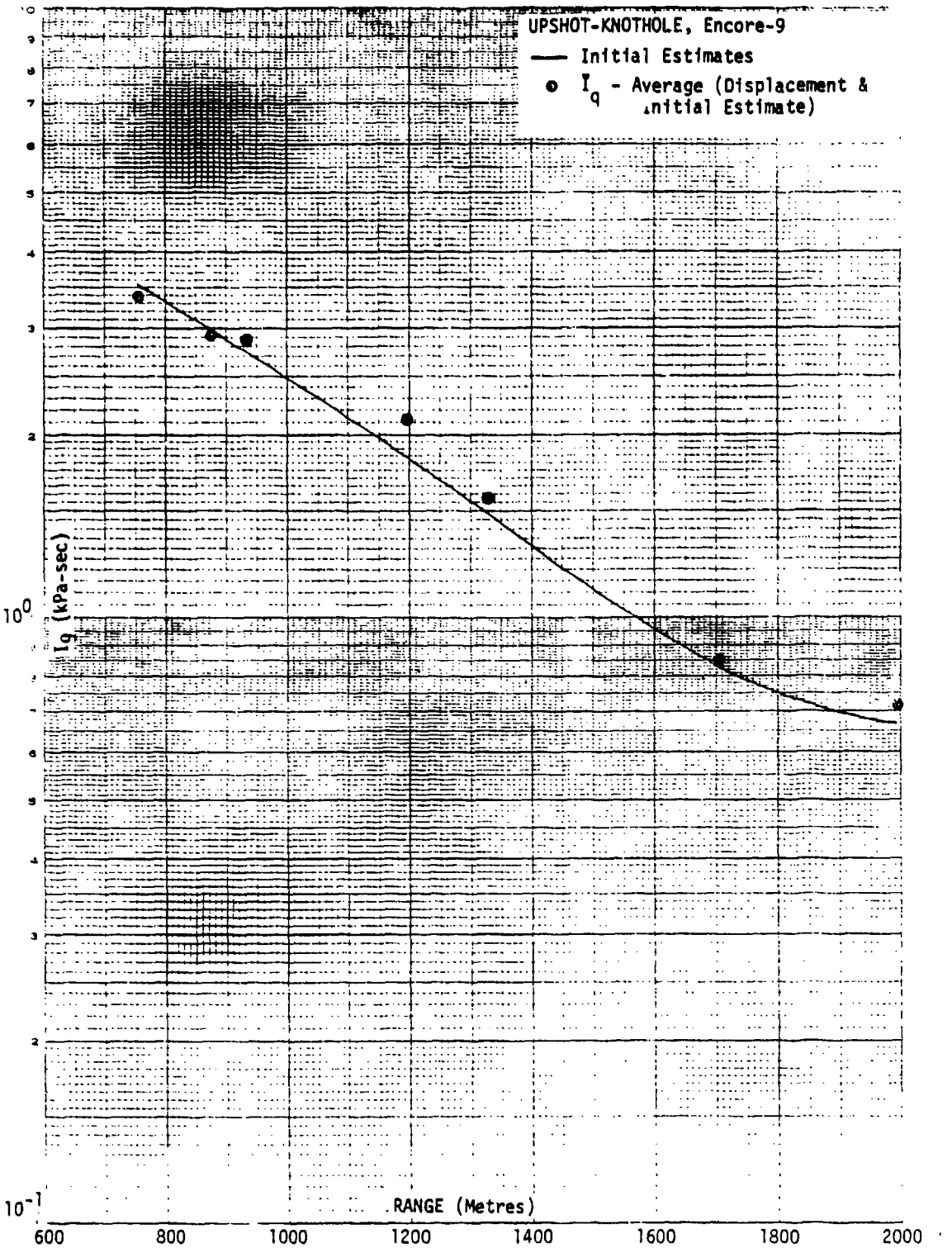

UNCLASSIFIED

FIGURE A.2 (U) Dynamic Pressure Impulse versus Range - Upshot/Knothole, Encore-9

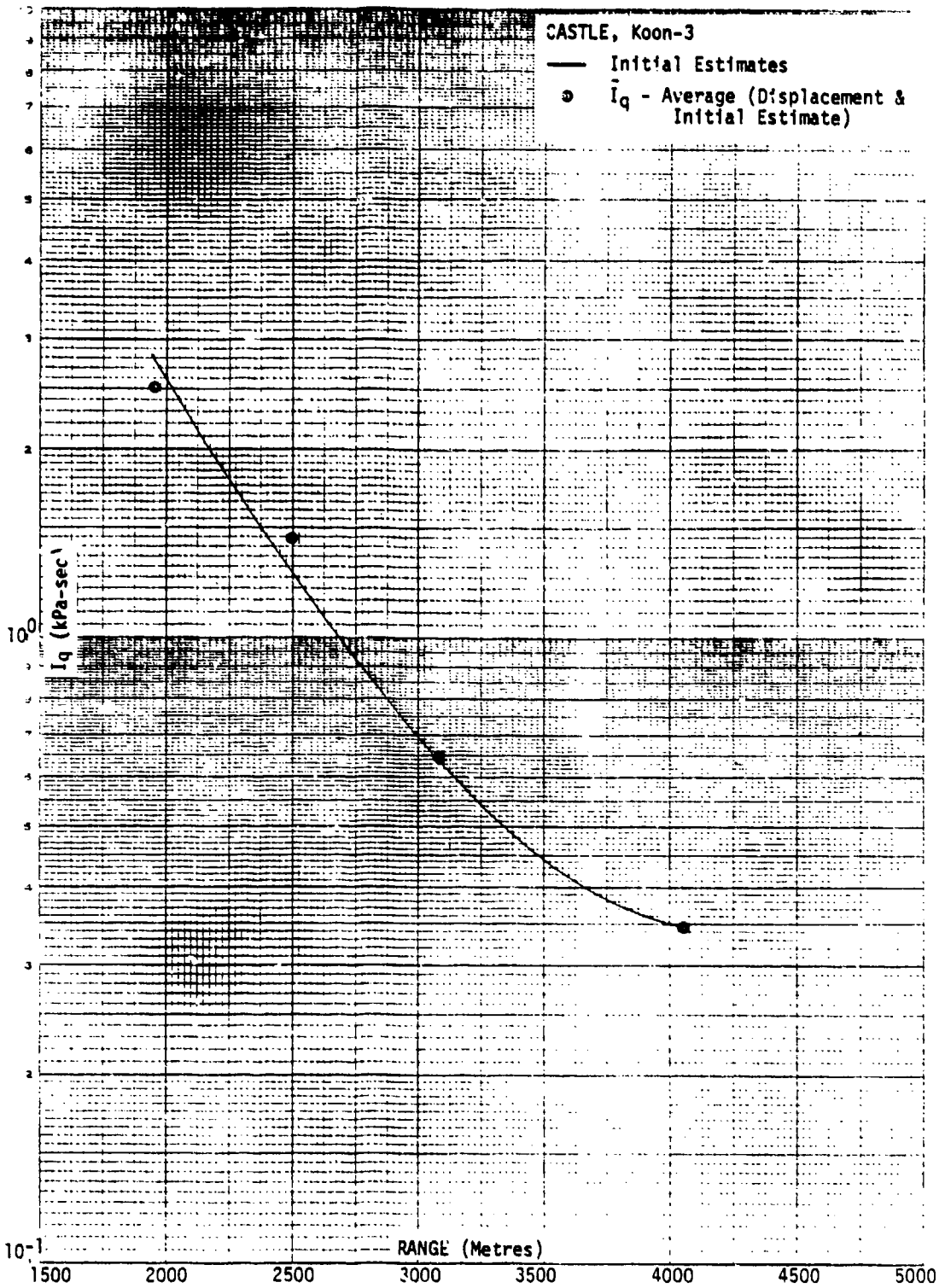

UNCLASSIFIED

FIGURE A.3 (U) Dynamic Pressure Impulse versus Range - Castle, Koon-3

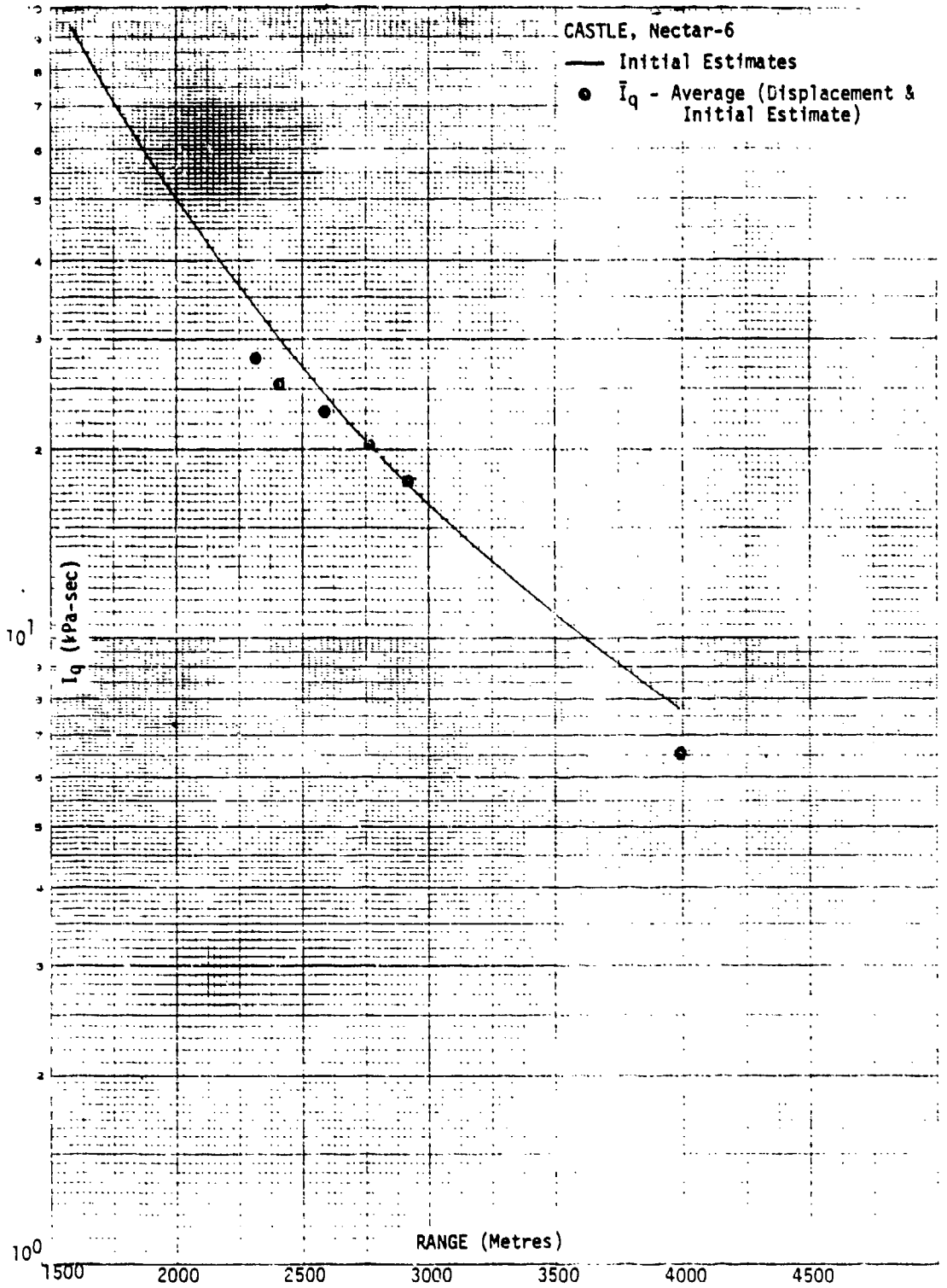

UNCLASSIFIED

FIGURE A.4 (U) Dynamic Pressure Impulse versus Range - Castle, Nectar-6

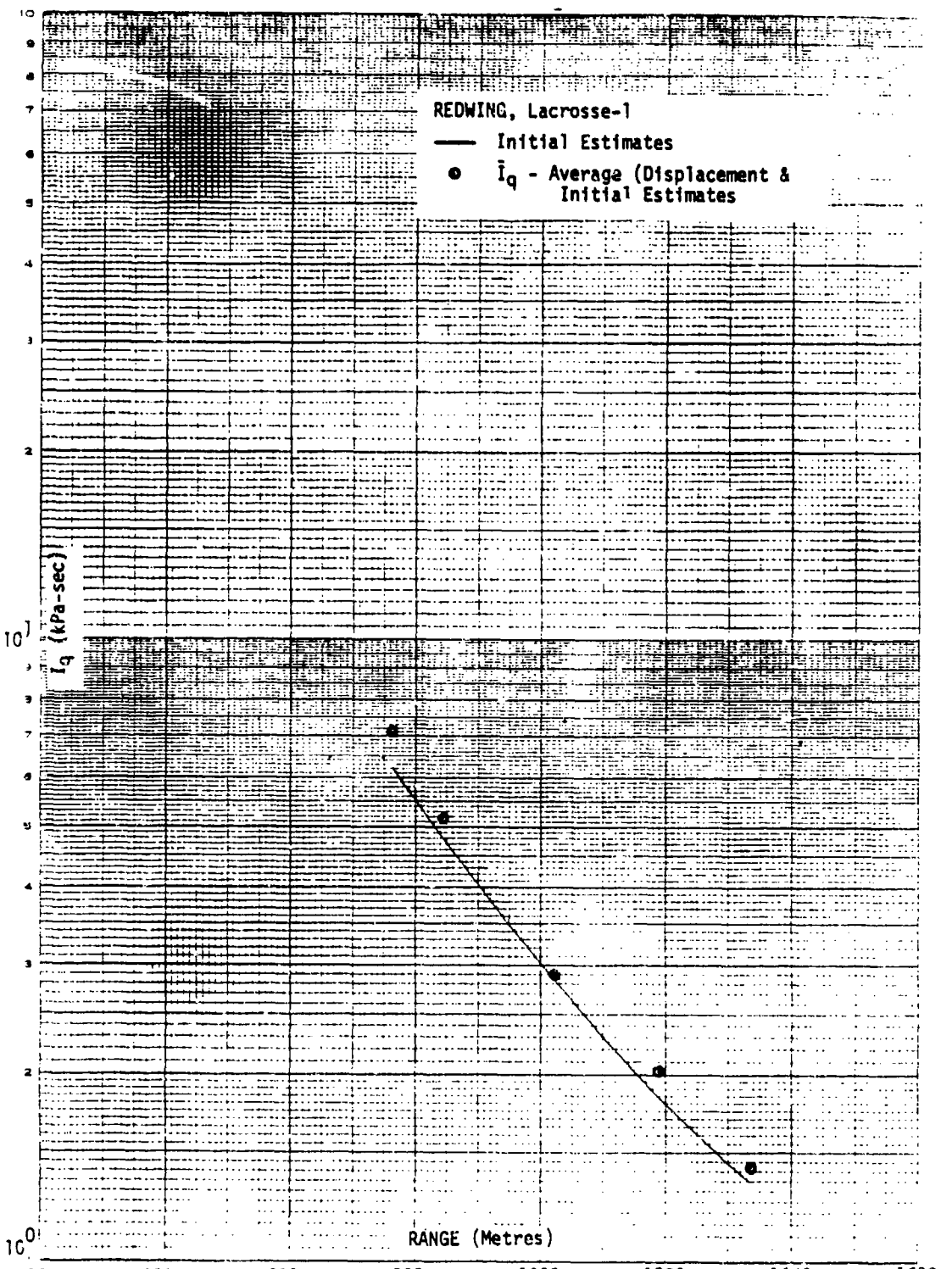

UNCLASSIFIED

FIGURE A.5 (U) Dynamic Pressure Impulse versus Range - Redwing, Lacrosse-1

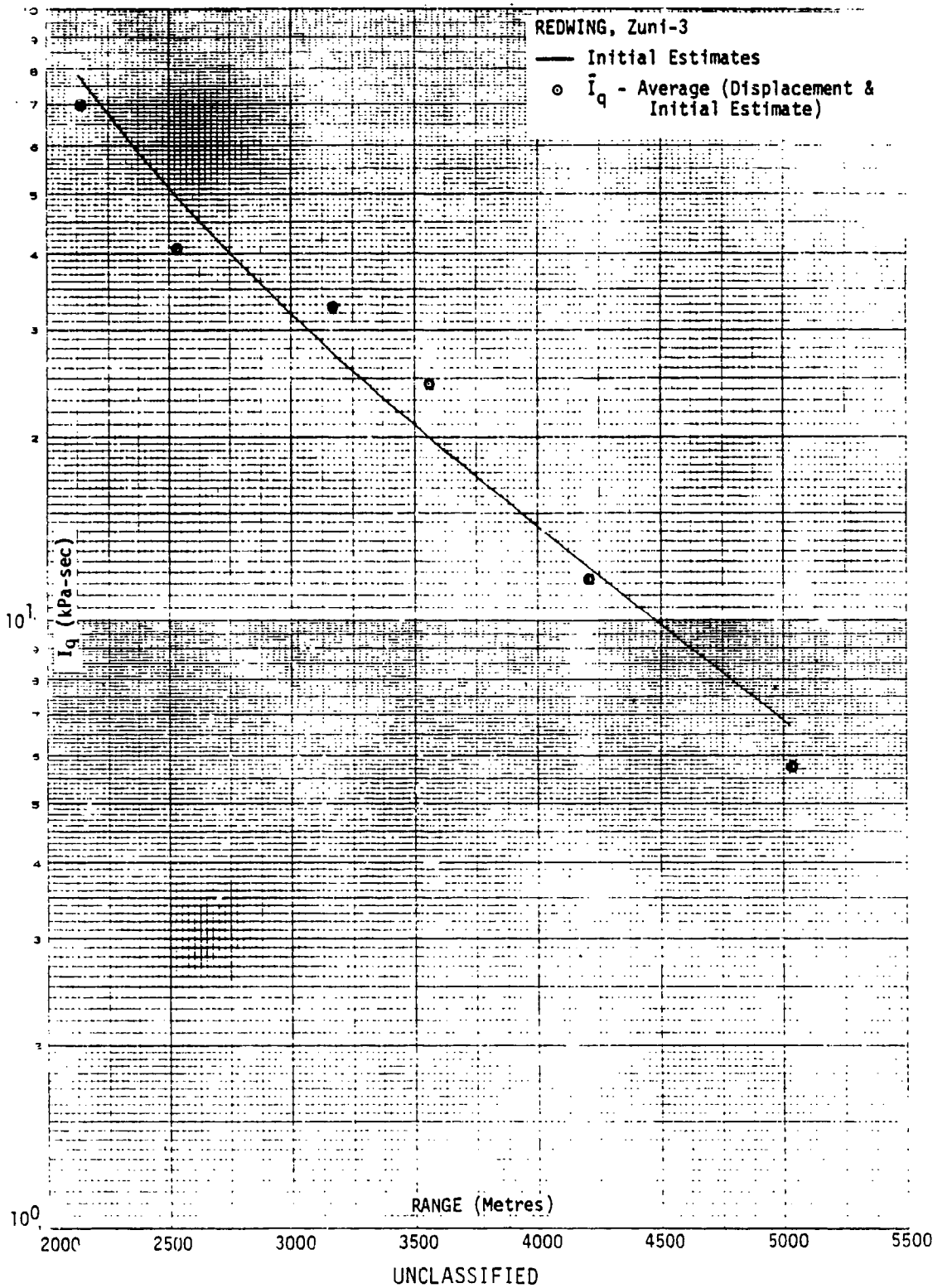

FIGURE A.6 (U) Dynamic Pressure Impulse versus Range - Redwing, Zuni-3

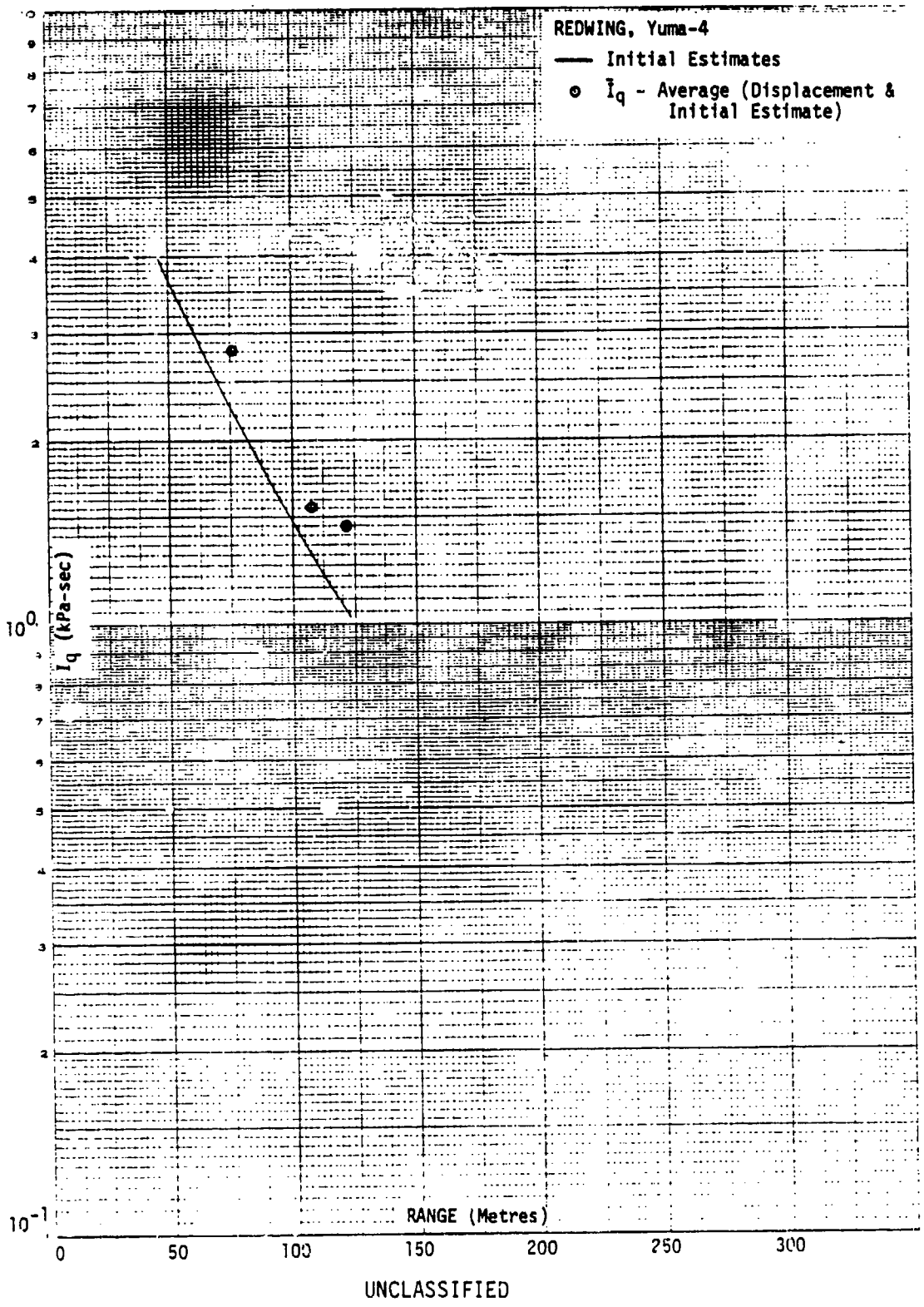

UNCLASSIFIED

FIGURE A.7 (U) Dynamic Pressure Impulse versus Range - Redwing, Yuma-4

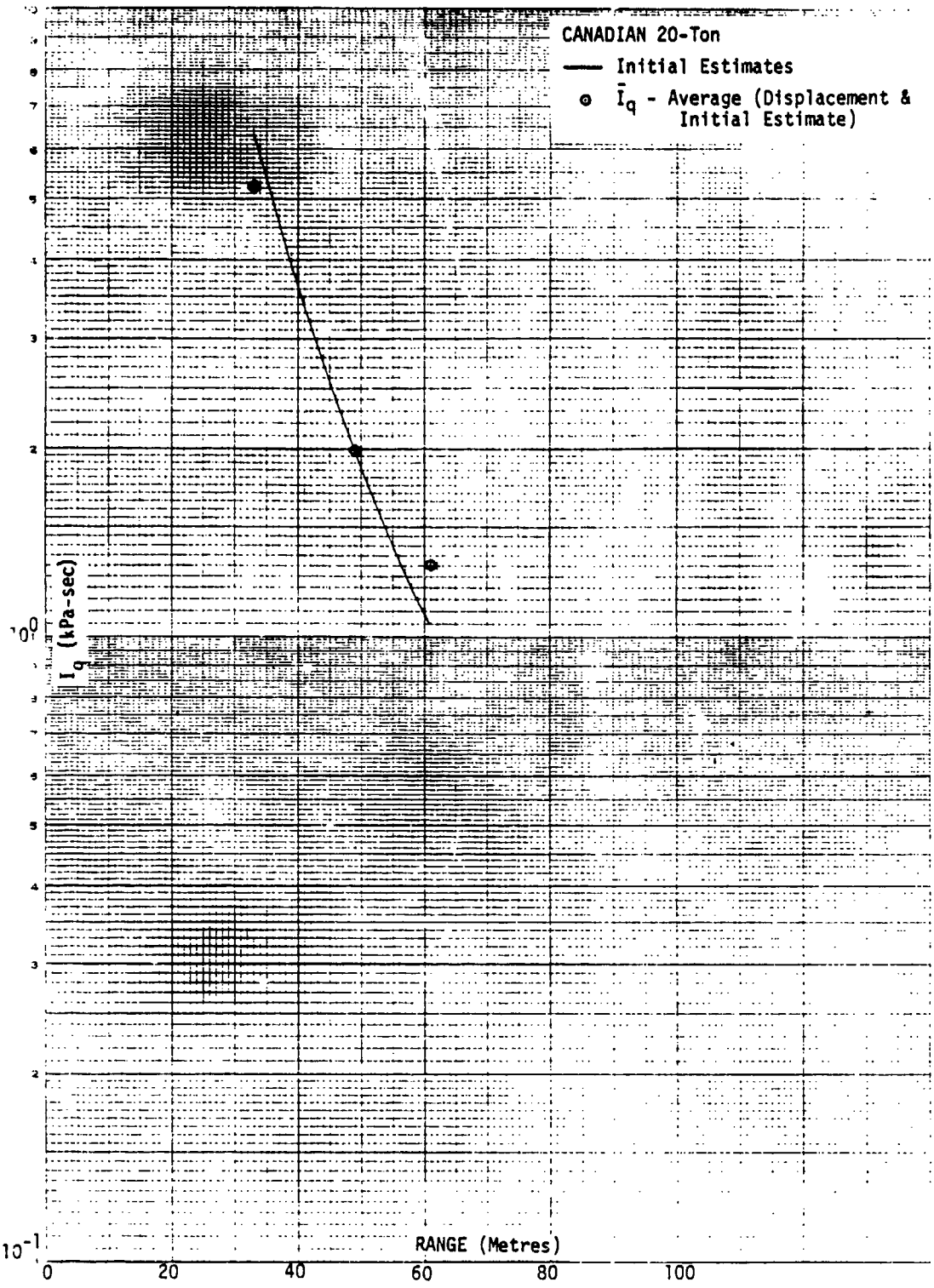

UNCLASSIFIED

FIGURE A.8 (U) Dynamic Pressure Impulse versus Range - Canadian 20 Ton

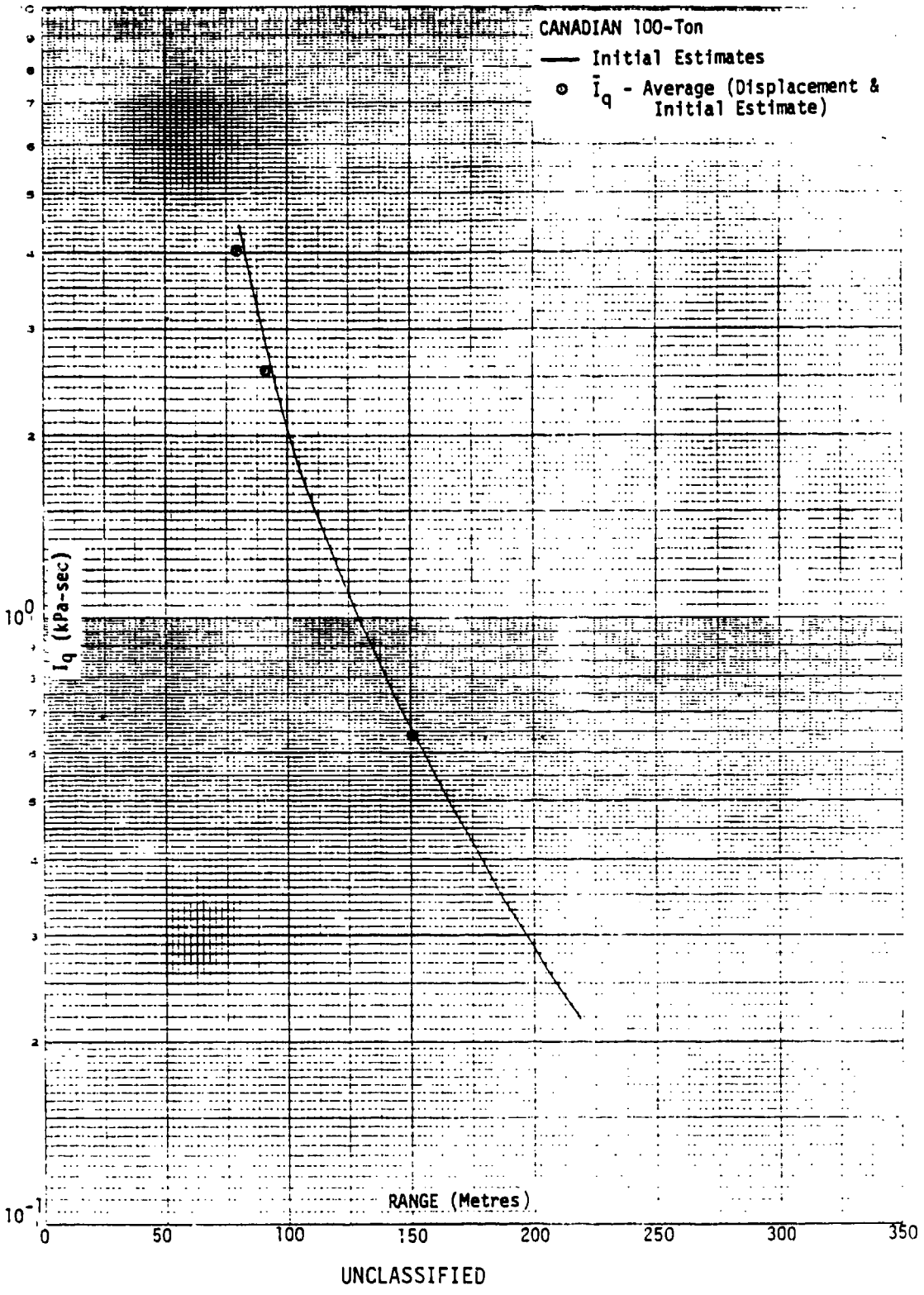

UNCLASSIFIED

FIGURE A.9 (U) Dynamic Pressure Impulse versus Range - Canadian 100 Ton

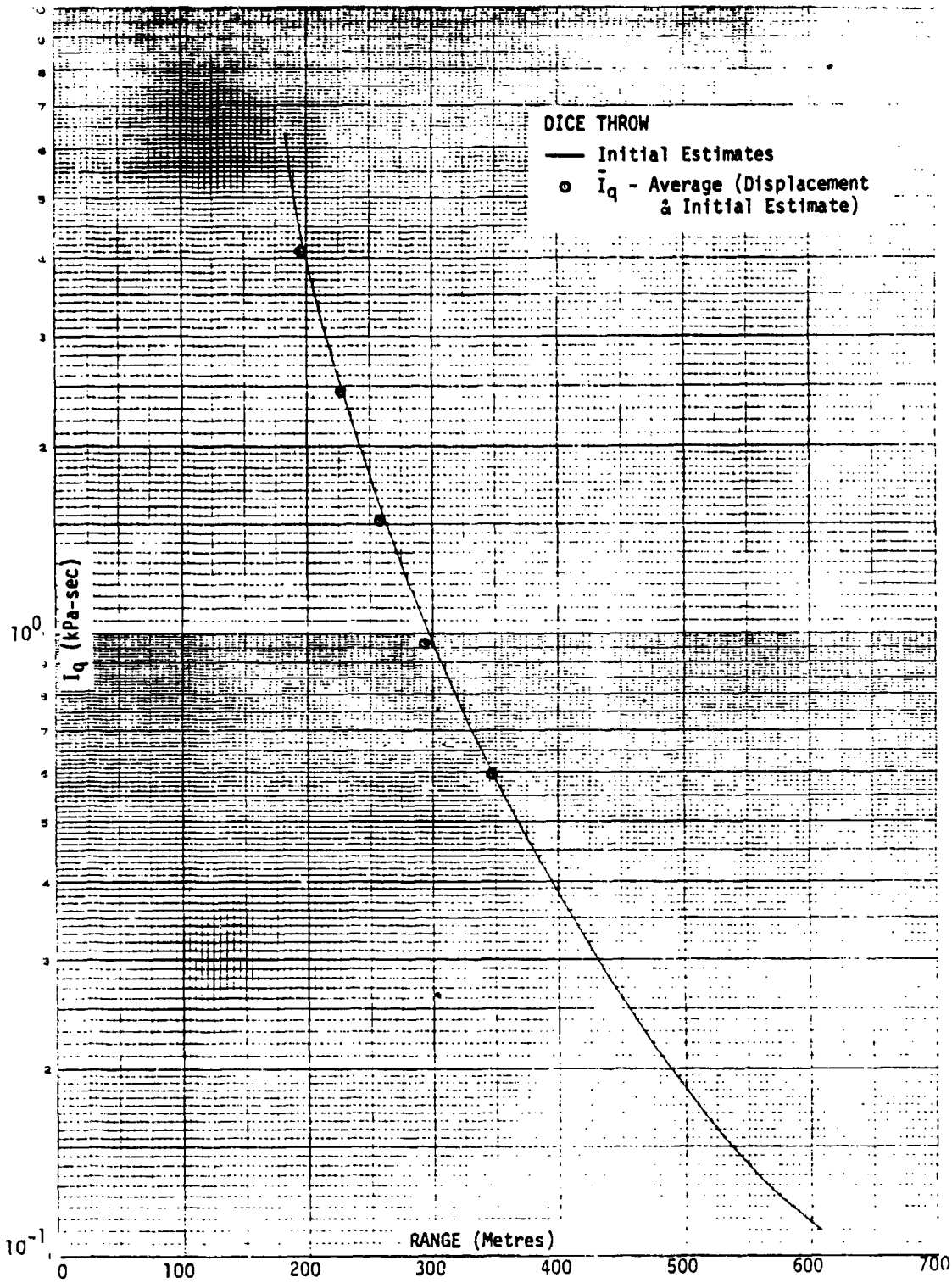

UNCLASSIFIED

FIGURE A.10 (U) Dynamic Pressure Impulse versus Range - Dice Throw

APPENDIX B
(This Section is Unclassified)

DETERMINATION OF DYNAMIC PRESSURE IMPULSE FOR NON-IDEAL SHOTS

B.1 DATA REDUCTION PROCESS

The shots involved in this section were all part of Operation Teapot.* We used two basic procedures and some variants of these to determine dynamic pressure impulse from the measured pressure-time histories. The measurements consisted of total head overpressure and static overpressure versus time, the latter at two locations: one at ground level and one at the same height, usually 0.91 metres (3 feet), as used to measure total head pressure. In addition, previously conducted reduction of this data (using only the two gages at the same height, not the ground level measurement) provided dynamic pressure versus time waveforms (not corrected to account for the perturbation to the pressure undergoing measurement by the gage used to make the measurement). In the following we describe the correction process for the dynamic pressure provided and an independent data reduction method we used to calculate dynamic pressure impulse from the original gage data.

We use the following nomenclature (Reference 3):

P_S - absolute free stream static pressure

P_T - absolute free stream total pressure

P_p - absolute total head Pitot pressure

P_o - ambient pressure

$\Delta P_S = P_S - P_o$ — free stream static overpressure

$\Delta P_T = P_T - P_o$ — free stream total overpressure

$\Delta P_p = P_p - P_o$ — total head overpressure

q - dynamic pressure

Q_i - dynamic pressure impulse; subscript i denotes ith method of obtaining result (4 values of i used)

γ - ratio of specific heat at constant pressure to specific heat at constant volume for air

M - local free stream Mach No. of flow behind blast front

Δt_i - ith time interval (in a pressure-time waveform)

$G(M)$ - Mach correction factor

$\overline{G(M)}$ - average value of G(M) over pressure-time history

* There was one exception to this: Plumbbob, Smoky-15.

W_i - weighting factor for ith time interval

To determine dynamic pressure impulse when q(t) is provided, without Mach correction, we must calculate the Mach correction and integrate the corrected dynamic pressure over time. This involves some of the operations used in calculating the dynamic pressure impulse from the raw data (pressure waveforms), so we start with the latter.

It can be shown (Reference 3) that

$$q(t) = [P_T(t) - P_S(t)]/\frac{2}{\gamma M^2}\left[\left(1 + \frac{\gamma-1}{2} M^2\right)^{\frac{\gamma}{\gamma-1}} - 1\right] \qquad (1)$$

and that for $\gamma = 1.4$ and $M < 2.24$ this can be replaced by

$$q(t) = \frac{P_T(t) - P_S(t)}{G(M)} \qquad (2)$$

where $G(M) = 1 + \frac{1}{4} M^2 + \frac{1}{40} M^4 + \frac{1}{1600} M^6 + \ldots$ (3)

Also $P_T/P_S = \left(1 + \frac{\gamma-1}{2} M^2\right)^{\frac{\gamma}{\gamma-1}}$. (4)

For $M \leq 1$, $P_p = P_T$. (5)

However, for $M > 1$, $P_p \neq P_T$ so that to determine P_T (from the gage result P_p) we must first find the Mach No., M.

To do this, following Reference 3, we have

$$\frac{P_p}{P_S} = \left[\frac{\left(\frac{\gamma+1}{2} M^2\right)^{\gamma}}{\frac{2\gamma}{\gamma+1} M^2 - \frac{\gamma-1}{\gamma+1}}\right]^{\frac{1}{\gamma-1}} \qquad (6)$$

Thus, for $M \leq 1$, we can determine M from Equation (4) since P_T and P_S are known (as functions of time). Then G(M) is determined from Equation (3) and q(t) from Equation (2). Breaking up the waveforms into time intervals (the same set of intervals for P_T and both P_S gages) and using this method then

yields a set of values of $q(t_i)$. Then $Q = \int q\,dt \cong \sum_i q(t_i)\Delta t_i$ (7)

For $M > 1$, we can determine M from Equation (6), then P_T from Equat (4) since P_p and P_S are known (as functions of time). The same procedure as above then determines Q. (γ is known as a function of the static overpressure, see Reference 11.)

In practice, the overpressure-time rather than the absolute pressure-time histories are the data provided. Therefore, we wished to transform the above relations to a form suitable for using the measured pressures directly. To do this we rewrite Equations (4) and (6):

$$\frac{P_T}{P_S} = f_1\ (M, \gamma),\ M \leq 1 \tag{4a}$$

$$\frac{P_p}{P_S} = f_2\ (M, \gamma),\ M > 1 \tag{6a}$$

and note that Equation (2) can be written:

$$q(t) = \frac{\Delta P_T(t) - \Delta P_S(t)}{G(M)} \tag{2a}$$

Equation (4a) may now be written:

$$\frac{\Delta P_T + P_o}{\Delta P_S + P_o} = f_1\ (M, \gamma)$$

or, $\Delta P_T = f_1\ (M, \gamma)\ \Delta P_S + P_o\ [f_1\ (M, \gamma) - 1],\ M \leq 1$ (8)

and similarly, $\Delta P_p = f_2\ (M,\gamma\ )\ \Delta P_S + P_o\ [f_2\ (M, \gamma) - 1],\ M > 1$.

Therefore, for fixed values of M, γ and P_o the desired relations, Equations (8), are straight lines. We plotted these relations using ΔP_p as ordinate, ΔP_S as abscissa, calculating f_1 and f_2 from the right hand sides of Equations (4) and (6) for assumed values of M and γ. We made separate linear plots for each decade of static overpressure, ΔP_S. This is convenient since γ can be

obtained as a function of static overpressure (Reference 11). For $1 \leq P_s \leq 100$ psi we took $\gamma = 1.4$. For $100 < P_S \leq 1000$ psi we took $\gamma = 1.35$.

It turns out that there were few instances of concern to us for which $P_S > 100$ psi. Further, it turns out, as will become apparent when we consider inaccuracies involved in the data reduction process, that changes in both γ and P_0 induce changes in the calculated results which are negligibly small compared with unavoidable inaccuracies in the data reduction process. We assumed $P_0 = 14$ psi. Also for $M \gtrsim 1.3$, the difference between P_p and P_T is completely negligible compared with inaccuracies involved in data reduction.

We plotted Equations (8) in the manner indicated for values of M between 0.2 and 2.0 in increments of 0.2. However, in reducing the Operation Teapot data we only rarely encountered a value of $M > 1.2$, so that the Mach corrections owing to perturbation of the flow by the measuring instrument are, in general, quite modest.* See Equation (3).

Prior to initiating the data reduction process we carefully examined the pressure-time waveforms (Reference 12) in order to devise a systematic method with as good accuracy as can be achieved. We noted several sources of inaccuracy: the waveforms are small, especially on the pressure axis, typically 0.5" peak value; the areas under the pressure-time curves are small, usually less than 1 square inch, this being especially true for the (already reduced, but not Mach corrected) dynamic pressure-time curves where the areas under the curves are typically in the range of 0.2 to 0.4 square inches (with a few smaller and a few larger than this); in many cases the waveforms are highly irregular, some of the irregularities probably being real, i.e., physically present at the gage, and some probably being instrumental; there are some problems which appeared to be due to baseline drift during recording and some which may well have been due to gage clogging (with dust).

The previous data reduction process, which provided the available dynamic pressure-time histories, used a point-by-point method; i.e., values of total and static pressures were taken at identical (or almost identical) times from the raw data and the dynamic pressure calculated at each such time (as the difference between the total and static overpressures). Sometimes the dynamic

* In reducing the data for the Plumbbob, Smoky-15 event, Equations (4) and (6) were used. Plots of these Equations are given in Figures B.1 and B.2.

pressure, as obtained in this manner, was negative — owing presumably to the difficulties enumerated in the previous paragraph.

Any attempt to use the pressure-time waveforms in the form in which they are now available to obtain a dynamic pressure-time curve via a point-by-point data reduction method seemed to us to be doomed to failure. We concluded that better accuracy (though not nearly as good as could be desired) could be achieved by use of a planimeter to measure areas under the curves in selected time intervals.

We used the sets of parametric curves (straight lines) corresponding to Equations (8) in conjunction with visual inspection of each set of waveforms (3 waveforms: P_p and two P_s, only one of the latter having been used in the previous data reduction process) to determine approximate average values of Mach No. over trial intervals. Where average values of M were relatively large or rapidly varying the time intervals were taken fairly small. We also looked visually at the waveforms in doing this in order to properly average out effects of irregularities in planimetering the areas under the curve for each time interval. When no (or only small) irregularities were present we took the relative contribution of each time interval to the total area under the pressure-time curve into account in choosing the intervals. Finally, since the waveforms had to be considered in sets, if one waveform had much more irregularity than others in the set of three, it largely determined the choice of time intervals, the same set of time intervals being used, however, for all three waveforms in each set. The number of time intervals used for each set varied from 1 to 6 in our data reduction procedure for Operation Teapot. We believe that the choices of intervals in each case are about the best we can make: using a greater number of intervals decreases the areas associated with them and results in greater inaccuracy in measuring the area with a planimeter. (In general, we planimetered each area twice, and in the case of the smaller areas three times — without resetting the planimeter; this improves the overall accuracy somewhat. Also, in many cases, including all those in which results could be questioned for any of several reasons, areas in question were replanimetered.)

B.2 PROCESSING OF REDUCED DATA

Having obtained the areas under the various pressure-time curves for

each selected interval and for the total curve (value obtained separately and checked against the sum over the intervals) we proceeded as follows to obtain (4) values of dynamic pressure impulse. First we calculated average values of ΔP_p and ΔP_S for each gage and for each time interval simply by dividing the planimeter value $\Delta P_p \Delta t_i$, for example, by Δt_i, the selected time interval. We then read the Mach No., M_i, for the time interval from our set of parametric straight line plots of ΔP_p versus ΔP_S corresponding to Equations (8). Interpolation between the lines of constant M, spaced at intervals of 0.2, caused negligible inaccuracy here compared with other inaccuracies in the data reduction process (alluded to previously and to be discussed later). Then Equation (3) — or a plot thereof — determines $G(M_i)$, the Mach correction factor for the ith time interval. Considering now the ΔP_p and one of the ΔP_S gages, we did this for each value of i and then formed $(\Delta P_p - \Delta P_S)_i \Delta t_i$ for each i and also $\sum_i (\Delta P_p - \Delta P_S)_i \Delta t_i$. Then we associated a weighting factor with each time interval:

$$W_i = \frac{(\Delta P_p - \Delta P_S)_i \Delta t_i}{\sum_i (\Delta P_p - \Delta P_S)_i \Delta t_i} \qquad (9)$$

This factor is the ratio of the dynamic pressure impulse associated with the i^{th} time interval to the entire dynamic pressure impulse at the gage location. (When the ground static overpressure gage is used for ΔP_S, the two gages are a few feet apart; however, the ground gage does not perturb the flow field.)

$$\text{Note that } \Sigma W_i = 1 . \qquad (10)$$

In using (9) we have assumed

$$\Delta P_p \cong \Delta P_T, \; M \gtrsim 1.3 \qquad (11)$$

since, as we have previously noted, the difference between ΔP_p and ΔP_T is negligible compared with unavoidable inaccuracies in data reduction. In fact in the Operation Teapot data reduction, use of (11) is justified in all cases. (Remember also that by use of time intervals rather than a point-by-point data reduction process we smooth out irregularities in M_i — real or instrumental and possibly made worse by data reduction procedure inaccuracy — and substitute an average value of M_i for the i^{th} time interval; in a point-by-point method some higher, and lower, values of M would be found in each of our time intervals in which there are significant waveform irregularities.)

With the aid of Equation (9) we are now in position to determine an average value of the Mach correction factor over the entire pressure-time history. Denoting this by $\overline{G(M)}$, we have

$$\overline{G(M)} = \Sigma W_i \, G(M_1) \, . \tag{12}$$

For reasons that will be clear when we discuss accuracy of the method in more detail this is the only use we made of the planimetered areas of the selected intervals for each set of waveforms; in the remainder of the data reduction process we used only total area under the pressure-time curves.

Note that $\overline{G(M)}$ as given by Equation (12) is greater than the value which would be obtained if only one "interval" — the entire waveform — were used. That is, if we were to base the average Mach correction factor on the areas under the entire P_p and P_s waveforms, we would get too low a value.

This is because the highest values of M and G(M) occur in intervals of time which have the greatest differences between ΔP_p and ΔP_s, i.e., which make the greatest contribution to dynamic pressure impulse. Since the Mach Nos. involved are fairly low for Operation Teapot events, values of G(M) are also fairly low so that the difference between $\overline{G(M)}$ as given by (12) and the value of $\overline{G(M)}$ which would be obtained based on the entire pressure pulse — one interval — never exceeds a few percent. We now can use the value of $\overline{G(M)}$ obtained from Equation (12) in two ways, separately for the two static overpressure gage results, each used in conjunction with the single total head overpressure gage result, to obtain 4 estimates of the value of dynamic pressure impulse. We denote these estimates by Q_i, i = 1 . . . 4.

$$Q_1 = \int(\Delta P_p - \Delta P_{S_1}) \, \Delta t/\overline{G(M_1)} \tag{13}$$

where the integral is the difference of the planimetered values of the areas under the entire curves of total head overpressure and static overpressure ($\Delta P_p = \Delta P_T$ for Operation Teapot events). $\overline{G(M)}$ is found from Equation (12). Q_1 is the value of dynamic pressure impulse associated with the static pressure gage placed at the same location as the total head overpressure gage [and $\overline{G(M_1)}$ is also so associated].

Q_2 is given by a similar equation, the only difference being that the planimetered value of $\Delta P_S \, \Delta t$ and the value of $\overline{G(M)}$ are associated with the

ground level static overpressure gage; we use the subscript 2 to connote this. Then

$$Q_2 = \int(\Delta P_p - \Delta P_{S_2})\ \Delta t/\overline{G(M_2)} \quad . \tag{14}$$

Next

$$Q_3 = \int q(t)\ \Delta t/\overline{G(M_1)} \tag{15}$$

and

$$Q_4 = \int q(t)\ \Delta t/\overline{G(M_2)} \quad . \tag{16}$$

Here $\int q(t)\,\Delta t$ is the planimetered value of the area under the dynamic pressure-time curve provided by the previous (point-by-point) data reduction.

$\overline{G(M_1)}$ and $\overline{G(M_2)}$ rarely differ by more than a few percent in this report, so that Q_3 and Q_4 likewise rarely differ by more than (the same) few percent. Since all 4 estimates are dependent on a single gage result, and 2 of the 4 estimates are based on one static overpressure gage, 2 on another, the 4 estimates are certainly not independent; however, as will soon be clear, inaccuracies in obtaining dynamic pressure impulse stem not only from the raw data but also from the data reduction process itself.

Thus Q_1 and Q_2 are both dependent upon the single total head overpressure gage result but are otherwise independent. Q_3 and Q_4 are almost completely dependent upon one another, differing only because of differences between $\overline{G(M_1)}$ and $\overline{G(M_2)}$, but from a data reduction standpoint are almost independent of Q_1 and Q_2. Put in another way, Q_1 and Q_3 are only dependent upon one another through $\overline{G(M_1)}$, which has the same effect on both, and Q_2 and Q_4 are only dependent upon one another through $\overline{G(M_2)}$ in carrying out the data reduction process.

In many cases, after the estimates of dynamic pressure impulse had been obtained, one or more of the four estimates were either missing (gage failure, or missing ΔP_S gage at the ground range in question) or obviously bad. When a reading was obviously bad a reason for this was almost always apparent. Most usual reasons were: $\int\Delta P_p\Delta t$ and $\int\Delta P_S\Delta t$ both considerably larger than the differences between them, which greatly magnifies errors in the data reduction process; baseline drift or instrumental noise problems associated with one or more of the gages; area under curve too small and/or irregular for accurate planimeter values to be obtained especially in the case of $\int q(t)\Delta t$.

Rather than attempt any, necessarily partly subjective, weighting of the

results obtained we, therefore, simply averaged the acceptable Q values (from 1 to 4 of them) in each case. We also made a comparison of results obtained with values of dynamic pressure impulse inferred from displacement (based on data from ideal shots, Reference 1). While these data have considerable scatter, values of dynamic pressure impulse inferred from side-on and face-on dynamic pressure impulse versus displacement curves are almost always within a factor of 1.5 of one another. We did not use any of these results to adjust any values of Q_i obtained from the pressure gage data. (See, however, Section 2.2.4 for a discussion of displacement-inferred values of dynamic pressure impulse; here we have recourse to a larger data base than in the previous work, Reference 1.)

Averaging the acceptable Q values obtained gives a somewhat higher weight to Q_3 and Q_4 than to either of Q_1 and Q_2; Q_3 and Q_4 correspond to the previously reduced data (point-by-point) with our Mach correction applied. As a comparative check of the results we plotted Q_2 versus Q_1, Q_1 versus Q_3, and Q_2 versus Q_4. Ideally the results should then lie on 45° lines. We found that:

1) For Q_1 versus Q_3 the points are scattered uniformly about a 45° line;

2) For Q_2 versus Q_1 and Q_2 versus Q_4 plots (with Q_2 as ordinate) the points are scattered about a slightly greater than 45° line;

3) The scatter of the points is about the same on all 3 plots.

This shows that the Q_i values are of equal reliability. The fact that Q_2 is, on the average, a little higher than the other Q_i values may be due to a physically real difference resulting from the ΔP_p and ΔP_s gage locations, or it may be associated with the fact that the ground level ΔP_s gage does not perturb the flow whereas the flow is perturbed at the other ΔP_s gage location. Thus, we cannot say that Q_2 is less reliable or less likely to be correct than the other values of Q_i.

B.3 ERROR ANALYSIS

Finally we must discuss the question of accuracy in more detail. We start with the planimeter result. When we measure the area under the entire pressure-time curve, a value expressed in square inches is obtained. This must be converted to pressure X time (psi-msec in this case although we convert the final results to kPa-sec). So in addition to the planimetering

error, there is an error in the scale length conversions on the raw data plots, psi per inch on the ordinate and msec per inch on the abscissa. We estimate typical measurements errors to be about 1% in the time scale, 2% in the (smaller) pressure scale, and ~3% in planimetering the small irregular areas, in spite of going around the areas more than once which diminishes part of the planimetering error; (it doesn't necessarily diminish the part of the latter error associated with inaccurate following of the contour, but it diminishes any planimeter resetting and vernier reading errors). In measuring areas under the curve for intervals within a pressure-time waveform there is a further error of placing the vertical lines which subdivide the waveform into intervals. That is, there is an error in Δt_i which in turn causes error in $\Delta P_p \Delta t_i$ and $\Delta P_S \Delta t_i$, as determined with the planimeter; since Δt_i for the ΔP_S gage waveform will not be precisely equal to the measured Δt_i for the ΔP_p waveform another small error is introduced, perhaps ~1%. We note also that the area within an interval is smaller than the total area under the waveform, usually by a factor of 2 or 3 for the most important intervals within a waveform, so that the percent error in planimetering the interval areas is larger than for the entire area. (This is the reason for not using a larger number of intervals than we have used.)

Thus before any calculations are undertaken, several small errors are introduced (in addition to instrumental errors in obtaining the raw data with which we begin.) The root mean square value of the errors discussed is typically ~4% for the entire waveform and perhaps about 5% for an important interval within a waveform — for each of $\Delta P_p \Delta t$ and $\Delta P_S \Delta t$. The absolute error bounds, however, can be anywhere from zero to 6 or 8%, for the waveform and an interval, respectively, depending on whether the several separate errors tend to cancel or reinforce one another.

The principal reason for the much greater inaccuracy in the final results achieved is due to the magnification of this error in the data reduction process. Dynamic pressure impulse is dependent upon the difference between $\Delta P_p \Delta t$ and $\Delta P_S \Delta t$ (for an interval or the whole waveform). With the estimate of typical error inputs given in the previous paragraph we can make a tabulation of expected and (approximate) upper bound errors as a function of the ratio of $\Delta P_S \Delta t$ to $\Delta P_p \Delta t$. We obtain for an entire waveform:

$\Delta P_S \Delta t / \Delta P_p \Delta t$	% ERROR RMS	% ERROR Approximate Upper Bound
0.25	5	10
0.50	9	18
0.75	20	40

For an important interval within a waveform, the entries in the last two columns should be increased by 25 to 40% (of the listed % error). For less important intervals, i.e., those that contribute small amounts to the total dynamic pressure impulse, still larger percent errors would be obtained. In each case the lower bound of the percent error is essentially zero, owing to possible cancellation of input errors. Random addition or cancellation of errors was undoubtedly involved in the elimination of obviously unacceptable results in some instances.

We have also combined the above analysis with inaccuracy caused by our use of $P_p \approx P_T$ (for $M < 1.3$), fixing $P_o = 14$ psi, and interpolating between the parametric curves (straight lines) given by Equations (8) to determine M. The inaccuracies involved here are completely negligible compared with the unavoidable inaccuracies just discussed. Likewise errors in $G(M_i)$ and $\overline{G(M)}$ owing to the assumptions of convenience just mentioned are negligible compared with the unavoidable inaccuracies.

The errors we have discussed so far relate to determination of Q_1 and Q_2. The errors we introduce in determining Q_3 and Q_4 stem from two sources: (1) planimetering of the dynamic pressure-time waveforms (already provided by a previous, point-by-point data reduction process, Reference (2); (2) determination of $\overline{G(M)}$.

The planimetering error involved here is larger than the error in planimetering ΔP_S and ΔP_p since the waveforms provided are smaller. However, there is no magnification of this error — this magnification has already taken place in forming $\Delta P_p - \Delta P_S$ in the previous data reduction from which we have q(t) waveforms. We cannot assess the detailed sources of error involved in obtaining q(t). We roughly estimate, however, that errors in Q_3 and Q_4 range from 7 to 10% when the area under q(t) curve is $\gtrsim 0.5$ square inch to perhaps 30% when the area under the curve is ~0.1 square inch. From our plots, previously mentioned, of Q_2 versus Q_1, Q_2 versus Q_4, and Q_1 versus Q_3, which show about equal point scatter in all cases, we conclude that the inaccuracy in our method based on planimetering areas and the inaccuracy in the point-

by-point method are roughly equal.

The fact that the errors are unavoidably as large as they are, and are still larger for individual intervals within a waveform, is the reason we used the areas under the total waveforms, Mach corrected with $\overline{G(M)}$, [with $\overline{G(M)}$ based on interval planimetering as previously described] to determine Q_1 and Q_2 — rather than using the planimetered areas $\Delta P_p \Delta t_i$ and $\Delta P_s \Delta t_i$ along with $G(M_i)$ to obtain the contribution of each interval to Q_1 and Q_2, then summing over the intervals to obtain Q_1 and Q_2. To show that the method we used was the more accurate of the two possible methods we simply explain why it is that we can determine $\overline{G(M)}$ accurately from planimetering values within intervals, even though the latter values are themselves rather inaccurate. The reasons for this are as follows:

1) intervals with sufficient planimetered area to have high weighting factors, W_i, associated with them can be planimetered much more accurately than small intervals;

2) G(M) is only "large" for high values of M and these are always associated with relatively large planimetered values;

3) the $\Delta P_p \Delta t_i$ and $\Delta P_s \Delta t_i$ values will not be nearly equal for any interval with a large value of W_i [except where M is small for the entire waveform, in which case G(M) is not much greater than unity, i.e., correction for Mach effect is small];

4) our weighting factor is normalized so that $\Sigma W_i = 1$ so that if one or more values of W_i are too high, others are necessarily too low thus providing some cancellation of errors; also in the important parts of a waveform G(M) varies less than over the total waveform and an error in one measured interval is most likely to be compensated in an adjacent interval, thus augmenting the error cancellation effect in determining $\overline{G(M)}$.

Had we decided to use the individual interval planimetered results, thus determining $q(t_i)\Delta t_i$ for each interval, some of the aforementioned cancellation would also have taken place. However, since use of the individual interval planimetered areas provides an accurate determination of $\overline{G(M)}$, the most accurate we can achieve, as previously explained — the method we have used yields as accurate a result as we can obtain without need for further use of the planimetered results for the individual intervals.

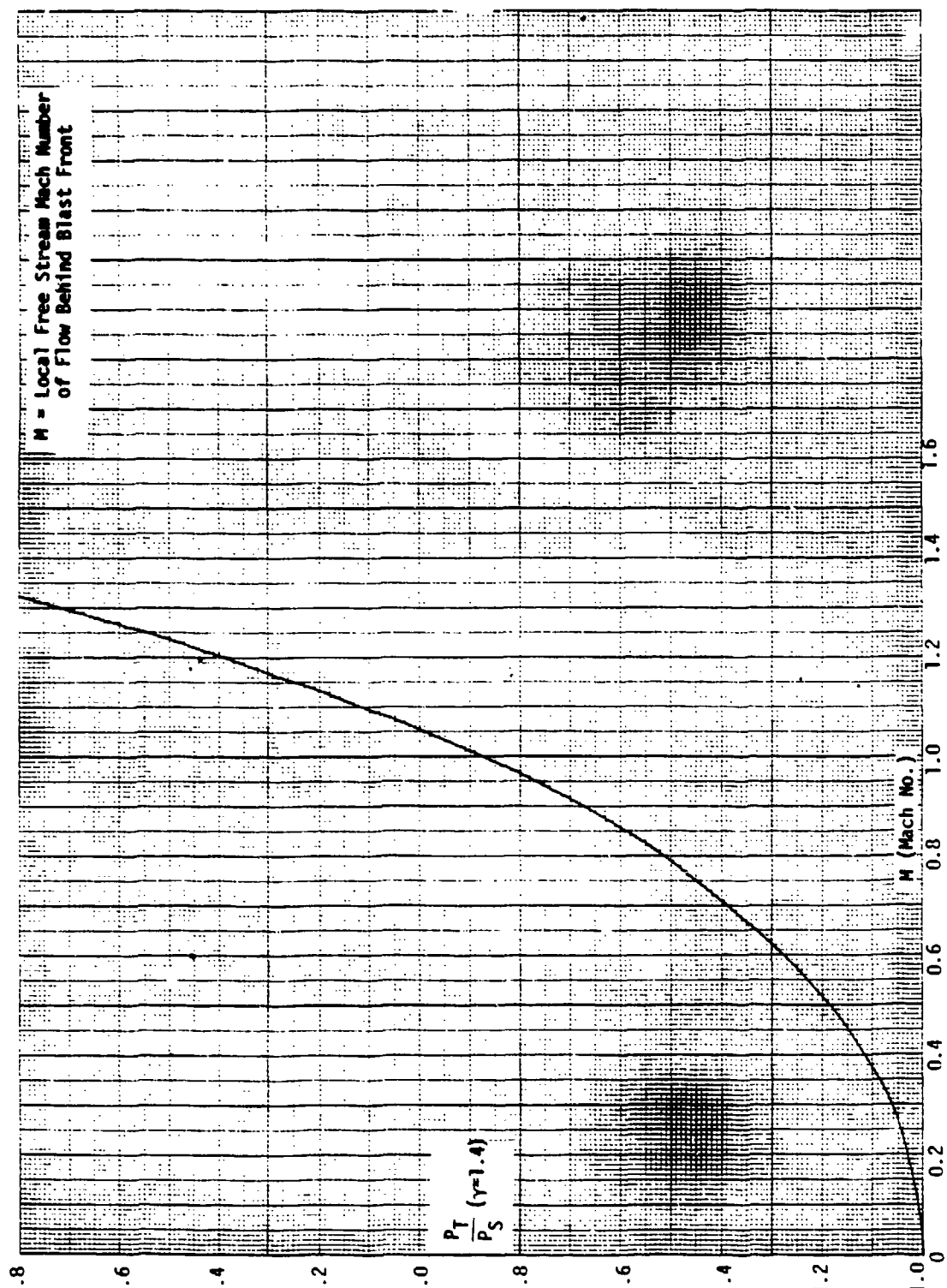

FIGURE B.1 Ratio of Absolute Free Stream Total Pressure to Absolute Free Stream Static Pressure vs. M

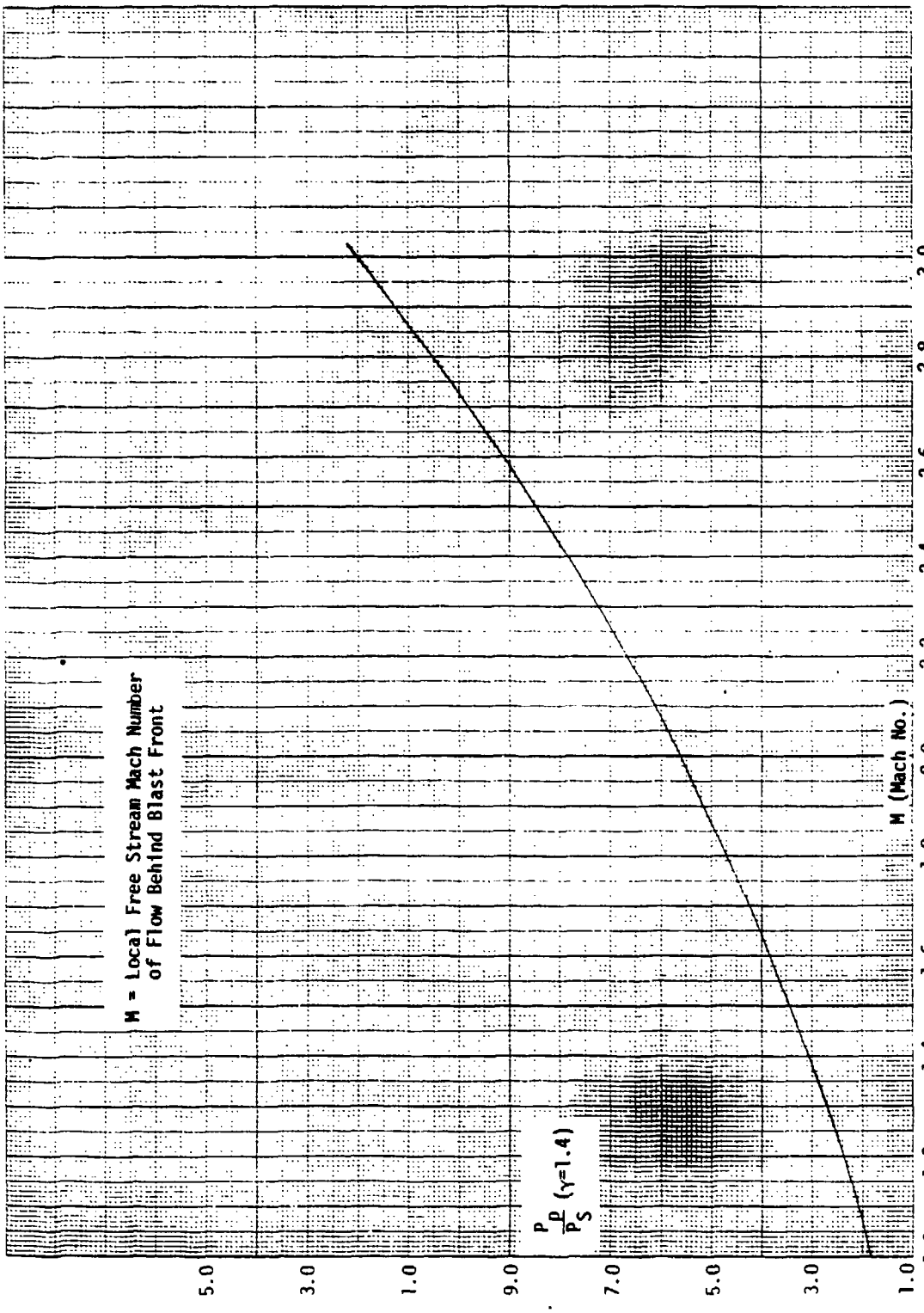

FIGURE B.2 Ratio of Absolute Total Head Pitot Pressure to Absolute Free Stream Static Pressure vs. M

APPENDIX C
(This Section is Unclassified)

THE LEAST SQUARES PROCEDURES

C.1 INTRODUCTION

All of the least squares fits in this report were obtained with the TI-59 calculator using library programs supplied by Texas Instruments.

All of the fits were either of the form

$$y = mx + b \tag{1}$$

or

$$y = a_0 + a_1x_1 + a_2x_2 \tag{2}$$

where y was the natural logarithm of the desired quantity; x was either the independent (controlled) variable or its logarithm and the least squares variables x_1, x_2 involved only the special case $x_1 = x$ and $x_2 = x^2$.

The least squares equations are obtained by minimizing the sum of the squares of the deviations of the data from the curve. If the experimental points have a variable scatter for a given small range of x, weights should be applied in the procedures so that the least squares equations corresponding to Equation (1), for example, are obtained by setting the derivatives of

$$S = \Sigma W_i[y_i - (mx_i + b)]^2 \tag{3}$$

with respect to m and b equal to zero, thus obtaining two linear algebraic equations which can be solved for m and b. Here S is the weighted sum of the squares of the residuals about the fitted curve and

$$W_i = \sigma^2/\sigma_i^2$$

where σ is a constant (to be determined from the deviations of the data from the fitted curve) and σ_i^2 is a measure of the expected deviation from the true value for an observation y_i (of unit weight).

In the Texas Instruments programs $W_i = 1$. In individual cases to be discussed we will point out that the programs used are nonetheless quite adequate for our needs. This is mainly due to the fact that in all cases, we minimized the sum of the squares of the logarithmic deviations of the desired function. This is equivalent to minimizing the sum of the squares of the percentage deviations from the curve since

$$\Delta(\ell n\ y) = \frac{\Delta y}{y} \tag{4}$$

That is, for small deviations from the curve, the fractional error $\frac{\Delta y}{y}$ is equal to $\Delta(\ell n\ y)$. For large deviations this is not exact and in our tabulation of results we show both

$$\sum_i (\ell n\ y_i - \ell n\ y_c)^2 \quad \text{and} \quad \sum_i \left(\frac{y_i - y_c}{y_c}\right)^2$$

where y_c = the value of $y(x_i)$ corresponding to the curve fit.*

The statistical analog of Equation (4) (Reference 13) is

$$\text{Var}\ (\ell n\ y) = \frac{1}{y^2}\ \text{Var}\ y \qquad (\text{Var} = \text{variance})\ . \qquad (4a)$$

Now in all of the cases in which we fitted the logarithm of the desired function y, the values of y covered a large range. If we consider, for example, a displacement measurement of 100 metres to be in error by 2%, the square of its deviation from the true value is 4; if we consider a displacement measurement of 1 metre to be in error by 20%, the square of its deviation from the true value is 0.04. So even though the percent errors in our data are not necessarily uniform (as best these errors are known), assuming them to be uniform is much closer to reality than any other assumption we can make. From the example just given we readily see that the coefficients in the least squares fits would be determined almost entirely by the data with large values of y if we were to minimize absolute rather than percent deviations from the fitted curves.

C.2 DYNAMIC PRESSURE IMPULSE VERSUS DISPLACEMENT (a)
DISPLACEMENT VERSUS DYNAMIC PRESSURE IMPULSE (b)

In application of our results we need fits of the data for cases (a) and (b), i.e., with each quantity used in the role of independent (controlled) and of dependent variable.

In each subcase of this case the data are fitted very will by straight lines on log-log plots. Thus for fitting on the TI-59 calculator the fit is of the form $y = mx + b$ (1)

with $y = \ell n\ I_q,\ x = \ell n\ D$ for Case (a)

and $y = \ell n\ D,\ x = \ell n\ I_q$ for Case (b)

* In most cases we omit the subscript i denoting the ith data point; the summations are taken over the data points in all cases so that omission of the subscript i will not lead to any confusion.

and $$b = \ell n\ B\ . \qquad (5)$$

Equation (1) can then also be written [for case (a)], $I_q = BD^m$ (1a) with a similar relation for Case (1b). However, after we have fitted case (a) we can calculate (b) directly (without fitting it) provided we recall certain data summations from the machine memory. For Equation (1) we obtain from the TI-59 fit:

$$\text{slope} = m = \frac{\Sigma xy - \Sigma x \Sigma y/N}{\Sigma x^2 - (\Sigma x)^2/N} \qquad (6)$$

$$y_{\text{intercept}} = b = \frac{\Sigma y - m\Sigma x}{N} \qquad (7)$$

and the correlation coefficient, $r = m\left(\frac{\sigma_x^2}{\sigma_y^2}\right)^{1/2}$. (8)

r^2 is called the coefficient of determination. The various summations can be recalled from the machine memory. σ_x^2 and σ_y^2 are the variances of the x-array and y-array data and are given by *

$$\sigma_x^2 = \frac{1}{N}\Sigma(x_i - \bar{x})^2 \qquad (9)$$

$$\sigma_y^2 = \frac{1}{N}\Sigma(y_i - \bar{y})^2 \qquad (10)$$

with $$\bar{x} = \frac{1}{N}\Sigma x \qquad (11)$$

and $$\bar{y} = \frac{1}{N}\Sigma y \qquad (12)$$

N is the number of data points.

Equations (6) to (8) are not symmetrical in x and y and the algebraic inverse of the least squares fit $I_q = BD^m$ (1a)

is $D = \left(\frac{1}{B}\right)^{1/m} I_q^{1/m}$ but this is <u>not</u> a least squares fit to the data with the role of I_q and D reversed.

However, manipulation of Equations (6) to (10) leads to the equation

* Bar over a quantity indicates an average value.

$$r = [\Sigma xy - \frac{1}{N}\Sigma x\Sigma y]\left([\Sigma x^2 - \frac{1}{N}(\Sigma x)^2][\Sigma y^2 - \frac{1}{N}(\Sigma y)^2]\right)^{-1/2} \quad (8a)$$

which is symmetrical in x and y, i.e., is unchanged when x and y are interchanged.

Thus, if we have obtained the least squares fit $I_q = BD^m$ we know that the correlation ratio r has the same value with the roles of I_q and D reversed. It can be shown (by taking the origin at the data centroid), (References 13 and 14), that the least squares fits

$$I_q = BD^m \quad (1a)$$

$$D = AI_q^{\ell} \quad (1b)$$

have values of ℓ and m which satisfy $\ell\, m = r^2$. (13)

Thus, having determined m (and r) in the least squares fit to case 1a we obtain ℓ in the least squares fit to case (1b) from Equation (13). The constant A in Equation 1b is then determined by the fact that both least squares fits (1a) and (1b) pass through the centroid of the data distribution. (Compare Reference 15.) Thus, from Equation (1b) we have

$$\ell n\, D = \ell n\, A + \ell\, \ell n\, I_q \quad (1b)$$

and in particular

$$\overline{\ell n\, D} = \ell n\, A + \ell\, \overline{\ell n\, I_q} \quad (14)$$

where from Equations (11) and (12)

$$\overline{\ell n\, D} = \frac{1}{N}\Sigma(\ell n\, D) \quad (15)$$

$$\overline{\ell n\, I_q} = \frac{1}{N}\Sigma(\ell n\, I_q)$$

and these values are available from the machine memory after running case (1a). Thus from Equation (14) we determine ℓn A, hence A, and the least squares fit to case (1b) is fully determined.

Having obtained the least squares fits, the coefficient of determination provides a measure of the goodness of fit. By manipulation of Equation (3), with $W_i = 1$, and Equations (6) through (12) it can be shown that

$$1 - r^2 = \frac{S}{N\sigma_y^2} \quad . \quad (16)$$

In this report we are concerned only with positive correlation, so that the

nearer r is to +1, the smaller is S, the sum of the squares of the deviations from the fitted curve, and hence the better the fit to the data. The expression for $1 - r^2$ can also be put in the form

$$1 - r^2 = \frac{\Sigma(y - y_c)^2}{\Sigma(y - \bar{y})^2} \tag{17}$$

thus expressing $1-r^2$ as a ratio of the sum of the squares of the deviations from the curve to the sum of the squares of the deviations from the mean (of the data). The denominator may be regarded as a normalizing factor. It is independent of the functional form used for the fitting function. Without such a denominator $1-r^2$ would tend to increase with the number of data points — even if the data were excellent.

Now letting $S_{\ell n\ I_q}$ and $S_{\ell n\ D}$ be the sum of the squares of the deviations from the fitted curve when $\ell n\ I_q$ and $\ell n\ D$, in turn, play the role of dependent variable, we have from Equation (16)

$$(1 - r^2) = \frac{S_{\ell n\ I_q}}{N\sigma^2_{\ell n\ I_q}} = \frac{S_{\ell n\ D}}{N\sigma^2_{\ell n\ D}} \tag{18}$$

Here
$$\sigma^2_{\ell n\ I_q} = \frac{1}{N}\left[\Sigma(\ell n\ I_q)^2 - \frac{1}{N}(\Sigma \ell n\ I_q)^2\right]$$
$$\sigma^2_{\ell n\ D} = \frac{1}{N}\left[\Sigma(\ell n\ D)^2 - \frac{1}{N}(\Sigma \ell n\ D)^2\right] \tag{19}$$

in accord with Equations (9) through (12). Since we have seen that r is unchanged when the roles of D and I_q are reversed, Equation (18) shows that the sums of the squares of the deviation from the curves are not the same for the two corresponding least squares fits (to the same data) but that

$$\frac{S_{\ell n\ I_q}}{S_{\ell n\ D}} = \frac{\sigma^2_{\ell n\ I_q}}{\sigma^2_{\ell n\ D}} \tag{20}$$

In all cases treated in this report we found $S_{\ell n\ I_q}$ to be considerably less than $S_{\ell n\ D}$.

In an application to be made of the results of this case we wish to know the standard deviation of the value of the slope of the curve as well as

the standard deviation of our observation. We use the following notation with the subscript c referring to the curve fit in each instance:

$\sigma^2_{\ell n\ I_q,C}$ = variance of an observation of $\ell n\ I_q$ relative to the curve; (note that we have assumed the variance of the percent error to be independent of the abscissa value)

σ^2_{ℓ}, σ^2_{m} = variances of slopes of curve fits.

Then it can be shown that (Reference 16)

$$\sigma^2_{\ell n\ I_q,C} = S_{\ell n\ I_q} / N-2^*$$

$$\sigma^2_{\ell n\ D,C} = S_{\ell n\ D} / N-2 \tag{21}$$

$$\sigma^2_{\ell} = \frac{S_{\ell n\ D}/N-2}{N\sigma^2_{\ell n\ I_q}} = \frac{1-r^2}{N-2} \quad \frac{\sigma^2_{\ell n\ D}}{\sigma^2_{\ell n\ I_q}}$$

$$\sigma^2_{m} = \frac{S_{\ell n\ I_q}/N-2}{N\sigma^2_{\ell n\ D}} = \frac{1-r^2}{N-2} \quad \frac{\sigma^2_{\ell n\ I_q}}{\sigma^2_{\ell n\ D}} \tag{22}$$

Using Equation (8) twice, first with D, I_q being independent and dependent variable and then with their roles reversed, we also see that

$$\frac{\sigma_{\ell}}{\sigma_m} = \frac{\ell}{m} \tag{23}$$

In the tabular results for the Displacement - Dynamic Pressure Impulse data curve fits, we list for each subcase the quantities N, $S_{\ell n\ I_q}$, $\sigma_{\ell n\ I_q,C}$, $S_{\ell n\ D}$, $\sigma_{\ell n\ D,C}$, ℓ, m, σ_{ℓ}, σ_m in addition to r and the fitting functions.

To gain further insight into the reliability of the data fits we have

* Here there are N-2 degrees of freedom; the two degrees of freedom lost correspond to the number of regression coefficients (two).

also tabulated the following additional quantities defined as follows:

$$S'_D = \Sigma\left(\frac{D-D_C}{D_C}\right)^2$$

$$S'_{I_q} = \Sigma\left(\frac{I_q - I_{qC}}{I_{qC}}\right)^2 \tag{24}$$

$$\sigma'_{D,C} = \left(\frac{S'_D}{N-2}\right)^{1/2}$$

$$\sigma'_{I_q,C} = \left(\frac{S'_{I_q}}{N-2}\right)^{1/2} \tag{25}$$

and finally the root mean square percent error which is

$$E_D = (S'_D/N)^{1/2} \times 100\%$$

$$E_{I_q} = (S'_{I_q}/N)^{1/2} \times 100\% \tag{26}$$

The σ' quantities, Equation (25), are standard deviations of the fractional error (percent error apart from a factor of 100). Thus when the number of data points N is fairly large (large enough so that the fit is fairly reliable) the values of σ'_D, σ'_{I_q} are almost the same as the values of E_D and E_{I_q}, respectively, (aside from the factor of 100 expressing the latter quantities in percent).

The reason we have chosen to list these additional quantities, in this and in other data fits to be discussed shortly, is that in many cases the data scatter is rather large (irrespective of the functional form selected for fitting the data). This means that a deviation $\Delta \ell n\ y$ in $\ell n\ y$ for a given data point may differ considerably from $\Delta y/y$. To illustrate, suppose the curve fit and data point values of a displacement are 10 metres and 6 metres. The contribution of this point to the sum of the squares of the deviations of ℓn D is then $(\ell n\ 10 - \ell n\ 6)^2 = 0.261$ (irrespective of which value is the curve fit values and which is the data point value).

The contribution to S'_D is

$$\left(\frac{10-6}{10}\right)^2 = 0.160$$

if the curve fit value is 10 and the data point value is 6; if, however, the curve fit value is 6 and the data point value is 10, the contribution to S'_D is $(\frac{10-6}{6})^2 = 0.444$.

Since the least squares curve tends to pass through the data region with a fairly uniform distribution of points on either side, on the average the curve fit will be below the data point about as often as above it. Averaging the above results yields $\frac{0.160 + 0.444}{2} = 0.302$ which is to be compared with the value 0.261 for the logarithmic deviation. Had we chosen the values 10 and 9.8 instead of 10 and 6, the two compared numbers would be virtually identical.

It is inherent in the nature of the data we are dealing with in this report, as is clear from the discussion of the data, that there is a fairly large data scatter in many cases. Also in many cases the number of data points is rather fewer than we desire. In cases where the scatter of the data is small we find that S'_D is fairly close in value to $S_{\ell n\ D}$ and similarly S'_{I_q} is fairly close to $S_{\ell n\ I_q}$. Usually $S_{\ell n\ D} < S'_D$, as in the case illustrated, and $S_{\ell n\ I_q} < S'_{I_q}$; the situation is sometimes reversed, however, usually because one or two data points with large deviations from the curve fit are below the curve. Conversely, for a case in which one or two data points are far <u>above</u> the curve it can happen that $S'_y >> S_{\ell n\ y}$ since there is no limit to the contribution such a point can make to S'_y, y here indicating any quantity whose ℓn has been fitted. (For a data point <u>below</u> the curve fit the maximum contribution to S'_y is

$$(\frac{y-y_c}{y_c})^2 = (\frac{0-y_c}{y_c})^2 = 1 \quad .$$

Finally, quantities such as $\sigma'_{I_q,C}$ and E_{I_q} are directly associated with the plotted data and are easily visualized. Since they pertain to fractional or percent errors they apply equally well at all points along the curve fit (although the curve fit has greater predictive accuracy in the vicinity of the data centroid than toward the ends of the data range). On the other hand $\sigma_{\ell n\ I_q}$ refers to the natural logarithm of the plotted data (ordinate) and the latter may be quite small or large (or even negative), so that while $\sigma_{\ell n\ I_q}$ is a standard measure of the data scatter with respect to the fitted curve, it is not as simple to interpret as are the additional quantities which we have tabulated.

In sum, the tabulated measures of goodness of fit provide some insight into the assessment of the reliability and utility of the data and the curve fits and help with the interpretation of results.

The quantities described here are also tabulated for various curve fits of data other than displacement - dynamic pressure impulse data. We discuss the least squares treatment of the remaining data in the following sections.

C.3 ADDITIONAL LEAST SQUARES FITS

Displacement versus Scaled Ground Range (a)

Dynamic Pressure Impulse versus Scaled Ground Range (b)

Scaled Dynamic Pressure Impulse versus Scaled Ground Range (c)

In each case the fitted curve is described by

$$\ell n\, y = a_0 + a_1 + a_2 x^2 \tag{27}$$

where x = scaled ground range. For cases (a) and (b) several scaling factors were used and an approximate optimum obtained.

In running these cases on the TI-59 calculator we feed in the natural logarithm of the y coordinate of each data point. Again, the machine generates a fit and all of the relevant summations over the data are available from the machine memory. For this type fit (trivariate), however, the machine provides a quantity R^2 rather than r as a measure of the goodness of fit. R is the multiple linear correlation coefficient between y and the other least squares variables $x_1 = x$ and $x_2 = x^2$; R^2 is called the coefficient of determination (see Reference 16) and is given by

$$R^2 = \frac{r_{y1}^2 + r_{y2}^2 - 2r_{12}\, r_{y1}\, r_{y2}}{1 - r_{12}^2} \tag{28}$$

The subscripts 1 and 2 refer to x_1 and x_2; r_{y1}, r_{y2}, and r_{12} are given by equations analagous to Equation (8a).

$$r_{y1} = \left[\Sigma xy - \frac{\Sigma x \Sigma y}{N}\right]\left(\left[\Sigma x^2 - \frac{(\Sigma x)^2}{N}\right]\left[\Sigma y^2 - \frac{(\Sigma y)^2}{N}\right]\right)^{-1/2}$$

$$r_{y2} = \left[\Sigma x^2 y - \frac{\Sigma x^2 \Sigma y}{N}\right]\left(\left[\Sigma x^4 - \frac{(\Sigma x^2)^2}{N}\right]\left[\Sigma y^2 - \frac{(\Sigma y)^2}{N}\right]\right)^{-1/2} \tag{29}$$

$$r_{12} = \left[\Sigma x^3 - \frac{\Sigma x \Sigma x^2}{N}\right]\left(\left[\Sigma x^2 - \frac{(\Sigma x)^2}{N}\right]\left[\Sigma x^4 - \frac{(\Sigma x^2)^2}{N}\right]\right)^{-1/2}$$

(The superficial lack of symmetry between r_{y1} and r_{y2} results from the fact that the least squares variables x_1 and x_2 as used here are x and x^2, respectively.) The quantities r_{y1}, r_{y2}, and r_{12} are the coefficients of correlation (also called simple correlation or zero-order coefficients) between y and x_1, y and x_2, and x_1 and x_2, respectively. The important point here is that

$$(1 - R^2) = \frac{\Sigma(y-y_c)^2}{\Sigma(y-\bar{y})^2} \tag{17a}$$

so that R^2 provides a measure of the goodness of fit precisely similar to that provided by r^2 in the previous discussion: R^2 is a measure of the closeness of fit of the regression plane (in ℓn y, x_1, x_2 space) to the data points.

There is one further change: replacement of N-2 by N-3 in Equations (21) and (25) so that

$$\sigma^2_{\ell n\ I_q,C} = S_{\ell n\ I_q}/N-3$$

$$\sigma^2_{\ell n\ D,\ C} = S_{\ell n\ D}/N-3 \tag{21a}$$

and

$$\sigma'_{D,C} = (S'_D/N-3)^{1/2}$$

$$\sigma'_{I_q,C} = (S'_{I_q}/N-3)^{1/2} \tag{25a}$$

We list the same quantities in the tabular results relating to the fitted curves in this subsection as in the previous subsection.

Some additional fits were required in the cases treated in this subsection owing to the form of Equation (27). This functional form entails either a maximum or a minimum (which may fall within the data range, near one end of the data range, or at a point remote from the range of the data). In the case of Dynamic Pressure Impulse versus Scaled Ground Range and Scaled Dynamic Pressure Impulse versus Scaled Ground Range, the experimental data are such that the curves are concave upward and have a minimum usually approximately at the large x (= scaled ground range) end of the data range. In these instances, in order to have a fit of the proper shape for large x, and capable of extrapolation with no more than the usual uncertainty in extrapolating a monotonic well-behaved function somewhat beyond the range validated by data, we generated additional fits (of the same functional form and with the same

scaling in each instance) over the data contained in the large x end of the data range. Thus, in these cases we have two fits of the form of Equation (27), one over the entire data base and one over the portion of the data base relevant to large scaled range.

The need for the additional fits stems from the fact that there are many targets susceptible to damage at lower levels of dynamic pressure impulse than are the vehicles of interest in this report.

There are possibly other methods of accomplishing this purpose, including use of functions other than provided by Equation (27) for fitting the data. We note, however, that the data itself is concave upward, so that any function conforming to this shape and consisting of more than two terms all either increasing or decreasing monotonically would seemingly have at least one positive and one negative term and therefore a possibility of a minimum somewhere (though not necessarily near or within the range of the data). In an attempt to avoid this we used a one term expression for the fit in one case:

$$y = a \exp[-b(x-x_0)^m] \quad .$$

We chose a and x_0 so that the curve was forced to pass through a selected point. The exponent m allows some flexibility in adjusting the curvature as a function of x as compared with a simple exponential and y decreases monotonically as x increases for $x > x_0$. ($x = x_0$ was chosen as the lowest value of x in the data range.) Then with a change of variable $Y = \ell n(\frac{a}{y})$ and $X = x-x_0$ the fitting equation takes the form $\ell n\ Y = \ell n\ b + m\ \ell n\ X$. We fitted this equation to the data for one case. It did not fit well at all. (At least part of the reason for this, however, is that the fitting equation is ill-conditioned to fitting the data without use of a weighting function — large percentage errors in y for small y have little effect on the data; as previously pointed out the Texas Instruments library programs for least squares fitting do not allow use of weighting functions.)

Thus, while it is possible that some other (probably not more than two term — however complicated) function or some transformation of variables may allow good fit to the data without a minimum (or maximum) in or near the data range we believe it simpler and quite justifiable to use Equation (27) for all of the fits in this subsection in the manner we have described. Equation (27) is a simple and convenient function to use.

APPENDIX D
(This Appendix Is Unclassified)

LIST OF ABBREVIATIONS, ACRONYMS, AND/OR SYMBOLS

I_p - static pressure impulse

I_q - dynamic pressure impulse

I_{q_0} - dynamic pressure impulse: initial estimates for ideal/near-ideal events; first iteration results for non-ideal events

$\bar{I}_q$ - final estimates of dynamic pressure impulse: iterated results for ideal/near-ideal events; second iteration results for non-ideal events

P_s - peak overpressure

D - displacement

da - damage

W, Y - weapon yield

R - ground range

X - scaled ground range

HOB - height of burst

P_0 - ambient pressure

T_0 - ambient temperature

S_d, S_d', S_i, S_p, S_t - scaling factors

n - exponent in scaling law

a_0, a_1, a_2, b, ℓ, m, x_0, A, B - constants in least squares fits

x, y - independent and dependent variables in least squares fits

f, f_1, f_2, G - functional forms

σ - standard deviation

σ^2 - variance

N - number of data points

r - correlation coefficient

R - multiple linear correlation coefficient

r^2, R^2 - coefficient of determination

S - sum of squares of deviations of data points from fitted curve

S' - sum of squares of fractional (relative) deviations of data points from fitted curve

$\sigma' - \left(\frac{S}{N - \text{number of regression coefficients}}\right)^{1/2}$ = standard deviation of fractional error

$E - \left(\frac{S'}{N}\right)^{1/2} \times 100$ = root mean square percent error

M - mass of vehicle

I - moment of inertia of vehicle (about designated axis)

A - projected area of vehicle

μ - coefficient of friction

V, V_0 - velocity, initial velocity

F - force

ω - angular velocity

α - angular acceleration

T - torque (vehicle overturning)

x - distance travelled by vehicle (in equations of motion)

F(V), g(V) - functions of velocity (in equations of motion)

C - constant in curve fits

K, K_1, K_2 - constants in equations of motion

P_S - absolute free stream static pressure

P_T - absolute free stream total pressure

P_p - absolute total head Pitot pressure

P_o - ambient pressure

$\Delta P_S = P_S - P_o$ — free stream static overpressure

$\Delta P_T = P_T - P_o$ — free stream total overpressure

$\Delta P_p = P_p - P_o$ — total head overpressure

q - dynamic pressure

Q_i - dynamic pressure impulse; subscript i denotes ith method of obtaining result (4 values of i used)

γ - ratio of specific heat at constant pressure to specific heat at constant volume for air

M - local free stream Mach No. of flow behind blast front

Δt_i - ith time interval (in a pressure-time waveform)

G(M) - Mach correction factor

$\overline{G(M)}$ - average value of G(M) overpressure-time history

W_i - weighting factor for ith time interval

THIS PAGE IS INTENTIONALLY LEFT BLANK.

DISTRIBUTION LIST

(This List is Unclassified)

DEPARTMENT OF DEFENSE

DEF RSCH & ENGRG
ATTN: STRAT & SPACE SYS (OS)
ATTN: STRAT & THEATER NUC FOR, F VAJDA

DEFENSE INTELLIGENCE AGENCY
ATTN: RTS-2A (TECH LIB)
ATTN: RTS-2B

DEFENSE NUCLEAR AGENCY
ATTN: SPAS C GALLOWAY
ATTN: SPAS D MUNNINGHOFF
ATTN: SPAS G ULLRICH
ATTN: SPAS R ROHR
4 CYS ATTN: STTI-CA

DEFENSE TECHNICAL INFORMATION CENTER
2 CYS ATTN: DD

FIELD COMMAND DEFENSE NUCLEAR AGENCY
ATTN: FCTT
ATTN: FCTT W SUMMA
ATTN: FCTXE

JOINT STRAT TGT PLANNING STAFF
ATTN: JLKS
ATTN: JPTM
ATTN: JPTP

DEPARTMENT OF THE ARMY

HARRY DIAMOND LABORATORIES
ATTN: SCHLD-NW-P
ATTN: SLCIS-IM-TL (TECH LIB)

U S ARMY BALLISTIC RESEARCH LAB
ATTN: SLCBR-SS-T (TECH LIB)

U S ARMY CORPS OF ENGINEERS
ATTN: DAEN-ECE-T

U S ARMY ENGINEER CTR & FT BELVOIR
ATTN: TECHNICAL LIBRARY

U S ARMY ENGINEER DIV HUNTSVILLE
ATTN: HNDED-SY

U S ARMY ENGR WATERWAYS EXPER STATION
ATTN: E JACKSON, WESSS-O
ATTN: J JACKSON, WESSD
ATTN: J ZELASKO, WESSD-R

U S ARMY NUCLEAR & CHEMICAL AGENCY
ATTN: LIBRARY
ATTN: MONA-NU MR LONG

U S ARMY STRATEGIC DEFENSE CMD
ATTN: DASD-H-SAV R C WEBB

U S ARMY STRATEGIC DEFENSE COMMAND
ATTN: ATC-T

DEPARTMENT OF THE NAVY

NAVAL RESEARCH LABORATORY
ATTN: CODE 2627 (TECH LIB)
ATTN: CODE 4040 D BOOK
ATTN: CODE 4040 J BORIS

NAVAL SURFACE WEAPONS CENTER
ATTN: CODE R44 H GLAZ
ATTN: CODE X211 (TECH LIB)

NAVAL SURFACE WEAPONS CENTER
ATTN: TECH LIB & INFO SVCS BR

DEPARTMENT OF THE AIR FORCE

AIR FORCE CTR FOR STUDIES & ANALYSIS
ATTN: AFCSA/SAMI (R GRIFFIN)

AIR FORCE WEAPONS LABORATORY, AFSC
ATTN: NTED-A
ATTN: SUL

BALLISTIC MISSILE OFFICE/DAA
ATTN: ENSN
ATTN: MYED D GAGE

STRATEGIC AIR COMMAND/NRI-STINFO
ATTN: NRI/STINFO

DNA 5826 (DL CONTINUED)

DEPARTMENT OF ENERGY

LOS ALAMOS NATIONAL LABORATORY
ATTN: C F KELLER
ATTN: M T SANDFORD
ATTN: R WHITAKER

SANDIA NATIONAL LABORATORIES
ATTN: DIV 7111 J W REED
ATTN: J R BANNISTER 7111
ATTN: ORG 7112 A CHABAI

OTHER GOVERNMENT

CENTRAL INTELLIGENCE AGENCY
ATTN: OSWR/NED

DEPARTMENT OF DEFENSE CONTRACTORS

AEROSPACE CORP
ATTN: H MIRELS
ATTN: LIBRARY ACQUISITION

APPLIED RESEARCH ASSOCIATES, INC
ATTN: N HIGGINS

APPLIED RESEARCH ASSOCIATES, INC
ATTN: D PIEPENBURG

BOEING CO
ATTN: S STRACK

CALIFORNIA RESEARCH & TECHNOLOGY, INC
ATTN: K KREYENHAGEN
ATTN: LIBRARY

CALIFORNIA RESEARCH & TECHNOLOGY, INC
ATTN: F SAUER

CARPENTER RESEARCH CORP
ATTN: H J CARPENTER

DENVER, UNIVEPSITY OF
ATTN: J WISOTSKI

H & H CONSULTANTS, INC
ATTN: J HALTINANGER
ATTN: W HALL

H-TECH LABS, INC
ATTN: B HARTENBAUM

KAMAN SCIENCES CORP
ATTN: R RUETENIK

KAMAN TEMPO
ATTN: DASIAC

KAMAN TEMPO
ATTN: DASIAC
2 CYS ATTN: E BRYANT

MCDONNELL DOUGLAS CORP
ATTN: H HERDMAN
ATTN: R HALPRIN

NEW MEXICO, UNIVERSITY OF
ATTN: J KOVARNA

PACIFIC-SIERRA RESEARCH CORP
ATTN: H BRODE, CHAIRMAN SAGE

PACIFIC-SIERRA RESEARCH CORP
ATTN: D GORMLEY

PACIFICA TECHNOLOGY
ATTN: R ALLEN
ATTN: TECH LIBRARY

PHYSICS INTERNATIONAL CO
ATTN: H W WAMPLER

R & D ASSOCIATES
ATTN: A KUHL
ATTN: T MAZZOLA
ATTN: TECHNICAL INFO CTR

R & D ASSOCIATES
ATTN: A POLK
ATTN: B WEBSTER

R & D ASSOCIATES
ATTN: G GANONG

RAND CORP
ATTN: B BENNETT

S-CUBED
ATTN: B PYATT
ATTN: C DISMUKES
ATTN: J BARTHEL
ATTN: LIBRARY

S-CUBED
ATTN: C NEEDHAM

SCIENCE APPLICATIONS INTL CORP
ATTN: H WILSON
ATTN: R SCHLAUG
ATTN: TECH LIB

SCIENCE APPLICATIONS INTL CORP
ATTN: J COCKAYNE
ATTN: W LAYSON

SCIENCE APPLICATIONS INTL CORP
ATTN: G BINNINGER

SRI INTERNATIONAL
ATTN: J COLTON

TELEDYNE BROWN ENGINEERING
ATTN: D ORMOND
ATTN: F LEOPARD

TRW ELECTRONICS & DEFENSE SECTOR
ATTN: A ZIMMERMAN
ATTN: M SEIZEW
ATTN: TECH INFO CTR,DOC ACQ

TRW ELECTRONICS & DEFENSE SECTOR
ATTN: E WONG, BLDG SB1
ATTN: G HULCHER
ATTN: N GUILES
ATTN: N LIPNER
ATTN: P DAI

WEIDLINGER ASSOC, CONSULTING ENGRG
ATTN: I SANDLER

Defense Special Weapons Agency
6801 Telegraph Road
Alexandria, Virginia 22310-3398

TRC

13 April 1998

MEMORANDUM TO DEFENSE TECHNICAL INFORMATION CENTER
ATTN: OCQ/MR BILL BUSH

The following reports have been reviewed by the Defense Special Weapons Agency Security Office:

~~DNA-4622F, AD-C015969, DTL-78,1304~~ Completed
DNA-5056F, AD-C021924, DTL-80,0808
DNA-5826F, AD-C040572, DTL-87,0355 C FRD
DNA-5826F-SUP, AD-C041417, DTL-871167 C FRD

The Security Office has **declassified** all of the listed reports. Further, distribution statement **"A"** applies to all of the reports.

Ardith Jarrett
ARDITH JARRETT
Chief, Technical Resource Center

Completed
15 May 2000
R.W.